PEPTIDOMIMETIC PROTEASE INHIBITORS: ACTIVITY AND MECHANISM OF INHIBITION

A thesis submitted for the
degree of Doctor of Philosophy

Xiaozhou Zhang, B.Sc. (Hons.)

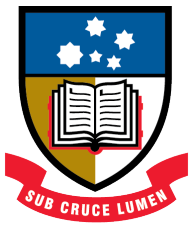

THE UNIVERSITY
of ADELAIDE

Department of Chemistry
The University of Adelaide
South Australia
August 2015

Table of Contents

Abstract

The study of protein mechanism and function is central to the development of biosensing tools and therapeutics for the treatment of diseases. This thesis describes an NMR and X-ray crystallography-based characterisation of the mechanism by which a macrocyclic peptidomimetic, the backbone of which is constrained into a β-strand conformation, inhibits α-chymotrypsin. This allowed the development of new peptidomimetic inhibitors that target the 26S proteasome and also inhibitors the activity of which can be modulated photochemically. This then provides a basis for biosensing and therapeutic applications.

Chapter one introduces the structures and mechanism of serine, cysteine and threonine proteases, and discusses how theses proteases universally bind ligands in an extended β-strand conformation. In addition, this chapter details the strengths and limitations of current peptidomimetic inhibitors of α-chymotrypsin, calpains and the 26S proteasome and their implications in the treatment of human diseases.

Chapter two describes optimisation of the synthesis of two macrocyclic peptidic aldehyde inhibitors **2.12** and **2.13** that target cysteine proteases and α-chymotrypsin, respectively. This allowed the preparation of an analogue of **2.13** containing a ^{13}C label in the aldehyde, which was used to confirm the mechanism of inhibition of α-chymotrypsin by ^{13}C NMR spectroscopy. This confirmed the formation of a stable hemiacetal intermediate upon the binding

of **2.13** with α-chymotrypsin. X-ray crystallography of a complex of **2.13** bound to α-chymotrypsin revealed that the backbone adopts a stable β-strand conformation as per its design. The binding of **2.13** to α-chymotrypsin is further stabilised by the oxyanion hole near the S_1 subsite and multiple hydrogen bonding interactions.

Chapter three details the development of new acyclic proteasome inhibitors **3.05**-**3.08** containing a peptidomimetic backbone and a *C*-terminal boronate. All analogues showed selectivity for the chymotrypsin-like subunit of the 26S proteasome with IC_{50} values in the low nanomolar range. Compound **3.08**, with an IC_{50} of 13 nM, was 2-fold more active than the anti-myeloma therapeutics bortezomib and carfilzomib. This inhibitor is more cytotoxic against a range of solid tumour cells and has a larger therapeutic window compared to existing FDA approved drugs.

Chapter four presents a new approach to the regulation of the activity of α-chymotrypsin using a new spiropyran-based moiety that can be reversibly switched between an 'on' (SP isomer) and 'off' (MC isomer) state photochemically. This is demonstrated in solution and also when attached to a microstructured optical fibre (MOF), as a first step to the development of a biosensor. The most active analogue in this series displayed a K_i of 115 nM in solution. The active SP isomer of an analogue **4.07** with a *C*-terminal Weinreb amide was significantly more active than the corresponding MC isomer both in solution and on fibre.

Declaration and Published Works

I certify that this work contains no material which has been accepted for the award of any other degree or diploma in my name, in any university or other tertiary institution and, to the best of my knowledge and belief, contains no material previously published or written by another person, except where due reference has been made in the text. In addition, I certify that no part of this work will, in the future, be used in a submission in my name, for any other degree or diploma in any university or other tertiary institution without the prior approval of the University of Adelaide and where applicable, any partner institution responsible for the joint-award of this degree. I give consent to this copy of my thesis when deposited in the University Library, being made available for loan and photocopying, subject to the provisions of the Copyright Act 1968. The author acknowledges that copyright of published works contained within this thesis resides with the copyright holder(s) of those works. I also give permission for the digital version of my thesis to be made available on the web, via the University's digital research repository, the Library Search and also through web search engines, unless permission has been granted by the University to restrict access for a period of time.

.....

Xiaozhou Zhang

.....

Date

Work in this thesis has appeared in the following publications:

"Photoregulation of α-Chymotrypsin Activity by Spiropyran-Based Inhibitors in Solution and Attached to an Optical Fiber", Zhang, X.; Heng, S.; Abell, A. D. *Chemistry – A European Journal* **2015**, *21*, 10703.

"Macrocyclic Protease Inhibitors with Reduced Peptide Character", Chua, K. C. H.; Pietsch, M.; Zhang, X.; Hautmann, S.; Chan, H. Y.; Bruning, J. B.; Gütschow, M.; Abell, A. D. *Angew. Chem. Int. Ed.* **2014**, *53*, 7828.

Acknowledgements

First of all I would like to thank Professor Andrew Abell for his guidance and supervision throughout my PhD. I am especially thankful for the time and energy he has put into revising and guiding me on writing scientific papers and this thesis. I am also grateful for the freedom he'd given me to pursue my own ideas. I would like to also thank my co-supervisor Dr. Jonathan George for his guidance and supervision in many aspects of my study. Thank you to Dr. Sabrina Heng for mentoring me through the most difficult time of my PhD, assisting in all my projects and proofreading this thesis. I would like to thank Dr. Andrew Harvey for his invaluable advice on my research.

Many thanks to all the past and present members of the Abell group for providing assistance in every aspect of my PhD, especially: to Dr. Krystle Chua for laying the foundation for my research, Dr. Ashok Pehere, Dr. Niels Krogsggard-Larsen, and Dr. William Tieu for helping me to overcome difficulties in synthesis, Dr. Markus Pietsch for assisting on enzyme assays, Dr. Denis Scanlon and Ms. Kelly Keeling for their assistance on HPLC and mass spectrometry, Dr. Herbert Foo and Mr. Daniel Stubing for helping me with fibre surface functionalization, and Mr. Jacko Feng for conducting high-resolution mass spectrometry experiments.

I would like to thank those who have helped me with my research, especially: Mr. Phil Clement (MS and NMR), Dr. Paul Neilsen and Ms. Alaknanda Alaknanda (proteasome assays and cell cytotoxicity assays), Mr. Roman

Kostecki and Dr. Erik Schartner (laser-aided MOF experiments) and Dr. John Bruning (X-ray crystallography).

I am grateful to the University of Adelaide for generously providing the AGRS scholarship for my research and Cancer Therapeutics CRC for providing a top-up scholarship.

And last, but most importantly, to my family: my mother and father, my husband Victor and my dear daughter Kimberley—Thank you for your enormous support, encouragement and love. Without you, I would not have been able to achieve all these.

Abbreviations

AAF-AMC	Ala-Ala-Phe-7-amido-4-methylcoumarin
Ac-nLPnLD-AMC	*N*-acetal-Nle-Pro-Nle-Asp-7-amino-4-methylcoumarin
ACN	acetonitrile
Ala	alanine
AMC	7-amino-4-methylcoumarin
Asn	asparagine
Asp	aspartic acid
ATP	adenosine triphosphate
bCT	bovine α-chymotrypsin
Boc	*tert*-butyloxycarbonyl
Boc-LSTR-AMC	*N*-Boc-Leu-Ser-Thr-Arg-7-amino-4-methylcoumarin
Boc_2O	di-*tert*-butyl dicarbonate
BOP	(benzotriazol-1-yloxy)tris(dimethylamino)phosphonium hexafluorophosphate
br s	broad singlet (in NMR)
Bz-VGR-AMC	*N*-benzyl-Val-Gly-Arg-7-amino-4-methylcoumarin
C-L	caspase-like activity (of the proteasome)
cat.	catalytic amount
Cbz	carboxybenzyl
CDK	cyclin-dependent kinase
CT-L	chymotrypsin-like activity (of the proteasome)
Cys	cysteine

d	doublet (in NMR)
DCM	dichloromethane
dd	doublet of doublet (in NMR)
ddd	doublet of doublet of doublet
DIC	*N,N′*-diisopropylcarbodiimide
DIPEA	N,N-diisopropylethylamine
DMAP	4-dimethylaminopyridine
DMF	dimethylformamide
DMSO	dimethyl sulfoxide
dt	doublet of triplet (in NMR)
EDCI	1-Ethyl-3-(3-dimethylaminopropyl)carbodiimide
equiv	equivalents
ESI	electrospray ionisation (in HRMS)
FDA	United States Food and Drug Administration
FTIR	fourier transform infrared spectroscopy
G1	growth-1 phase
G2	pre-mitotic phase
Glu	glutamic acid
Gly	glycine
HATU	1-[Bis(dimethylamino)methylene]-1H-1,2,3-triazolo[4,5-b]pyridinium 3-oxid hexafluorophosphate
HEPES	4-(2-hydroxyethyl)-1-piperazineethanesulfonic acid
His	histidine
HIV	human immunodeficiency virus
HIVPR	the human immunodeficiency virus protease

HMDS	bis(trimethylsilyl)amine
HOBt	hydroxybenzotriazole
HRMS	high-resolution mass spectrometry
Ile	isoleucine
LDA	lithium diisopropylamide
Leu	leucine
LiHMDS	lithium bis(trimethylsilyl)amide
M	mitosis phase
m	multiplet (in NMR)
MC	merocyanine
Met	methionine
min	minute
MMF	multi-mode fibre
MOF	microstructured optical fibre
n-Buli	n-butyllithium
NMR	nuclear magnetic resonance
o-CAPN2	ovine calpain 2 (m-calpain)
PDB	protein data bank
PG	protecting group
Phe	phenylalanine
PMP-C	pars intercerebralis major peptide-C
q	quartet (in NMR)
quant	quantitative (yield)
r.t.	room temperature
RCM	ring-closing metathesis

RMS	root mean square (in X-ray crystallography)
RP-HPLC	reverse phase high-performance liquid chromatography
S	synthesis phase
s	singlet (in NMR)
sat.	saturated
SEM	scanning electron microscopy
Ser	serine
SP	spiropyran
Suc-LLVY-AMC	*N*-succinyl-Leu-Leu-Val-Tyr-7-amino-4-methylcoumarin
t	triplet (in NMR)
T-L	trypsin-like activity (of the proteasome)
TBAI	tetrabutylammonium iodide
TES	*N*-[tris(hydroxymethyl)methyl]-2-aminoethanesulfonic acid
TFA	trifluoroacetic acid
THF	tetrahydrofuran
Thr	threonine
TLC	thin layer chromatography
TLCK	tosyllysine chloromethyl ketone
TMS	trimethylsilane
Tris	tris(hydroxymethyl)aminomethane hydrochloride
Trp	tryptophan
TTL	transistor-transistor logic
Tyr	tyrosine
UV	ultraviolet
Vis	visible light

Chapter 1

Introduction to Proteases and Protease Inhibitors

1.1 Overview of Proteases and Protease Inhibitors

Proteases occupy approximately 2% of the genomes of all living species.[1] Proteases catalyse the hydrolysis of the back bone amide bond of numerous substrates to facilitate protein activation, deactivation, modification and degradation.[2-3] Thus proteases are crucial in regulating a wide range of cellular processes including cell proliferation and differentiation,[4] signaling,[5] and apoptosis.[6] These cellular processes, in turn, have significant influences on a wide range of physiological functions.[1]

Protease activity is tightly regulated through a feedback mechanism.[7] This commonly involves the binding of either a signaling molecule or a protein substrate to various sites of the protease, which either diminishes or enhances its catalytic activity.[8-9] The loss of proper regulation of protease functions often results in abnormal protein activities associated with many disease conditions, such as neurodegenerative diseases,[10] cardiac dysfunction,[11] cancer,[12] and cataracts.[13] Consequently, inhibitors that can restore proper protease activity have promising therapeutic potentials to treat a wide range of human disease.[14-16]

Proteases are incredibly diverse in terms of size, structure and catalytic mechanism.[17] Based on the catalytic residue that facilitate substrate hydrolysis, proteases can be divided into six classes: cysteine, serine, threonine, aspartic, glutamic and metallo-proteases.[18] A protease can function through two possible catalytic mechanisms: 1) serine, cysteine and threonine

proteases have the key catalytic nucleophile located inside the active site; 2) aspartic, glutamic and metallo-proteases catalyse the cleavage of substrates through an activated water molecule.[17]

All proteases bind their substrates in an active site cleft. Based on a notation developed by Schechter and Berger (Figure 1.01),[19] the amino acids of a protease substrate are denoted as P_1-P_n to the *N*-terminal of the cleavage site and P_1'-P_n' to the *C*-terminal end. The hydrolysed amide bond lies between the P_1 and P_1' residues. The corresponding enzyme binding pockets denoted as S_n-S_n' interact with the substrate to define it into an extended β-strand conformation. Such conformation is critical to binding and inhibitor design.[18] This is discussed in detail in section 2.1.1.

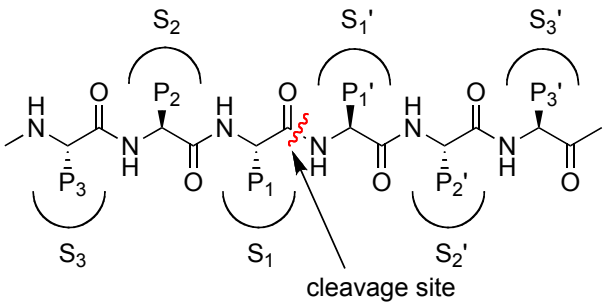

Figure 1.01 A schematic representation of a typical protease substrate: the substrate amino acid side chains are denoted P_n-P_n' whereas the corresponding binding pockets on the enzyme are denoted as S_n-S_n'. The cleavage site is between P_1 and P_1'.

Protease inhibitors can be divided into 'active-site directed' or allosteric inhibitors based on the mechanism of inhibition.[20] Active-site directed inhibitors compete with the substrates for binding to the active site residues,

most importantly S_1-S_3. Thus synthetic protease inhibitors are mostly small peptide-based molecules that mimic the natural substrates of their target proteases.[21] Many inhibitors have a *C*-terminal reactive functional group to covalently interact with the catalytic residue. This results in the formation of an intermediate that mimics the transition state of amide bond hydrolysis, thereby displaying a greater binding affinity than those that do not possess a reactive species.[22-23] These reactive functional groups are also commonly referred to as warheads. Warheads can form either irreversible or reversible bonds with the active site.[21] Reversible inhibitors are generally preferred over irreversible inhibitors in a therapeutic sense as the latter can covalently bind non-specifically to many nucleophiles and proteases in an *in vivo* environment, resulting in toxic side effects.[22] Thus the design of protease inhibitors presented in this thesis is primarily directed towards reversible inhibitors, as shown in Figure 1.02.[24] Some reversible warheads provide selectivity between proteases from different families. For example, peptidic boronates are highly selective for the proteasome while α-keto esters show selectivity for serine proteases over other proteases. Peptidic aldehydes, on the other hand, provide little selectivity between serine, cysteine and threonine proteases.

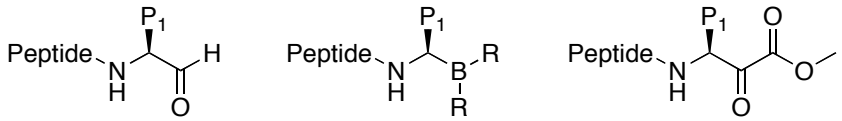

Figure 1.02 General design of reversible inhibitors discussed in this thesis: peptidic aldehyde, peptidic boronate and peptidic α-keto ester.

1.2 Serine Proteases and Inhibitors

Serine proteases account for ~30% of all proteases.[25,26] Most proteases in this class have catalytic triads consisting of aspartic acid (Asp), histidine (His) and serine (Ser),[27] Serine proteases play a critical role in the regulation of many biological processes such as inflammation, reproduction and apoptosis, and thus are closely associated with a wide range of diseases including metastatic cancer and thrombosis.[28-29] The key members of this class include: α-chymotrypsin, trypsin, elastases and thrombin.

α-Chymotrypsin is one of the best-characterised proteins, with its structure and substrate specificity resembling other important proteases, e.g. the chymotrypsin-like (β5) subunit of proteasome. It is an ideal model for studying the versatility of an inhibitor design for a system as complex as the proteasome. For these reasons, α-chymotrypsin was used in the mechanistic and crystallographic studies presented in this thesis. α-Chymotrypsin has a single polypeptide chain consists of 245 amino acids, which are arranged into two beta barrels (Figure 1.03).[30] The catalytic triad (Ser195, His57 and Asp102) in the active site facilitates substrate hydrolysis via the following mechanism: Ser195 is activated by His57 to facilitate nucleophilic attack onto the carbonyl of the substrate amide bond. The resulting negatively charged intermediate is stabilised by an oxyanion hole constructed by Ser195 and Gly193. Proton transfer from the oxygen to the side chain amine of His57 releases the amino component of the substrate from the enzyme. The remaining section of the substrate forms a new, negatively charged

intermediate with a water molecule. Electron transfer within this intermediate releases the acid component of the substrate, while restoring the catalytic triad for a new cycle.[31] The above mechanism is illustrated in Scheme 1.01. This mechanism has important implications in inhibitor design and optimisation.

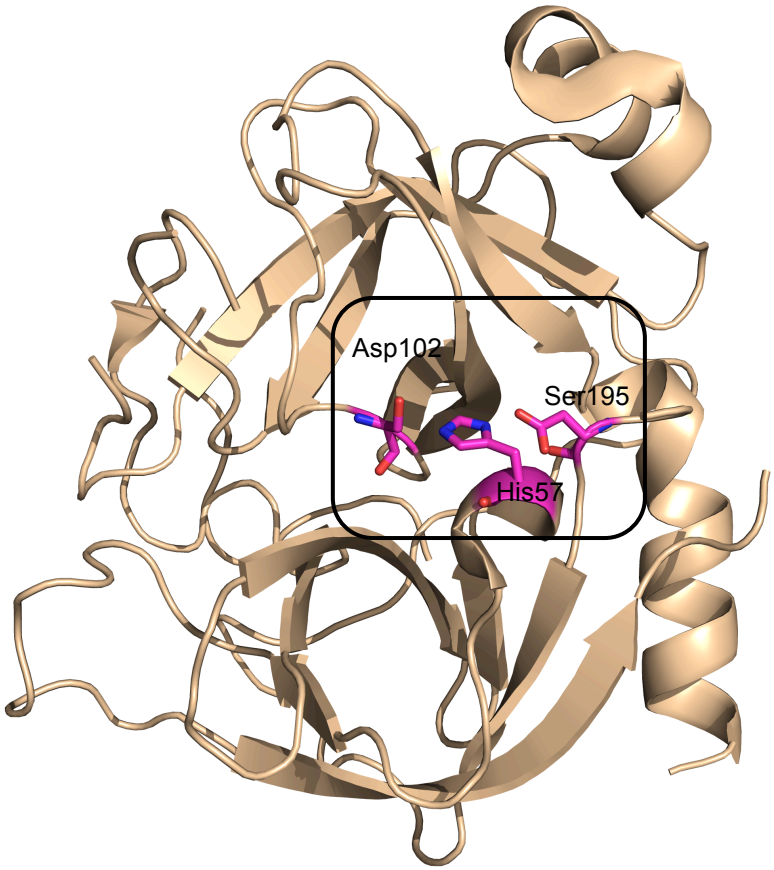

Figure 1.03 Structure of α-chymotrypsin (PDB code: 4Q2K). Catalytic triad is in a stick representation highlighted by a black square: Ser195, Asp102 and His57.[32]

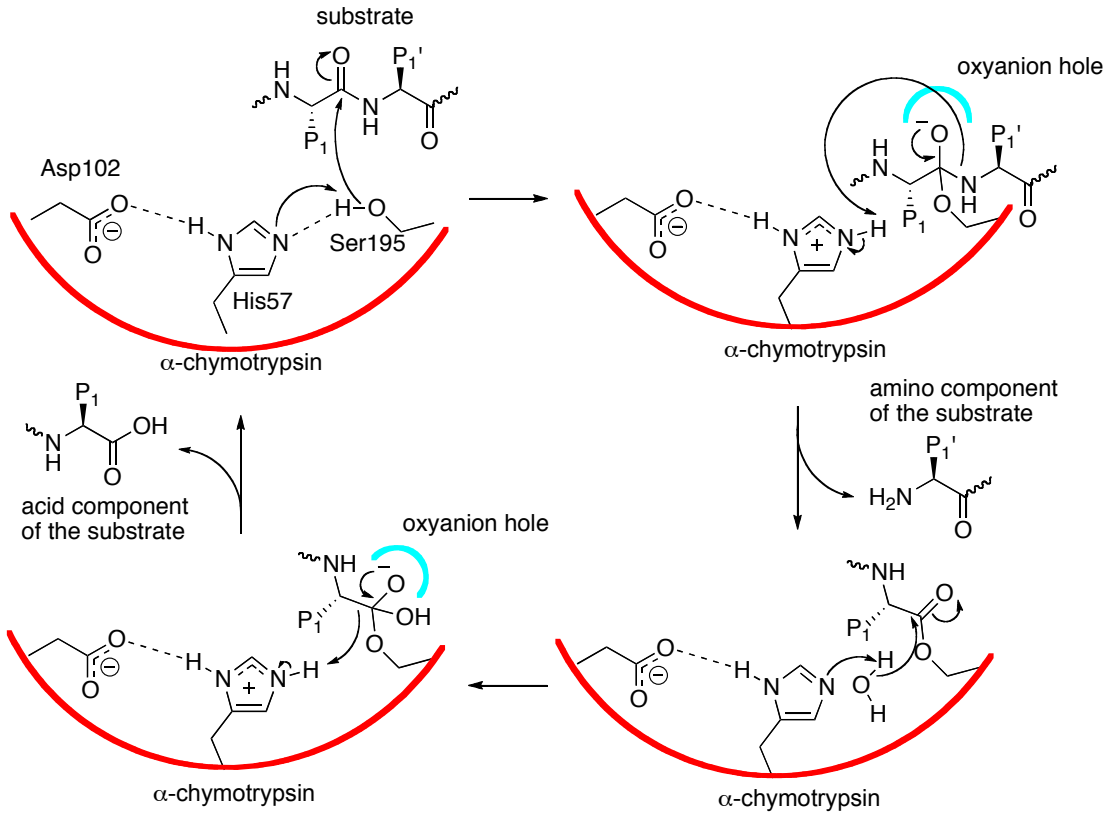

Scheme 1.01 The catalytic mechanism of α-chymotrypsin involving the catalytic triad of Ser195, His57 and Asp102. The enzyme is represented by the red arc and the oxyanion hole is represented by the blue arc.

Most serine proteases have a highly defined S_1 binding site that dictates substrate specificity. The S_1 site of α-chymotrypsin is a deep hydrophobic pocket and thus has a strong preference for large aromatic residues such as phenylalanine (Phe), tyrosine (Tyr) or tryptophan (Trp).[33] Thus the α-chymotrypsin inhibitors discussed in this thesis all bear a phenylalanine residue at P_1 to enhance binding. The S_2-S_3 subsites only have weak preference for hydrophobic residues and are less important in substrate discrimination. Overall, the active site of α-chymotrypsin is somewhat promiscuous so that it can accommodate a wide range of substrates during food digestion.[34] In addition, several hydrogen bonding interactions are crucial

for substrate recognition and binding (Figure 1.04): 1) the carbonyl group of Ser214 and the amine group of P_1; 2) the amine of Trp215 and the carbonyl of P_3; and 3) the carbonyl of Gly216 and the amine of P_3.[35]

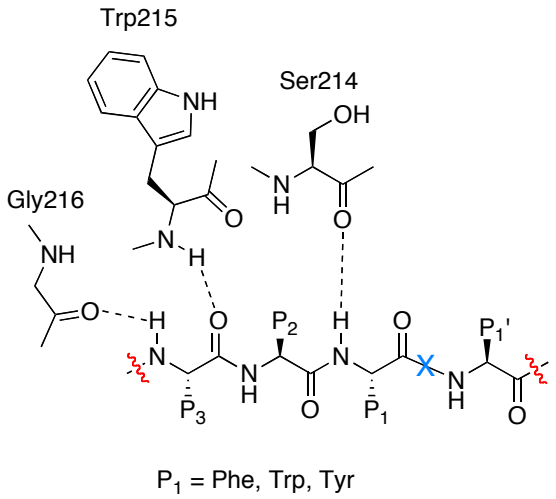

Figure 1.04 Key hydrogen bonding interactions between α-chymotrypsin and its typical substrate. The scissile bond is marked by 'X' (in blue).

Most inhibitors of α-chymotrypsin have warheads that react with Ser195 to form a transition-state mimicking complex with the enzyme.[22] In particular, the highly reactive aldehyde warhead has been extensively explored for the inhibition of α-chymotrypsin due to its ease of synthesis and reversible nature.[36-38] This warhead was reported to form a stable but reversible hemiacetal intermediate upon reaction with serine,[39] which can be detected by various techniques including NMR and X-ray crystallography. The detailed study is discussed in chapter 2. The intermediate formed between aldehyde and Ser is stabilised by the oxyanion hole to further improve activity. Abell et al. reported a number of aldehyde-containing peptide-based inhibitors that are highly active against α-chymotrypsin.[32] For example, compound **2.13** (Figure

1.05), with a macrocycle linking the side-chains of P_2 and P_4 and a pyrrole moiety replacing the P_3-P_4 backbone amide bond, showed K_i of 33 nM against α-chymotrypsin. The macrocycle and the pyrrole moiety constrain the peptide backbone into a β-strand conformation, which is critical to improve binding, as discussed further in chapter 2. These features also reduce the peptide-like character of the inhibitor and thus increase its stability to non-specific proteolytic degradation in an *in vivo* environment. The detailed design of this inhibitor is discussed in section 2.2.1.

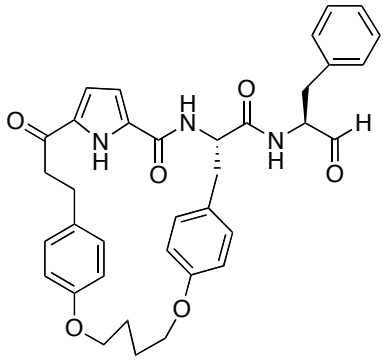

2.13
K_i = 33 nM

Figure 1.05 Compound **2.13**, a peptidic aldehyde inhibitor of α-chymotrypsin.

1.3 Cysteine Proteases and Inhibitors

Cysteine proteases are found in all species ranging from viruses to mammals. In human, cysteine proteases are ubiquitously expressed in all cells.[21] The common catalytic triads and dyads of cysteine proteases include Cys-His-Asn, Cys-His-His, Glu-His-Cys and Cys-His.[40] In mammals, cysteine cathepsins and cytoplasmic calpains are by far the most important members of this class as they play critical roles in immune response, neuronal signalling and cardiac

function. Failure to maintain an adequate activity level for these proteases is closely associated with diseases including cataract, Alzheimer's disease, stroke and rheumatoid arthritis.[41-42] Cysteine cathepsins and cytoplasmic calpains share the common catalytic triad of Cys-His-Asn.[40]

Calpains are popular pharmaceutical targets due to their significant role in the progression of cataract and neurodegenerative diseases. Calpains have shallow active site that can only accommodate structurally flat substrates/inhibitors. The S_1 pocket, which is crucial for inhibitor recognition, favours the binding of leucine, whereas the S_2 and S_3 sites prefer branched hydrophobic amino acids and aromatic residues respectively.[43] Similar to α-chymotrypsin, peptidic aldehydes are also highly active against calpains as the warhead is able to reversibly react with the catalytic residue Cys105.[44] The detailed mechanism of inhibition of a peptidic aldehyde inhibitor is shown in Scheme 1.02: The thiol group of Cys105 was activated by His262 in the catalytic triad to facilitate nucleophilic attack onto the aldehyde carbonyl. This results in the formation of a negatively charged thiolate intermediate, which obtains a proton from His262 to form a stable hemithioacetal intermediate. This prevents other substrates form entering the active site and thus diminishing catalytic activity.

Abell et al. reported a number of macrocyclic peptidic aldehyde calpain inhibitors with much improved activity and stability.[32,45-48] The macrocycle defines the inhibitors into an extended β-strand geometry that enables the inhibitors to bind favourably with the shallow active site of calpains. The most

potent analogues, **CAT811** and compound **2.12** (Figure 1.06), is at the forefront for cataract treatment.[48]

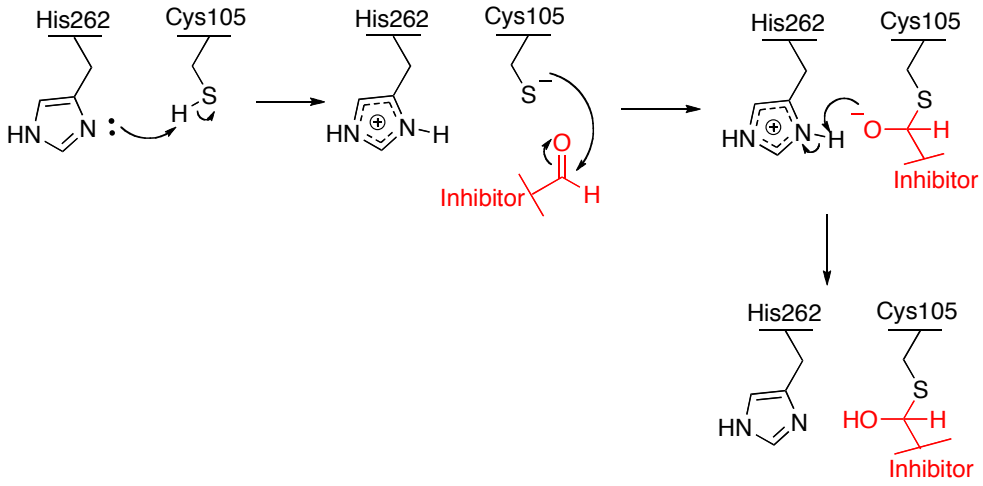

Scheme 1.02 Mechanism of inhibition of calpain by a peptidic aldehyde.

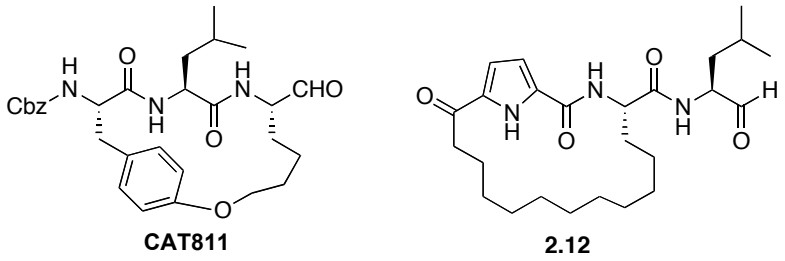

Figure 1.06 Structures of the most potent calpain inhibitors developed by Abell et al., compound **2.12**[32] and **CAT811**[48].

1.4 Threonine Proteases and Inhibitors

Threonine proteases contain a threonine residue (Thr1) at the *N*-terminus to facilitate proteolysis.[49] Unlike serine and cysteine proteases, the catalytic activity of threonine proteases largely relies on a water molecule and the

enzyme's *N*-terminal amine.[50] The 26S proteasome is the most important member of this class.

The 26S proteasome is an ATP-dependent protease complex that is expressed ubiquitously in all eukaryotic cells.[51] This 2000 kDa complex is commonly composed of two major components: a 20S catalytic complex and a 19S regulatory particle containing a lid and a base (Figure 1.07a).[52] The 20S complex is found in both prokaryotes and eukaryotes with different subunit compositions.[53] The eukaryotic 20S catalytic complex is 750 kDa in size and organized into a cylindrical arrangement.[54] It is formed by two outer α-rings and two inner β-rings (Figure 1.07b). The α-ring consists of 7 structurally similar α-subunits. It regulates the entry and release of the substrates through interactions with the 19S particles. The β-rings form a proteolytic chamber, in which the protein substrates are degraded into smaller fragments via amide bond hydrolysis.[55] Each β-ring is composed of 7 different subunits that are all classified as threonine proteases. Three of the β subunits, β1, β2 and β5, have well-characterised substrate specificity. The β1 subunit, also known as the caspase-like (C-L) subunit, has selectivity for substrates with acidic residues, whereas the β2 subunit cleaves peptide bonds at the *C*-terminus of basic amino acids, thus it is called the trypsin-like (T-L) subunit. The β5 or the chymotrypsin-like (CT-L) subunit prefers to bind substrates consist of hydrophobic amino acids.[54,56]

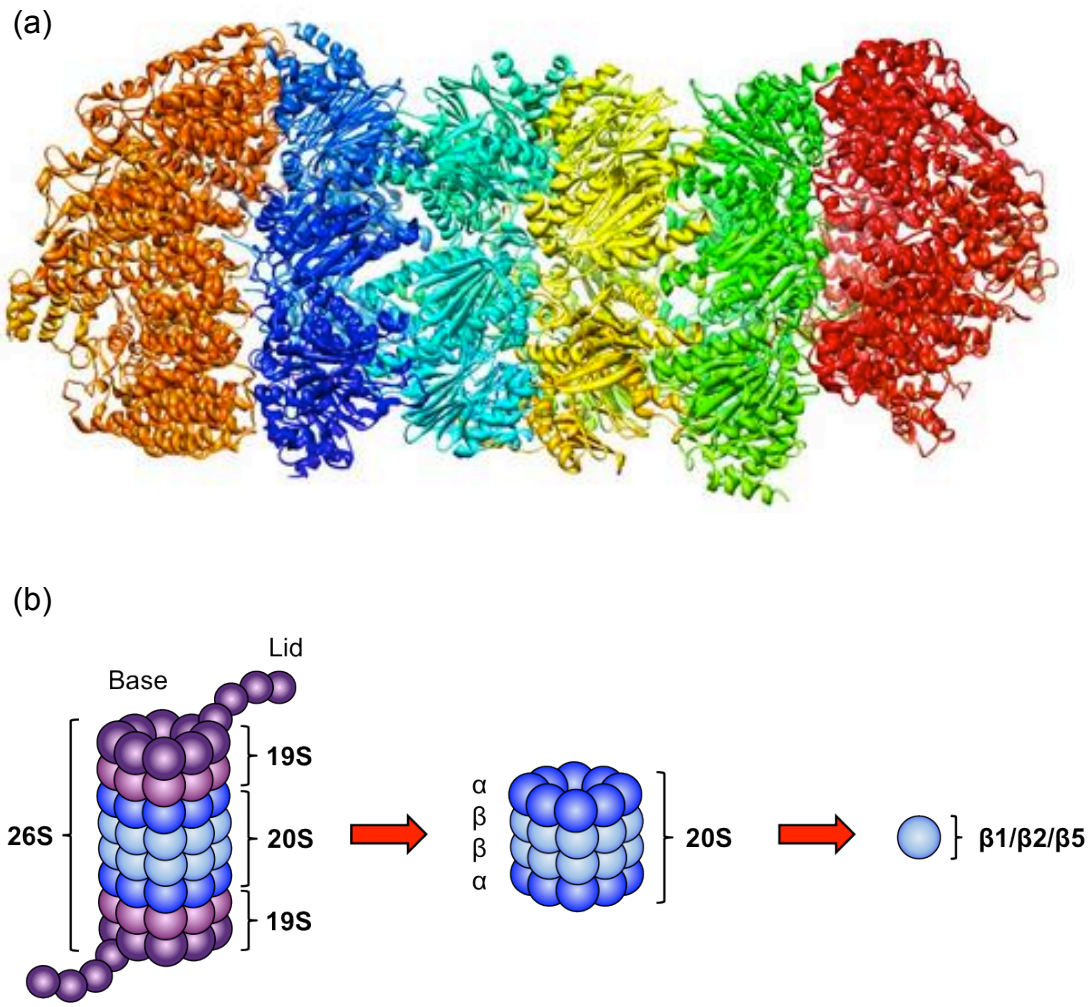

Figure 1.07 (a) An X-ray crystallographic structure of the 26S proteasome isolated from *S. cerevisiae* (PDB code: 4V7O).[57] The 19S particles are coloured red and orange. The α-rings are coloured blue and green. The β-rings are coloured aqua and yellow; (b) a schematic representation of the 26S proteasome, which contains two 19S regulatory complexes (purple) and one 20S catalytic complex (blue). The 20S complex consists of two α-rings (dark blue) and two β-rings (light blue). Each ring contains seven subunits named α1-α7 or β1-β7 respectively.

The proteolytic mechanism of the proteasome is demonstrated in Scheme 1.03:[58] the hydroxyl group on the *N*-terminal threonine is activated by a

nearby lysine residue to perform nucleophilic attack onto the carbonyl group of the P_1-P_1' amide bond of the substrate, consequently forming a tetrahedral intermediate. Proton transfer from the negatively charged oxygen to the positively charged amine releases the amino component of the substrate. Lastly, a water molecule attacks the carbonyl group and cleaves the acidic component of the substrate from the enzyme. The catalytic threonine is thus restored for another proteolytic cycle.

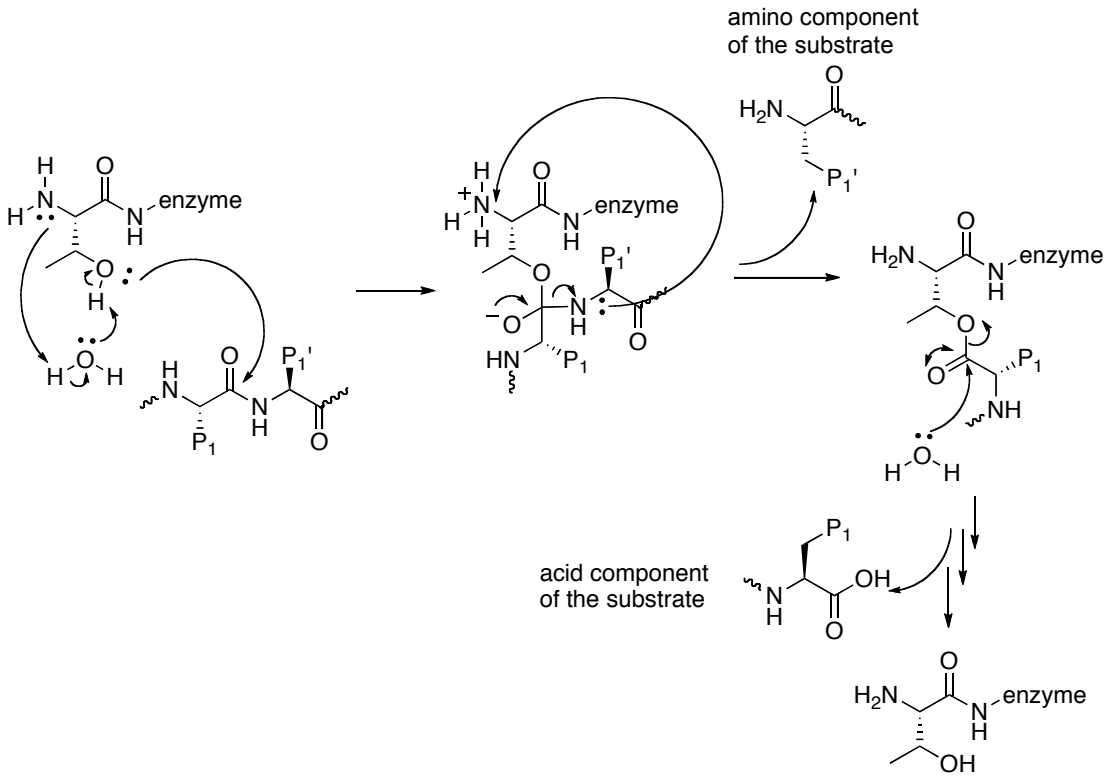

Scheme 1.03 The catalytic mechanism of a typical threonine protease.

The 26S proteasome facilitates approximately 80% of all intracellular protein degradation. Thus it is involved in a wide range of biological processes, such as immune response, transcription, post-translational modification, DNA repair, apoptosis and cell cycle progression.[59] In addition, the proteasome is

highly important for maintaining intracellular protein homeostasis.[60] Therefore it is closely associated with a vast number of disease conditions including cardiac dysfunction, cataract, neurodegenerative diseases, autoimmune diseases and most importantly, cancer (see Table 1.01).[61] The role of the proteasome in cancer will be discussed in detail in chapter 3. The inhibition of proteasome activity to reduce intracellular protein breakdown is central to the treatment of these pathological conditions.

Table 1.01 Proteasome-related diseases and the protein substrates involved.

Disease	Symptoms	Proteasome affected
Cardiac:		
Pressure overload	Apoptosis	26S proteasome
Inclusion body myositis	Inclusion bodies	26S and immuno-proteasome
Cataract	Protein aggregation	20S proteasome
Neurodegenerative:		
Alzheimer's	Plaque formation	20S/26S proteasome
Huntington's	Lewy body formation, neuronal loss	20S/26S proteasome
Parkinson's	poly-glutamine inclusions, neuronal dysfunction	20S/26S, immuno-proteasome
Autoimmune:		
Sjogren's syndrome	Tissue destruction	Subunit β1i

Cancer:		
Multiple myeloma	Suppression of apoptosis, promotion of proliferation	20S/26S, immuno-proteasome
Leukemia	Suppression of apoptosis, promotion of proliferation	20S/26S, immuno-proteasome

Empirical data shows that inactivation of β5 subunit significantly retards cell growth, whereas inactivation of the other two subunits doesn't result in significant change in cellular functions.[62] Therefore, β5 subunit is the primary target for the development of proteasome inhibitors. In contrast to other proteases, the proteasome has a unique catalytic feature: its catalytic threonine is the first amino acid of each catalytic subunit and facilitates proteolysis through coordination with the *N*-terminal amine and a nearby water molecule (Scheme 1.03). Inhibitors that utilise this feature are likely to achieve higher selectivity for the proteasome over other intracellular proteases, e.g. calfilzomib (Figure 1.08c), which potentially reduces adverse effects and toxicity when used in disease treatment.[63]

As for cysteine and serine protease inhibitors, synthetic proteasome inhibitors generally bear a peptidomimetic backbone that defines specificity and a warhead to react with Thr1.[64] Based on the type of warhead, these inhibitors can be divided into five classes: boronates,[65-66] epoxyketones,[67-68] aldehydes,[69-70] semicarbazones[71-72] and vinyl-sulfones.[73-74] The first three are discussed in detail in this section (Figure 1.08).

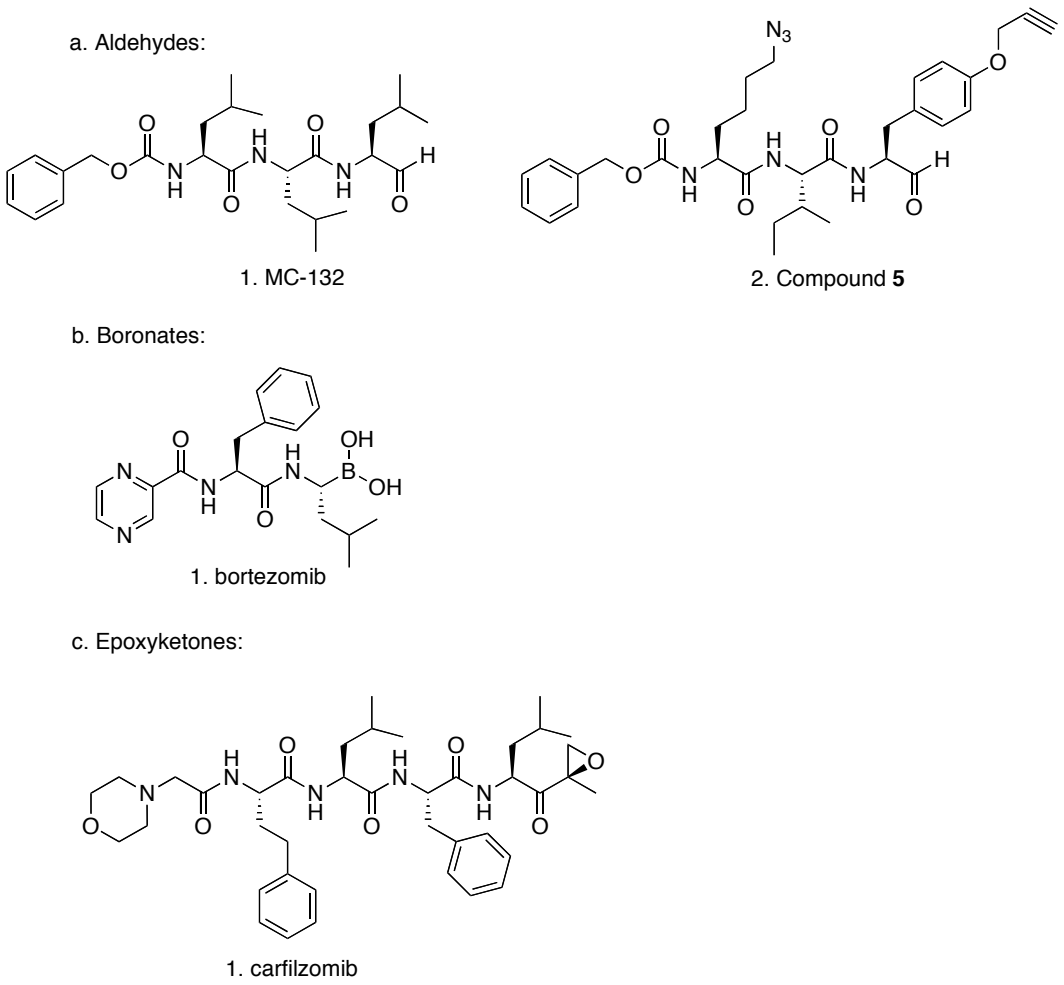

Figure 1.08 Examples of the three categories of common proteasome inhibitors: a. peptidic aldehydes MG132[75] and compound **5**[69]; b. peptidic boronates bortezomib[66] and MLN2238[76]; c. peptidic epoxyketones carfilzomib[67] and epoxomicin[68].

Peptidic aldehydes (Figure 1.08a) were the first inhibitors developed for the proteasome and are still widely used as a research tool owing to the high *in vitro* activity.[70] The terminal aldehyde reacts with Thr1 to form a highly stable hemiacetal adducts, which is rapidly reversible upon hydrolysis.[77] Although peptidic aldehydes preferentially inhibit the chymotrypsin-like active site in the proteasome, many are also found to weakly inhibit the trypsin-like and

caspase-like subunits.[78] One classic example of these inhibitors is MG-132 (Figure 1.08, a1). This tri-leucinal inhibitor with an *N*-terminal Cbz group was reported by Tsubuki et al. to inhibit the proteasome with high potency (IC_{50} = 4 nM),[79] thus it has been widely used as a benchmark compound for newly developed peptidic aldehyde inhibitors of the proteasome.[69] MG-132 has inspired the design of many peptidic aldehyde inhibitors with higher potency and selectivity. For example, Abell et al.[69] reported a tripeptidyl aldehyde (compound **5**, Figure 1.08) with an azide at P_3 and a propargyloxyphenyl group at P_1. This modification gave the inhibitor a higher degree of selectivity for β5 over the other subunits.

Proteasome inhibitors with aldehyde warhead have been used mainly as research tools instead of therapeutic candidates due to several major drawbacks: Peptidic aldehydes also inhibit other proteases. For example, MG-132 also demonstrates moderate activity against calpains and cathepsins.[80] The low selectivity has led to much controversy on whether the cytotoxicity effect observed for the inhibitor-treated cancer cells are resulted from proteasome inhibition or inhibition of other proteases.[64] The lack of specificity also potentially results in severe side effects if these inhibitors are used as drugs. In addition, aldehydes are rapidly oxidized *in vivo* before they can bind and function as proteasome inhibitors.[81]

In comparison to peptidic aldehydes, peptidic boronates (Figure 1.08b) exhibit much higher potency and selectivity for the proteasome.[65] The *C*-terminal boron accepts electrons from active site threonine alcohol to form a

tetrahedral adduct, which are further stabilized by a hydrogen bond between the *N*-terminal amino group of the threonine and one of the hydroxyl groups of the boronic acid (Scheme 1.04).[82] Although boronates were originally developed as serine protease inhibitors, these compounds were found to be much more active against the proteasome due to the unique hydrogen bonding interaction.[65]

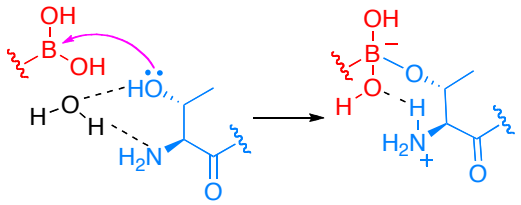

Scheme 1.04 Mechanism of the inhibition of the proteasome by a peptidic boronate. The inhibitor is in red. The N-terminal threonine is coloured in blue.

A well-known example of peptidic boronates, bortezomib (Figure 1.08, b1), was developed and FDA-approved for the treatment of multiple myeloma.[83] It consists of a simple phenylalanine-leucine dipeptide with the *N*-terminal amine protected by a pyrazine group and a *C*-terminal boronic acid. Bortezomib shows excellent *in vitro* activity against the purified 20S proteasome (K_i = 0.62 nM), which is 2500-fold higher than the corresponding aldehyde.[65] Bortezomib was initially claimed to have extremely high selectivity for the proteasome over common serine proteases. However, it was later revealed that bortezomib inhibits an ATP-dependent serine protease in mitochondria named HtrA2.[84] In the treatment of myeloma, this causes approximately one third of the patients to develop peripheral neuropathy, which is extremely painful and potentially lethal.[85] Bortezomib's inhibition is

considered as irreversible due to the slow dissociation rate.[86] This leads to limited distributions of bortezomib into solid tumours, as it cannot be released from the red blood cells once it binds to the proteasome.[87]

Peptidic epoxyketones are found to have exquisitely specific inhibition against the proteasome, which can be explained by its unique mechanism of inhibition: the catalytic threonine hydroxyl first attacks the carbonyl group of the inhibitor. Then, the N-terminal amine of the threonine opens up the epoxide and forms a highly stable, irreversible morpholino adduct (Scheme 1.05).[68] Catalytic residues of serine and cysteine proteases do not have the adequate amine to form such adduct. A representative member of this class, carfilzomib (Figure 1.08c), showed great promises as a therapeutic agent due to its high selectivity for the β5 subunit that potentially minimizes adverse effects.

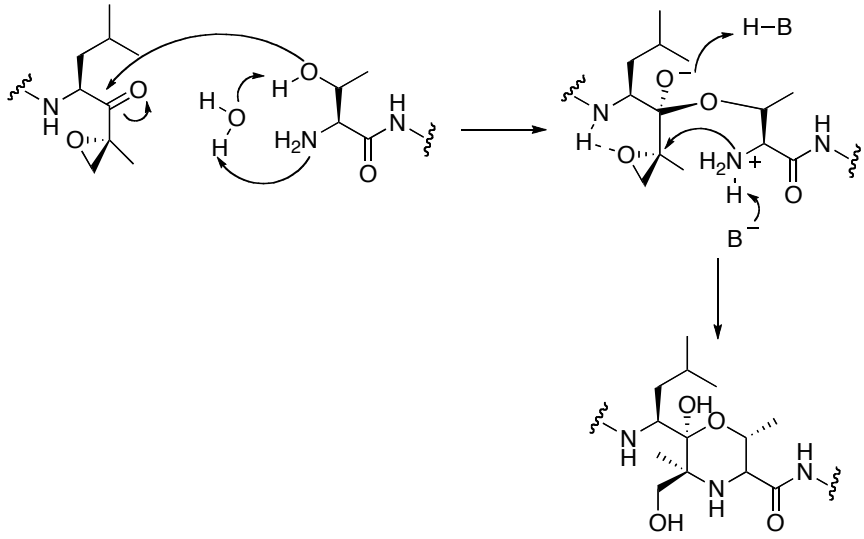

Scheme 1.05 The mechanism of inhibition of a peptidic epoxyketone inhibitor.

1.5 Overview of Thesis

The study of protein mechanism and function is central to the development of biosensing tools and therapeutics for the treatment of disease. Understanding the mechanism of inhibition of a current inhibitor allows the development of new inhibitors with improved therapeutic potential and reusable biosensing tools with higher sensitivity and versatility.

This thesis describes optimisation of the synthesis of macrocyclic protease inhibitors **2.12** and **2.13** targeting cysteine proteases and α-chymotrypsin respectively. An analogue of **2.13** containing a ^{13}C label in the *C*-terminal aldehyde was prepared using the optimised conditions. ^{13}C NMR spectroscopy of this analogue confirmed the formation of a hemiacetal intermediate upon binding with α-chymotrypsin. X-ray crystallography of the α-chymotrypsin-**2.13** complex revealed the conformation of the bound inhibitor key non-covalent interactions between **2.13** and α-chymotrypsin. In addition, the thesis presents the development and characterisation of new acyclic proteasome inhibitors **3.05**-**3.08** containing a *C*-terminal boronate and a peptidomimetic backbone. The inhibitory activity and cancer cell cytotoxicity of these inhibitors were investigated in collaboration with Ms. Alaknanda Alaknanda and Prof. David Callen[1]. Finally, a new class of spiropyran-based photoswitchable inhibitor of α-chymotrypsin was developed to achieve photocontrol of enzyme activity both in solution and on the surface of a microstructured optical fibre (MOF). The activity of these inhibitors against α-

[1] Cancer Therapeutics Laboratory, Hanson Institute, The University of Adelaide.

chymotrypsin is investigated *in vitro*. The photoswitching of a particularly stable analogue with a *C*-terminal Weinreb amide is demonstrated both in solution and on surface of a MOF core. The binding affinity of its two photoisomers, spiropyran (SP) and merocyanine (MC), to α-chymotrypsin is investigated both in solution by *in vitro* assays and on surface by fluorescence spectroscopy.

1.6 References

(1) Turk, B. *Nat. Rev. Drug Discov.* **2006**, *5*, 785.

(2) Hooper, N. M. *Biochemical Education* **1990**, *18*, 55.

(3) Goll, D. E.; Thompson, V. F.; Li, H.; Wei, W.; Cong, J. *Physiol. Rev.* **2003**, *83*, 731.

(4) Wells, J. M.; Strickland, S. *Development* **1994**, *120*, 3639.

(5) Soh, U. J. K.; Dores, M. R.; Chen, B.; Trejo, J. *British Journal of Pharmacology* **2010**, *160*, 191.

(6) Fiandalo, M.; Schwarze, S.; Kyprianou, N. *Apoptosis* **2013**, *18*, 766.

(7) Solomon, M.; Belenghi, B.; Delledonne, M.; Menachem, E.; Levine, A. *The Plant Cell* **1999**, *11*, 431.

(8) Thornberry, N. A.; Lazebnik, Y. *Science* **1998**, *281*, 1312.

(9) Flaumenhaft, R.; Rifkin, D. B. *Current Opinion in Cell Biology* **1991**, *3*, 817.

(10) Getz, G. S. *The American Journal of Pathology* **2012**, *181*, 388.

(11) Lutgens, S. P. M.; Cleutjens, K. B. J. M.; Daemen, M. J. A. P.; Heeneman, S. *The FASEB Journal* **2007**, *21*, 3029.

(12) Iqbal, M.; Messina McLaughlin, P. A.; Dunn, D.; Mallya, S.; Husten, J.; Ator, M. A.; Chatterjee, S. *Biorg. Med. Chem.* **2012**, *20*, 2362.

(13) Biswas, S.; Harris, F.; Dennison, S.; Singh, J.; Phoenix, D. A. *Trends Mol. Med.* **2004**, *10*, 78.

(14) Rastogi, N.; Mishra, D. P. *Cell Division* **2012**, *7*, 26.

(15) Fukiage, C.; Azuma, M.; Nakamura, Y.; Tamada, Y.; Nakamura, M.; Shearer, T. R. *Biochim. Biophys. Acta, Mol. Basis Dis.* **1997**, *1361*, 304.

(16) Katunuma, N. *Proc. Jpn. Acad., Ser. B* **2011**, *87*, 29.

(17) López-Otín, C.; Bond, J. S. *J. Biol. Chem.* **2008**, *283*, 30433.

(18) Tyndall, J. D. A.; Nall, T.; Fairlie, D. P. *Chem. Rev. (Washington, DC, U. S.)* **2005**, *105*, 973.

(19) Schechter, I.; Berger, A. *Biochem. Biophys. Res. Commun.* **1967**, *27*, 157.

(20) Krantz, A. *Bioorg. Med. Chem. Lett.* **1992**, *2*, 1327.

(21) Otto, H.-H.; Schirmeister, T. *Chem. Rev.* **1997**, *97*, 133.

(22) Abbenante, G.; Fairlie, D. P. *Med. Chem.* **2005**, *1*, 71.

(23) Sanderson, P. E., *Med. Res. Rev.* **1999**, *19*, 179

(24) Leung, D.; Abbenante, G.; Fairlie, D. P. *J. Med. Chem.* **2000**, *43*, 305.

(25) Yousef, G. M.; Kopolovic, A. D.; Elliott, M. B.; Diamandis, E. P. *Biochem. Biophys. Res. Commun.* **2003**, *305*, 28.

(26) Chai, J.; Zhong, G. In *Handbook of Proteolytic Enzymes*; Salvesen, N. D. R., Ed.; Academic Press: 2013, p 3616.

(27) Hedstrom, L. *Chem. Rev.* **2002**, *102*, 4501.

(28) Heutinck, K. M.; ten Berge, I. J. M.; Hack, C. E.; Hamann, J.; Rowshani, A. T. *Mol. Immunol.* **2010**, *47*, 1943.

(29) Antalis, T. M.; Bugge, T.; Wu, Q. *Progress in Molecular Biology and Translational Science* **2011**, *99*, 1.

(30) D'Souza, V. T.; Lu, X. L.; Ginger, R. D.; Bender, M. L. *Proceedings of the National Academy of Sciences* **1987**, *84*, 673.

(31) Whiting, A. K.; Peticolas, W. L. *Biochemistry* **1994**, *33*, 552.

(32) Chua, K. C. H.; Pietsch, M.; Zhang, X.; Hautmann, S.; Chan, H. Y.; Bruning, J. B.; Gütschow, M.; Abell, A. D. *Angew. Chem. Int. Ed.* **2014**, *53*, 7828.

(33) Czapinska, H.; Otlewski, J. *Eur. J. Biochem.* **1999**, *260*, 571.

(34) Schellenberger, V.; Braune, K.; Hofmann, H. J.; Jakubke, H. D. *European journal of biochemistry / FEBS* **1991**, *199*, 623.

(35) Perona, J. J.; Craik, C. S. *J. Biol. Chem.* **1997**, *272*, 29987.

(36) Ito, A.; Tokawa, K.; Shimizu, B. *Biochem. Biophys. Res. Commun.* **1972**, *49*, 343.

(37) Stein, R. L.; Strimpler, A. M. *Biochemistry* **1987**, *26*, 2611.

(38) Cleary, J. A.; Doherty, W.; Evans, P.; Malthouse, J. P. G. *Biochim. Biophys. Act. - Proteins and Proteomics* **2014**, *1844*, 1119.

(39) Kuramochi, H.; Nakata, H.; Ishij, S.-i. *J. Biochem.* **1979**, *86*, 1403.

(40) Vernet, T.; Tessier, D. C.; Chatellier, J.; Plouffe, C.; Lee, T. S.; Thomas, D. Y.; Storer, A. C.; Ménard, R. *J. Biol. Chem.* **1995**, *270*, 16645.

(41) Reiser, J.; Adair, B.; Reinheckel, T. *The Journal of Clinical Investigation* **2010**, *120*, 3421.

(42) Zatz, M.; Starling, A. *New England Journal of Medicine* **2005**, *352*, 2413.

(43) Cuerrier, D.; Moldoveanu, T.; Davies, P. L. *J. Biol. Chem.* **2005**, *280*, 40632.

(44) Barrett, D. *Drug Discovery Today* **2002**, *7*, 1124.

(45) Payne, R. J.; Brown, K. M.; Coxon, J. M.; Morton, J. D.; Lee, H. Y.-Y.; Abell, A. D. *Aust. J. Chem.* **2004**, *57*, 877.

(46) Morton, J. D.; Lee, H. Y. Y.; McDermott, J. D.; Robertson, L. J. G.; Bickerstaffe, R.; Jones, M. A.; Coxon, J. M.; Abell, A. D. *Investigative Ophthalmology & Visual Science* **2013**, *54*, 389.

(47) Pehere, A. D.; Abell, A. D. *Org. Lett.* **2012**, *14*, 1330.

(48) Abell, A. D.; Jones, M. A.; Coxon, J. M.; Morton, J. D.; Aitken, S. G.; McNabb, S. B.; Lee, H. Y. Y.; Mehrtens, J. M.; Alexander, N. A.; Stuart, B. G.; Neffe, A. T.; Bickerstaffe, R. *Angew. Chem., Int. Ed.* **2009**, *48*, 1455.

(49) Polgár, L. In *Handbook of Proteolytic Enzymes*; Salvesen, N. D. R., Ed.; Academic Press: 2013, p 2524.

(50) Wlodawer, A. *Structure* **1995**, *3*, 417.

(51) Naujokat, C.; Hoffmann, S. *Lab. Invest.* **2002**, *82*, 965.

(52) Bochtler, M.; Ditzel, L.; Groll, M.; Hartmann, C.; Huber, R. *Annu. Rev. Biophys. Biomol. Struct.* **1999**, *28*, 295.

(53) Mogk, A.; Schmidt, R.; Bukau, B. *Trends in Cell Biology* **2007**, *17*, 165.

(54) Murata, S.; Yashiroda, H.; Tanaka, K. *Nat. Rev. Mol. Cell. Biol.* **2009**, *10*, 104.

(55) Peters, J. M.; Cejka, Z.; Harris, J. R.; Kleinschmidt, J. A.; Baumeister, W. *J. Mol. Biol.* **1993**, *234*, 932.

(56) Kisselev, A. F.; Akopian, T. N.; Castillo, V.; Goldberg, A. L. *Molecular cell* **1999**, *4*, 395.

(57) Sadre-Bazzaz, K.; Whitby, F. G.; Robinson, H.; Formosa, T.; Hill, C. P. *Molecular Cell*, **2010**, *37*, 728

(58) Marques, A. J.; Palanimurugan, R.; Matias, A. C.; Ramos, P. C.; Dohmen, R. J. *Chem. Rev. (Washington, DC, U. S.)* **2009**, *109*, 1509.

(59) Lecker, S. H.; Goldberg, A. L.; Mitch, W. E. *Journal of the American Society of Nephrology* **2006**, *17*, 1807.

(60) Chondrogianni, N.; Gonos, E. In *Protein Metabolism and Homeostasis in Aging*; Tavernarakis, N., Ed.; Springer US: 2010; Vol. 694, p 38.

(61) Dahlmann, B. *BMC Biochemistry* **2007**, *8*, S3.

(62) Heinemeyer, W.; Fischer, M.; Krimmer, T.; Stachon, U.; Wolf, D. H. *J. Biol. Chem.* **1997**, *272*, 25200.

(63) Molineaux, S. M. *Clinical Cancer Research* **2012**, *18*, 15.

(64) Kisselev, A. F.; van, d. L. W. A.; Overkleeft, H. S. *Chem. Biol. (Oxford, U. K.)* **2012**, *19*, 99.

(65) Adams, J.; Behnke, M.; Chen, S.; Cruickshank, A. A.; Dick, L. R.; Grenier, L.; Klunder, J. M.; Ma, Y. T.; Plamondon, L.; Stein, R. L. *Bioorg. Med. Chem. Lett.* **1998**, *8*, 333.

(66) Chen, D.; Frezza M.; Schmitt, S.; Kanwar, J.; Dou, Q. P., *Current Cancer Drug Targets* **2011**, *11*, 239.

(67) Vij, R.; Wang, L.; Orlowski, R. Z.; Stewart, A. K.; Jagannath, S.; Lonial, S.; Trudel, S.; Jakubowiak, A. J.; Belch, A.; Alsina, M.; Bahlis, N. J.; Le, M. H.; Cruickshank, S.; Bennett, M. K.; Molineaux, S.; Kauffman, M.; Siegel, D., *ASH Annual Meeting Abstracts* **2009**, *114*, 430.

(68) Groll, M.; Kim, K. B.; Kairies, N.; Huber, R.; Crews, C. M. *J. Am. Chem. Soc.* **2000**, *122*, 1237.

(69) Neilsen, P. M.; Pehere, A. D.; Pishas, K. I.; Callen, D. F.; Abell, A. D. *ACS Chemical Biology* **2012**, *8*, 353.

(70) Martin, M. E.; Kim, J. S.; Rice, K. G. *Mol. Ther.* **2006**, *13*, S65.

(71) Leban, J.; Blisse, M.; Krauss, B.; Rath, S.; Baumgartner, R.; Seifert, M. H. J. *Bioorg. Med. Chem.* **2008**, *16*, 4579.

(72) Baumann, P.; Müller, K.; Mandl-Weber, S.; Leban, J.; Doblhofer, R.; Ammendola, A.; Baumgartner, R.; Oduncu, F.; Schmidmaier, R. *British Journal of Haematology* **2009**, *144*, 875.

(73) Overkleeft, H. S.; Bos, P. R.; Hekking, B. G.; Gordon, E. J.; Ploegh, H. L.; Kessler, B. M. *Tetrahedron Lett.* **2000**, *41*, 6005.

(74) Bogyo, M.; McMaster, J. S.; Gaczynska, M.; Tortorella, D.; Goldberg, A. L.; Ploegh, H. *Proceedings of the National Academy of Sciences* **1997**, *94*, 6629.

(75) Yuan, B. Z.; Chapman, J. A.; Reynolds, S. H. *Translational Oncology* **2008**, *1*, 129.

(76) Gu, J. J.; Hernandez-Ilizaliturri F.; Mavis, C.; Czuczman, N. M.; Deeb, G.; Gibbs, J.; Skitzki, J. J.; Patil, R.; Czuczman, M. S., *Anti-cancer Drugs* **2013**, *24*, 1030.

(77) Genin, E.; Roeboud-Ravaux, M.; Vidal, J. *Curr. Top. Med. Chem.* **2010**, *10*, 232.

(78) Gaczynska, M.; Osmulski, P. In *Ubiquitin-Proteasome Protocols*; Patterson, C., Cyr, D., Eds.; Humana Press: 2005; Vol. 301, p 1.

(79) Tsubuki, S.; Kawasaki, H.; Saito, Y.; Miyashita, N.; Inomata, M.; Kawashima, S. *Biochem. Biophys. Res. Commun.* **1993**, *196*, 1195.

(80) Rivett, A. J.; Gardner, R. C. *J. Pept. Sci.* **2000**, *6*, 478.

(81) Lindsten, K.; Menendez-Benito, V.; Masucci, M. G.; Dantuma, N. P. *Nat. Biotech.* **2003**, *21*, 897.

(82) Groll, M.; Berkers, C. R.; Ploegh, H. L.; Ovaa, H. *Structure* **2006**, *14*, 451.

(83) Field-Smith, A., Morgan, J. G., Davies, F. E. *Therapeutics and Clinical Risk Management* **2006**, *2*, 271.

(84) Arastu-Kapur, S.; Anderl, J. L.; Kraus, M.; Parlati, F.; Shenk, K. D.; Lee, S. J.; Muchamuel, T.; Bennett, M. K.; Driessen, C.; Ball, A. J.; Kirk, C. J. *Clinical Cancer Research* **2011**, *17*, 2734.

(85) Richardson, P. G.; Sonneveld, P.; Schuster, M. W.; Irwin, D.; Stadtmauer, E. A.; Facon, T.; Harousseau, J. L.; Ben-Yehuda, D.; Lonial, S.; Goldschmidt, H.; Reece, D.; San-Miguel, J. F.; Bladé, J.; Boccadoro, M.; Cavenagh, J.; Dalton, W. S.; Boral, A. L.; Esseltine, D. L.; Porter, J. B.; Schenkein, D.; Anderson, K. C. *New England Journal of Medicine* **2005**, *352*, 2487.

(86) Tsu, C. A.; Blank, J.; Garcia, K.; Liu, J.; Bruzzese, F.; Lee, E.; Kao, Y.; Bannerman, B.; Fitzgerald, M.; Fleming, P.; Ciavarri, J.; Hales, P.; Yu, J.; Yang, Y.; Berger, A.; Sintchak, M.; Kupperman, E.; Manfredi, M.; Dick, L. *Molecular Cancer Therapeutics* **2011**, *10*, C99.

(87) Wheat, L. M. C.; Kohlhaas, S. L.; Monbaliu, J.; De Coster, R.; Majid, A.; Walewska, R. J.; Dyer, M. J. S. *Leukemia* **2006**, *20*, 1646.

Chapter 2

Characterising the Mechanism of Inhibition of Macrocyclic Protease Inhibitors

2.1 Introduction

2.1.1 Importance of β-Strand Conformation

A study of more than 1500 X-ray crystal structures of proteases in the Protein Data Bank shows that substrates almost universally bind with their backbone in an extended β-strand conformation.[1] This conformation has ϕ, ψ and ω backbone torsion angles of 120°, 120° and 180°, respectively (Figure 2.01a). A β-strand is represented as an extended or "saw-tooth" arrangement of amino acids with the amide bonds being nearly co-planar. This results in the amino acid side chains alternating above and below the plane of the peptide backbone (Figure 2.01b).[2] The planar β-strand conformation allows the substrate to bind with the shallow active site of a protease,[3] while maximising intermolecular hydrogen bonding interactions between substrates and the enzyme. This, in turn, allows rapid binding of the substrates to protease active sites and facile dissociation of the cleaved peptides, which are required for efficient turnover of cellular proteins.[4] In addition, the β-strand conformation efficiently exposes the amino acid side chain residues to the active sites of proteases, where well-defined binding pockets are able to selectively recognize these residues to allow specific binding. Therefore, the extended β-strand conformation is crucial to all protease substrates and inhibitors.[5] For example, an overlay of the backbones of 12 natural substrates bound to HIV-1 protease (Figure 2.02) shows all substrates binding in a β-strand conformation.[1] The importance of the β-strand conformation for the binding of

protease substrates also has profound implications in protease inhibitor design.

(a)

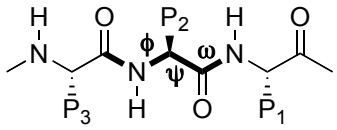

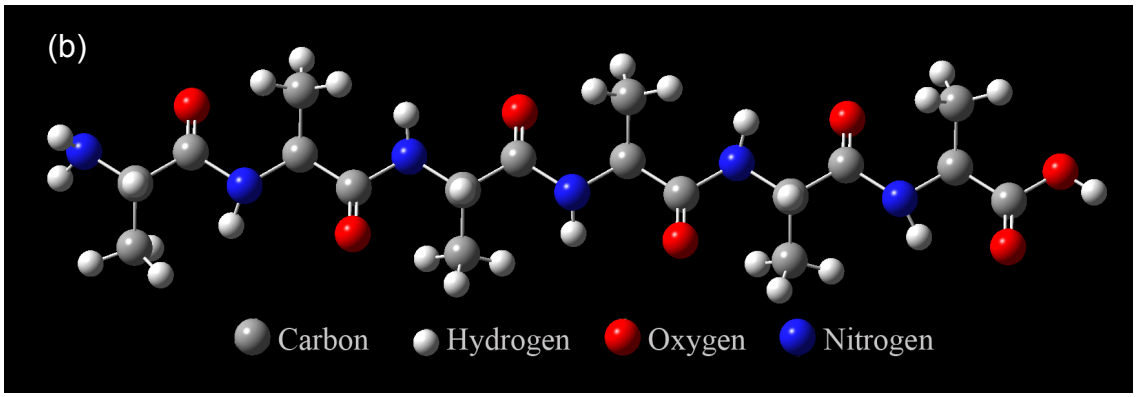

Figure 2.01 (a) Torsion angles, phi (ϕ), psi (ψ) and omega (ω); and (b) "saw-tooth" arrangement for amino acids for a peptide β-strand.

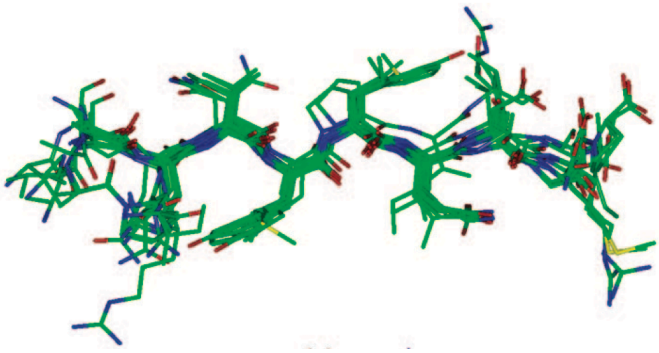

Figure 2.02 An overlay of the X-ray crystal structures of 12 natural substrates bound to HIV-1 protease.[1]

Most small-molecule protease inhibitors are designed to mimic the natural substrates and thus are commonly based on short peptides or peptidomimetic compounds.[6] It is well known that short peptides adopt random conformations, such that these peptides are entropically disfavoured to bind with proteases.[7] Therefore, preorganising the inhibitor backbone into a well-defined β-strand geometry with the inclusion of an appropriate macrocycle are expected to significantly reduce the entropic barrier for binding and the formation of inhibitor-enzyme complex.[8]

2.1.2 Stabilization of the Inhibitor Backbone into an Extended β-strand Conformation

There are multiple methods to stabilize the β-strand conformation of a peptidomimetic inhibitor. Firstly, it can be achieved by the substitution of amide bonds with heteroaromatic rings, such as pyrroles[9-10] and triazoles[11-12]. The bond length and the planar nature of the heterocycles mimic the backbone amide bond of a peptidomimetic inhibitor.[13] In addition, these heterocycles are more rigid than an amide bond and as a consequence, constrain the peptide backbone into a particular conformation, such as an extended β-strand. For example, Angelo et al.[14] demonstrated that a tetrapeptide could be constrained in a conformation closely mimicking the β-strand by replacing all the backbone amide bonds with 1,2,3-triazoles, as shown in Figure 2.03.

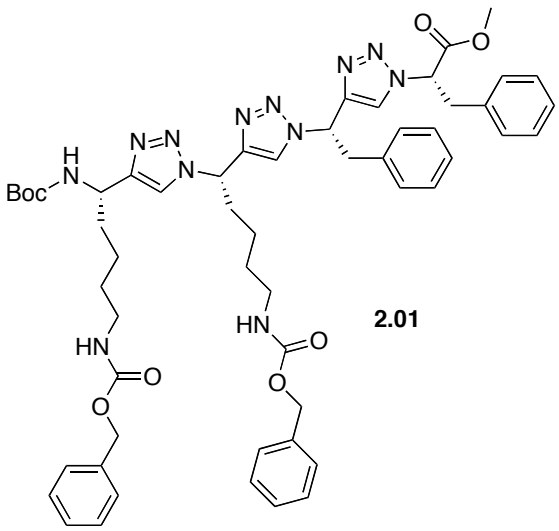

Figure 2.03 An example of peptidomemitic with backbone amide bonds replaced by triazole moieties.[14]

The introduction of a macrocycle linking the side chains of a peptidomimetic is also used to constrain its backbone into an extended β-strand geometry.[5,15-17] The cyclisation of the side chains minimises the entropic loss upon binding of a peptidomimetic to a protease by preorganising the backbone into a favourable conformation. An appropriate macrocycle also allows sufficient flexibility for an induced fit of the peptidomimetic to the target active site and thus maximizing its interactions with the target protease.[18] Therefore the introduction of an appropriate macrocycle can increase both potency and specificity of a ligand. In addition, a macrocyclic peptidomimetic has reduced peptide character and hence is more resistant to off-target proteolysis. This increases the stability, bioavailability and druggability of the inhibitor.[19]

Bartlett et al.[20] and Ksander et al.[21] reported that macrocyclic constraints play an active role in stabilising the backbone conformation of peptidomimetic protease inhibitors and thus improve the inhibitory activity. Fairlie et al.[15]

developed a number of such macrocyclic HIV protease inhibitors that adopt a β-strand conformation preferred by the protease active site, see compound **2.02** in Figure 2.04. Examples of these macrocyclic peptidomimetics were particularly potent with sub-nanomolar IC_{50}s. Tsantrizos et al.[17] reported a potent NS3 protease inhibitor (Figure 2.04, **2.03**) with its P_1 and P_3 side chains linked by a macrocycle, which constrained it into an extended β-strand geometry. This compound was 36-fold more potent than the corresponding acyclic analogue. Chen et al.[22] reported a related analogue with significantly improved bioavailability (Figure 2.04, compound **2.05**). The above examples demonstrate that a macrocycle can preorganise a protease inhibitor backbone into a β-strand conformation, while also cause a significant increasing potency and bioavailability.

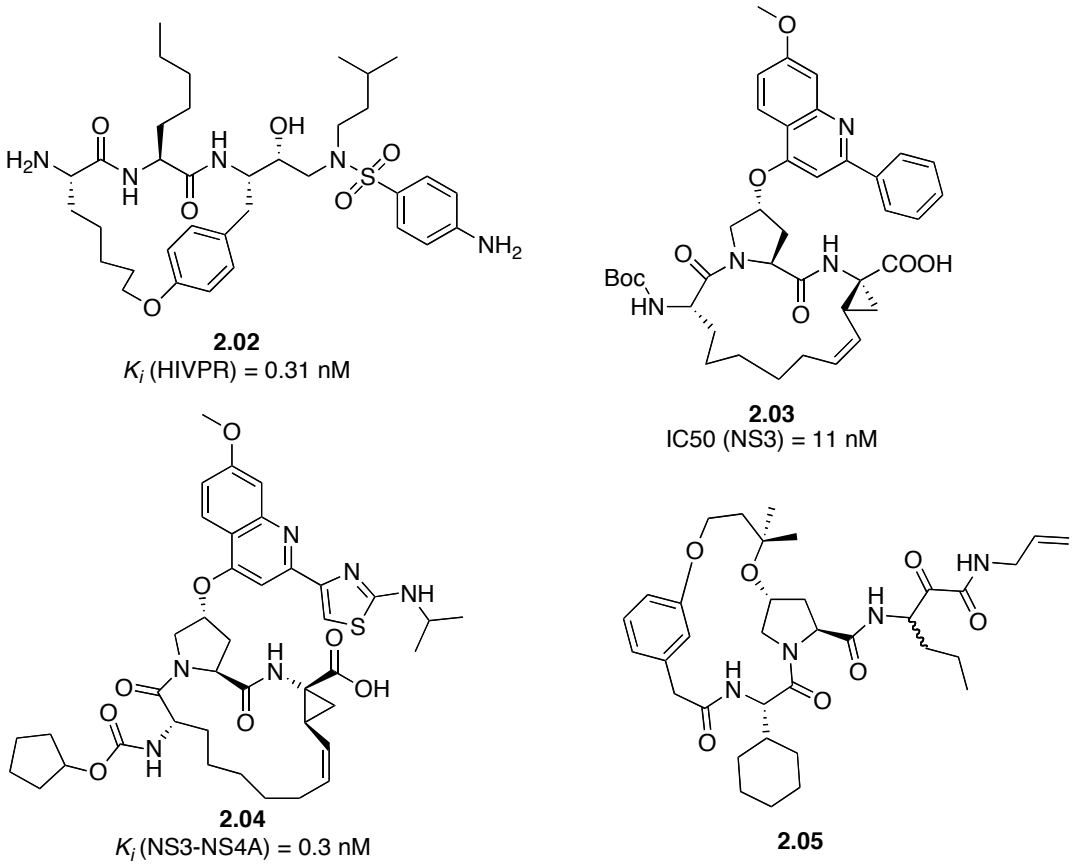

Figure 2.04 Examples of macrocyclic protease inhibitors.[15,17,20]

2.1.3 First-Generation Macrocyclic Inhibitors

Our group has developed a large number of macrocyclic inhibitors targeting various proteases including calpains, α-chymotrypsin, the proteasome, the HIV proteases, and cathespsins.[5,16,23-25] These inhibitors share a common feature: a macrocycle linking the side chains of P_1 and P_3 residues as discussed in section 2.1.2 (Figure 2.05).

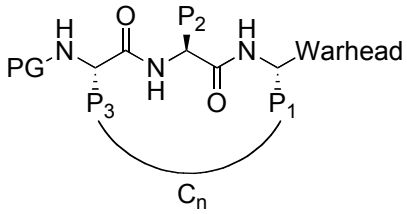

2.06

Figure 2.05 The general structure of the first-generation inhibitors reported by Abell et al.

One such macrocyclic calpain inhibitor, **CAT0811**, was identified to have excellent activity against bovine m-calpain and shows significant promises in treating corneal cataract.[26] **CAT0811** is currently undergoing trials using human lenses for cataract treatment.

In silico conformational searches on this compound and its related analogues (Figure 2.06) demonstrate that the 17- and 18-membered macrocycles (**CAT0811**, **2.07**) provide adequate flexibility for active-site binding and hence optimal activity against calpain.[16] With this in mind, our group[24] developed 17- and 18-membered macrocyclic inhibitors targeting HIV protease with high

potency and selectivity. For example, the most potent HIV protease inhibitor in this series has a K_i of 62 nM (**2.10**, Figure 2.07). This provides an important basis for the development of novel macrocyclic protease inhibitors with reduced peptide-like character and thus improved bioavailability.

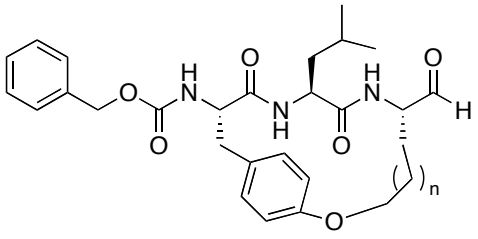

2.07, n = 1
CAT0811, n = 2
2.08, n = 3
2.09, n = 4

Figure 2.06 Calpain inhibitors previously prepared by Abell and co-workers.

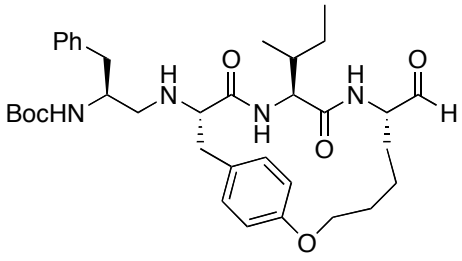

2.10
K_i (HIV-1B)= 62 nM

Figure 2.07 Example of the macrocyclic HIV protease and proteasome inhibitors.

Despite being highly active against a range of proteases, inhibitors with macrocycles that link the P_1 and P_3 side chains have several drawbacks: 1) considerable peptide-like character is retained due to the requirement for a tripeptide or modified tripeptide backbone with appropriate side chains for macrocyclisation. This makes the inhibitors prone to proteolysis by off-target

proteases when applied *in vivo*; 2) the P_1 residue is part of the macrocycle, which is problematic for modification of this group to target a particular protease. Thus there is a real need for a new generation of peptidomimetic protease inhibitor with reduced peptide-like character and with the macrocycle shifted from P_1-P_3 to P_2-P_n. This chapter presents studies on a new class of such protease inhibitor with a macrocycle linking the side chains of P_2 and P_4 and a pyrrole moiety replacing the P_3-P_4 amide bond. The design and synthesis of these inhibitors are discussed in detail in the following sections.

2.2 Results and Discussion

2.2.1 The Design of the Second-Generation Macrocyclic Protease Inhibitors

The second-generation peptidomimetic inhibitors contain a pyrrole moiety in place of the P_3 amino acid and the adjacent peptide bond (Figure 2.08, in blue) to reduce the peptide-like character of the inhibitors, thus potentially increasing their resistance to proteolytic degradation.[10] The pyrrole group also provides additional rigidity to the backbone of the inhibitor, such that it can still adopt the desired β-strand geometry. The inhibitors consist of two modules: the P_1 residue with a *C*-terminal warhead (Figure 2.08, in red) and the P_2-P_4 cyclised peptidomimetic template (Figure 2.08, in black). This modular approach allows easy modification of both modules to provide selectivity for different proteases (for detailed discussion on proteases and selectivity, see section 1.1).

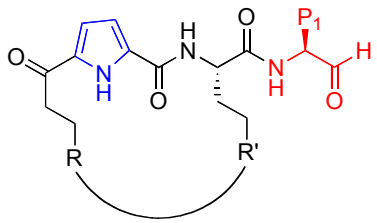

2.11

Figure 2.08 General structure of second-generation protease inhibitors

The S_1 binding site of a protease is critical in determining its specificity and thus the corresponding P_1 residue of a protease inhibitor is central to its potency and selectivity. The P_1 residue of the second-generation inhibitors is not part of the macrocycle, thus allowing appendage of a range of groups at this position (e.g. amino aldehyde or amino dicarbonyl moieties) for targeting a specific protease. The macrocycle linking the side chains of P_2 and P_4 provides the significant advantage that it preorganises the inhibitor backbone into the desired β-strand geometry while also reducing peptide-like character. The size of the macrocycle and its functionality can be tailored to target different proteases. Proteases with extended non-polar binding domains, for example α-chymotrypsin, favour the binding of aryl-containing macrocycles. Macrocycles lacking such functionality are more conformationally mobile, and hence bind with the shallow active sites of cysteine proteases.[27-28] The introduction of a macrocycle can be achieved through several synthetic methods, e.g. Huisgen 1,3-dipolar cycloaddition (Click reaction),[29] lactamization[30] and ring-closing metathesis (RCM).[31] RCM has been widely applied to synthesise conformationally constrained peptidomimetics owing to its compatibility with a wide range of functionality, high yields and mild reaction conditions.[32-34] Grubbs second-generation ruthenium-based catalyst

was used in RCM to improve the yield. This class of catalyst generally has excellent tolerance to most functional groups. The second-generation catalyst provides additional advantage of higher tolerance to water and moisture. Our group has successfully applied RCM to the synthesis of a number of macrocyclic protease inhibitors.[10,16,24] This strategy was also used to prepare the macrocyclic protease inhibitors discussed in this chapter.

Compound **2.12** and **2.13** (Figure 2.09) are examples of the second-generation inhibitors developed by our group. Compound **2.12** with a P_1 leucinal was designed to specifically target cysteine proteases (Figure 2.09) whose S_1 subsites generally favour the binding of a leucine residue. The flexible P_2-P_4 macrocycle favours binding with cysteine proteases. This inhibitor was identified as a promising candidate for treating calpain-induced cataract, with a reported IC_{50} of 35 nM against bovine m-calpain.[10] Compound **2.13** was designed to specifically target α-chymotrypsin (for detailed discussion on α-chymotrypsin, see section 1.1.2).[10] An earlier report by Chua et al. confirmed that analogue **2.13** is a potent inhibitor of α-chymotrypsin, with a K_i of 33 nM.[10] This compound contains a benzyl group at P_1 that binds favourably with the S_1 binding pocket of α-chymotrypsin.[35] The macrocycle links P_2 and P_4 side chains and contains two aryl rings to interact with the large hydrophobic surface of the S_2 and S_4 subsites. The *C*-terminal aldehyde warhead of compound **2.13** is anticipated to react with Ser195 upon active site binding with the mechanism of inhibition shown in Scheme 2.01. This would result in the formation of a stable hemiacetal intermediate, which is in equilibrium with the aldehyde and serine alcohol.[36] This chapter presents the

optimisation of synthetic procedures to produce sufficient quantities of inhibitors **2.12**, **2.13** and an analogue of inhibitor **2.13** with a ^{13}C label at the *C*-terminal aldehyde (compound **2.14**, Figure 2.09) for mechanistic studies and *in vivo* biological experiments. In particular, the formation of the intermediate is demonstrated through ^{13}C NMR experiments of compound **2.14** (Scheme 2.02). The detailed structure of the **2.13**-α-chymotrypsin complex would be solved by X-ray crystallography to determine the conformation of the bound inhibitor and identify the key non-covalent interactions between **2.13** and α-chymotrypsin.

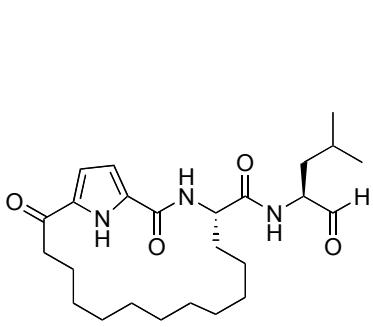

2.12
IC_{50} (o-CAPN2) = 35 nM

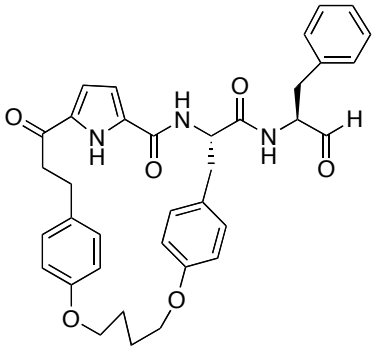

2.13
K_i (bCT) = 33 nM

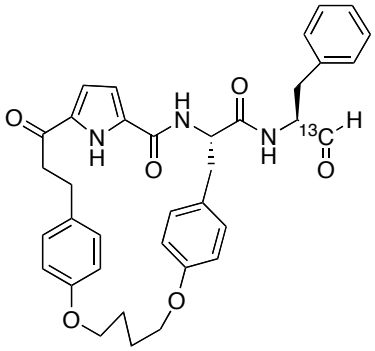

2.14

Figure 2.09 Cysteine protease inhibitor **2.12** and α-chymotrypsin inhibitors **2.13** and **2.14**.

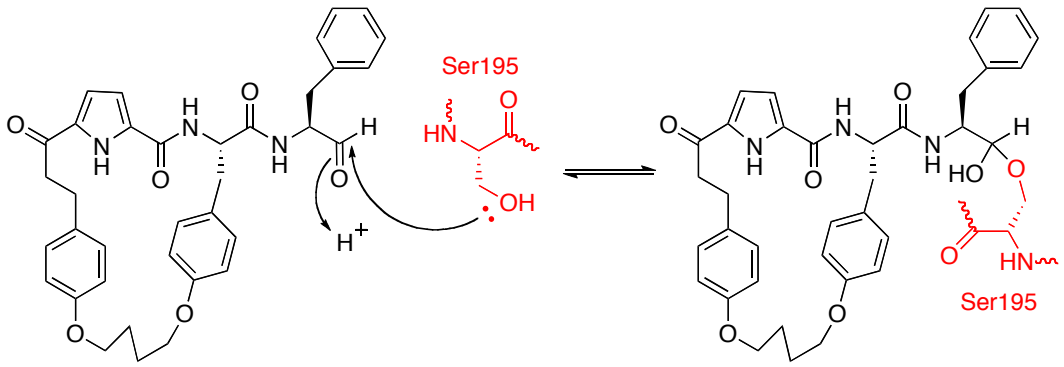

Scheme 2.01 Covalent attachment formed between **2.13** and Ser_{195} of α-chymotrypsin.

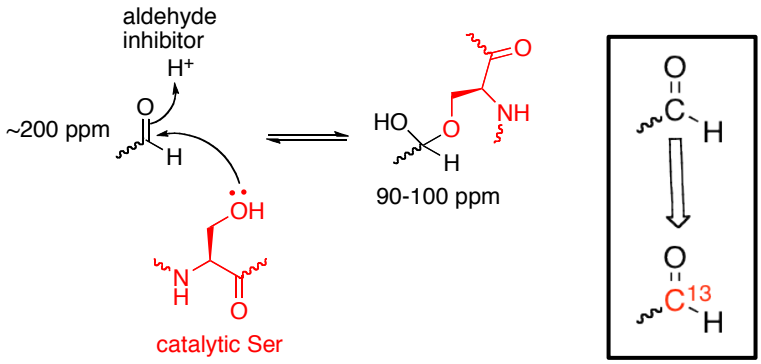

Scheme 2.02 The proposed mechanism of inhibition of α-chymotrypsin by an inhibitor with an aldehyde warhead. The structure of the catalytic serine is in red and the structure of the inhibitor is in black. Insert: replacing the aldehyde C with a ^{13}C atom (highlighted in red).

2.2.2 Optimising the Synthesis of Macrocycles 2.12 and 2.13

The P_2-P_4 macrocyclic cores of compound **2.12** and **2.13** is prepared from a common pyrrole-containing building block via key synthetic steps including Friedel-Craft acylation, ring-closing metathesis and hydrogenation, as illustrated in Scheme 2.03. An initial attempt to synthesise **2.12** revealed

these steps to significantly limit the scale and overall yield of the synthesis. Large-scale (> 1 g) Friedel-Crafts acylation of pyrrole **2.16** with acid chloride **2.17** using $Yb(OTf)_3$ as the catalyst[10] gave a low yield (16%) of **2.19** due to incomplete reaction (Entry 1, Table 2.01). The Low yield is also a result of competing reactions that produced a complex mixture of products, which could not be efficiently separated. This compares with an isolated yield of **2.19** of 61% in the corresponding small-scale reaction (<100 mg). Increasing the reaction time of the large-scale Friedel-Crafts acylation from 21 h to 48 h gave **2.19** in a significantly improved yield of 33% (Entry 2, Table 2.01). An increase in the reaction temperature from ambient to 45°C further improved the yield of **2.19** to 65% (Entry 3, Table 2.01).

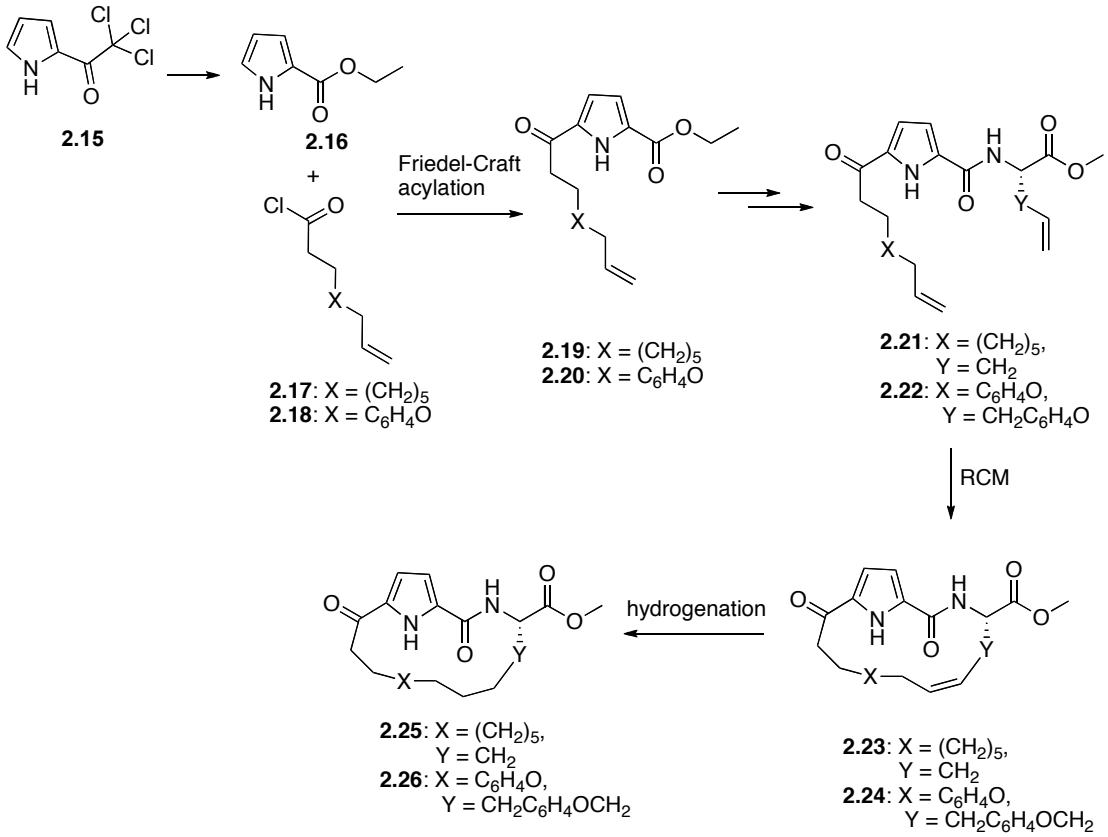

Scheme 2.03 General synthetic scheme for P_2-P_4 macrocycles of compound **2.12**-**2.14**

Table 2.01 Optimisation of Friedel-Craft acylation of pyrrole **2.16** and acid chloride **2.17**

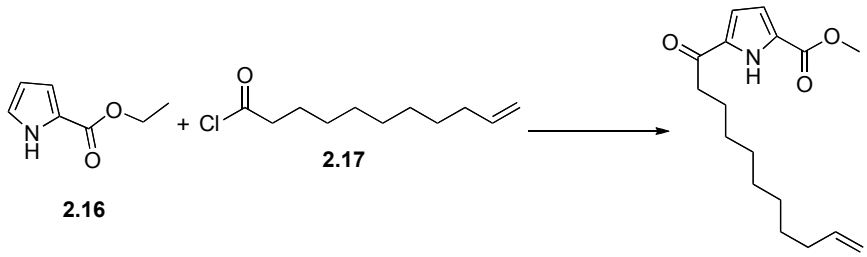

2.16 **2.17** **2.18**

	Equivalents $Yb(OTf)_3$	Reaction time (h)	Temperature	Yield of **2.18** (%)
Entry 1	0.1	21	Ambient	16
Entry 2	0.1	48	Ambient	33
Entry 3	0.1	48	45^{o}C	65

The key RCM cyclisation of **2.21** requires highly dilute conditions (2.5 ml of DCM/mg of diene), which limits the scalability of this reaction. The use of a single portion of Grubbs catalyst gave a 30% yield of **2.23** (Entry 1, Table 2.02). In attempt to improve this, Grubbs catalyst was added in two portions with the second added after 1 h to maintain a constant concentration of the active catalyst. This gave an improved yield of 50% (Entry 2, Table 2.02). The yield of the RCM product was maintained at a higher reaction concentration (1 ml/mg of diene) (Entry 3, Table 2.02). This significantly reduced the volume of solvent required and thus allowing scale up of the RCM reaction.

Table 2.02 Optimisation of RCM of diene **2.21**

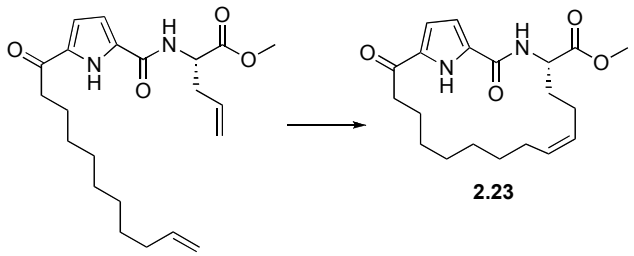

2.21 **2.23**

	Entry 1	Entry 2	Entry 3
Portions of catalyst	1	2.5	28
Concentration of **2.21** (ml/mg of **2.21**)	2	2.5	50
Catalyst used	Grubbs II	Grubbs II	Grubbs II
Temperature (^{o}C)	45	45	45
Reaction time (h)	2	2	2
Yield of **2.23** (%)	2	1	47

The reported hydrogenation of alkene **2.23** with 10% w/w Pd/C catalyst gave a low yield (24%) of the required saturated macrocycle (Entry 1, Table 2.03). The catalyst loading was initially increased from 10% to 50% in an attempt to improve this reaction (Entry 2, Table 2.03). This resulted in an improved yield of 66%. Some unidentified side products resulting from reduction of the ketone (red, Scheme 2.04) were also isolated after chromatography, however these were not characterised. An attempt was made to reduce the amount of side product by decreasing the catalyst loading to 33%. This gave an improved yield of 72% (Entry 3, Table 2.03). TLC analysis of the crude mixture from this reaction still revealed the presence of the side product. Therefore the reaction was monitored by TLC to define the optimal reaction time to minimise side product formation. It was found that using 33% of catalyst, hydrogenation was complete after 3 h with no side product observed.

This gave a significantly improved yield of 95% (Entry 4, Table 2.03). These conditions were then used to prepare compounds **2.12**-**2.14** for mechanistic studies and biological characterisation.

Table 2.03 Optimisation of hydrogenation of macrocycle **2.23**

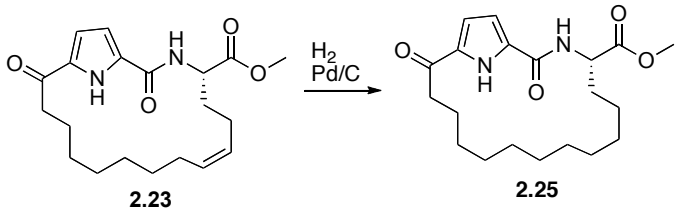

2.23 **2.25**

	Amount of Pd catalyst (% w/w)	Reaction time (h)	Yield of **2.25** (%)
Entry 1	0.1	18	24
Entry 2	0.5	18	66
Entry 3	0.33	18	72
Entry 4	0.33	3	95

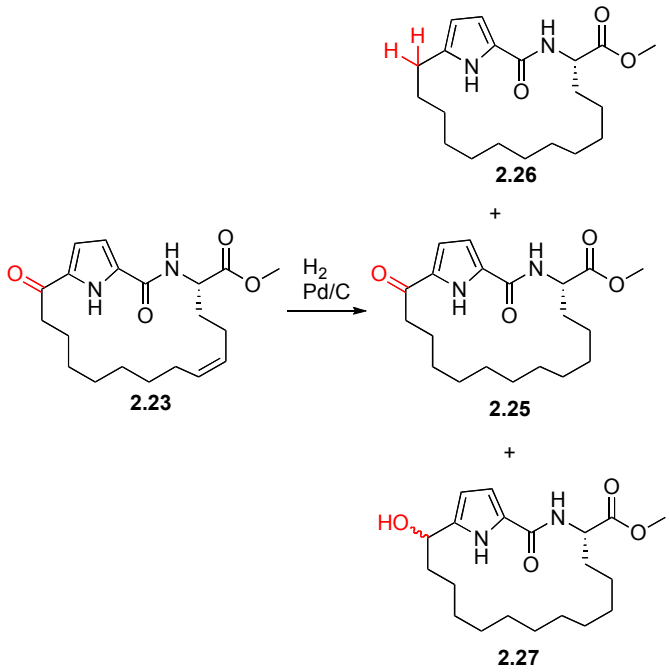

2.26 + **2.23** **2.25** + **2.27**

Scheme 2.04 Reduction of macrocycle **2.23** gave three possible products: the desired product **2.25** and over-reduced side products **2.26** and **2.27**.

2.2.3 The Optimised Synthesis of Calpain Inhibitor 2.12

Commercially available 2-(trichloroacetyl)pyrrole **2.15** was converted to ethyl 1*H*-pyrrole-2-carboxylate **2.16** on a multi-gram scale on reaction with a freshly prepared solution of sodium ethoxide in anhydrous ethanol. A subsequent Friedel-Crafts acylation of **2.16** with 10-undecenoyl chloride **2.17** using optimised conditions gave product **2.19** with the yield of 65%. Compound **2.19** was then hydrolysed with KOH to give the corresponding carboxylic acid **2.28** in excellent yield.

Attempts were then made to couple the carboxylic acid **2.28** with *L*-allylglycine methyl ester **2.30**, which was obtained from *N*-Boc-deprotection and *C*-terminal methylation of commercially available *N*-Boc-allylglycine. An initial attempt using EDCI in DCM gave diene **2.21** in a modest yield of 38% yield. An equivalent coupling using HATU in DMF to increase solubility improved the yield of **2.21** to 78%. Diene **2.21** was then cyclised by RCM using the optimised conditions under mild heating (45^{o}C) to form the desired macrocyclic alkene **2.23**. The cross-metathesis product and other impurities were removed by flash column chromatography in petroleum ether and ethyl acetate to give pure **2.23** in 47% yield, as a 1:1 mixture of *E*/*Z* isomers based on ^{1}H NMR spectroscopy. The formation of the *E/Z* mixture was of little significance as the alkene was subsequently reduced by palladium-catalysed hydrogenation. Using the optimised conditions, hydrogenation of the alkene of **2.23** gave the desired saturated macrocycle **2.25** in an excellent yield.

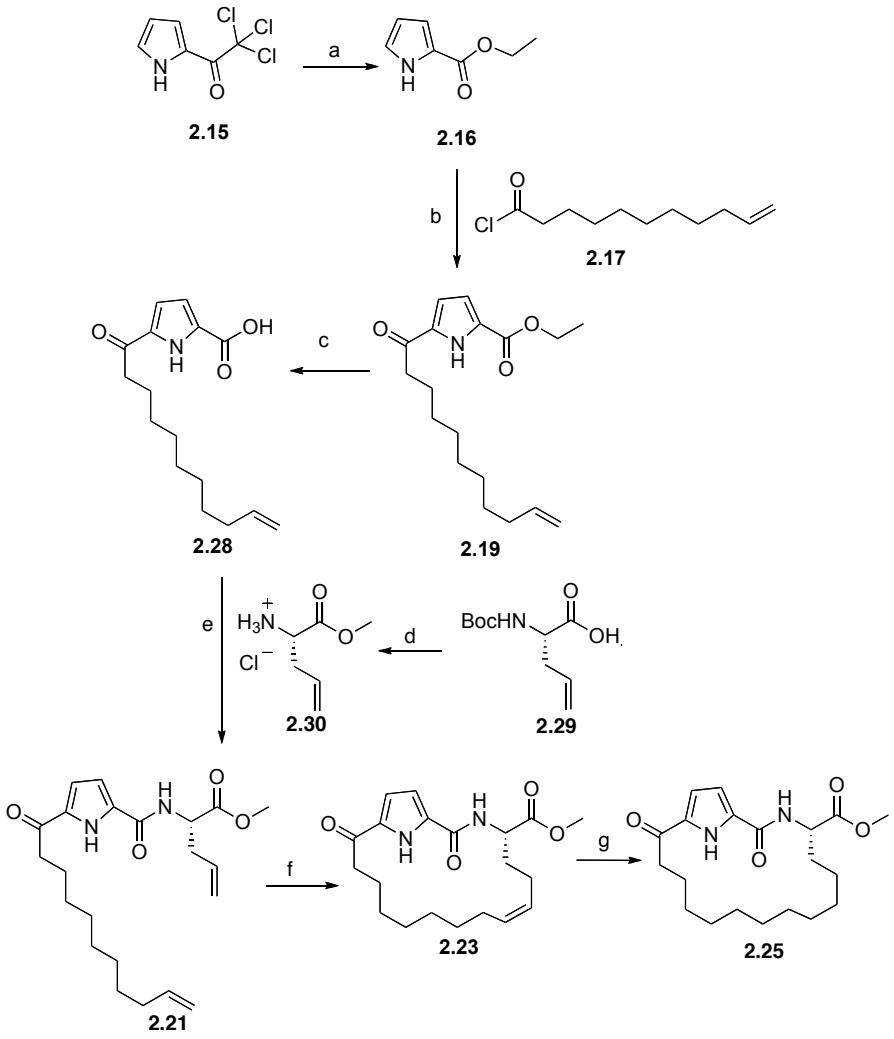

Scheme 2.05 Reagents and conditions: a) Na, anhydrous EtOH, Ar, r.t., 2 h, (77%); b) Yb(III)$(OTf)_3$, CH_3NO_2, r.t., 48 h, (66%); c) KOH, THF/H_2O, 50 ^oC, 18 h, (74%).; d) $SOCl_2$, anhydrous DMF, MeOH, N_2, r.t., 5 h, (quant.); e) HATU, HOBt, DIPEA, anhydrous DMF, r.t., 21 h, (78%); f) Grubbs 2nd generation catalyst, anhydrous DCM, 45 ^oC, 2 h, (47%); g) Pd/C, EtOAc, H_2, r.t., 3 h, (95%).

The methyl ester of the macrocyclic peptidomimetic **2.25** was hydrolysed with aqueous NaOH to give the corresponding carboxylic acid **2.31**, which was used in the subsequent reaction without further purification. A HATU-mediated coupling of **2.31** with *L*-leucinol in DMF gave alcohol **2.32** in 61% yield.

Subsequent Dess-Martin oxidation of the primary alcohol gave the desired macrocyclic aldehyde **2.12** as a single epimer after purification by RP-HPLC (Figure 2.10). A total of 135 mg of this compound was obtained for *in vivo* human lens studies that are still in progress.

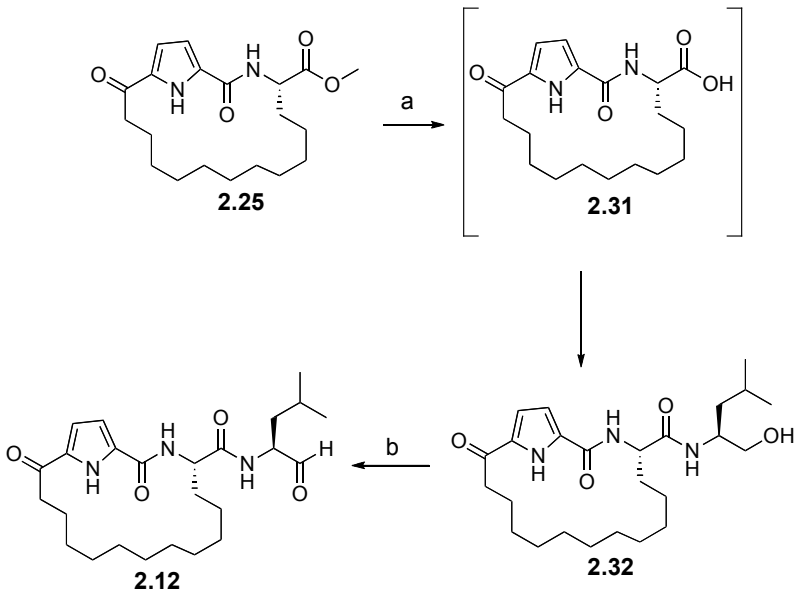

Scheme 2.06 Reagents and conditions: a) NaOH, THF/H_2O, r.t., 18 h; then L-leucinol, HATU, HOBt, DIPEA, anhydrous DMF, N_2, r.t., 21 h, (61%); b) Dess-Martin periodinane, anhydrous DCM, r.t., 1 h, (28%*).

*Yield calculated after RP-HPLC purification.

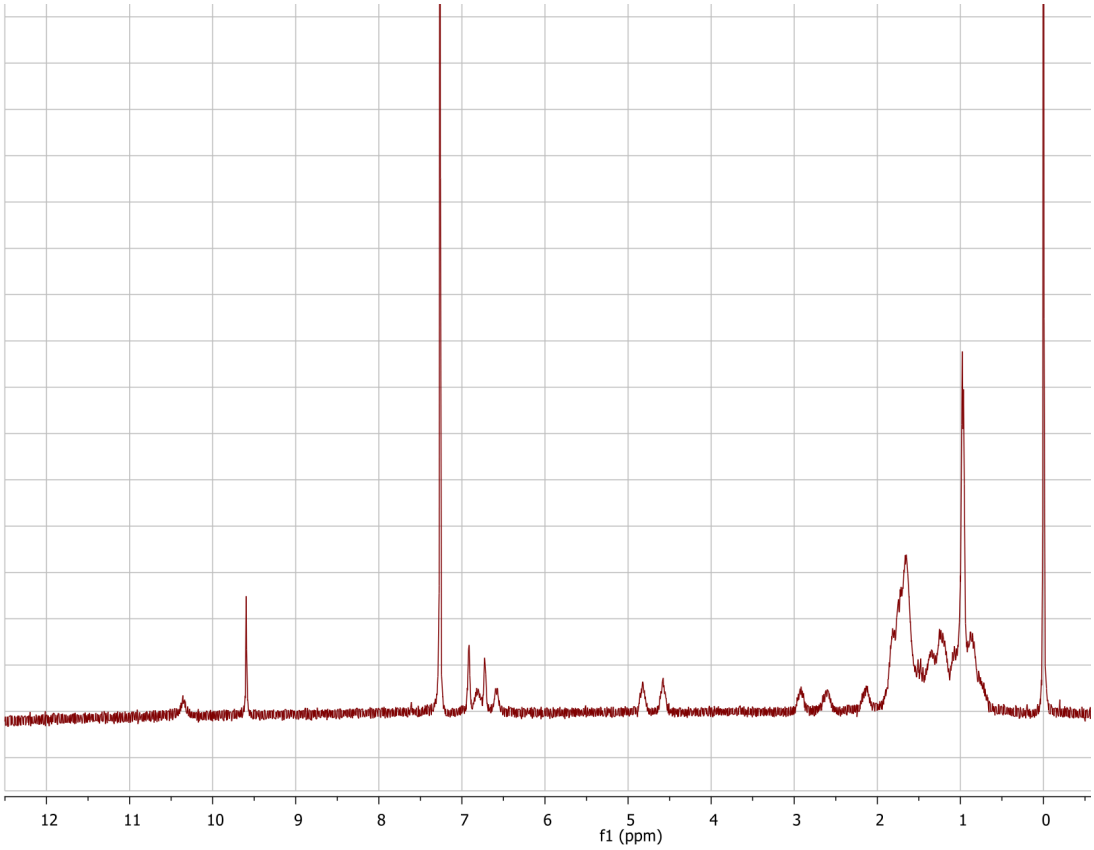

Figure 2.10 ^{1}H NMR spectrum of compound **2.12**.

2.2.4 The Optimised Synthesis of 2.13 and its ^{13}C-labelled Analogue 2.14

The key acid chloride **2.18** was prepared from commercially available methyl 3-(4-hydroxyphenyl) proprionate in three synthetic steps in an overall yield of 96%. Reaction of methyl 3-(4-hydroxyphenyl) proprionate with allyl bromide gave allyl ester **2.34**. The ester of this compound was hydrolysed with LiOH in THF/H_2O to give carboxylic acid **2.35**, which was subsequently converted to the corresponding acid chloride **2.18** on reaction with $SOCl_2$. These three steps were carried out without purification of the intermediates.

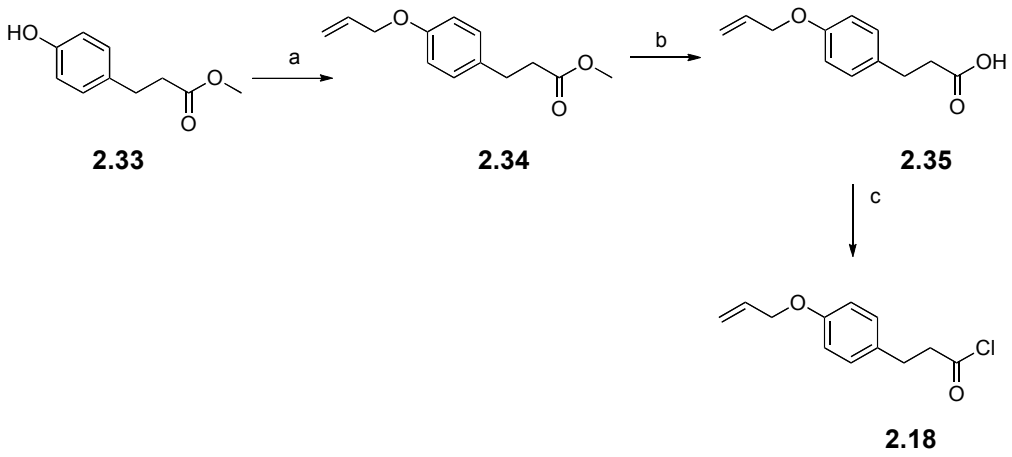

Scheme 2.07 Reagents and conditions: a) TBAI, allyl bromide, K_2CO_3, DMF, N_2, r.t., 18 h, (97%); b) LiOH, THF/H_2O, 40 ^oC, 3 h, (99%); c) $SOCl_2$, DCM, 40 ^oC, 18 h, (quant.).

Friedel-Crafts acylation of the pyrrole derivative **2.16** with acid chloride **2.18** under the optimised conditions gave the key dipeptide-mimic **2.20** in 58% yield. Hydrolysis of **2.22** with KOH gave carboxylic acid **2.36** in excellent yield, which was directly used in the next step without further purification. HATU-mediated coupling of **2.36** and **2.38** in the presence of HOBt and DIPEA gave diene **2.22** in 78% yield over two steps. The starting material **2.38** was obtained from concomitant *N*-terminal Boc-deprotection and *C*-terminal methylation of **2.37** with $SOCl_2$ in MeOH. The diene **2.22** was then cyclised using the optimised RCM conditions to give the desired unsaturated macrocycle **2.24**, which was used directly in the subsequent hydrogenation without purification. Hydrogenation in the presence of Pd/C (33% mol %) gave the saturated macrocycle **2.26** in excellent yield. The progress of this reaction was carefully monitored by TLC analysis to prevent the reduction of the ketone group (highlighted in red in Scheme 2.08).

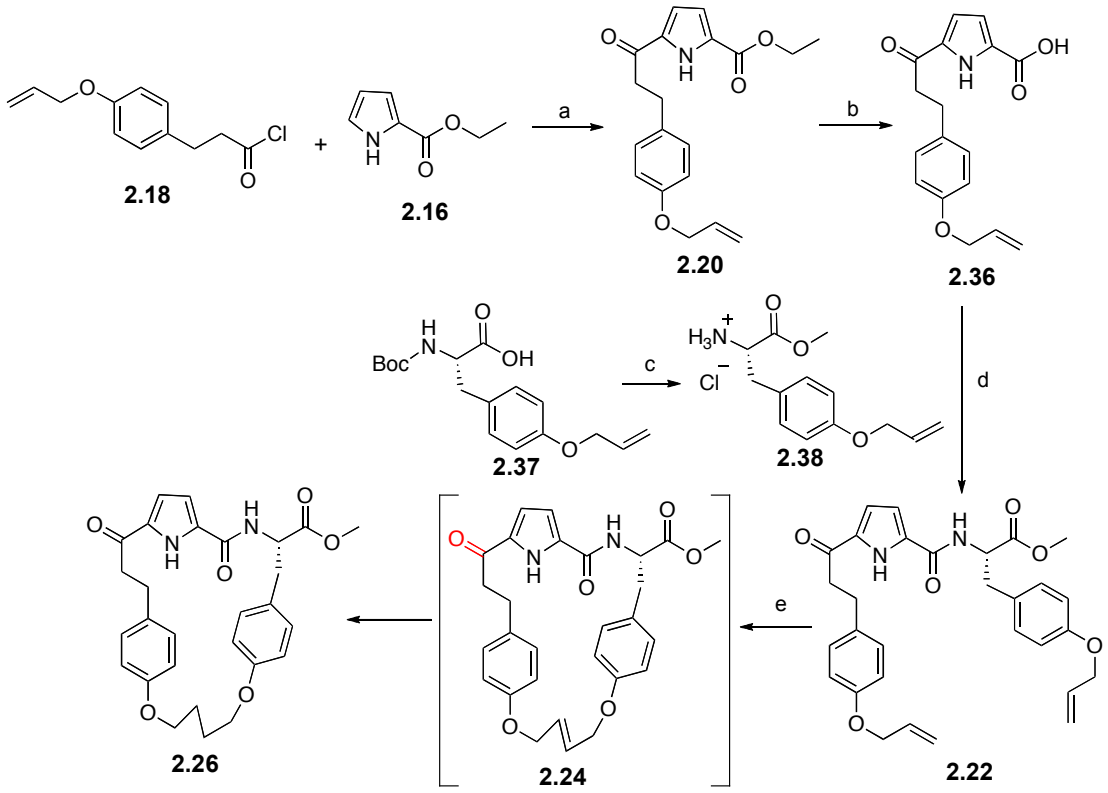

Scheme 2.08 Reagents and conditions: a) $Yb(OTf)_3$, nitromethane, r.t., 21 h, (58%); b) KOH, THF/H_2O, 40 ^oC, 21 h, (85%); c) $SOCl_2$, DMF, MeOH, r.t., 5 h, (quant.); d) HATU, DIPEA, DMF, N_2, r.t., 21 h, (78%); e) Grubbs 2nd generation catalyst, anhydrous DCM, N_2, 45 ^oC, 2 h; then Pd/C, EtOAc, H_2, r.t., 4 h, (76%).

The methyl ester of **2.26** was hydrolysed with NaOH to give carboxylic **2.39**, which was coupled to commercially available *L*-phenylalaninol in the presence of HATU, HOBt and DIPEA to give alcohol **2.40** in 48% yield. The alcohol was subsequently oxidized with Dess-Martin periodinane to give a crude mixture containing aldehyde **2.13**, which was purified by flash column chromatography. An ^1H NMR spectrum of this material indicated the presence of both epimers in a ratio of 3:1 (Figure 2.11a). This is likely due to

epimerisation alpha to the aldehyde carbonyl. The major epimer was then isolated by RP-HPLC. A ^{1}H NMR spectrum of **2.13** confirmed the presence of a single epimer as shown by the singlet at 9.67 ppm (Figure 2.11b, in red).

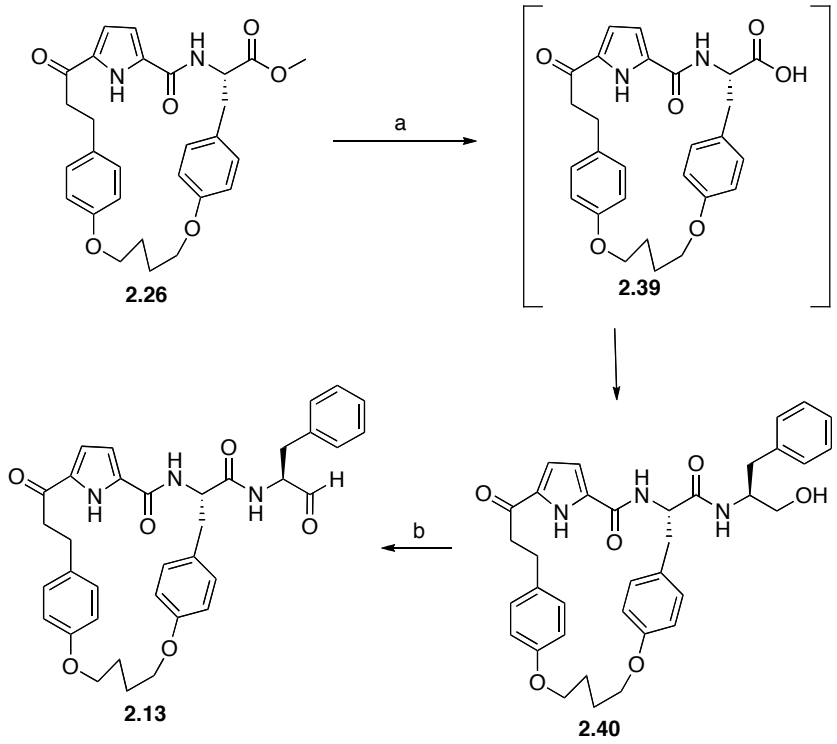

Scheme 2.09 Reagents and conditions: a) NaOH, THF/H_2O, r.t., 18 h; then L-phenylalaninol, HATU, HOBt, DIPEA, DMF, N_2, r.t., 21 h, (48%); b) Dess-Martin periodinane, DCM, N_2, r.t., 1.5 h, (22%*).

*Yield calculated after RP-HPLC purification.

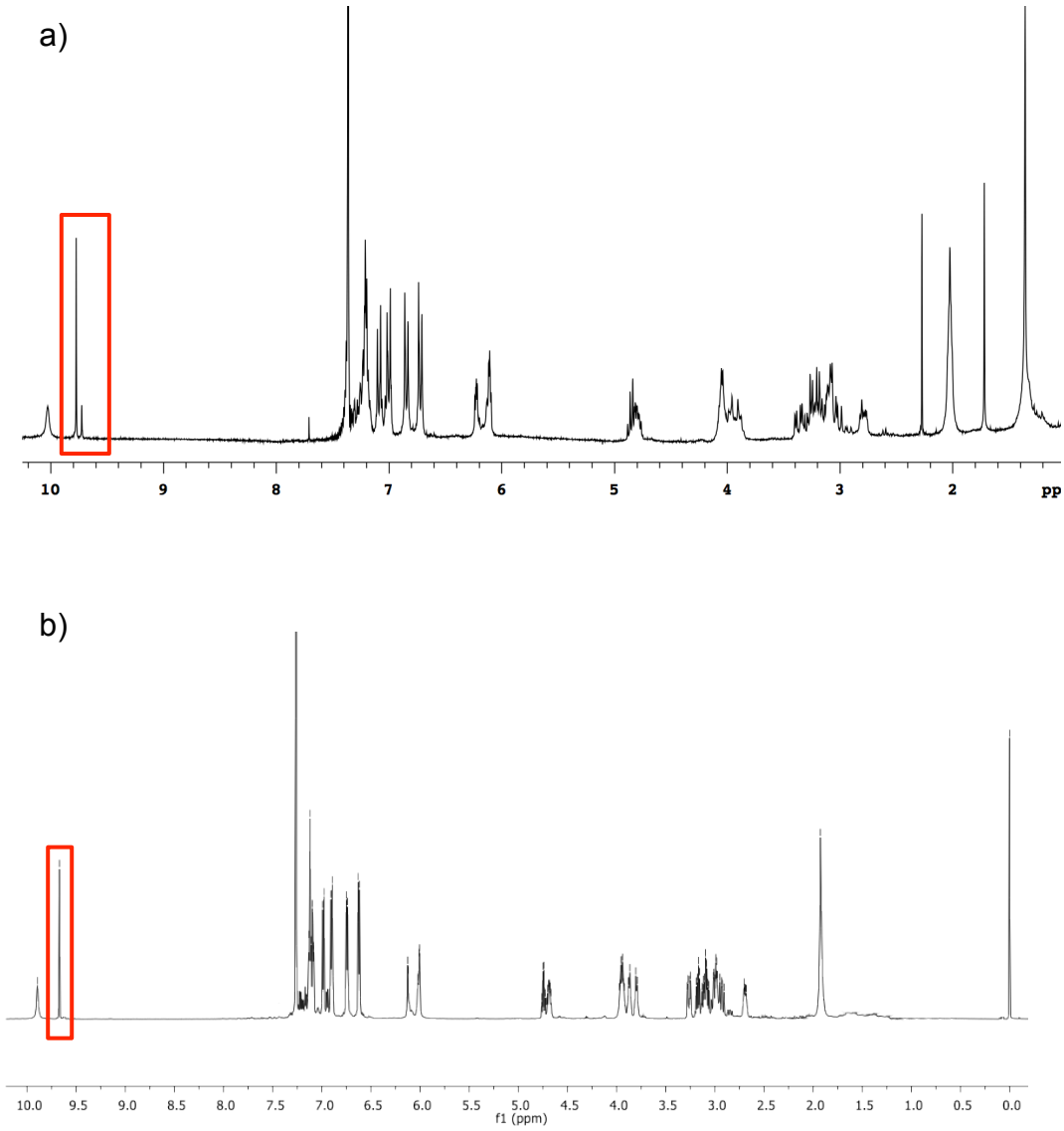

Figure 2.11 a) ^{1}H NMR spectrum of **2.13** showing a large single resonance and a small single resonance (in red) for the aldehyde group; b) ^{1}H NMR spectrum of **2.13** after RP-HPLC purification showing a single resonance for at 9.67 ppm (in red).

The synthesis of *L*-phenylalaninol-1-^{13}C (**2.44**) began with *N*-Boc-protection of commercially available *L*-phenylalanine-1-^{13}C. The resulting protected amino acid **2.42** was reduced with $LiAlH_4$ to give Boc-protected *L*-phenylalninol-1-^{13}C **2.43**. The Boc group of this compound was subsequently removed on

treatment of TFA in DCM to give the desired labelled alcohol **2.44**. HATU-mediated coupling of **2.44** to carboxylic acid **2.39** as described previously, followed by Dess-Martin oxidation, gave the crude ^{13}C-labelled aldehyde inhibitor **2.14**, which was purified by flash column chromatography. Similar to **2.13**, a ^{1}H NMR spectrum of this material indicated the presence of both epimers in a ratio of approximately 3:1 (Figure 2.12a, in red). Therefore, the compound was again purified by reverse-phase high-pressure liquid chromatography (RP-HPLC) to give a single epimer. The epimeric purity was confirmed by an RP-HPLC trace showing a single peak at 18 min (Figure 2.12c). This epimer is assigned the natural isomer based on the chemical shift of the formyl resonance at 9.71 ppm (Figure 2.12b).

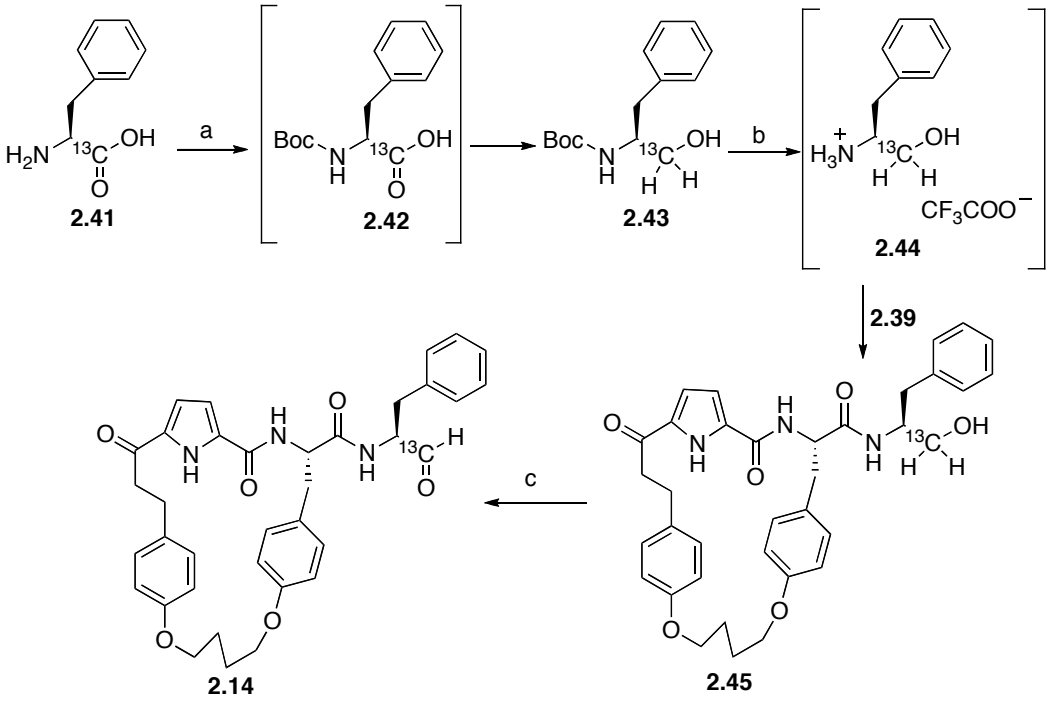

Scheme 2.10 Reagents and conditions: a) Boc_2O, Et_3N, THF/MeOH, r.t., 18 h,; then $LiAlH_4$, THF, N_2, 0 ^{o}C – r.t., 18 h, (quant); b) TFA, DCM, 0 ^{o}C, 2 h,;

then HATU, HOBt, DIPEA, DMF, N_2, r.t., 21 h, (39%); c) Dess-Martin periodinane, DCM, N_2, r.t., 1.5 h, (27%*).

*Yield calculated after RP-HPLC purification

a)

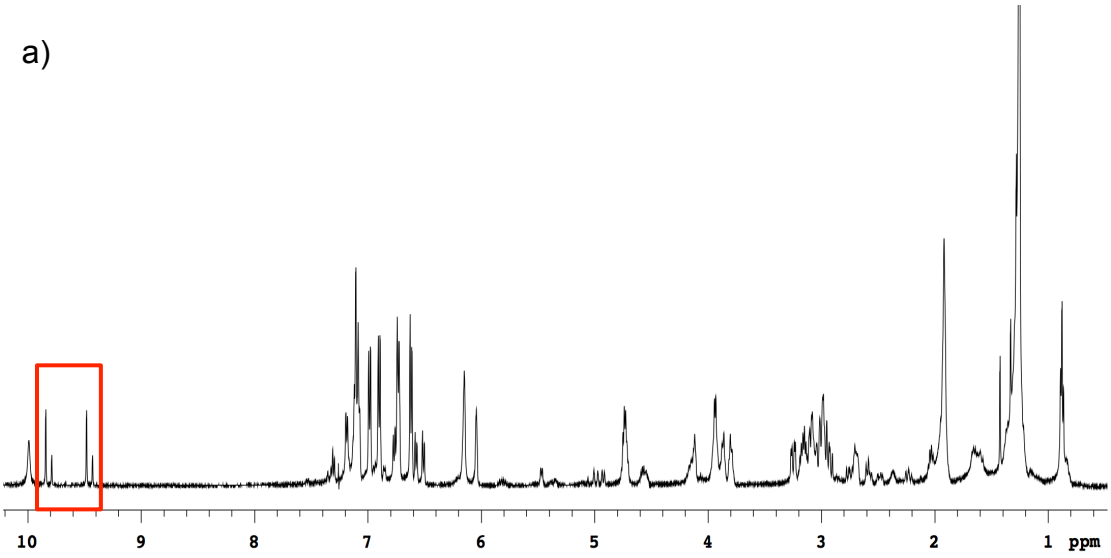

b)

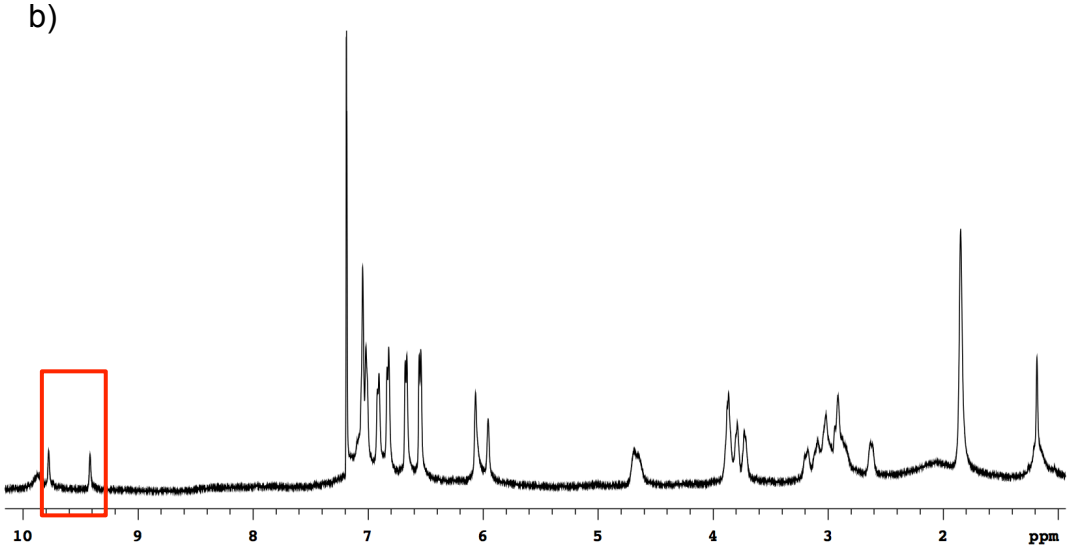

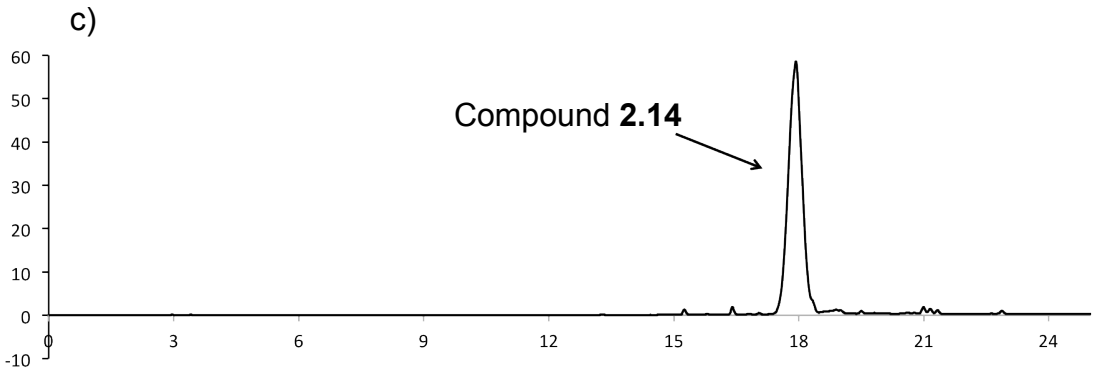

Figure 2.12 a) ^{1}H NMR spectrum of **2.14** showing a large double resonance and a small double resonance (in red) for the ^{13}C-labelled aldehyde groups of the two epimers; b) ^{1}H NMR spectrum of compound **2.14** showing a single set of double resonance (highlighted in red) for the ^{13}C-labelled aldehyde groups; c) analytical HPLC trace of compound **2.14** showing a single peak at 18 min.

2.2.5 Determining the mechanism of inhibition of the α-Chymotrypsin inhibitor 2.14 by ^{13}C NMR

A ^{13}C NMR spectrum of inhibitor **2.13** and its labelled analogue **2.14** revealed a 100-fold enhancement in the intensity of the aldehyde resonance at 199.6 ppm (Figure 2.13). This then provides an opportunity to follow the fate of this label in enzyme inhibition studies.

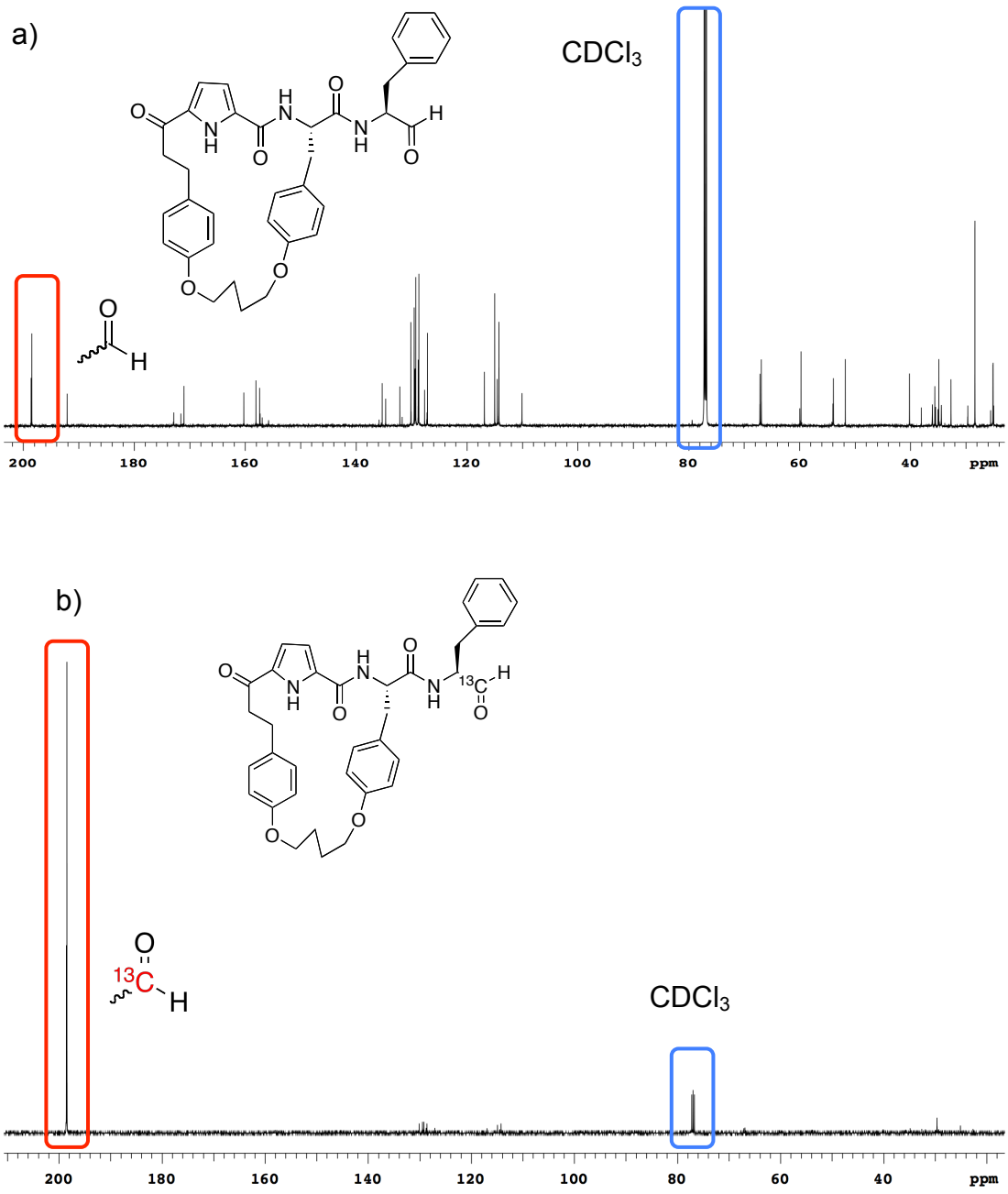

Figure 2.13 (a) ^{13}C NMR spectrum of **2.13** (2.8 mM in $CDCl_3$); (b) ^{13}C NMR spectrum of **2.14** (2.8 mM in $CDCl_3$). The aldehyde peaks are highlighted in red; the solvent residue peaks of $CDCl_3$ are highlighted in blue.

Some initial experiments were carried out to optimise the solvent system for the enzyme inhibition studies using the labelled material. A sample of labelled aldehyde **2.14** was not completely soluble in a 7.5% solution of α-chymotrypsin in DMSO-d_6 in D_2O and gave rise to a suspension. This is the

solvent system reported previously for α-chymotrypsin ^{13}C NMR studies using unrelated inhibitors.[37-38] Solubility was not improved on stirring this suspension for 1 h at room temperature, or in a second experiment by first dissolving aldehyde **2.14** in DMSO-d_6 and diluting with D_2O to give 7.5% DMSO-d_6 in D_2O. Thus it was not possible to determine the concentration of inhibitor **2.14** under these conditions. The maximum concentration of **2.14** obtainable in 7.5% DMSO-d_6 in D_2O was next determined.

A standard curve of **2.14** was constructed by RP-HPLC to determine the concentration of this compound in a solvent system containing variable amounts of DMSO (Figure 2.14): Six solutions of **2.14** in DMSO (concentration = 0.2, 0.3, 0.4, 1, 1.5 and 2 mM) were prepared and 20 µL of each solution were analysed by HPLC. A UV absorption spectrum (λ = 280 nm) of each injection was obtained. The major peak at 18.1 min was identified to correspond to compound **2.14**. The absolute integral of this peak was then calculated for each injection (Table 2.04) and these results were plotted against the amount of **2.14** injected to construct a standard curve for determining unknown concentrations of **2.14** for a given amount of DMSO in H_2O. Next, a saturated solution of **2.14** was prepared by adding an excess to 7.5% DMSO in H_2O with stirring at room temperature for 1 h. This was centrifuged and filtered to give a homogeneous solution and 20 µL of this solution was analysed by RP-HPLC to generate a UV absorption spectrum. An analysis using the standard curve indicated a concentration of 0.69 mM, which represents the saturation concentration in 7.5% DMSO/H_2O. This is 3-fold less concentrated than the optimal conditions reported for the ^{13}C-NMR-

based analysis of α-chymotrypsin activity. The ^{13}C NMR spectrum of a solution of **2.14** and α-chymotrypsin in 7.5% DMSO-d_6/D_2O (0.69 mM) gave poor signal to noise such that not even the enhanced aldehyde signal could be observed, as shown in Figure 2.15. We thus set about establishing the maximum concentration of DMSO that α-chymotrypsin can tolerate *in vitro* without losing significant activity.

Table 2.04 The RP-HPLC analysis of solutions of **2.14** in DMSO.

Solution Concentration (mM)	Volume of Injection (uL)	Amount of **2.14** injected (nmol)	Integral
0.2	20	4	1419.0
0.3		6	2110.0
0.4		8	2333.0
1		20	6976.0
1.5		30	10449.0
2		40	13739.0

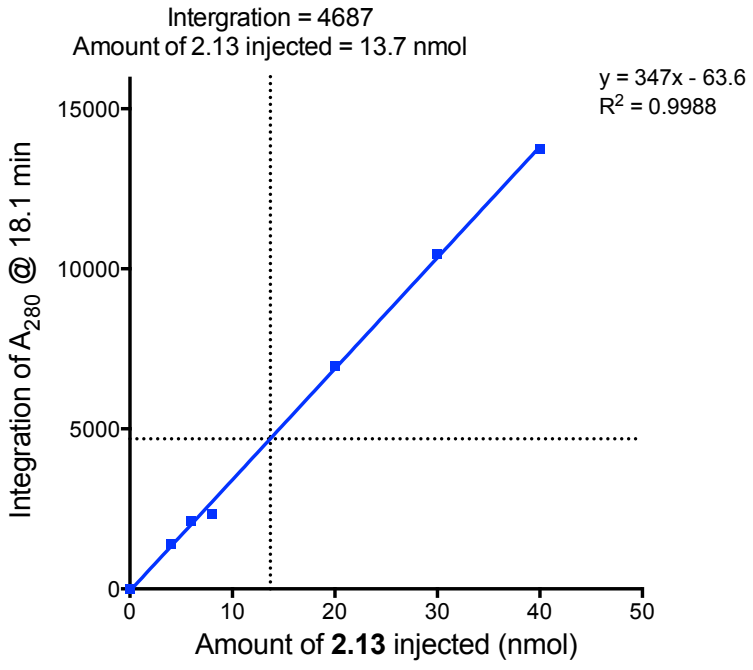

Figure 2.14 A graph of peak integration versus amount of compound **2.14** injected. A linear line was fitted to the graph with GraphPad Prism 6. The equation and R^2 value calculated were displayed above the line. The dotted line parallel to the x-axis represents the peak integration of **2.14** in 7.5% DMSO in H_2O (20 µL injection) while the dotted line parallel to the y-axis represents the amount of compound injected in nmol.

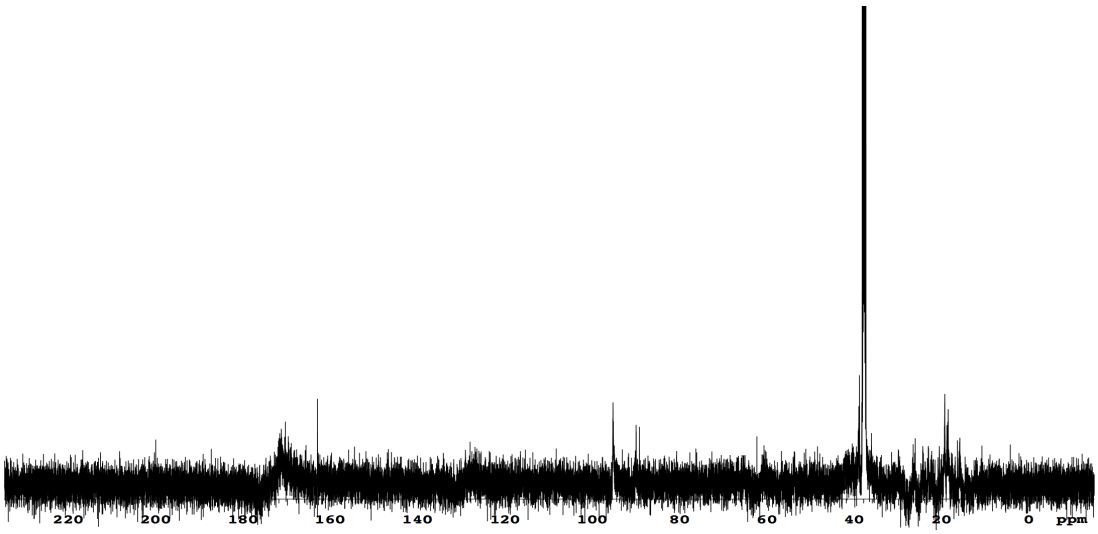

Figure 2.15 ^{13}C NMR spectrum of **2.14** and α-chymotrypsin in 7.5% DMSO-d_6 in D_2O (concentration = 0.69 mM).

The activity of α-chymotrypsin was assayed *in vitro* using a fluorogenic substrate alanine-alanine-phenylalanine-AMC (AAF-AMC). The fluorescent AMC group is cleaved by chymotrypsin upon the binding of the substrate and consequently causes an increase in fluorescence over time. α-Chymotrypsin activity is directly proportional to the rate of fluorescence increase, which is equivalent to the slope of the linear plot shown in Figure 2.16. The increase of fluorescence was entirely due to substrate cleavage by α-chymotrypsin as the negative control (Figure 2.16, magenta) containing only the substrate gave no

change in fluorescence. A positive control (Figure 2.16, blue) containing α-chymotrypsin and AAF-AMC in 2.5% DMSO in H_2O gave a slope of 139.7. Increasing the DMSO content to 10% (Figure 2.16, green) and 20% (Figure 2.16, red) gave slopes of 119.1 and 96.5 respectively. This indicates that α-chymotrypsin in 20% DMSO in H_2O retained its activity by 69% in comparison with the positive control. It was anticipated that this level of activity would be sufficient for the purpose of the ^{13}C NMR experiments using labelled **2.14**. An RP-HPLC analysis of a solution of **2.14** under these conditions revealed the saturation concentration of **2.14** in 20% DMSO in H_2O to be 2.6 mM. This is comparable with the literature value of 2.8 mM discussed above. Therefore this solvent system was used in subsequent ^{13}C NMR experiments with α-chymotrypsin.

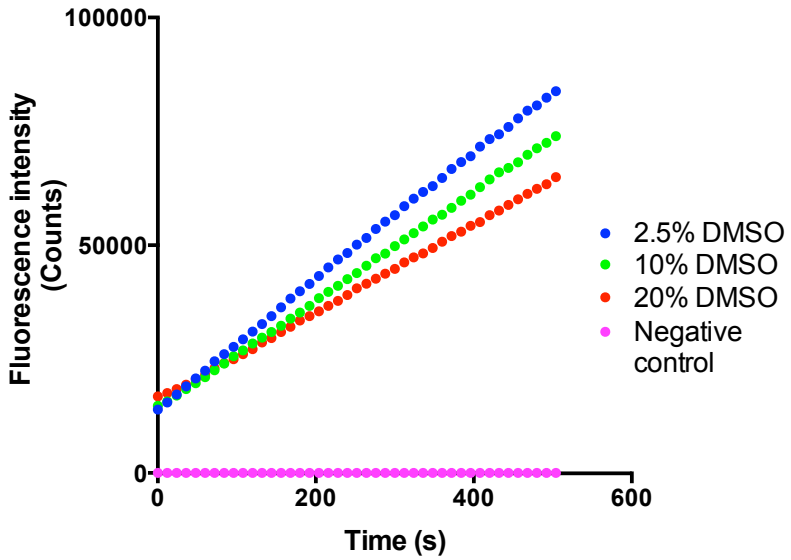

Figure 2.16 α-Chymotrypsin activity in water containing 2.5% (blue), 10% (green) or 20% (red) DMSO. The negative control containing only substrate in 2.5% DMSO in H_2O is shown in magenta.

Next, the interactions of **2.14** (2.6 mM) and α-chymotrypsin (2.6 mM) in 20% DMSO-d_6/D_2O was analysed by ^{13}C NMR, with the resulting spectrum shown in red in Figure 2.20. A negative control containing only the inhibitor was also analysed. The resulting spectrum (in blue, Figure 2.17) shows a resonance at 200 ppm corresponding to the *C*-terminal aldehyde of **2.14**, and a second resonance at 90.0 ppm, which is consistent with a hemiacetal formed on reaction of the aldehyde with D_2O. The ^{13}C NMR of the test sample containing α-chymotrypsin (shown in red, Figure 2.17) reveals a single resonance at 92.1 ppm, which is consistent with a hemiacetal formed on reaction of the aldehyde with active site Ser195. In addition, the absence of resonances at 200 and 90 ppm is consistent with an efficient formation of this intermediate. This study confirms that the aldehyde of **2.14** is covalently reacting with the active site of α-chymotrypsin.

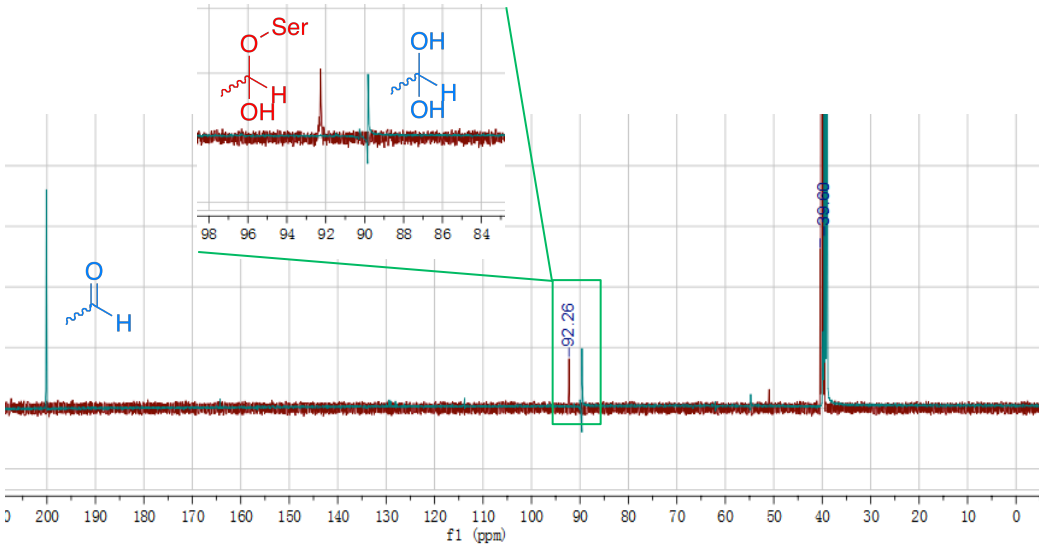

Figure 2.17 An overlay of two ^{13}C NMR spectra: in blue: negative control with only **2.14** in 20% DMSO-d_6 in D_2O (2.6 mM); in red: sample with α-chymotrypsin (2.6 mM) and **2.14** (2.6 mM) in 20% DMSO-d_6 in D_2O. The

region of interest is highlighted in green. Insert: an expansion of the spectra in the region of 84-100 ppm.

2.2.6 X-Ray Crystallography of the α-Chymotrypsin-2.13 Complex

X-ray crystallography of α-chymotrypsin bound by aldehyde inhibitor **2.13** was conducted in collaboration with Dr. John Bruning to further explore the structure and interactions of the enzyme-inhibitor complex. The detailed procedure of the experiment is presented below. A solution of compound **2.13** (0.1 equiv.) in 0.1 M HEPES buffer (pH = 7) was added to a solution of crystallography-grade α-chymotrypsin (2 mg/ml) in the same buffer. The solution was concentrated by centrifugation to 20 mg/ml of α-chymotrypsin + **2.13** to enable more efficient crystallisation. The complex was crystallized by the sitting drop vapour diffusion method. The 96-well sitting drop crystallisation tray was set up as illustrated in Figure 2.21: 1 μL of the enzyme solution was set up as the 'drop' in each small well while 75 μL of crystallisation matrix was placed into the adjoining deep well as the 'mother liquor'. A small amount of the 'mother liquor' (1 μL) was transferred into the 'drop' and the plate was sealed for incubation at 16 ^{o}C. The water vapour slowly diffused between the 'drop' and 'mother liquor' to gradually increase the concentration of the enzyme solution until an equilibrium was achieved. Nucleation slowly occurred over 4 weeks resulting in the formation of crystals, which were harvested and carefully coated with paratone-N solution and cryo-protected with liquid N_2 to reduce radiation damage caused by X-rays. A crystal was mounted onto the goniometer for X-ray irradiations with 1 min

exposures and 1° oscillations. A total of 360 diffraction patterns were collected. Each diffraction pattern was then indexed and integrated before all 360 frames were scaled and merged into a single reflection file. The phase problem was overcome by molecular replacement. Refinement was carried out by iterative rounds of positional and β-factor refinement followed by manual rebuilding in Coot until R-factors converged. The structure generated was visualized using Chimera 1.9, Pymol 1.3, and Coot 0.7.

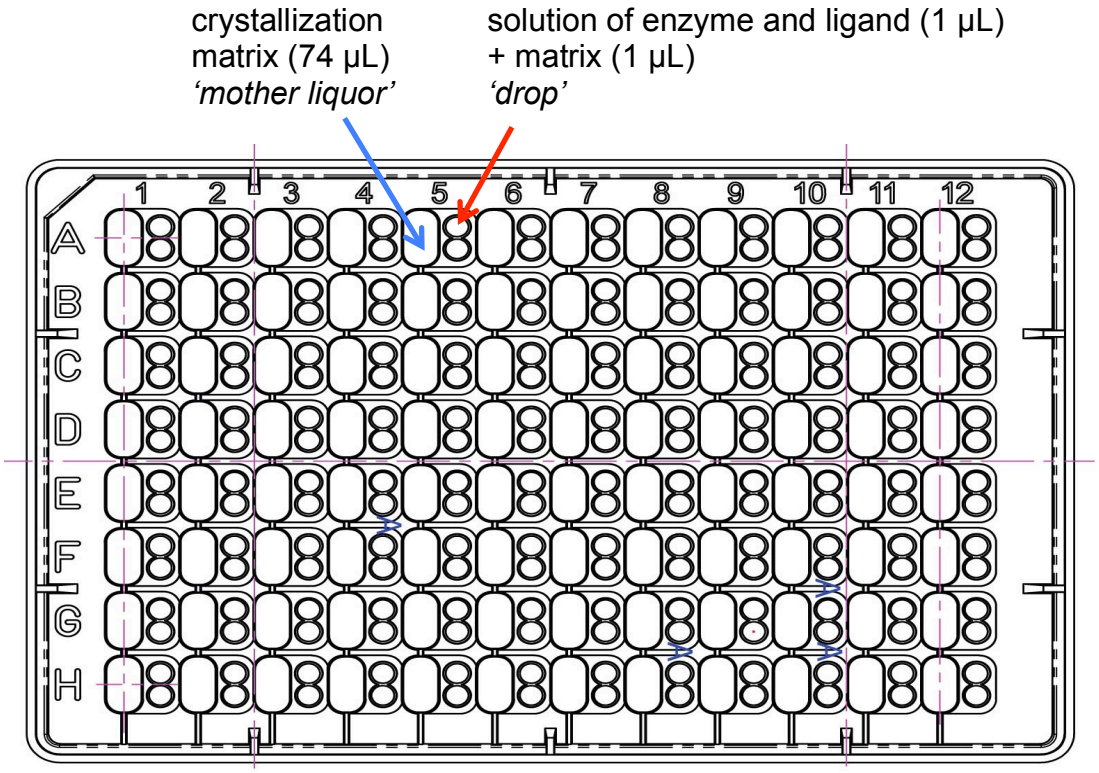

Figure 2.18 A schematic representation of a sitting drop crystallisation plate consists of 96 sample sets. Each sample set contains a deep well (annotated by the blue arrow) and two small wells (annotated by the red arrow). For the purpose of this experiment, only one of the two small wells was used to contain 1 µL of enzyme solution known as the 'drop' and 1 µL of the

crystallisation matrix known as the ‘mother liquor’, while the deep well contained 74 µL of the ‘mother liquor’.

Overall, α-chymotrypsin crystallised in a tetrameric form in the asymmetric unit with each monomer bound by one molecule of compound **2.13**. As expected, compound **2.13** binds with the active site of α-chymotrypsin (Figure 2.19, a). The P_1 phenylalanine of **2.13** binds tightly with the S_1 subsite defined by amino acids Ser189-Met192, Ser214-Gly216 and Trp224-Tyr228. This orients the *C*-terminal aldehyde to less than 1.5 Å away from the catalytic Ser195 of α-chymotrypsin, which is a feasible distance for the formation of a covalent bond. In addition, the electron density map (Figure 2.20) shows continuous electron density between **2.13** and Ser195. This also indicates the existence of a covalent bond between the aldehyde carbon of **2.13** and the side-chain hydroxyl group of Ser195, which is consistent with the observations of the ^{13}C NMR experiments reported in section 2.2.6. The P_2 aryl group as a part of the macrocycle binds with the S_2 pocket of α-chymotrypsin. The binding is stabilised by a π-π interaction with His57, a member of the catalytic triad. As per our design, the backbone of the bound inhibitor adopts an extended geometry similar to a β-strand (Figure 2.21, a), with dihedral angles $\phi = 147^{o}$, $\psi = -88^{o}$, and $\varpi = 178^{o}$ (Figure 2.21, b) respectively. The pyrrole group of the inhibitor clearly helps to define its backbone geometry while occupying the space between the S_3 and S_4 subsites of the enzyme. Furthermore, the inhibitor backbone overlays perfectly with the backbone of PMP-C, a natural α-chymotrypsin inhibitor that binds in a β-strand geometry (Figure 2.22).

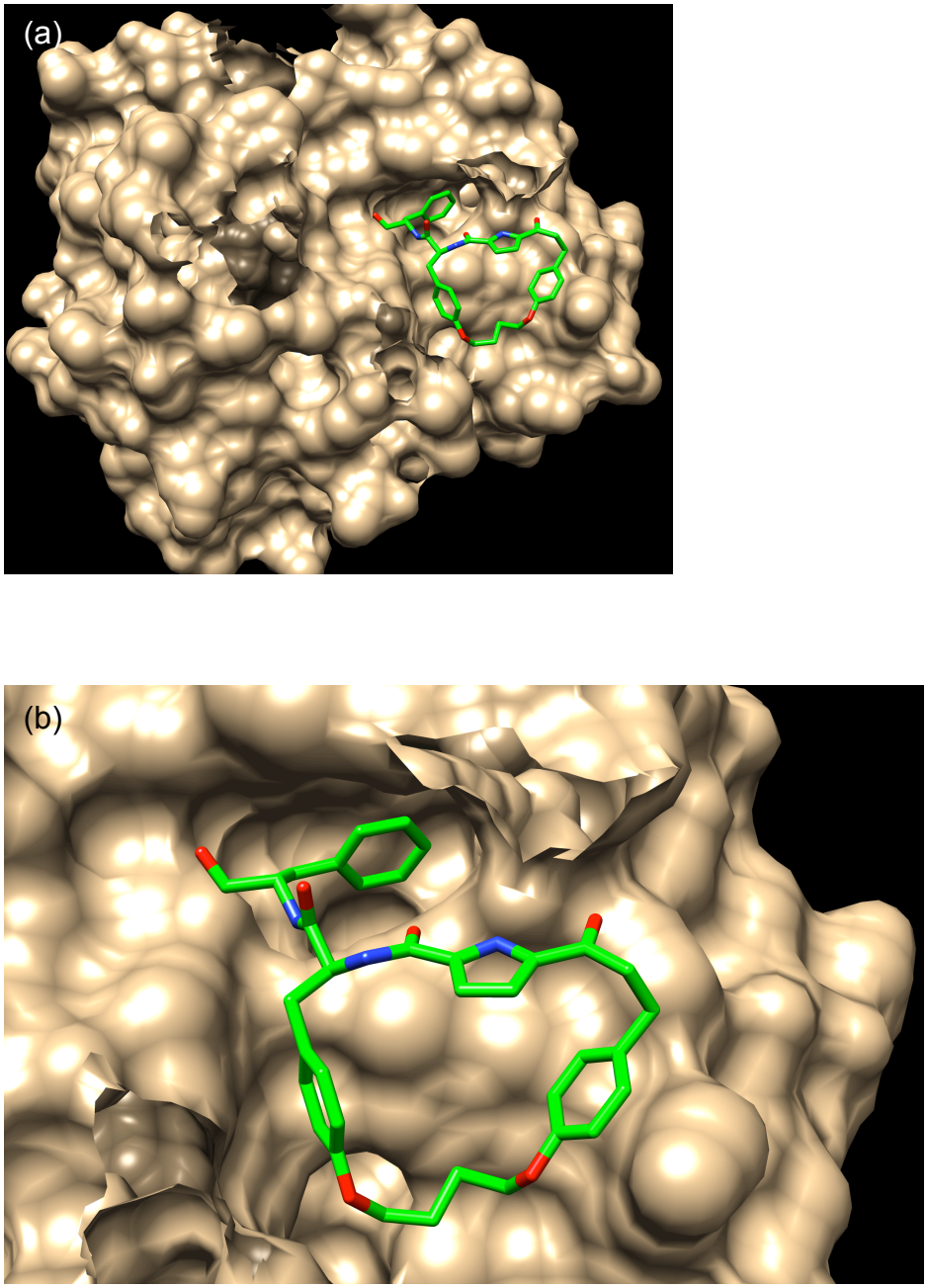

Figure 2.19 (a) An X-ray crystal structure of an α-chymotrypsin monomer bound by compound **2.13** in its active site; (b) the expansion to the active site region of α-chymotrypsin. The enzyme is displayed as surfaces in light brown and the inhibitor is displayed as sticks in green.

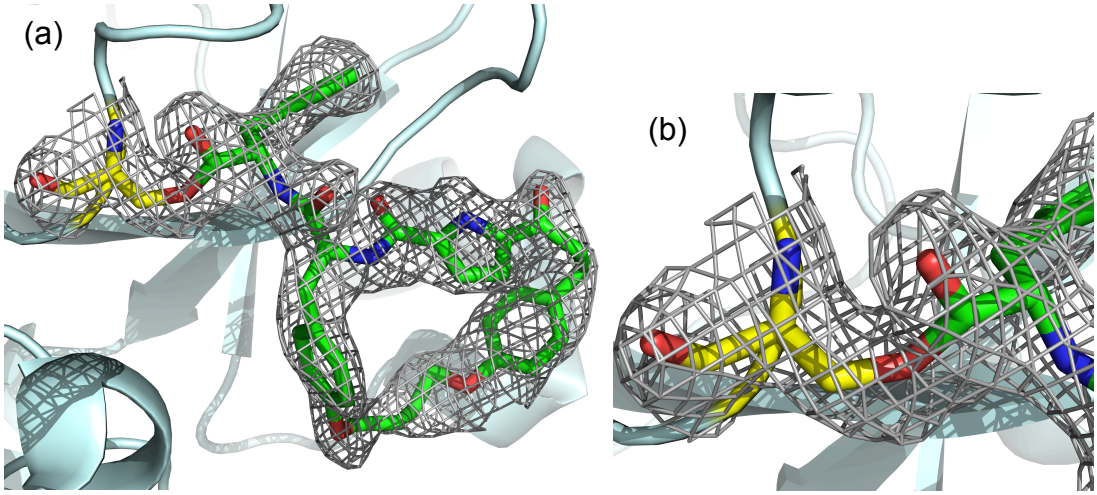

Figure 2.20 (a) $2F_o$-F_c kicked electron density map (in grey) of compound **2.13** contoured at 1σ, the inhibitor is displayed in sticks and the enzyme is displayed in ribbons; (b) an expansion to the region of Ser195 and the warhead.

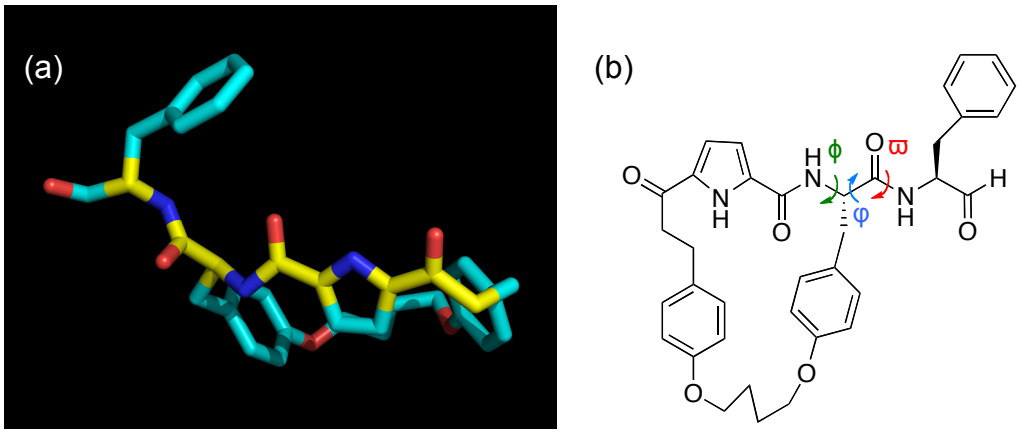

Figure 2.21 (a) X-ray crystallographic structure of compound **2.13** bound to α-chymotrypsin (backbone highlighted in yellow); (b) Structure of **2.13** showing the measured dihedral angles.

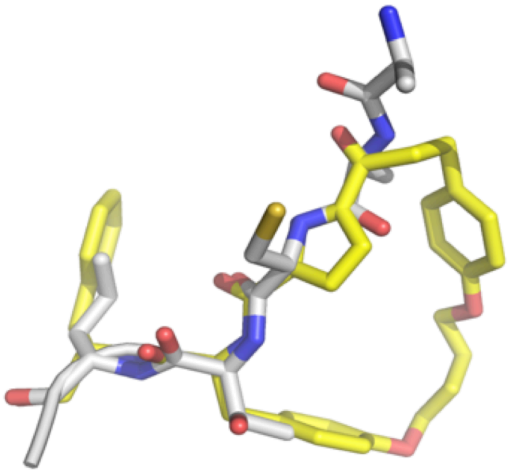

Figure 2.22 Superimposition of compound **2.13** with truncated PMP-C (PDB: 1GL1), a natural inhibitor of α-chymotrypsin.

Compound **2.13** forms a number of hydrogen bonding interactions with α-chymotrypsin's active site as illustrated in Figure 2.23. For example, the aldehyde oxygen of **2.13** interacts directly with the backbone amine of Ser195 and Gly193 that form the oxyanion hole. The oxyanion hole stabilises the negatively charged oxygen atom of the hemiacetal intermediate (Figure 2.24, green), which, in this case, is formed upon reaction with the aldehyde of compound **2.13**. This would be expected to enhance the potency of inhibitor **2.13.** Many of the hydrogen bonding interactions are mediated by water molecules. Two of these molecules, denoted as Hoh260 and Hoh491 in Figure 2.23, have particular importance in mediating hydrogen bonding interactions. Hoh260 interacts with Thr222 of the enzyme, C33 of the inhibitor and two other water molecules, while Hoh491 interacts with Gly216 and Ser217 of the enzyme, pyrrole NH and O30 of **2.13** and Hoh430. These hydrogen bonding interactions play crucial roles in the stabilisation of the α-

chymotrypsin-**2.13** complex. The binding affinity of the inhibitor is further enhanced by hydrophobic and ionic interactions with other critical active site residues, including His57 and Asp102 of the catalytic triad. Upon binding, the macrocycle linking P_2 and P_4 side chains of **2.13** lies exactly parallel to Trp215, which potentially results in π-π interactions with the enzyme.

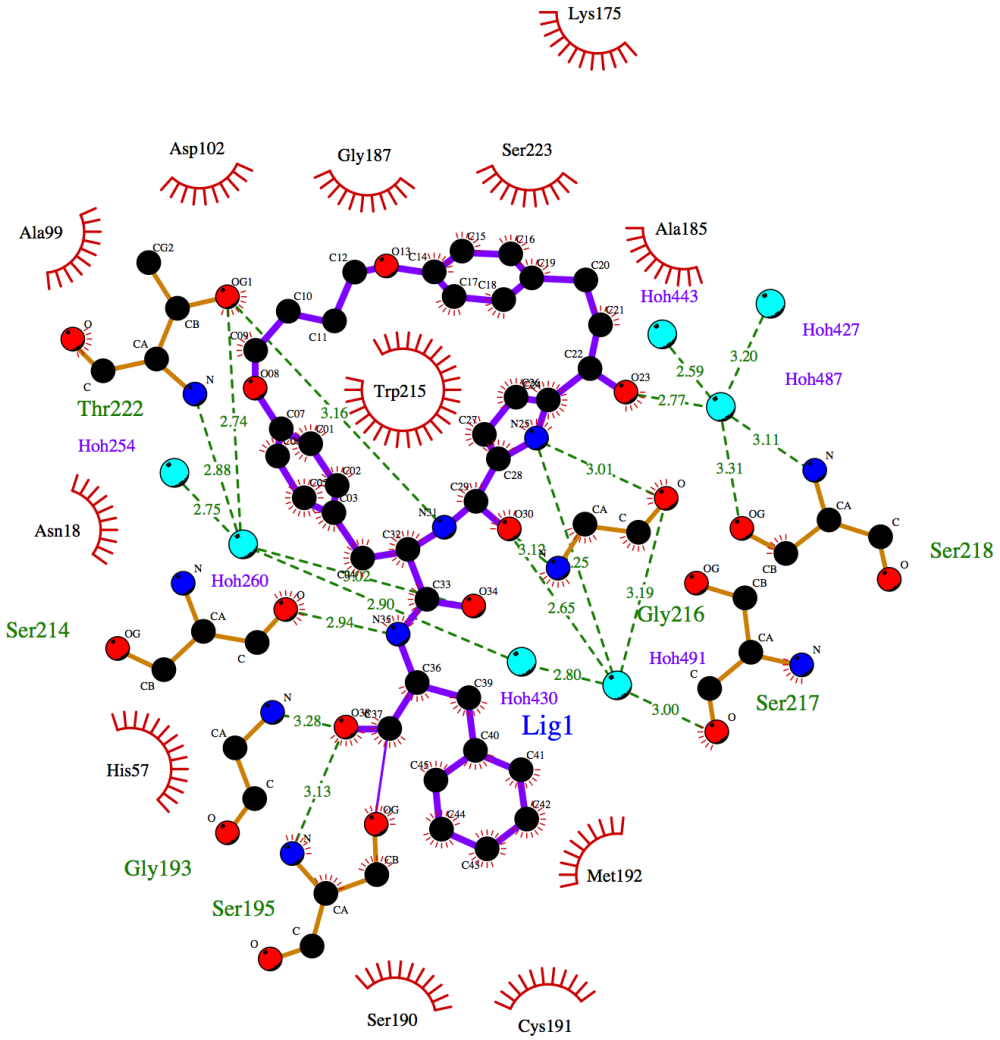

Figure 2.23 A ligplot showing non-covalent interactions of compound **2.13** and α-chymotrypsin. The inhibitor and amino acids of α-chymotrypsin involved in hydrogen bonding interactions are displayed in a ball-and-stick

representation. The amino acids involved in other non-covalent interactions are displayed as arcs

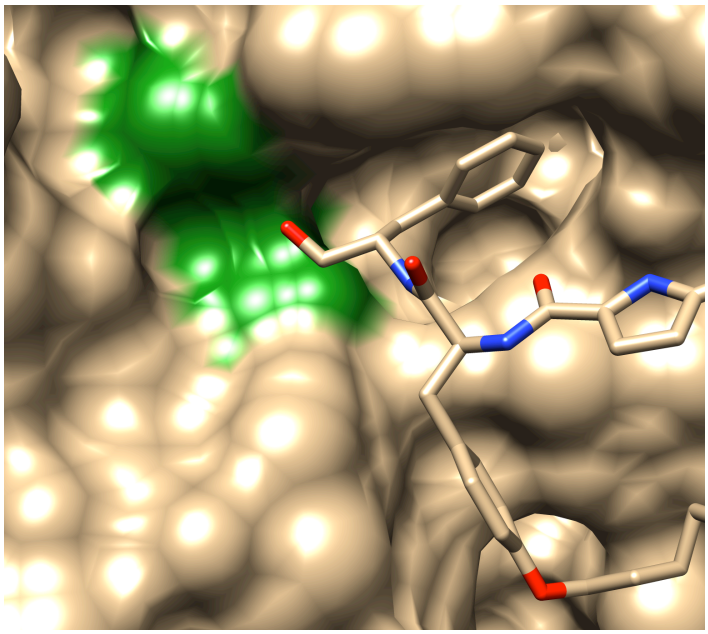

Figure 2.24 The oxyanion hole (in green) of chymotrypsin and compound **2.13**. The enzyme is displayed as surfaces and the inhibitor is displayed as sticks.

2.3 Conclusions

In summary, a new generation of P_2-P_4 cyclised peptidomimetic protease inhibitor was characterized by NMR and X-ray crystallography. The key features of these inhibitors include a pyrrole moiety replacing the P_3-P_4 amide bond of the inhibitor backbone and a macrocycle linking the P_2 and P_4 side chains. These features work in synergy to constrain the inhibitor backbone into an extended β-strand geometry while increasing the resistance to random

proteolysis. The P_2-P_4 cyclisation also allows easy modification of the P_1 residue, which is critical for providing selectivity and potency.

Analogues **2.12** and **2.13** are designed to specifically inhibit cysteine proteases and α-chymotrypsin respectively. The key Friedel-Crafts acylation, RCM and hydrogenation steps were carefully optimised to produce sufficient quantities of the desired inhibitors for mechanistic studies and in vivo biological experiments. In particular, a ^{13}C-labelled analogue of **2.13** (compound **2.14**) was synthesised to explore its mechanism of inhibition of α-chymotrypsin using NMR. In ^{13}C NMR, the labelling in **2.14** amplified the signal intensity of the aldehyde by 100-fold, making it easily distinguishable from other carbon signals of the inhibitor and enzyme. The poor water solubility of the inhibitor was overcome by increasing the DMSO content of the solvent system from 7.5% to 20%. The ^{13}C NMR spectrum of the inhibitor-enzyme complex shows a new resonance at 92 ppm corresponding to the hemiacetal formed on reaction of the aldehyde with the active site serine of α-chymotrypsin. Therefore it can be concluded that the aldehyde inhibitor **2.13** is a covalent inhibitor for α-chymotrypsin.

X-ray crystallography of the enzyme-inhibitor complex further confirmed that inhibitor **2.13** forms a hemiacetal intermediate with the active site serine of α-chymotrypsin upon binding. Furthermore, it demonstrates that the inhibitor binds to the enzyme in an extended β-strand-mimicking geometry. The crystal structure also reveals a number of important non-covalent interactions between the enzyme and the inhibitor, including hydrogen bonding, non-polar

and ionic interactions. These are critical for enhancing the activity of the inhibitor. The hemiacetal is further stabilized by the oxyanion hole in the S_1 subsite of α-chymotrypsin to further increase the binding affinity of inhibitor **2.13** into the low nanomolar range.

2.4 References

(1) Madala, P.; Tyndall, J. D. A.; Nall, T.; Fairlie, D. P. *Chem. Rev. (Washington, DC, U. S.)* **2010**, ACS ASAP.

(2) Loughlin, W. A.; Tyndall, J. D. A.; Glenn, M. P.; Fairlie, D. P. *Chem. Rev.* **2004**, *104*, 6085.

(3) Li, P.; Roller, P. P.; Xu, J. *Curr. Org. Chem.* **2002**, *6*, 411.

(4) Tyndall, J. D. A.; Nall, T.; Fairlie, D. P. *Chem. Rev. (Washington, DC, U. S.)* **2005**, *105*, 973.

(5) Pehere, A.; Abell, A. In *Proteases in Health and Disease*; Chakraborti, S., Dhalla, N. S., Eds.; Springer New York: 2013; Vol. 7, p 181.

(6) Leung, D.; Abbenante, G.; Fairlie, D. P. *J. Med. Chem.* **2000**, *43*, 305.

(7) Maurer-Stroh, S.; Debulpaep, M.; Kuemmerer, N.; de la Paz, M. L.; Martins, I. C.; Reumers, J.; Morris, K. L.; Copland, A.; Serpell, L.; Serrano, L.; Schymkowitz, J. W. H.; Rousseau, F. *Nat Meth* **2010**, *7*, 237.

(8) Fuchs, J. E.; von Grafenstein, S.; Huber, R. G.; Margreiter, M. A.; Spitzer, G. M.; Wallnoefer, H. G.; Liedl, K. R. *PLoS Comput Biol* **2013**, *9*, e1003007.

(9) Abell, A. D.; Hoult, D. A.; Jamieson, E. J. *Tetrahedron Lett.* **1992**, *33*, 5831.

(10) Chua, K. C. H.; Pietsch, M.; Zhang, X.; Hautmann, S.; Chan, H. Y.; Bruning, J. B.; Gütschow, M.; Abell, A. D. *Angew. Chem. Int. Ed.* **2014**, *53*, 7828.

(11) Angell, Y. L.; Burgess, K. *Chem. Soc. Rev.* **2007**, *36*, 1674.

(12) Angelo, N. G.; Arora, P. S. *J. Org. Chem.* **2007**, *72*, 7963.

(13) Valverde, I. E.; Bauman, A.; Kluba, C. A.; Vomstein, S.; Walter, M. A.; Mindt, T. L. *Angew. Chem. Int. Ed.* **2013**, *52*, 8957.

(14) Angelo, N. G.; Arora, P. S. *J. Am. Chem. Soc.* **2005**, *127*, 17134.

(15) Glenn, M. P.; Pattenden, L. K.; Reid, R. C.; Tyssen, D. P.; Tyndall, J. D. A.; Birch, C. J.; Fairlie, D. P. *J. Med. Chem.* **2001**, *45*, 371.

(16) Abell, A. D.; Jones, M. A.; Coxon, J. M.; Morton, J. D.; Aitken, S. G.; McNabb, S. B.; Lee, H. Y. Y.; Mehrtens, J. M.; Alexander, N. A.; Stuart, B. G.; Neffe, A. T.; Bickerstaffe, R. *Angew. Chem., Int. Ed.* **2009**, *48*, 1455.

(17) Tsantrizos, Y. S.; Bolger, G.; Bonneau, P.; Cameron, D. R.; Goudreau, N.; Kukolj, G.; LaPlante, S. R.; Llinàs-Brunet, M.; Nar, H.; Lamarre, D. *Angew. Chem. Int. Ed.* **2003**, *42*, 1356.

(18) Driggers, E. M.; Hale, S. P.; Lee, J.; Terrett, N. K. *Nat. Rev. Drug Discovery* **2008**, *7*, 608.

(19) Marsault, E.; Peterson, M. L. *J. Med. Chem.* **2011**, *54*, 1961.

(20) Meyer, J. H.; Bartlett, P. A. *J. Am. Chem. Soc.* **1998**, *120*, 4600.

(21) Ksander, G. M.; de Jesus, R.; Yuan, A.; Ghai, R. D.; McMartin, C.; Bohacek, R. *J. Med. Chem.* **1997**, *40*, 506.

(22) Chen, K. X.; Njoroge, F. G.; Arasappan, A.; Venkatraman, S.; Vibulbhan, B.; Yang, W.; Parekh, T. N.; Pichardo, J.; Prongay, A.; Cheng, K.-

C.; Butkiewicz, N.; Yao, N.; Madison, V.; Girijavallabhan, V. *J. Med. Chem.* **2006**, *49*, 995.

(23) Jones, M. A.; Coxon, J. M.; McNabb, S. B.; Mehrtens, J. M.; Alexander, N. A.; Jones, S.; Chen, H.; Buisan, C.; Abell, A. D. *Aust. J. Chem.* **2009**, *62*, 671.

(24) Jones, S. A.; Duncan, J.; Aitken, S. G.; Coxon, J. M.; Abell, A. D. *Aust. J. Chem.* **2014**, *67*, 1257.

(25) Neilsen, P. M.; Pehere, A. D.; Pishas, K. I.; Callen, D. F.; Abell, A. D. *ACS Chemical Biology* **2012**, *8*, 353.

(26) Morton, J. D.; Lee, H. Y. Y.; McDermott, J. D.; Robertson, L. J. G.; Bickerstaffe, R.; Jones, M. A.; Coxon, J. M.; Abell, A. D. *Investigative Ophthalmology & Visual Science* **2013**, *54*, 389.

(27) Wanichawan, P.; Hafver, T. L.; Hodne, K.; Aronsen, J. M.; Lunde, I. G.; Dalhus, B.; Lunde, M.; Kvaløy, H.; Louch, W. E.; Tønnessen, T.; Sjaastad, I.; Sejersted, O. M.; Carlson, C. R. *J. Biol. Chem.* **2014**, *289*, 33984.

(28) Corvo, I.; O'Donoghue, A. J.; Pastro, L.; Pi-Denis, N.; Eroy-Reveles, A.; Roche, L.; McKerrow, J. H.; Dalton, J. P.; Craik, C. S.; Caffrey, C. R.; Tort, J. F. *PLoS Negl Trop Dis* **2013**, *7*, e2269.

(29) Pehere, A. D.; Abell, A. D. *Org. Lett.* **2012**, *14*, 1330.

(30) Song, Z. J.; Tellers, D. M.; Journet, M.; Kuethe, J. T.; Lieberman, D.; Humphrey, G.; Zhang, F.; Peng, Z.; Waters, M. S.; Zewge, D.; Nolting, A.; Zhao, D.; Reamer, R. A.; Dormer, P. G.; Belyk, K. M.; Davies, I. W.; Devine, P. N.; Tschaen, D. M. *The Journal of Organic Chemistry* **2011**, *76*, 7804.

(31) Grisi, F.; Costabile, C.; Grimaldi, A.; Viscardi, C.; Saturnino, C.; Longo, P. *Eur. J. Org. Chem.* **2012**, *2012*, 5928.

(32) Ersmark, K.; Nervall, M.; Gutiérrez-de-Terán, H.; Hamelink, E.; Janka, L. K.; Clemente, J. C.; Dunn, B. M.; Gogoll, A.; Samuelsson, B.; Åqvist, J.; Hallberg, A. *Biorg. Med. Chem.* **2006**, *14*, 2197.

(33) Poupart, M.-A.; Cameron, D. R.; Chabot, C.; Ghiro, E.; Goudreau, N.; Goulet, S.; Poirier, M.; Tsantrizos, Y. S. *The Journal of Organic Chemistry* **2001**, *66*, 4743.

(34) Goudreau, N.; Brochu, C.; Cameron, D. R.; Duceppe, J.-S.; Faucher, A.-M.; Ferland, J.-M.; Grand-Maître, C.; Poirier, M.; Simoneau, B.; Tsantrizos, Y. S. *The Journal of Organic Chemistry* **2004**, *69*, 6185.

(35) Hedstrom, L. *Chem. Rev.* **2002**, *102*, 4501.

(36) Lowe, G.; Nurse, D. *J. Chem. Soc., Chem. Commun.* **1977**, 815.

(37) Groutas, W. C.; Stanga, M. A.; Brubaker, M. J. *J. Am. Chem. Soc.* **1989**, *111*, 1931.

(38) Neidhart, D.; Wei, Y.; Cassidy, C.; Lin, J.; Cleland, W. W.; Frey, P. A. *Biochemistry* **2001**, *40*, 2439.

Chapter 3

The Design and Synthesis of the 26S Proteasome Inhibitors

3.1 Introduction

3.1.1 The Role of the 26S Proteasome in Cancer Development and Treatment

It is widely reported that tumour cells generally express a higher level of the 26S proteasome than non-cancerous cells.[1-3] This is because the proteasome is responsible for the degradation of crucial proteins controlling cell-cycle progression[4], cell proliferation[5] and apoptosis[6]. The up-regulation of proteasome helps the cancer cells to escape cell cycle and apoptosis thus ultimately enables them to stay immortal.[7] Inhibiting the proteasome has significant clinical relevance since it results in the restoration of cell cycle and apoptosis of cancer cells.[8]

The most important substrates for the proteasome such as cyclins and cyclin-dependent kinases (CDKs),[9] caspases,[10] and tumour suppressors[11] all play key roles in maintaining a healthy cell cycle. In mammals, cyclins provide tight control to all stages of the cell cycle through interactions with CDKs (Figure 3.01): cyclin D and E are known to regulate cell growth (G1) phase; cyclin E and A act during the DNA synthesis phase (S); in addition, cyclin A and B dictate cell proliferation and differentiation through regulation of the mitosis phase (M).[12] Cyclins are rapidly turned over by the ubiquitin-proteasome pathway. The precisely programmed degradation of cyclins by the proteasome is the key to promote cell growth and proliferation. Therefore the

inhibition of this proteasome-mediated degradation can lead to cell cycle arrest and ultimately, apoptosis.[13]

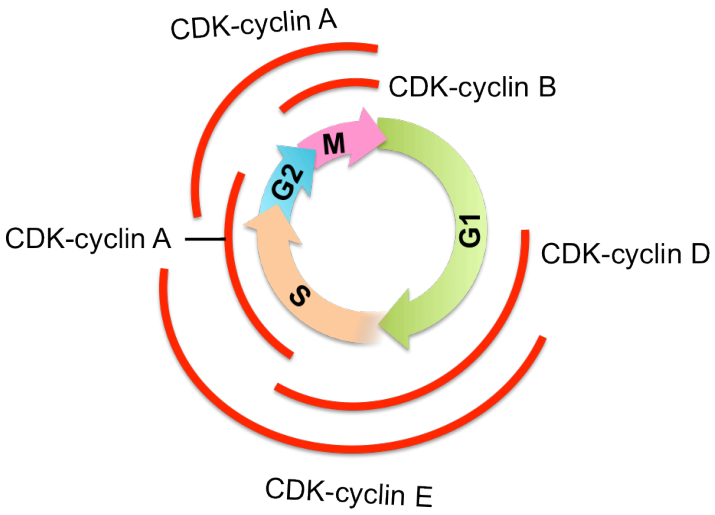

Figure 3.01 Cyclins and CDKs are involved in the regulation of all cell cycle stages. Red lines represent the stages that each cyclin has impact on. Figure adapted from Adams.[9]

In addition, the proteasome can cause an increase or decrease in apoptotic activity through the modulation of caspases.[14] Amongst the total of 12 caspases identified to date, caspase-8 and caspase-3 are specifically recognized as essential for cell apoptosis.[15] The proteasome regulates caspases through various pathways. For example, the proteasome-mediated activation of NF-kB inactivates the caspases to enable the survival of the cell. To promote apoptosis, the proteasome activity needs to be inhibited to prevent the activation of NF-κB thus potentiate caspase activity.[16]

The p53 tumour suppressor is another crucial substrate of the proteasome that is present in low quantities in normal cells.[17] Multiple stimuli in the tumour

cells such as DNA damage and hypoxia lead to accumulation of the p53 protein, which triggers responses including cell-cycle arrest, DNA repair, differentiation and apoptosis.[18] MDM2, a ubiquitin ligase that tags the p53 protein for degradation by the proteasome is often overexpressed in cancer cells.[19] The use of proteasome inhibitors to attack these cancer cells is a valid approach to salvaging the p53 regulatory cascade and inducing apoptosis of these tumour cells.[20]

The fact that the proteasome is crucial for the growth, proliferation and apoptosis for all cells indicates that compounds that induce proteasome inhibition in a highly controlled manner, preferentially specific to neoplastic cells, have great potential for treating cancer.[21] However, it is challenging to selectively target proteasome in cancer cells and maintain a reasonable therapeutic window for non-cancerous cells since the proteasome in both cell types are anticipated to have similar mechanism.[9] Nevertheless, experimental results show that the malignant cells are more sensitive to proteasome inhibition than non-cancerous cells, which makes the proteasome an ideal target for treatment of cancers.[22-24] The downstream mechanism for the increased susceptibility of malignant versus normal cells to proteasome inhibitors has not been conclusively determined.

3.1.2 Limitations of Existing Proteasome Inhibitors

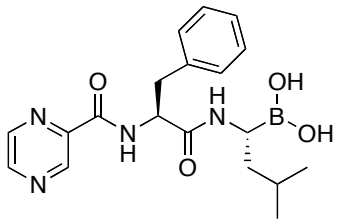

Bortezomib

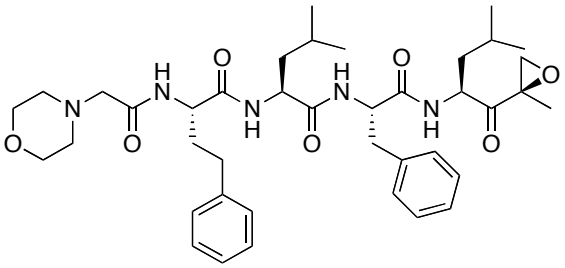

Carfilzomib

Figure 3.02 The structures of two FDA-approved drugs for treating multiple myeloma, bortezomib and calfilzomib.

Despite having high efficacy in the treatment of multiple myeloma, both bortezomib and carfilzomib still possess major limitations: 1) approximately 30% of patients develop neuropathy due to bortezomib's off-target inhibition of an ATP-dependent protease in mitochondria.[25] In extreme cases, this side effect can be lethal. Bortezomib also induces other serious side-effects including shingles and digestive abnormality.[26] On the other hand, carfilzomib has significantly reduced side effects compared to bortezomib due to high specificity for the proteasome.[27] However, its toxic side effects resulted in 24 deaths (9% of patients) in a phase II clinical trial.[28] Peripheral edema are also commonly observed in patients treated with carfilzomib.[29] The exact mechanisms that cause these side effects remain unknown; 2) bortezomib, in particular, has very narrow therapeutic window. The therapeutic dose of bortezomib is 1.3 mg/m^2, whereas 1.6 mg/m^2 produced dose-limiting toxic effects in phase I studies.[30] New proteasome inhibitors with higher selectivity for cancer cells over normal cells are required to enhance the therapeutic

window; 3) drug resistance remains one of the most clinically significant problems of proteasome inhibitors, where 65% of myeloma patients are resistant to bortezomib.[31] Treated human leukemia cell lines showed over-expression of the chymotrypsin-like subunit of the proteasome, which also bears a mutation in the active site that makes binding of inhibitors largely unfavourable.[32] This provides a possible explanation for the prominent drug resistance associated with proteasome inhibitors. To overcome these limitations, there is a real need for a new class of proteasome inhibitors with improved potency, selectivity for cancer cells over non-cancerous cells, and reduced off-target effects.

3.2 Results and Discussion

3.2.1 The Design of the Proteasome Inhibitors

MG132 is a potent inhibitor for all three main catalytic activities of the proteasome, which may cause potential side effects.[33] A new variant of MG132 has been developed to selectively target the chymotrypsin-like activity (CT-L) of the proteasome.[34] These inhibitors display the following features: 1) they all bear leucine or isoleucine at P_2 since a sterically bulky substituent at this position is known to enhance selectivity for CT-L activity; 2) an aryl group was incorporated at P_1 to interact with the large hydrophobic S_1 pocket of CT-L activity; 3) an N-terminal Cbz group was incorporated to probe the S_4 binding pocket in an attempt to improve specificity and potency. The inhibitors also bear unique aliphatic azide at P_3 to provide additional opportunities for

hydrogen bonding interactions with the binding pockets. The aryl amino acid at P_1 contains an unusual acetylenic group to further probe this binding pocket. This substituent also provided an opportunity to cyclise the P_1 to P_3 through [3+2] azide-alkyne cycloaddition. Such macrocycle stabilises a β-strand conformation of the backbone, which is known to universally favoured for binding to proteases (discussed in detail in section 2.1.1).

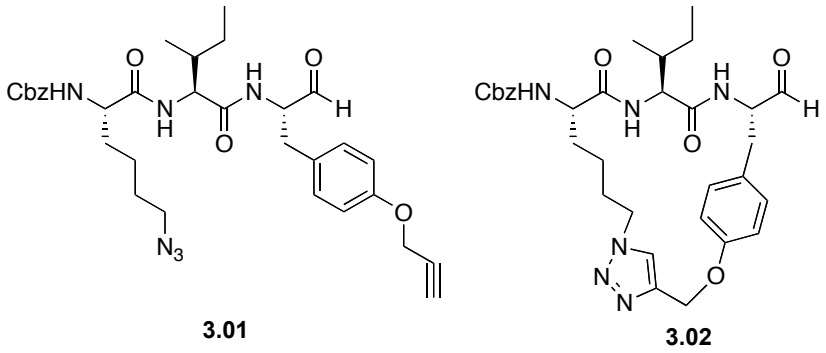

Figure 3.03 Representative inhibitors **3.01** and **3.02** developed by Pehere and Abell et al. Inhibitor **3.01** is an acyclic tripeptidic aldehyde while inhibitor **3.02** is a macrocyclic tripeptidic aldehyde.

In vitro assays and subsequent *in vivo* cell cytotoxicity data revealed that these inhibitors had extremely high selectivity for CT-L activity over the other two activities. In general, the acyclic inhibitors were significantly more potent than the macrocyclic inhibitors. For example, **3.01** (Figure 3.03) had an IC_{50} of 21 nM, which is 10-fold more potent than the corresponding macrocyclic inhibitor **3.02** (IC_{50} = 250 nM) and is slightly more potent than a related inhibitor differs only by a leucine at the P_2 position. Inhibitor **3.01** was also more potent than bortezomib in the *in vitro* assay. More importantly, this

inhibitor demonstrated an 1.55-fold larger therapeutic window compared to bortezomib in the in vivo cellular assays, which makes it a promising pharmacophore. However, cell cytotoxicity assay showed that bortezomib was much more cytotoxic to most cancer cells than **3.01**. Therefore improving potency of **3.01** while retaining or even enlarging its therapeutic window is greatly desirable.

Another series of interesting protease inhibitors developed by Chua and Abell et al.[35] showed excellent potential as proteasome inhibitors (Figure 3.04). The current proteasome inhibitors commonly have peptidic backbones that are prone to non-specific proteolytic degradation in in vivo enviroments. This has significant impact on the effectiveness of the inhibitors. To overcome this limitation, the newly developed inhibitors bear a pyrrole residue in the peptide backbone to reduce the peptide-like character of the compounds, making them highly resistant to off-target protease degradation. The pyrrole is also responsible for restraining the peptide backbone into the desired beta-strand conformation. This is particularly desirable since the proteasome, like most other proteases, prefers to bind substrate with extended geometry but disfavors inhibitors with macrocycles due to increased rigidity.[36] This series of inhibitors showed promising activity against a plethora of proteases including calpains, α-chymotrypsin and cathepsins. In particular, compound **3.03** (Figure 3.04) is a potent inhibitor for α-chymotrypsin with a K_i of 33 nM. This inhibitor was thought to be a potential candidate for inhibiting the proteasome since α-chymotrypsin closely resembles the CT-L activity of the proteasome. Amongst the 12 inhibitors of this series tested in *in vitro* assays against the

20S proteasome, only **3.04** (Figure 3.04), the acyclic analogue of **3.03** with a leucine at P_1, showed weak inhibitory activity at the concentration of 25 μM for the CT-L subunit and no inhibition for other activities (unpublished data). All other inhibitors of this type were inactive against the proteasome. Further modification of **3.04** is required to maintain the specificity for CT-L activity while the potency needs to be significantly increased.

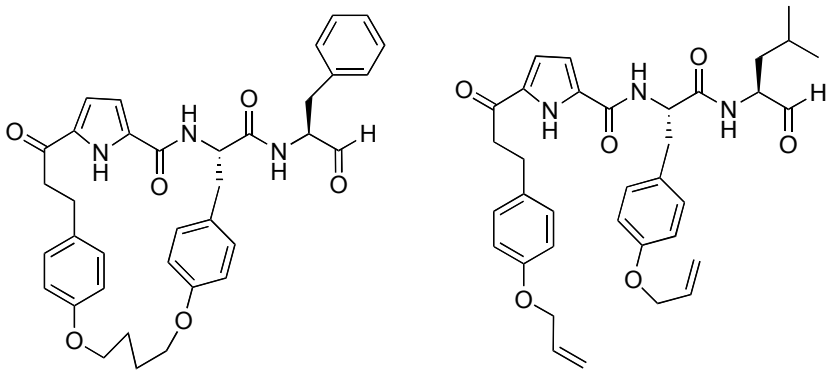

3.03 **3.04**

Figure 3.04 Representative protease inhibitors **3.03** and **3.04** developed by Chua and Abell et al. **3.03** is a macrocyclic peptidic aldehyde inhibitor while **3.04** is an acyclic peptidic aldehyde inhibitor.

A new class of acyclic proteasome inhibitors (see compounds **3.05**-**3.08** in Figure 3.05) was designed to combine the P_2-P_4 or P_2-P_3 templates of the previously identified inhibitors **3.01** and **3.04** with a boronate warhead on the *C*-terminus. A boronate is known to inhibit the proteasome with much higher selectivity compared to an aldehyde with potentially reduced off-target effects. The favourable characteristics such as the P_2 isoleucine and P_3 azide of **3.01** and the pyrrole isostere of **3.01** are maintained. This leads to target

compounds presented in Figure 3.05, with the specific design of each discussed in detail in the following section.

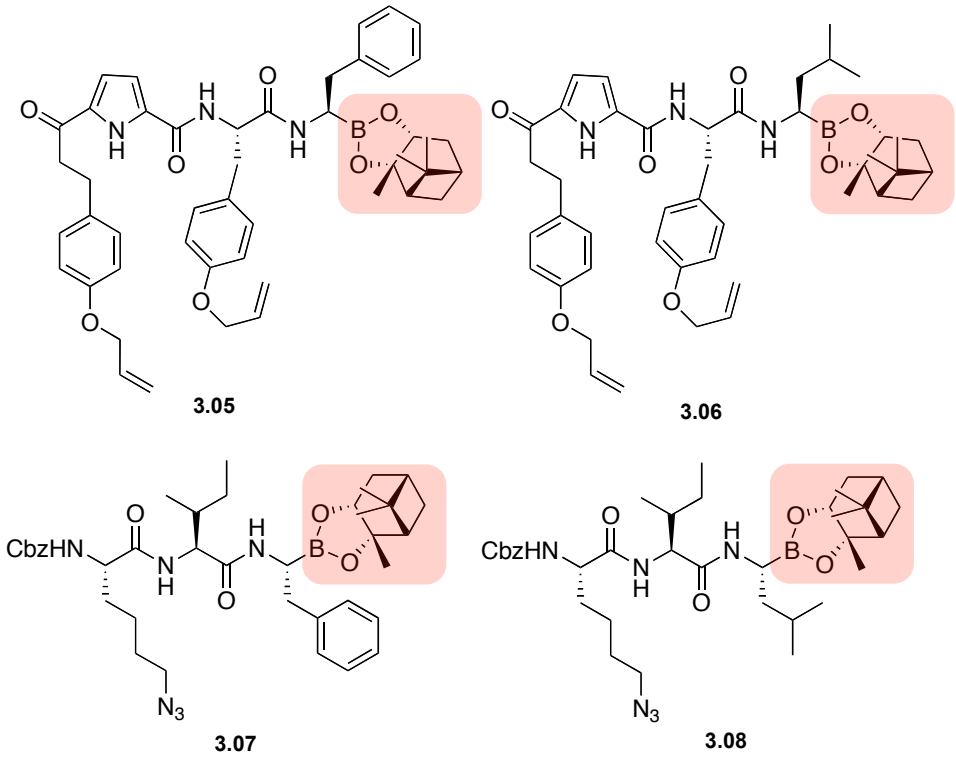

Figure 3.05 Structures of the four target compounds **3.05-3.08**. The *C*-terminal boronate is highlighted in pink.

Compounds **3.05** and **3.06** were designed based on inhibitor **3.04** (Figure 3.04) that is a weak inhibitor of the CT-L activity of the proteasome at 25 μM. Both of the new compounds bear a pyrrolic moiety that replaces the peptide bond in the backbone as well as the aromatic groups at P_2 and P_4 capable of binding with the deep, hydrophobic S_2 and S_4 pockets.[37] However, the two compounds have different P_1 residues. Compound **3.06** has a leucine at P_1 as found in most known inhibitors.[38-40] In comparison, **3.05** has a phenylalanine at this position since the S_1 binding pocket is known to favour the binding of a

large hydrophobic group.[41] Limited work has been done to explore these types of interactions.

Compounds **3.07** and **3.08** differ only at P_1. The P_2 and P_3 substituents are based on the most potent inhibitor **3.01** (Figure 3.03) identified by Pehere & Abell et al. This P_2-P_3 template provides compounds with high potency against the proteasome.[34] The template consists of a preferred isoleucine at P_2, aliphatic azide at P_3 with a Cbz group to interact with the S_4 pocket. The P_1 phenylalanine of **3.07** favours binding with the hydrophobic S_1 pocket as observed with a potent inhibitor **3.01**. Compound **3.08** has a leucine residue that is also favoured by the S_1 pocket of the proteasome.

Boronic acids are challenging to synthesise and difficult to fully characterise as they form a number of complexes with water. A related *C*-terminal boronate that is easier to synthesise and characterise, while retaining the potency, would be beneficial. The activity of 36 peptide boronic pinanediol esters against human 20S proteasome has been reported, of these, 29 showed low-nanomolar inhibition. In addition, bortezomib-pinanediol ester has very similar IC_{50} (1.92 nM) compared to bortezomib (IC_{50} = 1.90 nM).[42] This suggests that boronic pinanediol esters are capable of retaining the inhibitory potencies against the proteasome, possibly indicating this ester is a prodrug for the active free acid. This remains to be confirmed. The same boronic pinanediol ester (highlighted in pink, Figure 3.05) was used in the current study. This chiral ester also defines the absolute configuration of the P_1 group

during the synthesis. This then negates the need for the final deprotection to produce boronic acid.

3.2.2 The Synthesis of Target Inhibitors 3.05-3.08

The target compounds **3.05** and **3.06** was prepared from a common acyclic P_2-P_4 template **3.09**, which was produced by hydrolysis of **2.26**, an intermediate in the synthesis of the inhibitors **2.12** and **2.13** (Scheme 3.01). The synthesis of **2.26** is discussed in detail in section 2.3.1 (see Scheme 2.5-2.7).

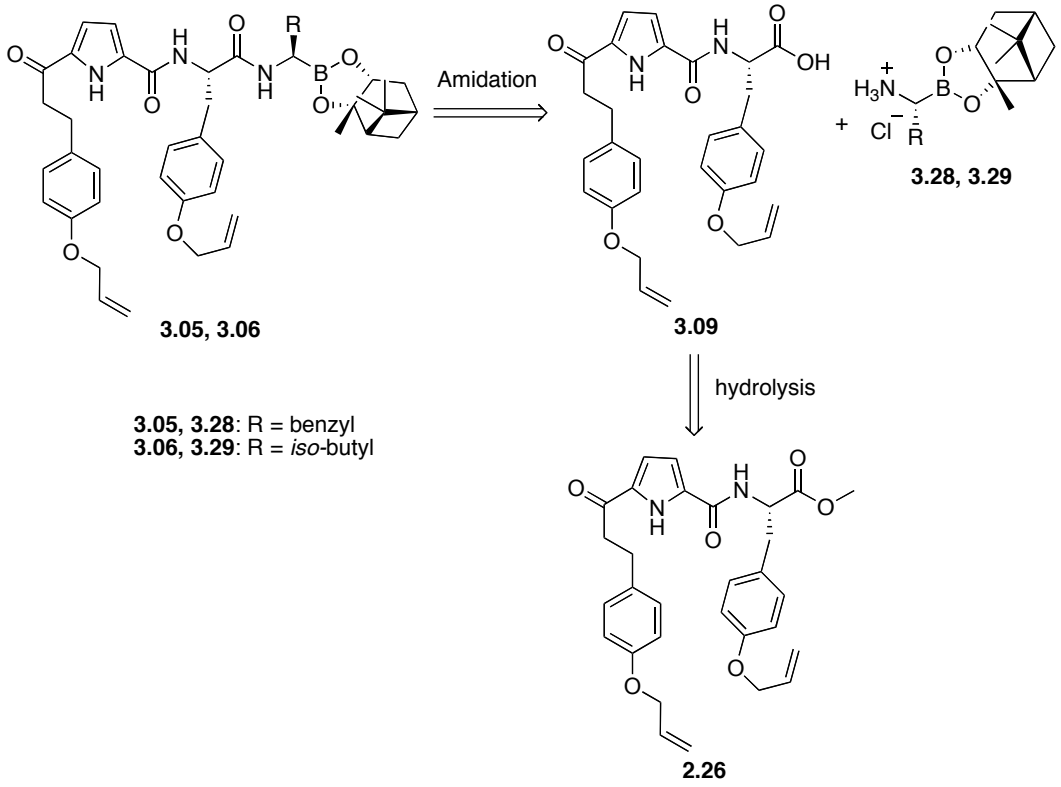

Scheme 3.01 Retrosynthetic analysis of **3.05** and **3.06**.

As for compounds **3.05** and **3.06**, target compounds **3.07** and **3.08** would be prepared by coupling the common acyclic template **3.15**[35] with amino boronates **3.28** or **3.29**. This template would be obtained in two steps from two key intermediates **3.11** and **3.13**. Compound **3.11** would be obtained from the conversion of the side-chain amine of the commercially available Cbz protected lysine **3.10** to the corresponding azide.

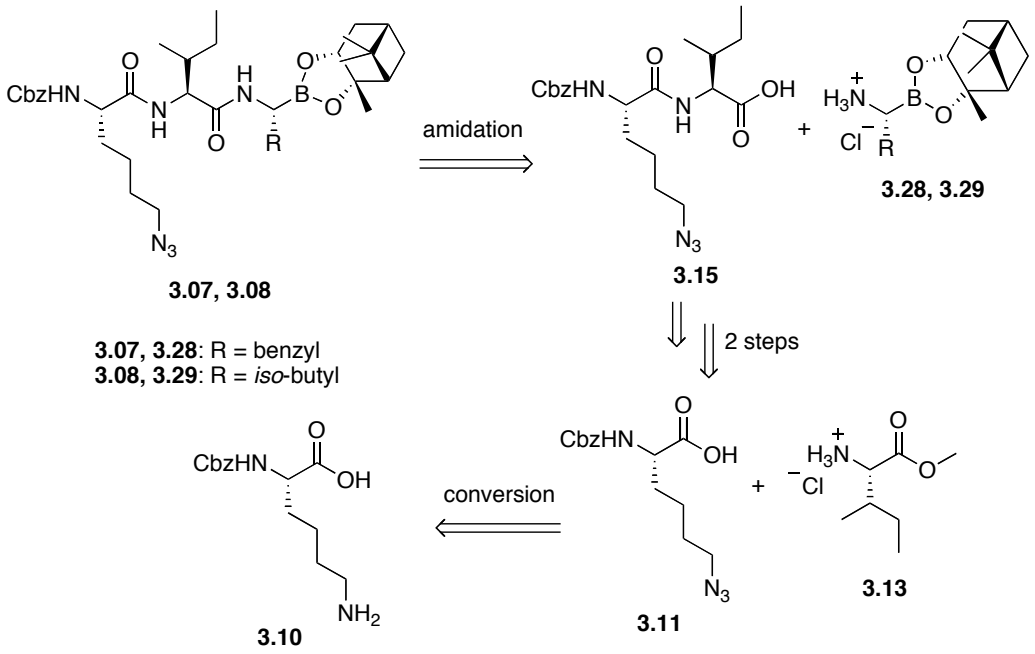

Scheme 3.02 Retrosynthetic analysis of **3.07** and **3.08**.

The key azide **3.11** was prepared by treating commercially available Cbz-Lys-OH (**3.10**) with triflic azide under basic conditions. The presence of an azide was confirmed by the characteristic absorption at 2100 cm^{-1} in the FTIR spectrum (Figure 3.06). Compound **3.11** was subsequently coupled with compound **3.13** in the presence of EDCI, HOBt and DIPEA to give the dipeptide **3.14**. Amino acid **3.13** was prepared by concomitant Boc-

deprotection and *C*-terminal methylation of Boc-Ile-OH (**3.12**). Hydrolysis of the methyl ester of **3.14** in the presence of LiOH then gave the free acid **3.15**.

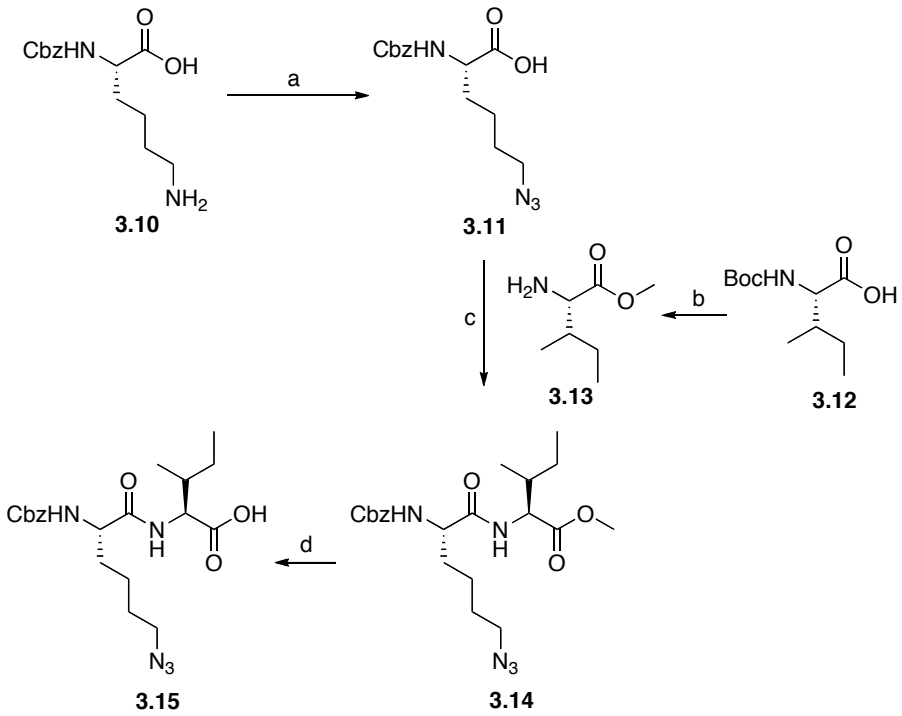

Scheme 3.03 Reagents and conditions: a) triflic anhydride, NaN_3, ACN, N_2, 0 ^oC, 2 h then; Et_3N, $CuSO_4.5H_2O$, H_2O/CH_3CN, 0 ^oC-r.t., 21 h, (28%); b) $SOCl_2$, DMF, MeOH, r.t., 5 h, (quant.); c) EDC, HOBt, DIPEA, DCM, N_2, r.t., 21 h, (36%); d) LiOH, THF/H_2O, r.t., 18 h, (93%).

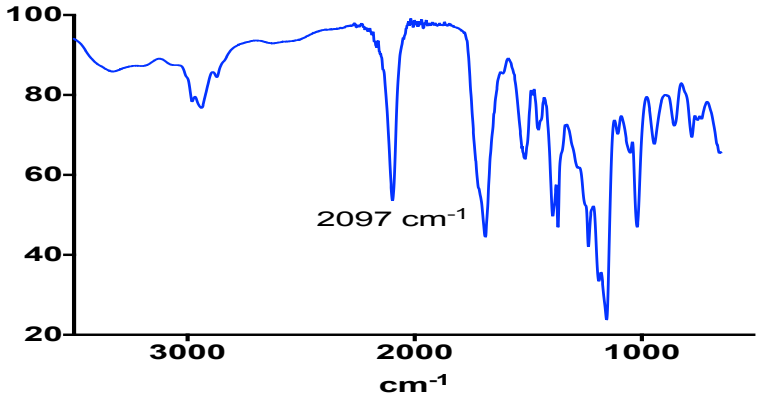

Figure 3.06 FTIR spectrum of compound **3.11**.

Compound **3.20** was initially targeted as a key intermediate to the final product **3.29**.[43] Isobutylboronic acid **3.16** was treated with optically pure, commercially available (+)-pinanediol to obtain isobutylboronic pinanyl ester **3.18**. This was then added to a solution of $LiCHCl_2$ in anhydrous THF at -100°C under N_2**.** $LiCHCl_2$ was prepared by either treating anhydrous DCM with *n*-BuLi at -100 °C, or with LDA at -78 °C. The reaction was gradually allowed to warm to room temperature overnight and the product was analysed by NMR, which revealed the presence of both the starting material **3.18** and the desired product **3.20** in a ratio of 1:9 (Figure 3.07). Product formation was not obtained unless freshly titrated *n*-BuLi or LDA was used. It was not possible to isolate the desired product by flash column chromatography, despite investigating a number of different solvent systems. Therefore, an alternative synthetic route was investigated.

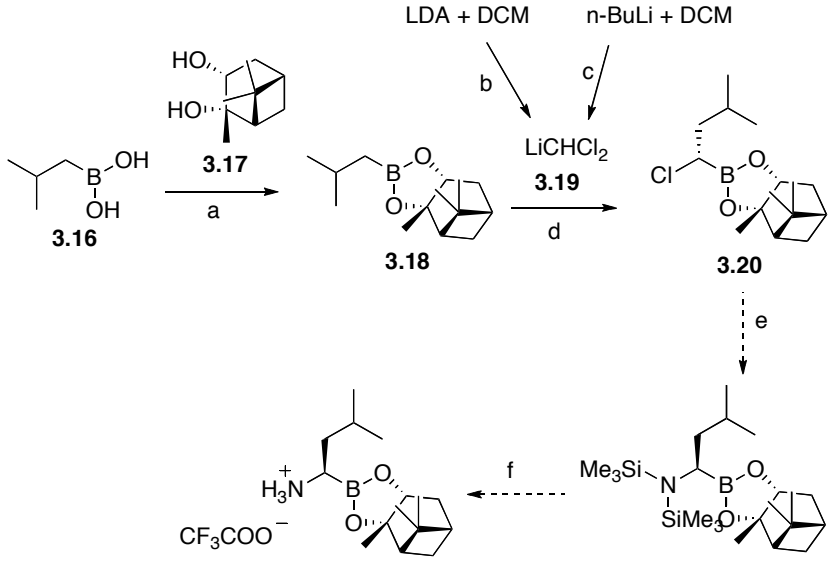

Scheme 3.04 Reagents and conditions: a) (+)-pinanediol, Et_2O, r.t., 18 h, (45%); b) THF, N_2, -78 °C, 2 h (quant.); c) THF, N_2, -100 °C, 40 min, (quant.);

d) $ZnCl_2$, THF, N_2, -100 ^oC, 18 h, (crude yield ~90%); e) LiHMDS, THF, N_2, -78 ^oC, 18 h; f) TFA, DCM, 0 ^oC, 2 h.

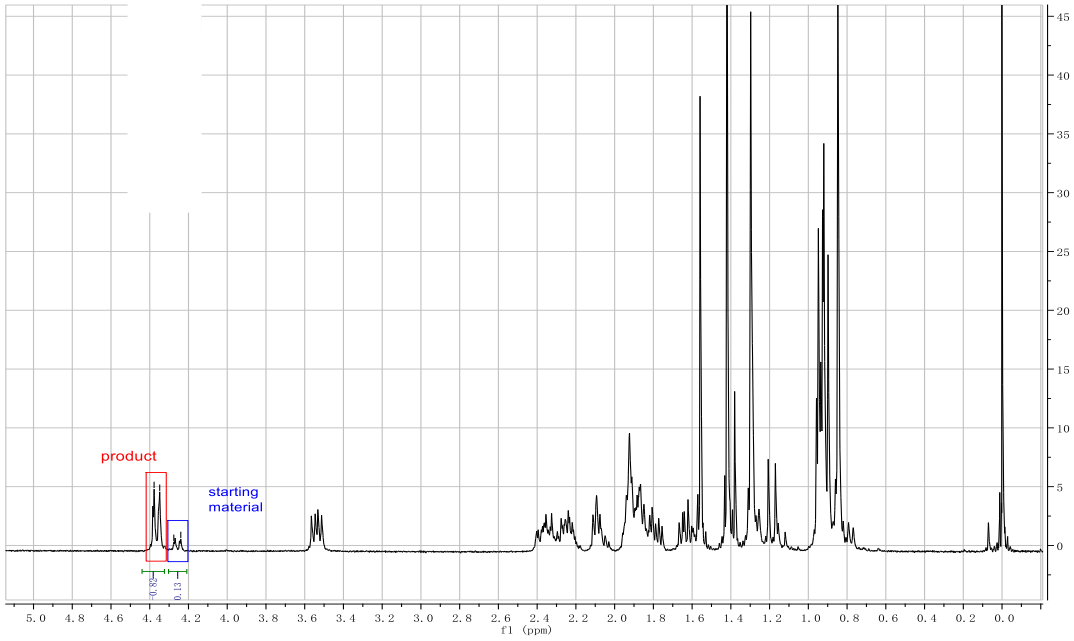

Figure 3.07 ^1H NMR of compound **3.20** showing trace amount of starting material.

The desired amino boronates **3.28** and **3.29** were however successfully obtained as outlined in Scheme 3.5.[42] $LiCHCl_2$ prepared as above (Scheme 3.04, step c) was treated with trimethyl borate to give **3.22**. This was subsequently transesterified on reaction with (+)-pinanediol to give dichloro-boronate **3.23** in excellent yield. This intermediate was separately treated with either benzylmagnesium bromide or isobutylmagnesium bromide in the presence of $ZnCl_2$ to give the mono-substituted chloroboronates **3.24** and **3.25** respectively in good yields. S_N2 reaction of **3.24** or **3.25** with LiHMDS freshly prepared in anhydrous THF gave intermediate **3.26** and **3.27**, which were not isolate but simply treated with HCl in Et_2O to remove the TMS

groups to give the desired amino boronate **3.28** and **3.29** in good yields. The reaction of **3.24** with commercially available LiHMDS solution gave only a 20% yield of **3.28**. The reaction was also attempted using commercially available solid LiHMDS, which was dissolved in anhydrous THF immediately before the reaction. This, however, only gave a slightly improved yield of 35%.

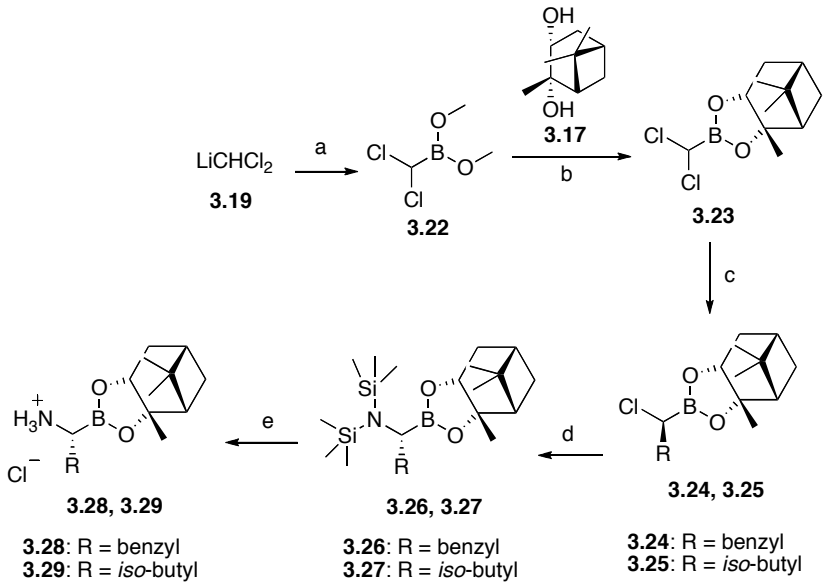

Scheme 3.05 Reagents and conditions: a) $B(OCH_3)_3$, THF, N_2, -100 ^oC-r.t., 40 min (quant.); b) (+)-pinanediol, Et_2O, r.t., 18 h, (88%); c) benzylmagnesium bromide or isobutylmagnesium bromide, $ZnCl_2$, Et_2O, N_2, -78 ^oC-r.t., 18 h, (**3.24**: 68%, **3.25**: 50%); d) LiHMDS, THF, N_2, -78 ^oC-r.t., 18 h; and e) 2 M HCl in Et_2O, petroleum ether, N_2, -78 ^oC-r.t., 12 h, (**3.28**: 79% over 2 steps, **3.29**: 60% over 2 steps).

A number of alternative acidic conditions for the deprotection of the TMS group of **3.26** and **3.27** were investigated in an attempt to improve the yield of **3.28** and **3.29** repsectively (Table 3.01). TFA was initially selected according to literature[44] but gave no desired product (Entry 1). The conventional

deprotection method with 4 M HCl in dioxane (Entry 2) successfully removed the TMS groups as indicated by TLC analysis. However, the product failed to form precipitation, resulting in difficult product isolation. With 2 M HCl in Et_2O and compound **3.26** dissolved in Et_2O (Entry 3), there was a limited precipitation leading to a low yield of 26%. Deprotection with 2 M HCl in ether and petroleum ether for starting material dissolution[42] (Entry 4) gave the highest yield (67%) compared to all other entries and enabled easy isolation of product by vacuum filtration. Therefore, the most optimal method, entry 2, was used to deprotect all amino boronates in this chapter.

Table 3.01 Optimisation of acid-catalysed TMS deprotection of **3.28**

Entry	Type of acid	Acid concentration	Solvent for acid	Solvent for **3.40**	Yield of **3.42** (Over 2 steps)
1	TFA	25%	--	DCM	0%[b]
2	HCl	4 M	dioxane	THF	0%[a]
3	HCl	2 M	Et_2O	Et_2O	26%
4	HCl	2 M	Et_2O	petroleum ether	67%

[a] Compound could not be isolated since it did not precipitate in THF;
[b] Removal of TFA and DCM in vacuo gave incorrect products.

Inhibitors **3.05-3.08** were prepared using the thus prepared key amino boronates **3.28** or **3.29.** In particular, pyrrole-containing peptide **3.09** was coupled with phenylalanine boronate **3.28** or leucine boronate **3.29** in the presence of HATU and DIPEA to give inhibitors **3.05** and **3.06** respectively.

The acyclic peptide **3.15** was also coupled with the same boronates to give inhibitors **3.07** and **3.08**. All four inhibitors were purified by RP-HPLC for subsequent biological experiments (for details see Sections 3.4 and 3.5). The integrity and purity of all four inhibitors were confirmed by proton NMR. An example is included in Figure 3.08 showing the proton NMR of compound **3.07**. The multiple small peaks at 1-2.5 ppm are the characteristic feature for a boronic pinanediol ester.

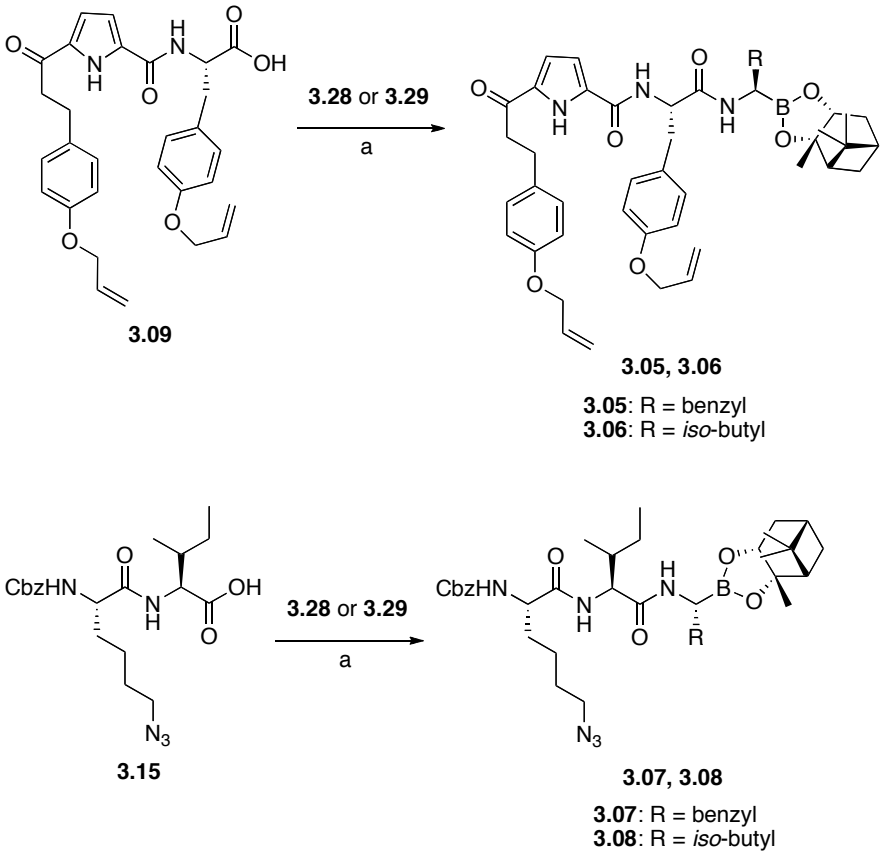

Scheme 3.07 Reagents and conditions: a) HATU, DIPEA, DMF, N_2, r.t. 21 h, (**3.05**: 38%, **3.06**: 16%, **3.07**: 10%, **3.08**: 15%)*.

* Yields calculated after RP-HPLC purification.

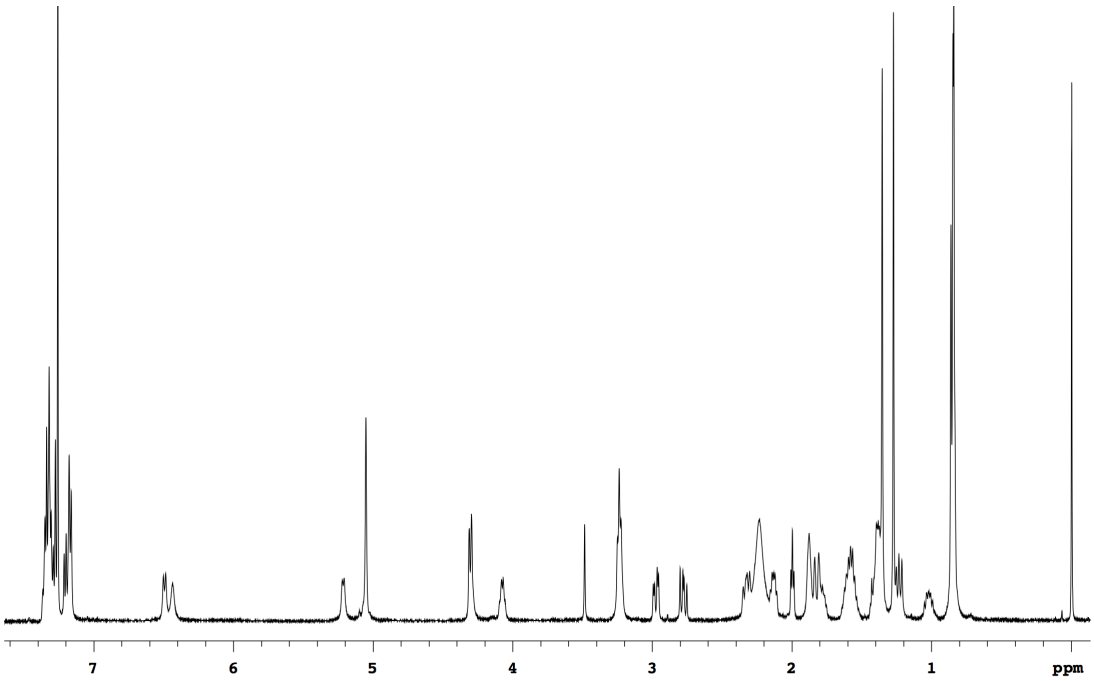

Figure 3.08 ^{1}H NMR ($CDCl_3$, 600 MHz) of compound **3.07**.

3.2.3 In vitro Inhibition Assays with Pure Rabbit 20S Proteasome

All four inhibitors were assayed against the chymotrypsin-like activity (CT-L), trypsin-like activity (T-L) and caspase-like activity (C-L) of the purified 20S proteasome. Bortezomib, carfilzomib and bortezomib ester were also assayed under the same conditions to provide references. The structures of the assay compounds are presented in Figure 3.11.

Each activity was assayed using a specific substrate bearing a 7-amino-4-methylcoumarin group (AMC, Figure 3.09, insert) as a fluorescent tag to allow monitoring of the enzyme activity. The substrates used were Suc-LLVY-AMC for CT-L,[45] Bz-VGR-AMC for T-L[45] and Ac-nLPnLD-AMC for C-L[46]. A schematic representation of the assay is provided in Figure 3.09. The proteasome-catalysed cleavage of the substrate releases an

aminomethylcoumarin group that has greater fluorescence compared to the methylcoumarin amide substrate. The fluorescence can be measured overtime. The addition of a proteasome inhibitor reduces the cleavage, leading to a lower rate of fluorecence increase.

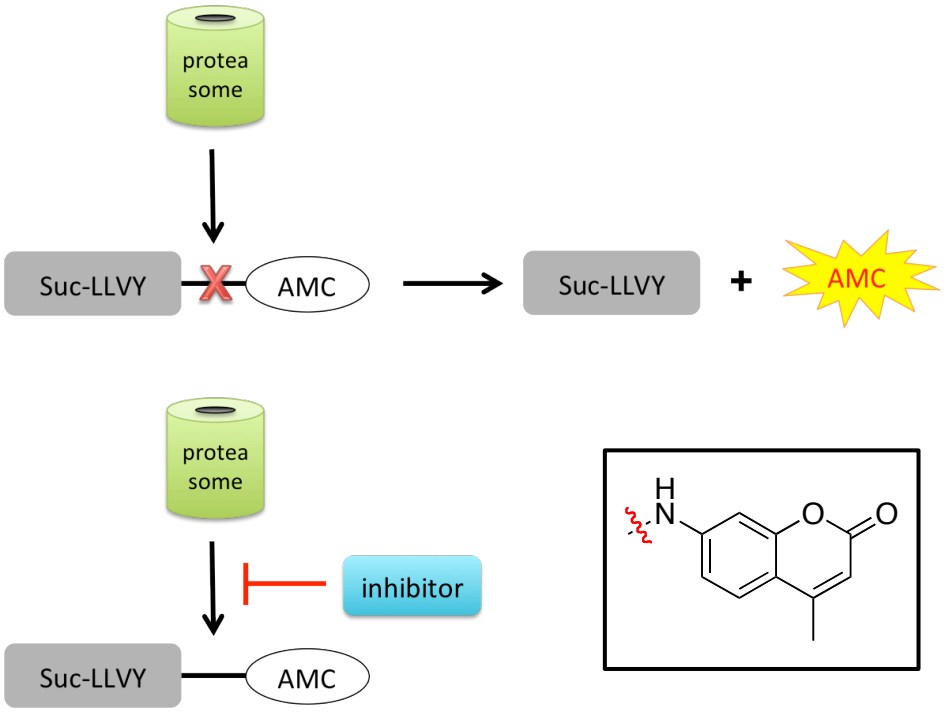

Figure 3.09 Schematic representation of fluorescence 20S proteasome assay. Insert: structure of 7-amino-4-methylcoumarin.

The assays were performed in black 96-well plates with three separate controls: 1) a positive control with 40 ng of proteasome and 50 μM substrate but no inhibitor; 2) a buffer blank with Tris buffer only; and 3) a substrate blank with 50 μM substrate only. Assays were performed in triplicate, with serial dilutions of each inhibitor (7 dilutions) ranging from 25 μM to 25 pM. Fluorescence readings were obtained after 120-min incubation at 37 ^{o}C. The IC_{50} value of each inhibitor was then calculated from a plot of the %

proteasome activity normalized with the positive control against the inhibitor concentrations (Figure 3.10).[47]

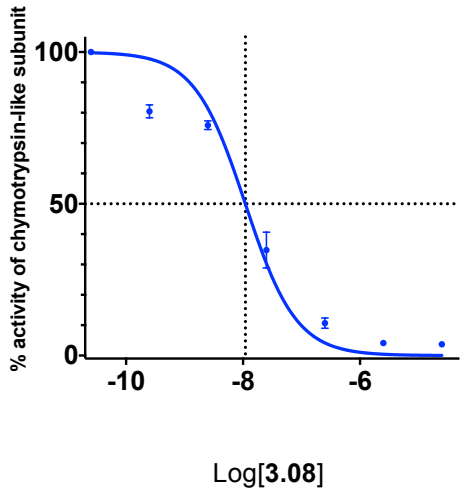

Figure 3.10 IC_{50} analysis of compound **3.08** against the rabbit 20S proteasome. IC_{50} represents the concentration of inhibitor required to reduce the enzyme activity by 50%, which is usually used to quantify inhibitor potencies.

The resulting IC_{50} values are presented in Table 3.02. All four compounds **3.05-3.08** inhibit the CT-L activity of the 20S proteasome with an IC_{50} in the nanomolar range. Compounds **3.06-3.08** are all more potent than the benchmark bortezomib and carfilzomib, however, **3.05** was 3-fold less active. The most potent inhibitor in this series, **3.08**, has an IC_{50} of 13 nM against the CT-L activity, which is more than 2-fold more potent than bortezomib. Overall, inhibitors with leucine residue at P_1 (**3.06** and **3.08**) inhibit the CT-L activity with higher potencies compared to the inhibitors bearing a P_1 phenylalanine (**3.05** and **3.07**). Compounds bearing the P_2-P_3 template containing P_2 isoleucine and P_3 azide (see **3.07** and **3.08**) were more potent than the

inhibitors with the pyrrole-containing peptide (see **3.05** and **3.06**). Bortezomib and its ester (see Figure 3.11) are reported to have essentially identical activity against the CT-L activity of the proteasome.[42] Under our conditions the IC_{50} of bortezomib ester was 2-fold higher than bortezomib.

All inhibitors were inactive against the T-L activity at or below 25000 nM, which is consistent with data for similar acyclic inhibitors. Bortezomib was the most potent C-L inhibitor in this series with an IC_{50} of 213 nM. Bortezomib shows a 6-fold selectivity for the CT-L over C-L. All four target inhibitors **3.05**-**3.08** are higly selective for CT-L over the C-L. In comparison, bortezomib and its ester show significantly reduced selectivity. Inhibitor **3.06** was the most selective inhibitor of CT-L over C-L, with a 200-fold difference in activities. Consistent with previous reported data in literature[39], carfilzomib is inactive against the C-L and T-L subunits at 25000 nM, indicating that it is highly specific for the CT-L activity.

In summary, the four target inhibitors **3.05-3.08** show nanomolar inhibition against the CT-L activity of the 20S proteasome. Inhibitor **3.06-3.08** are more potent than the benchmark bortezomib and carfilzomib. All target inhibitors are significantly more selective for CT-L over C-L compared to bortezomib, as reflected by the lower activity agianst C-L. This increase in selectivity for the CT-L subunit may reduce side effects associated with the low subunit selectivity of bortezomib. The increased potencies may provide an opportunity to limit drug resistance caused by the mutation in CT-L activity of the proteasome found in bortezomib-treated patients (discussed in section 3.1.3)

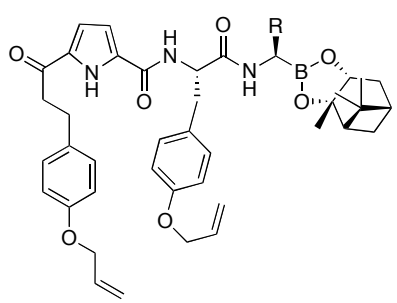

3.05: R = CH_2Ph
3.06: R = $CH_2(CH_3)_2$

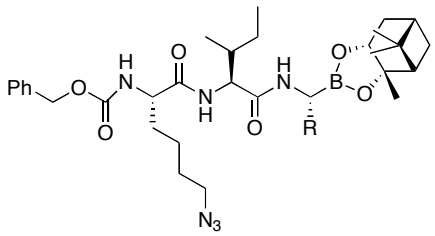

3.07: R = CH_2Ph
3.08: R = $CH_2(CH_3)_2$

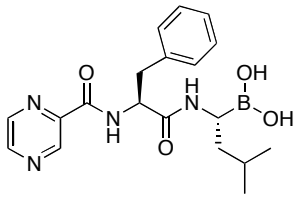

Bortezomib

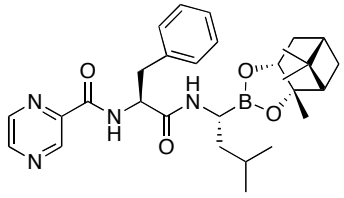

Bortezomib ester

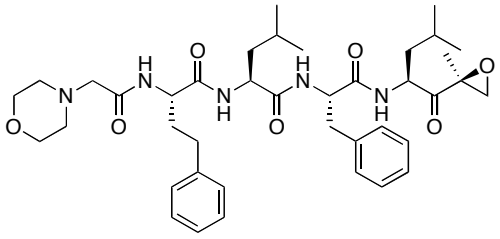

Carfilzomib

Figure 3.11 Structures of compounds **3.05**-**3.08**, bortezomib, bortezomib ester and carfilzomib.

Table 3.02 *IC_{50}* values for compounds **3.05-3.08**, bortezomib, bortezomib ester and carfilzomib against the CT-L, C-L and T-L activities of the purified rabbit 20S proteasome. (Standard Errors <10% of Mean)

Analogues	IC_{50} (chymotrypsin-like) (nM)	IC_{50} (trypsin-like) (nM)	IC_{50} (caspase-like) (nM)
3.05	114	>25000	3415
3.06	20	>25000	3976
3.07	21	>25000	2449

3.08	13	>25000	1599
bortezomib	35	>25000	213
bortezomib-ester	67	>25000	447
carfilzomib	23	>25000	>25000

3.2.4 In vitro Assays with Proteasome in Cellular Extracts and Cell Cytotoxicity Assays

The two most active inhibitors **3.06** and **3.08** (see Figure 3.11) were also assayed for proteasome activity in cytosolic extracts of certain cancer and normal cell lines, as well as for their cytotoxicity against cancer and normal cells. The work presented in this section was performed by our collaborator Ms. Alaknanda Alaknanda in Cancer Therapeutic Group, Hanson Institute.

The cell lines used to obtain the cytosolic proteasome are listed in Table 3.03. The assay against cytosolic proteasome in cancer and normal cells were conducted according to literature methods[48] (Figure 3.12): To a sample of cellular extract obtained from lysed cells (either cancer cells or normal cells) was added a fluorogenic substrate that is specific for a proteasome subunit, e.g. Suc-LLVY-AMC for CT-L activity. The corresponding subunit of the proteasome in the extract hydrolysed the amide bond between the peptide and AMC tag, releasing the AMC group to produce fluorescence. In the absence of inhibitor, the amount of substrate cleaved increased over time, resulting in a linear increase in fluorescence intensity (Figure 3.12, right, in

blue). In the presence of a proteasome inhibitor, the proteasome's activity would be inhibited thus less substrate would be hydrolysed, leading to a lower rate of fluorecence increase compared to the sample with no inhibitor (Figure 3.12, right, in red).

Table 3.03 Cell lines used in the *in vitro* inhibition assays. Cancer cell lines are highlighted in pink. Normal cell lines are highlighted in green.

Cell types	Cell lines	Histology
Cancer cells	WE-68	Ewing sarcoma
	RDES	Ewing sarcoma
	KGN	Ovarian
	SKOV3	Ovarian
	MCF7	Breast
	MDAMB468	Breast
Normal cells	MCF10A	Breast
	IMR-90	Lung fibroblast
	DSF	Skin fibroblast

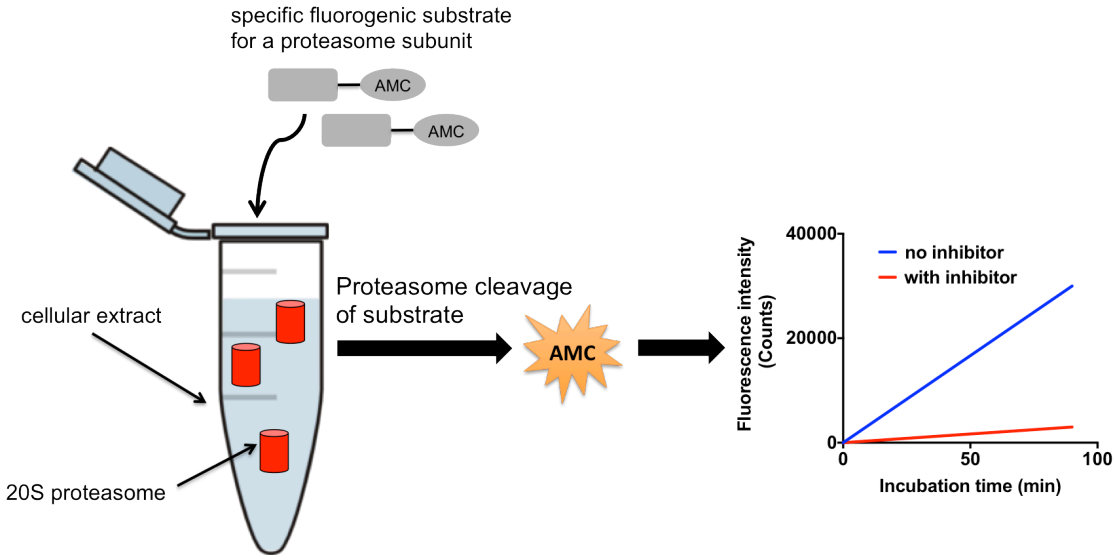

Figure 3.12 Schematic representation of an *in vitro* inhibition assay against the proteasome in cell-free extract.

The results of the assays are reported in Figure 3.13 with the structures of the compounds shown in Figure 3.11. The IC_{50} values of each inhibitor are grouped into four clusters: 1) determined against the CT-L activity in extracts of cancer cells; 2) determined against the CT-L activity in extracts of normal cells; 3) against the C-L activity in extracts of cancer cells and 4) against the same activity in extracts of normal cells. A mean value of the IC_{50} in each cluster was determined to compare the potencies of the inhibitors for cancer and normal cells.

The results for the CT-L activity are presented in Figure 3.13a. The left section of the graph shows the IC_{50} values of each inhibitor obtained using six different cancer cell lines (Table 3.03, in pink), while the right section shows values obtained with three normal cell lines (Table 3.03, in green). Consistent with previous *in vitro* assays performed with the purified 20S proteasome,

compounds **3.06** and **3.08** inhibit the CT-L subunit in cancer cell lines with similar potencies as the benchmark molecules bortezomib and carfilzomib. All compounds are slightly less active against the normal cellular extracts compared to the cancer cell extracts. In particular, compound **3.08** shows a 3-fold selectivity for the proteasome in cancerous extracts over the normal extracts, while the benchmarks only have approximately 2-fold selectivity. This increase in selectivity of **3.08** may lead to a larger therapeutic window.

The IC_{50} values of the inhibitors are similarly presented for the C-L activity. As with the purified 20S proteasome, the data again show that compounds **3.06** and **3.08** are less active than bortezomib but more active than carfilzomib in cancerous extracts. Compound **3.08** is significantly less potent than all other inhibitors and is 2-fold lower in potency compared to the cancer cells in normal cellular extracts. Interestingly, carfilzomib shows relatively potent inhibition of the C-L activity in both cancer and normal cellular extracts, however, it is inactive against the C-L activity of the purified 20S proteasome. This may reflect the possibility that carfilzomib acts on other cytosolic enzymes in the extract that turn off the C-L activity of the proteasome indirectly.

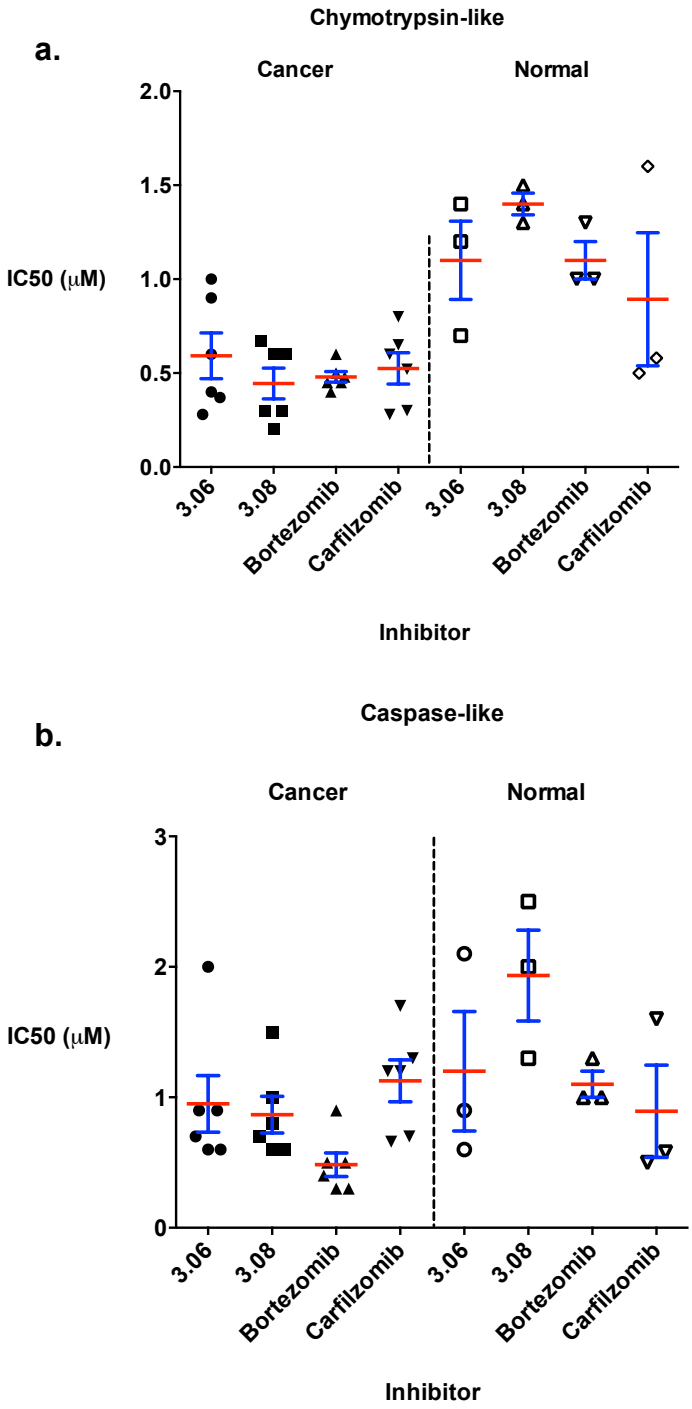

Figure 3.13 *IC_{50}* values of compounds **3.06**, **3.08**, bortezomib and carfilzomib against: a) the CT-L activity of proteasome in cancer cellular extracts (left) and the CT-L activity of proteasome in normal cellular extracts (right); b) the C-L activity of proteasome in cancer cellular extracts (left) and the C-L activity of proteasome in normal cellular extracts (Right).

In summary, inhibitors **3.06** and **3.08** are similarly potent against the CT-L activity with enhanced subunit selectivity compared to the benchmarks in cancerous extracts. This is consistent with the results obtained with the purified 20S proteasome where **3.06** and **3.08** are more selective for CT-L over C-L. This may provide an opportunity to reduce side effects associated with the low subunit selectivity of existing proteasome inhibitor used in cancer therapy. More importantly, inhibitor **3.08** shows significantly higher selectivity for cancerous extracts over the normal extracts compared to the benchmarks. Ultimately, this may provide an opportunity to improve the therapeutic window of proteasome inhibitors.

Cytotoxicity of compounds **3.06**, **3.08**, benchmarks bortezomib and carfilzomib was investigated. A total of 12 cell lines including 8 cancer cell lines (Table 3.04, in pink) and 4 immortalised normal cell lines (Table 3.04, in green) were treated with each inhibitor at a titration of concentrations. The cell viability was measured with flow cytometry after 48 h-incubation at 37 ^{o}C. LD_{50} was then calculated from this measurement to quantify the cytotoxic efficiency of each inhibitor against a certain cell line. These values are presented in Table 3.04.

Two cancerous cell lines were selected to represent each cancer histology. An immortalised normal cell line was also used in parallel with each cancer type to test the inhibitor's selectivity for cancer cells over normal cells. The chosen cancer histologies belong to two categories: solid (sarcoma, breast and ovarian cancers) and liquid tumours (myeloma). The two cell lines of each

cancer histology mainly differ by their p53 status: one possesses wild-type tumour suppressor protein p53 ($p53^{+/+}$) while the other has null-mutated p53 ($p53^{-/-}$). This explores the role of p53 tumour suppressor in the cytotoxic effects of each inhibitor against a cancer type, thus lays basis for the study of the cytotoxic mechanism for a certain inhibitor. The importance of p53 and the significance of its role in eliminating tumours have been discussed in section 3.1.1. All normal cell lines have wild-type p53 protein.

All four inhibitors have potent cytotoxicity against both ewing sarcoma cell lines. In the $p53^{+/+}$ cell line (WE-68), both **3.06** and **3.08** are more cytotoxic than the benchmarks, bortezomib and carfilzomib. In particular, the most potent inhibitor, **3.08** demonstrates a 3-fold lower LD_{50} than bortezomib. The cytotoxicity of **3.06** and **3.08** remain unchanged in the absence of p53, suggesting that their cytotoxicity is achieved through a p53-independent pathway. On the contrary, assays with KGN and SKOV3 cell lines show that the three inhibitors besides carfilzomib have p53-dependent cytotoxicity against the ovarian cancer cells. Carfilzomib has similar LD_{50} values for both cell lines, which suggests that its cytotoxicity may be p53-independent. The cytotoxicity of **3.08** against ovarian cancer cells is 3-fold higher than bortezomib and is very similar to carfilzomib. Compound **3.06** has compatible cytotoxicity to bortezomib. All compounds show low micromolar potencies against the breast cancer $p53^{+/+}$ cell line (MCF7). Unexpectedly, a decrease in cytotoxicity was observed for all inhibitors against the $p53^{-/-}$ cell line (MDAMB468). In addtion, both **3.06** and **3.08** are more potent against MCF7 cell line compared to the benchmarks. In summary, **3.08** is significantly more

cytotoxic against all solid tumours tested compared to the benchmarks. Since both bortezomib and carfilzomib are reported to be ineffective against most solid tumours, the increase in cytotoxicity of compound **3.08** may provide promising potential in solid cancer treatments.

All three inhibitors (carfilzomib's result is pending) show low nanomolar cytotoxicity against $p53^{+/+}$ myeloma cell line (NCI-H929) while in $p53^{-/-}$ cells, their potencies slightly decrease. This suggests that the cytotoxicity in this cancer type is p53-dependent. Compound **3.08** is slightly more cytotoxic compared to bortezomib though the significance of this difference requires further validation. This compound is also 4-fold more cytotoxic than the second-generation anti-myeloma drug carfilzomib against the $p53^{-/-}$ myeloma cells.

Table 3.04 Cytotoxicity of proteasome inhibitors against a panel of cancer cell lines or normal cell lines. LD_{50} values of the four inhibitors for cancer cell lines are highlighted in pink. LD_{50} values for normal cell lines are highlighted in green.

Cell line	**p53**	**Histology**	LD_{50} **(nM)**			
			3.06	**3.08**	**Bortezomib**	**Carfilzomib**
WE-68	+/+	Ewing sarcoma	65	35	100	80

RDES	-/-	Ewing sarcoma	65	35	40	43
KGN	+/+	Ovarian	180	65	180	450
SKOV3	-/-	Ovarian	1500	370	1600	320
MCF7	+/+	Breast	3000	1500	9800	4500
MDAMB468	-/-	Breast	50	30	37	330
NCI-H929	+/+	Myeloma	9	6.4	6.6	PENDING
U266	-/-	Myeloma	29	15	18	60
MCF10A	+/+	Breast	9000	5000	1500	320
IMR-90	+/+	Lung fibroblast	150	200	130	130
DSF	+/+	Skin fibroblast	1080	500	480	350
LCL	+/+	Lymphoblastoid	90	30	20	30

The therapeutic windows of **3.06, 3.08,** bortezomib and carfilzomib were calculated based on the cytotoxic potencies against a certain cancer cell line and a corresponding immortalised normal cell line. Comparison was made between breast cancer cells and normal cells from lactating glands as well as between myeloma cells and lymphoblastoid cells. Some cancer cell lines, such as ewing sarcoma and ovarian cancer, do not have corresponding

normal cell lines. Therefore the LD_{50} of the inhibitors against these cell lines were compared with the mean of LD_{50} against all four normal cell lines. The results are shown in Table 3.05. The target compounds **3.06** and **3.08** show larger therapeutic windows compared to the benchmarks in all types of tumour cells. In particular, both compounds have therapeutic windows above 2 against breast cancer while both benchmarks are more cytotoxic to normal cells than cancer cells. Similar trends were observed for ovarian cancer. This suggests that bortezomib and carfilzomib may not be suitable for treating ovarian and breast cancers whereas the target molecules are promising drug candidates for these cancer types oweing to their adequate therapeutic windows. Myeloma is the marketed target for the benchmark molecules. Bortezomib has a therapeutic window of 1.6 against myeloma, which is consistent with the literature value. Compound **3.06**, in particular, has a 3-fold larger therapeutic window compared to bortezomib. As discussed in section 3.1.2, enlarging the therapeutic window can lead to a potential solution for the severe side effects induced by bortezomib. Therefore, it can be concluded that compound **3.06** may have a better performance in minimising side effects in myeloma treatment compared to currently available chemotherapy agents.

Table 3.05. Therapeutic windows[a] of the inhibitors against the cancer cell line and normal cell line.

Tumor type	**3.06**	**3.08**	**Bortezomib**	**Carfilzomib**
Sarcoma	x52	x54	x10	x4
Ovarian	x4	x8	x0.7	x0.6
Breast	x2.2	x2.4	x0.1	x0.1
Myeloma	x4.7	x2.8	x1.6	PENDING

[a] Therapeutic window represents the fold change in potency (LD_{50} value) of the proteasome inhibitor against the cancer cell line versus the normal cell line.

3.3 Conclusion

In summary, four analogues **3.05-3.08** with pinanyl ester-protected boronate at the *C*-terminus were designed and synthesised to specifically target the chymotrypsin-like activity of the 26S proteasome. All four analogues and two benchmarks, bortezomib and carfilzomib, were assayed against the purified rabbit 20S proteasome as well as the cytosolic proteasome in extracts of various cancer and normal cell lines. All four analogues show low nanomolar activity against the CT-L subunit of the purified 20S proteasome and are much more selective for CT-L over the C-L subunit compared to bortezomib. The assay results obtained with cytosolic extracts agree with the results of the

purified enzyme. The cell cytotoxicity assays show that inhibitor **3.08** is significantly more cytotoxic against solid tumour cells compared to both benchmarks. More importantly, **3.08** provides larger therapeutic windows than the benchmarks for all tumour types tested including myeloma. From these results, it can be concluded that compound **3.08** is a much more attractive drug candidate compared to the commercially available chemotherapy agents bortezomib and carfilzomib due to its improved *in vitro* activity, higher selectivity for CT-L subunit, enhanced cytotoxicity against both solid and liquid tumour and larger therapeutic windows.

3.4 References

(1) Pingdou, D. C. Q. *Current Protein & Peptide Science* **2010**, *11*, 459.

(2) Kumatori, A.; Tanaka, K.; Inamura, N.; Sone, S.; Ogura, T.; Matsumoto, T.; Tachikawa, T.; Shin, S.; Ichihara, A. *Proceedings of the National Academy of Sciences* **1990**, *87*, 7071.

(3) Kanayama, H.-o.; Tanaka, K.; Aki, M.; Kagawa, S.; Miyaji, H.; Satoh, M.; Okada, F.; Sato, S.; Shimbara, N.; Ichihara, A. *Cancer Research* **1991**, *51*, 6677.

(4) Yanagawa, Y.; Hasezawa, S.; Kumagai, F.; Oka, M.; Fujimuro, M.; Naito, T.; Makino, T.; Yokosawa, H.; Tanaka, K.; Komamine, A.; Hashimoto, J.; Sato, T.; Nakagawa, H. *Plant and Cell Physiology* **2002**, *43*, 604.

(5) Naujokat, C.; Hoffmann, S. *Lab Invest* **0000**, *82*, 965.

(6) Orlowski, R. Z. *Cell Death & Differentiation* **1999**, *6*, 303.

(7) Rothbarth, K.; Stammer, H.; Werner, D. *Cancer Cell International* **2002**, *2*, 1.

(8) Rastogi, N.; Mishra, D. P. *Cell Division* **2012**, *7*, 26.

(9) Adams, J. *Nat. Rev. Cancer* **2004**, *4*, 349.

(10) Cohen, G. M. *Cell Death Differ* **0000**, *12*, 1218.

(11) Asher, G.; Tsvetkov, P.; Kahana, C.; Shaul, Y. *Genes & Development* **2005**, *19*, 316.

(12) King, R. W.; Deshaies, R. J.; Peters, J.-M.; Kirschner, M. W. *Science* **1996**, *274*, 1652.

(13) Concannon, C. G.; Koehler, B. F.; Reimertz, C.; Murphy, B. M.; Bonner, C.; Thurow, N.; Ward, M. W.; Villunger, A.; Strasser, A.; Kogel, D.; Prehn, J. H. M. *Oncogene* **2006**, *26*, 1681.

(14) Fiandalo, M.; Schwarze, S.; Kyprianou, N. *Apoptosis* **2013**, *18*, 766.

(15) Wang, C.-Y.; Mayo, M. W.; Korneluk, R. G.; Goeddel, D. V.; Baldwin, A. S. *Science* **1998**, *281*, 1680.

(16) Nawrocki, S. T.; Bruns, C. J.; Harbison, M. T.; Bold, R. J.; Gotsch, B. S.; Abbruzzese, J. L.; Elliott, P.; Adams, J.; McConkey, D. J. *Molecular Cancer Therapeutics* **2002**, *1*, 1243.

(17) Leng, R. P.; Lin, Y.; Ma, W.; Wu, H.; Lemmers, B.; Chung, S.; Parant, J. M.; Lozano, G.; Hakem, R.; Benchimol, S. *Cell*, *112*, 779.

(18) Meek, D. W. *Nat Rev Cancer* **2009**, *9*, 714.

(19) Kulikov, R.; Letienne, J.; Kaur, M.; Grossman, S. R.; Arts, J.; Blattner, C. *Proceedings of the National Academy of Sciences* **2010**, *107*, 10038.

(20) Lopes, U. G.; Erhardt, P.; Yao, R.; Cooper, G. M. *J. Biol. Chem.* **1997**, *272*, 12893.

(21) Orlowski, R. Z.; Kuhn, D. J. *Clinical Cancer Research* **2008**, *14*, 1649.

(22) Kudo, Y.; Takata, T.; Ogawa, I.; Kaneda, T.; Sato, S.; Takekoshi, T.; Zhao, M.; Miyauchi, M.; Nikai, H. *Clinical Cancer Research* **2000**, *6*, 916.

(23) Masdehors, P.; Omura, S.; Merle-Béral, H.; Mentz, F.; Cosset, J.-M.; Dumont, J.; Magdelénat, H.; Delic, J. *British Journal of Haematology* **1999**, *105*, 752.

(24) Drexler, H. C. A. *Proceedings of the National Academy of Sciences* **1997**, *94*, 855.

(25) Field-Smith, A., Morgan, J. G., Davies, F. E. *Therapeutics and Clinical Risk Management* **2006**, *2*, 271.

(26) O'Connor, O. A.; Wright, J.; Moskowitz, C.; Muzzy, J.; MacGregor-Cortelli, B.; Stubblefield, M.; Straus, D.; Portlock, C.; Hamlin, P.; Choi, E.; Dumetrescu, O.; Esseltine, D.; Trehu, E.; Adams, J.; Schenkein, D.; Zelenetz, A. D. *Journal of Clinical Oncology* **2005**, *23*, 676.

(27) Vij, R.; Wang, L.; Orlowski, R. Z.; Stewart, A. K.; Jagannath, S.; Lonial, S.; Trudel, S.; Jakubowiak, A. J.; Belch, A.; Alsina, M.; Bahlis, N. J.; Le, M. H.; Cruickshank, S.; Bennett, M. K.; Molineaux, S.; Kauffman, M.; Siegel, D.; The Multiple Myeloma Research, C. *ASH Annual Meeting Abstracts* **2009**, *114*, 430.

(28) Siegel, D. S.; Martin, T.; Wang, M.; Vij, R.; Jakubowiak, A. J.; Lonial, S.; Trudel, S.; Kukreti, V.; Bahlis, N.; Alsina, M.; Chanan-Khan, A.; Buadi, F.; Reu, F. J.; Somlo, G.; Zonder, J.; Song, K.; Stewart, A. K.; Stadtmauer, E.; Kunkel, L.; Wear, S.; Wong, A. F.; Orlowski, R. Z.; Jagannath, S. *Blood* **2012**, *120*, 2817.

(29) O'Connor, O. A.; Stewart, A. K.; Vallone, M.; Molineaux, C. J.; Kunkel, L. A.; Gerecitano, J. F.; Orlowski, R. Z. *Clinical Cancer Research* **2009**, *15*, 7085.

(30) Bross, P. F.; Kane, R.; Farrell, A. T.; Abraham, S.; Benson, K.; Brower, M. E.; Bradley, S.; Gobburu, J. V.; Goheer, A.; Lee, S.-L.; Leighton, J.; Liang, C. Y.; Lostritto, R. T.; McGuinn, W. D.; Morse, D. E.; Rahman, A.; Rosario, L. A.; Verbois, S. L.; Williams, G.; Wang, Y.-C.; Pazdur, R. *Clinical Cancer Research* **2004**, *10*, 3954.

(31) Chen, D. F., M.; Schmitt, S.; Kanwar, J.; Dou, Q. P. *Curr Cancer Drug Targets.* **2011**, *11*, 239.

(32) Oerlemans, R.; Franke, N. E.; Assaraf, Y. G.; Cloos, J.; van Zantwijk, I.; Berkers, C. R.; Scheffer, G. L.; Debipersad, K.; Vojtekova, K.; Lemos, C.; van der Heijden, J. W.; Ylstra, B.; Peters, G. J.; Kaspers, G. L.; Dijkmans, B. A. C.; Scheper, R. J.; Jansen, G. *Blood* **2008**, *112*, 2489.

(33) Yuan, B.-Z.; Chapman, J. A.; Reynolds, S. H. *Translational Oncology* **2008**, *1*, 129.

(34) Neilsen, P. M.; Pehere, A. D.; Pishas, K. I.; Callen, D. F.; Abell, A. D. *ACS Chemical Biology* **2012**, *8*, 353.

(35) Chua, K. C. H.; Pietsch, M.; Zhang, X.; Hautmann, S.; Chan, H. Y.; Bruning, J. B.; Gütschow, M.; Abell, A. D. *Angewandte Chemie International Edition* **2014**, n/a.

(36) Liu, C.-w.; Millen, L.; Roman, T. B.; Xiong, H.; Gilbert, H. F.; Noiva, R.; DeMartino, G. N.; Thomas, P. J. *J. Biol. Chem.* **2002**, *277*, 26815.

(37) Huber, Eva M.; Basler, M.; Schwab, R.; Heinemeyer, W.; Kirk, Christopher J.; Groettrup, M.; Groll, M. *Cell* **2012**, *148*, 727.

(38) Mroczkiewicz, M.; Winkler, K.; Nowis, D.; Placha, G.; Golab, J.; Ostaszewski, R. *J. Med. Chem.* **2010**, *53*, 1509.

(39) Demo, S. D.; Kirk, C. J.; Aujay, M. A.; Buchholz, T. J.; Dajee, M.; Ho, M. N.; Jiang, J.; Laidig, G. J.; Lewis, E. R.; Parlati, F.; Shenk, K. D.; Smyth, M. S.; Sun, C. M.; Vallone, M. K.; Woo, T. M.; Molineaux, C. J.; Bennett, M. K. *Cancer Research* **2007**, *67*, 6383.

(40) Hideshima, T.; Richardson, P.; Chauhan, D.; Palombella, V. J.; Elliott, P. J.; Adams, J.; Anderson, K. C. *Cancer Res.* **2001**, *61*, 3071.

(41) Borissenko, L.; Groll, M. *Chem. Rev.* **2007**, *107*, 687.

(42) Zhu, Y.; Zhao, X.; Zhu, X.; Wu, G.; Li, Y.; Ma, Y.; Yuan, Y.; Yang, J.; Hu, Y.; Ai, L.; Gao, Q. *J. Med. Chem.* **2009**, *52*, 4192.

(43) Matteson, D. S.; Sadhu, K. M.; Lienhard, G. E. *J. Am. Chem. Soc.* **1981**, *103*, 5241.

(44) Adams, J.; Behnke, M.; Chen, S.; Cruickshank, A. A.; Dick, L. R.; Grenier, L.; Klunder, J. M.; Ma, Y.-T.; Plamondon, L.; Stein, R. L. *Bioorg. Med. Chem. Lett.* **1998**, *8*, 333.

(45) Kisselev, A. F.; Akopian, T. N.; Castillo, V.; Goldberg, A. L. *Molecular cell* **1999**, *4*, 395.

(46) Dange, T.; Smith, D.; Noy, T.; Rommel, P. C.; Jurzitza, L.; Cordero, R. J. B.; Legendre, A.; Finley, D.; Goldberg, A. L.; Schmidt, M. *J. Biol. Chem.* **2011**, *286*, 42830.

(47) Yung-Chi, C.; Prusoff, W. H. *Biochem. Pharmacol.* **1973**, *22*, 3099.

(48) Rodgers, K. J.; Dean, R. T. *The International Journal of Biochemistry & Cell Biology* **2003**, *35*, 716.

Chapter 4

Photoregulation of α-Chymotrypsin Activity by Spiropyran-Based Inhibitors in Solution and Attached to an Optical Fibre

Statement of Authorship

Title of Paper	Photoregulation of α-Chymotrypsin Activity by Spiropyran-Based Inhibitors in Solution and Attached to an Optical Fiber
Publication Status	☑ Published ☐ Accepted for Publication ☐ Submitted for Publication ☐ Unpublished and Unsubmitted work written in manuscript style
Publication Details	"Photoregulation of α-Chymotrypsin Activity by Spiropyran-Based Inhibitors in Solution and Attached to an Optical Fiber", Zhang, X.; Heng, S.; Abell, A. D. *Chemistry – A European Journal* **2015**, *21*, 10703.

Principal Author

Name of Principal Author (Candidate)	Xiaozhou Zhang
Contribution to the Paper	Performed synthesis of all the analogues, all *in vitro* assays, in-solution fluorescence experiments and fibre-based experiments. Analysed data. Wrote and edited the manuscript.
Overall percentage (%)	50%
Certification:	This paper reports on original research I conducted during the period of my Higher Degree by Research candidature and is not subject to any obligations or contractual agreements with a third party that would constrain its inclusion in this thesis. I am the primary author of this paper.
Signature	Date 30/10/2015

Co-Author Contributions

By signing the Statement of Authorship, each author certifies that:

i. the candidate's stated contribution to the publication is accurate (as detailed above);

ii. permission is granted for the candidate in include the publication in the thesis; and

iii. the sum of all co-author contributions is equal to 100% less the candidate's stated contribution.

Name of Co-Author	Sabrina Heng
Contribution to the Paper	Perfomed *in silico* docking experiments Assisted with synthesis, fiber-based experiments and data analysis Wrote and edited the manuscript
Signature	Date 04 11 2015

Name of Co-Author	Andrew Abell
Contribution to the Paper	Supervised the work published Wrote and edited the paper
Signature	Date 30/10/2015

Please cut and paste additional co-author panels here as required.

Photoregulation of α-Chymotrypsin Activity by Spiropyran-based Inhibitors in Solution and Attached to an Optical Fibre[2]

Xiaozhou Zhang, Sabrina Heng, Andrew. D. Abell*[a]

[a] ARC Centre of Excellence for Nanoscale BioPhotonics, Institute for Photonics & Advanced Sensing and Department of Chemistry, The University of Adelaide, South Australia, Australia 5005

E-mail: andrew.abell@adelaide.edu.au

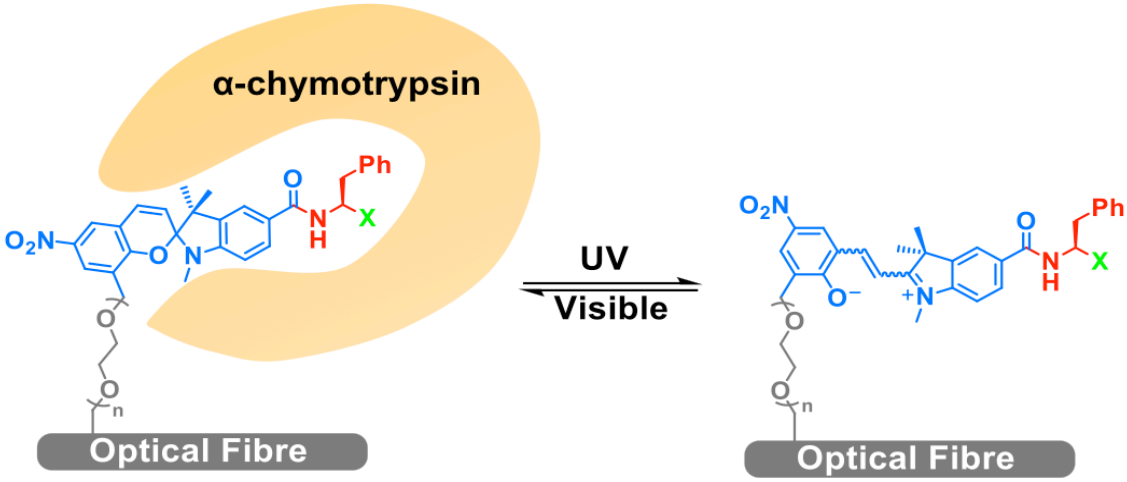

[2] Zhang, X.; Heng, S.; Abell, A. D. *Chemistry – A European Journal,* **2015**, *21*, 10703.

4.1 Abstract

Here we report the synthesis and characterization of a new class of spiropyran-based protease inhibitor that can be reversibly photoswitched between an active spiropyran (SP) isomer and a less active merocyanine (MC) isomer upon irradiation with UV and visible light respectively, both in solution and on a surface of a microstructured optical fibre (MOF). The most potent inhibitor in the series (**SP**-**4.09**) has a *C*-terminal phenylalanyl-based α-ketoester group and inhibits α-chymotrypsin with a K_i of 115 nM. An analogue containing a *C*-terminal Weinreb amide (**SP-4.07**) demonstrated excellent stability and photoswitching in solution and was attached to the surface of a MOF. The SP isomer of Weinreb amide **4.07** is a competitive reversible inhibitor in solution and also on fibre, while the corresponding MC isomer was significantly less active in both media. The ability of this new class of spiropyran-based protease inhibitor to modulate enzyme activity on a MOF paves the way for sensing applications.

4.2 Introduction

An ability to detect the on/off binding of a bio-ligand to a complementary surface bound receptor provides a basis of real time sensors of wide applicability.[1-5] The associated 'on' and 'off' states are typically modulated photochemically, by means of a component azobenzene, or other photochromic substructure.[6] One problem with switchable sensors of this type is that they generally lack an ability to be tailored to a range of ligands, with each specific application requiring a different base system.[2,5-12] For example, an azobenzene-based molecular glue has been reported to hybridise DNA strands with mismatch mutations on a gold surface.[7] While this permits reversible control of DNA hybridization by external light stimulus, the molecule only binds to a specific nucleotide sequence rather than a range of such structures.

More general and modular photoswitchable systems capable of targeting families of biomolecules, in a controlled and predictable manner, are needed to advance this area. With this in mind we recently reported a switchable surface containing an azobenzene core to which was attached a peptidomimetic trifluoromethyl ketone, the backbone structure of which can be tailored to inhibit a particular class or example of protease.[13] This system was immobilized onto gold surface by Huisgen 1,3-dipolar cycloaddition to provide an on/off switch and basis of a biosensor. Irradiation with UV (or visible light) reversibly controls the geometry of the azobenzene, and the associated inhibitory activity.[13-17]

The use of azobenzenes to regulate enzyme activity in this way is, however, somewhat limited since the two photostationary states often exhibit only a small difference in activity.[18] In addition, the fluorescence intensities of both switchable states are low,[19] such that detecting and measuring the extent of isomerization can be problematic. Finally, the cis-azobenzene usually undergoes spontaneous thermal isomerization back to the low-energy trans-isomer.[20] Given these limitations, there is a need to develop new photoswitchable systems.

We now present a new class of serine protease inhibitor based on a photoswitchable spiropyran core that mimics a peptide backbone as found in protease inhibitors. This structure is amenable to functionalization to target a particular protease, and also for attachment to a microstructured optical fibre (MOF) core surface for biosensor development (Figure 4.01). The fibre has a duel function; it facilitates irradiation of the spiropyran with light of a specific wavelength (532 nm) to bring about photoswitching and also the detection of changes in fluorescence produced on binding to the protease. There are reports on the non-specific covalent attachment of a spiropyran to α-chymotrypsin in order to modulate its activity.[21-23] However, our system is unique in that we designed this structural unit to mimic the extended backbone of a competitive inhibitor. Proteases are known to almost universally recognize the backbone of substrates and inhibitors in a β-strand.[24-25] Binding in this geometry is dictated by the juxtaposition of active site binding pockets that accommodate the side chains of the peptide-based ligands.[24]

Irradiation of the spiropyran core of these new inhibitors results in reversible ring opening (Figure 4.01), with an associated change in polarity and geometry[26] to affect inhibitor binding and hence potency. The change in dipole moment would be expected to be greater than that observed with an azobenzene.[2,27] A spiropyran has the added advantage that it is resistant to reductive environments and thermal relaxations in aqueous environment, while providing excellent fluorescence intensity to allow easy detection of inhibitor binding.[28] In addition, isomerization of a spiropyran is more efficient and the products are easier to detect compared to other photoswitchable systems such as an azobenzene.[28]

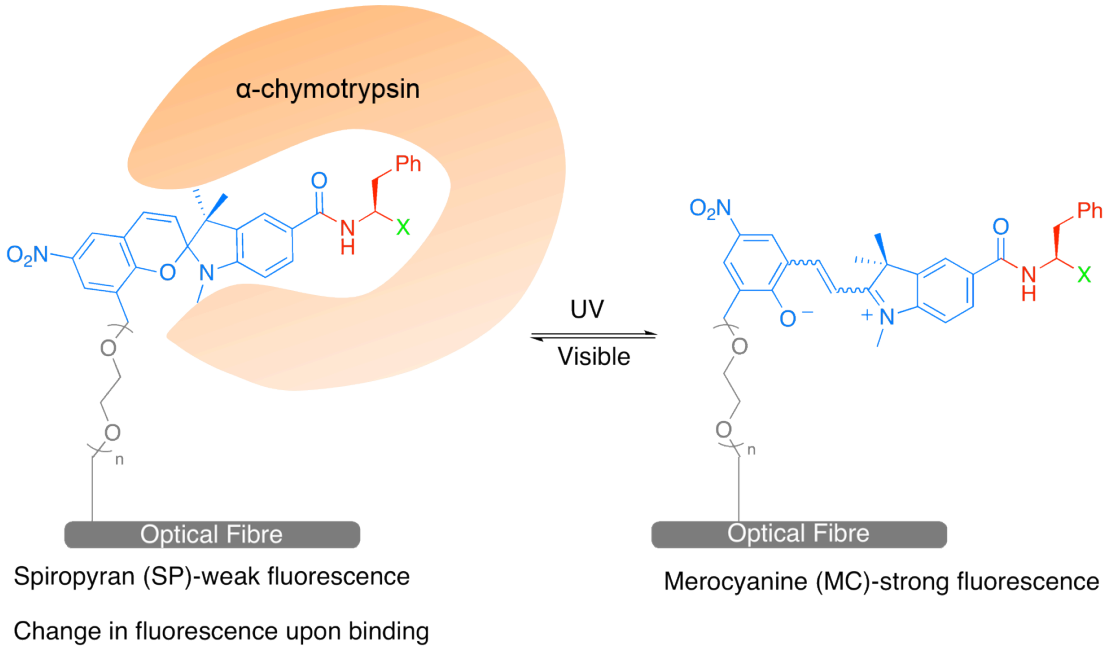

Figure 4.01 Schematic representation of spiropyran-based α-chymotrypsin inhibitors. The photoswitch is highlighted in blue, the sensing platform and linker grey, amino acid residue red and the *C*-terminal electrophile green.

4.3 Results and Discussion

The system reported here and depicted in Figure 4.01, consists of four components: a photoswitchable spiropyran backbone core (blue), an amino acid-based group (red) capable of binding to the active site of a given protease e.g. α-chymotrypsin (orange), an attached *C*-terminal electrophile (X, green) to bring about inhibition once bound, and a microstructured optical fibre (MOF)-based sensing platform to guide light and detect changes in fluorescence (grey). The key photoswitchable spiropyran core was designed to reversibly switch the inhibitor geometry and polarity to modulate active-site binding. This group is known to provide an excellent fluorescence emission profile for sensing purposes,[28] where the ring-closed spiropyran (SP) (Figure 4.01, left) generally exhibits weak fluorescence and the switched merocyanine isomer (MC) (produced on UV irradiation, Figure 4.01, right) has an enhanced fluorescence emission[29] that can be detected through the MOF. The isomerization from MC to SP is promoted by visible light typically provided by a halogen lamp. We can then detect changes in fluorescence through the fibre upon selective active-site binding of one isomer, anticipated to be the SP isomer given that α-chymotrypsin prefers non-polar substrates.

The design allows for incorporation of suitable amino acid and sensing components to target a particular protease and/or sensing application. Here we use a phenylalanine-based amino acid mimic since such a group is known to bind in the primary S_1 pocket[30] (and also other neighboring pockets) of our target protease, α-chymotrypsin. Both an aldehyde and a α-ketoester were

investigated as *C*-terminal electrophilic groups capable of interacting with the protease. α-Chymotrypsin was chosen for study as a model protease, where much is known about its structure and inhibition.[31-34] The overall system also contains a spacer to link the photoswitchable inhibitor to the sensing platform (in grey, Figure 4.01). A relatively short spacer was chosen in this study for ease of synthesis and since the active site of α-chymotrypsin is located close to the enzyme surface.[35]

A MOF (as depicted in Figure S1, Supporting Information) has additional advantages. Fluorescence of spiropyran is known to be greatly enhanced when coupled to a MOF,[36-37] to provide significantly improved sensitivity compared to the equivalent solution-based experiments. This is particularly important when using the small sample volumes required for subcellular-scale biological samples.[36] A MOF also provides a potential platform for performing *in vivo* assays in confined and well-defined locations such as would be expected in potential *in vivo* sensing applications. Furthermore, the air holes within the MOF can be used to guide light to interact with both the attached molecules and the sample solution within. These voids simultaneously act as micro sample chambers.

4.3.1 Synthesis of the Inhibitors

The photoswitchable inhibitors prepared for this study are depicted in Figure 2. Compounds **4.04-4.10** contain a phenylalanine (Phe) analogue at the *C*-terminus for binding to α-chymotrypsin. Derivatives **4.08**/**4.10** and **4.09** also

contain a *C*-terminal electrophilic warhead (an aldehyde and α-ketoester respectively) that is capable of interacting with the protease active site once bound. Compounds **4.01-4.03** and **4.11** were prepared to investigate possible sites and functionality for surface attachment. Compound **4.07** provides a combination of the *C*-terminal Phe mimetic and a suitable C8' tether for surface attachment. This compound also contains a chemically stable Weinreb amide at the *C*-terminus, which is capable of hydrogen bonding with the enzyme's active site.

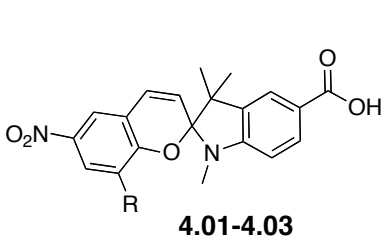

4.01-4.03

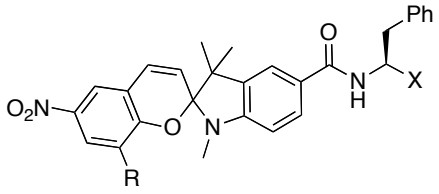

4.04-4.10

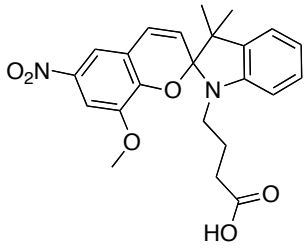

4.11

	R	X
4.01	$(CH_2OCH_2)_3CH_3$	—
4.02	CH_2N_3	—
4.03	$CH_2O(CH_2)_2OH$	—
4.04	$(CH_2OCH_2)_3CH_3$	CH_2OH
4.05	$(CH_2OCH_2)_3CH_3$	$CHOHCOOCH_3$
4.06	CH_2N_3	CH_2OH
4.07	$CH_2O(CH_2)_2OH$	$CONCH_3OCH_3$
4.08	$(CH_2OCH_2)_3CH_3$	CHO
4.09	$(CH_2OCH_2)_3CH_3$	$COCOOCH_3$
4.10	CH_2N_3	CHO

Figure 4.02 Structures of target spiropyrans.

Compounds **4.01-4.03** were prepared in three steps starting from 4-hydrazinobenzoic acid, see Scheme 4.01. In particular, reaction with 3-methylbutan-2-one, under acidic conditions, gave indoline **4.13**. This was subsequently N-alkylated on treatment with methyl iodide in toluene and acetonitrile to give **4.14** in 87% yield over two steps. Separate condensation of **4.14** with the hydroxyl nitro-benzaldehydes **4.15-4.17**, under reflux, gave the desired spiropyran analogues **4.01-4.03** in 45%-60% yield.

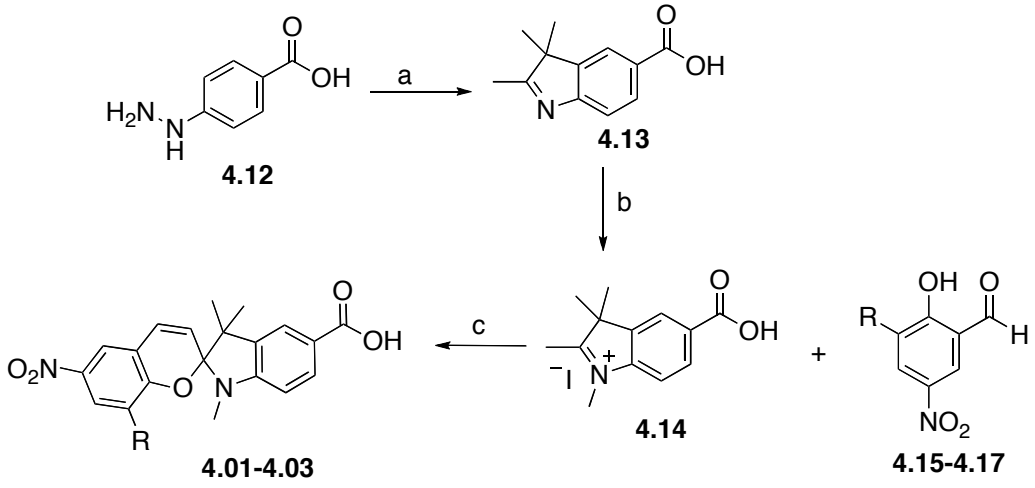

	R
4.01	$CH_2(CH_2OCH_2)_3CH_3$
4.02	CH_2N_3
4.03	$CH_2O(CH_2)_2OH$

Scheme 4.01 Synthesis of the core spiropyran unit. Reagents and conditions: a) 3-methyl-2-butanone, 98% H_2SO_4, anhydrous EtOH, N_2, Δ, 18 h, (91%); b) CH_3I, ACN/toluene, Δ, 18 h, (quant); c) anhydrous EtOH, N_2, Δ, 3h, (4.01: 27%, 4.02: 13%, 4.03: 45%).

HATU-mediated coupling of **4.01** and **4.02** with either phenylalaninol (**4.18**) or methyl-3-amino-2-hydroxy-4-phenylbutanoate (**4.19**)[38] then gave **4.04-4.06**

(Scheme 4.02). The phenylalaninol groups of **4.04** and **4.06** were oxidized with Dess-Martin periodinane to give the corresponding aldehydes **4.08** and **4.10**, respectively. The α-ketoester **4.09** was similarly obtained by Dess-Martin oxidation of the α-hydroxymethylester group of **4.05**.

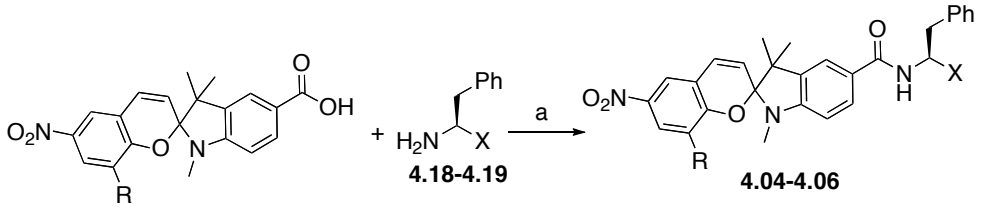

	R	X
4.04	$(CH_2OCH_2)_3CH_3$	CH_2OH
4.05	$(CH_2OCH_2)_3CH_3$	$CHOHCO_2CH_3$
4.06	CH_2N_3	CH_2OH

	R	Y
4.08	$(CH_2OCH_2)_3CH_3$	CHO
4.09	$(CH_2OCH_2)_3CH_3$	$COCO_2CH_3$
4.10	CH_2N_3	CHO

	X
4.18	CH_2OH
4.19	$CHOHCO_2CH_3$

Scheme 4.02 Preparation of *C*-terminal substituted spiropyrans. Reagents and conditions: (a) HATU, DIPEA, anhydrous DMF, N_2, r.t., 18 h (**4.04**: 62%, **4.05**: 47%, **4.06**: 87%); (b) for **4.08** and **4.10**: Dess-Martin periodinane, DCM, r.t., 1.5 h, (**4.08**: 8%*, **4.10**: 10%*); for **4.09**: Dess-Martin periodinane, DCM, r.t., 3 h, (6%*).

*Yields calculated after RP-HPLC purification.

The spiropyran **4.07** was prepared as shown in Scheme 4.03. BOP-mediated coupling of commercially available N,O-dimethylhydroxylamine hydrochloride

with *N*-Boc-*L*-phenylalanine, followed by removal of the Boc group on treatment with TFA, gave the key intermediate **4.21**. This was coupled with **4.03**, in the presence of HATU, to give the spiropyran **4.07**.

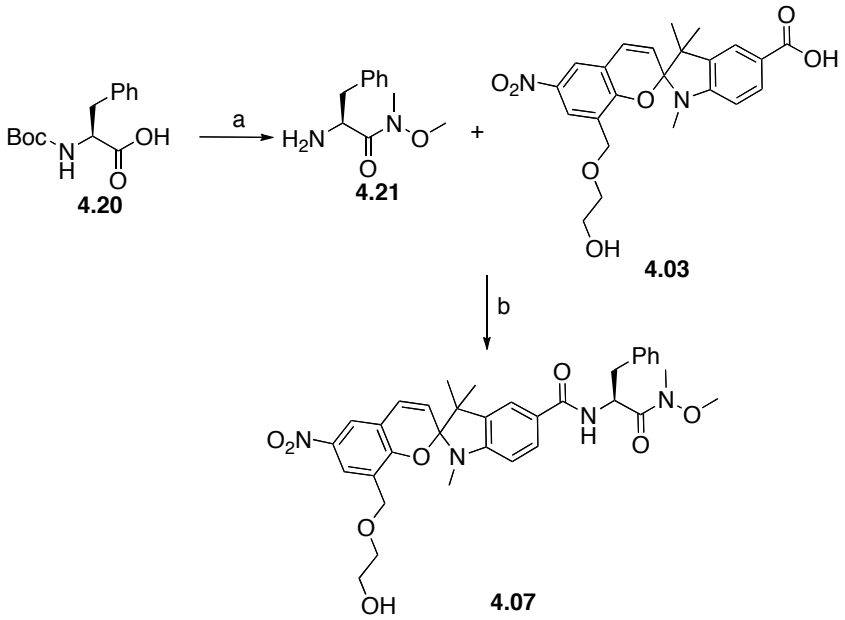

Scheme 4.03 Synthesis of **4.07**. Reagents and conditions: (a) $CH_3ONHCH_3.HCl$, EDCI, HOBt, DIPEA, DCM, N_2, r.t., 21 h, (quant); (b) HATU, DIPEA, anhydrous DMF, N_2, r.t., 18 h, (57%).

4.3.2 In vitro Inhibition Assay against α-Chymotrypsin

The spiropyrans **4.01-4.11** were assayed against bovine α-chymotrypsin as described in supporting data and the results are shown in Table 4.01. K_i values for all the inhibitors were determined graphically according to Dixon methodology.[39]

Table 4.01. *In vitro* inhibition of α-chymotrypsin by compounds **4.01-4.02**, and **4.04-4.11**.

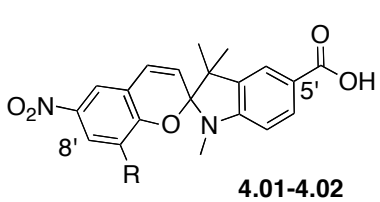

4.01-4.02

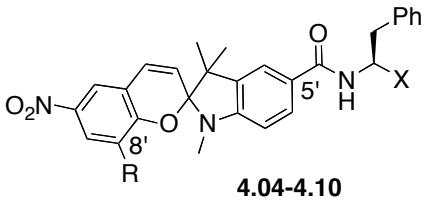

4.04-4.10

	R	X	K_i (μM)
4.01	$(CH_2OCH_2)_3CH_3$	---	305 ± 45
4.02	CH_2N_3	---	170 ± 27
4.04	$(CH_2OCH_2)_3CH_3$	CH_2OH	48 ± 6
4.05	$(CH_2OCH_2)_3CH_3$	$CHOHCO_2CH_3$	75 ± 9
4.06	CH_2N_3	CH_2OH	23 ± 4
4.07	$CH_2O(CH_2)_2OH$	$CONCH_3(OCH_3)$	86 ± 11
4.08	$(CH_2OCH_2)_3CH_3$	CHO	1.7 ± 0.26
4.09	$(CH_2OCH_2)_3CH_3$	$COCO_2CH_3$	0.12 ± 0.016
4.10	CH_2N_3	CHO	1.8 ± 0.56
4.11	OCH_3	---	> 1000

Compounds **4.01** and **4.02**, which lack a hydrophobic phenylalanine mimic at their *C*-termini, were weak inhibitors of α-chymotrypsin, with similar K_i values of 305 μM and 170 μM, respectively. Even weak inhibitory activity here is particularly interesting given that these compounds lack any significant peptide character normally associated[40] with protease inhibitors. The nature of the R group at the C8 of the benzopyran ring appears to have little

influence on potency (c.f. **4.01** and **4.02**), an important observation given that this is a potential site for attachment to the MOF as discussed later. On the other hand, compound **4.11**, with a pentanoic acid linker on the indole nitrogen, was inactive against α-chymotrypsin at a concentration of 1000 μM. Thus this is not a suitable site for surface attachment.

The incorporation of phenylalanine mimetic at C5 of the indole (**4.04-4.06)** results in a significant improvement in potency, with K_i values of 48 μM, 75 μM and 23 μM respectively. This suggests that the substituted spiropyran-core can act as a surrogate of the backbone of a protease inhibitor or substrate. The introduction of a reactive *C*-terminal group as in the aldehyde of **4.08** and **4.10** further improves potency, with these compounds having K_i values of 1.7 μM and 1.8 μM respectively. Compound **4.09**, with a *C*-terminal α-ketoester as found in other serine protease inhibitors,[41] proved to be particularly potent with a K_i of 115 nM. This compound is >1000-fold more potent than **4.01** that contains the spiropyran base unit only. Gratifyingly, the spiropyran **4.07**, with an ethylene glycol substituent at C8 suitable for attachment to a MOF, was a reasonable inhibitor of α-chymotrypsin in solution with a K_i = 86 μM. It was deemed advantageous to use a compound without a reactive *C*-terminal warhead for initial surface studies. Importantly, compound **4.07** was also shown to be a competitive reversible inhibitor of α-chymotrypsin by Dixon plot and Cornish-Bowden plot analyses,[39,42] see Figure S2 Supporting Information. This compound thus competes for substrate, an important observation if the spiropyran is to bind in the active site as a peptide backbone mimetic.

4.3.3 Solution-Based Photoisomerism of Compound 4.07

Studies on the photoswitching of spiropyran **4.07** in solution were undertaken in order to compare the relative potencies of the two photoswitchable states against α-chymotrypsin. These two switchable isomers are depicted in Scheme 4.04 as ring-closed spiropyran (SP) and ring opened merocyanine (MC).

A solution of **4.07** in the assay buffer was irradiated with UV light at 365 nm, for 5 min, and the resulting sample was incubated with α-chymotrypsin in the dark to minimize any isomerization back to the SP isomer. This sample proved to be a very weak inhibitor of α-chymotrypsin, with an IC_{50} greater than 500 μM. Thus the SP-based photostationary state is significantly more potent (> 5-fold) than the equivalent MC-based state. This observation presumably reflects significant differences in polarity and conformation of the two isomers, and hence their abilities to bind to the protease.

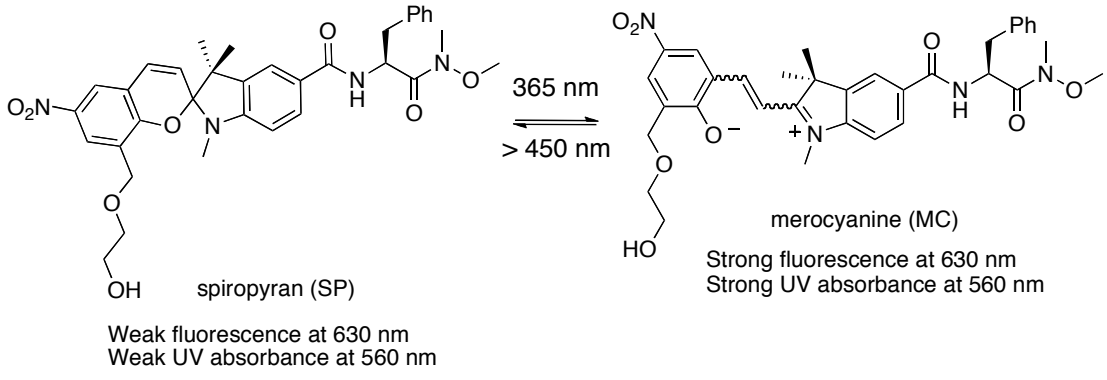

Scheme 4.04 Photoisomerization of **4.07**, where SP depicts the ring-closed non-fluorescent isomer and MC the ring-opened fluorescent isomer.

The ability of **4.07** to photoswitch between its two isomers was then studied. Specifically, a sample of **4.07** was irradiated with visible light (> 400 nm) and the resulting UV-visible (UV-vis) absorption spectrum was measured as shown in Figure 4.03 (red). The lack of absorption at 550 nm indicates that the sample consists predominantly as the SP isomer, where the MC isomer typically has strong absorption in this region.[43] The solution of **4.07** in methanol was then irradiated with UV light (365 nm) for 15 min to induce isomerization to the MC isomer as evidenced by a significant and characteristic increase in absorption at 550 nm (Figure 4.03a, blue). The sample was further irradiated with visible light to give a spectrum essentially the same as the initial one (black and red, Figure 4.03a). Switching between the two isomers was apparent after multiple cycles of alternate irradiation with UV and visible light, without any evidence of photobleaching, as shown in Figure 4.03b and Figure S5 in Supporting Information. A significant increase in fluorescence of **4.07** was also observed upon UV irradiation and switching to the MC isomer, while a decrease in fluorescence was apparent upon visible light irradiation to switch the compound back to the SP isomer (Figure S3, Supporting Information). Consistent with the UV-Vis absorption experiments, the fluorescence experiments also demonstrate the ability of compound **4.07** to reversibly photoisomerise between two isomers.

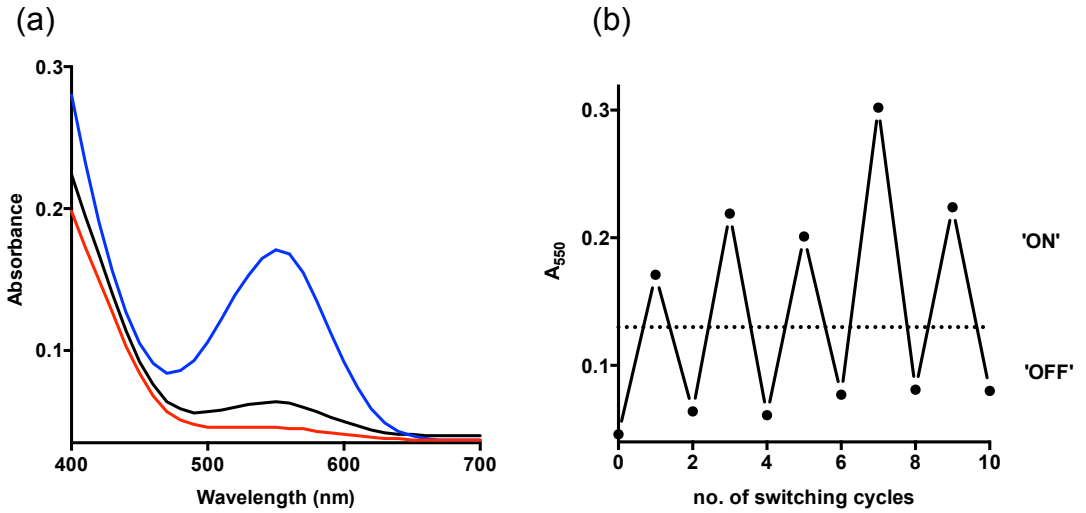

Figure 4.03 (a) The UV-vis absorption spectra of **4.07** in MeOH under visible light (red), after irradiation with UV light (365 nm) for 15 min (blue). Compound **4.07** was then isomerized by visible light irradiation again to produce spectrum in black. (b) Photoswitching of **4.07** induced by UV (365 nm) and visible light (> 400 nm) irradiations. Cycle 0 represents the state before **4.07** was irradiated with UV light. Cycles 1, 3, 5, 7 and 9 represent the state of **4.07** after irradiated with UV light for 15 min. Cycles 2, 4, 6, 8, and 10 represent the state of **4.07** after irradiated with visible light for 15 min.

4.3.4 In silico Docking

The SP and MC isomers of **4.07** were separately docked into a structure of α-chymotrypsin (*Bos Taurus,* PDB entry 1GGD)[44] using AutoDock4.2[45] in order to gain some insight into the potential mode of active site binding and associated differences in potency. Docking studies were carried out by performing 25 docking runs on each isomer using the Lamarckian Genetic Algorithm[46] and a maximum of 500,000 energy evaluations. The results of these studies are shown in Figure 4.04. The SP isomer of **4.07** docked with a

binding energy of -7.04 kcal/mol and docking energy of -13.57 kcal/mol (Figure 4.04a) while the apparently less active MC isomer docked less well with a binding energy of -0.61 and a docking energy of -8.93 kcal/mol respectively (Figure 4.04b). Figure 4a reveals that the SP isomer sits within the active site, with the amide carbonyl near the key active site serine as would be expected for a competitive reversible inhibitor. In comparison, the MC isomer docks poorly at the periphery of the active site (Figure 4.04b). Figure 4.04c depicts interactions of SP isomer of **4.07** with key binding pockets within the enzyme's active site as observed in the docked structures. Interestingly, the benzyl group of Phe mimic resides in the S_2' binding pocket (highlighted in green). This pocket is known to bind favorably with aromatic amino acids,[33] however this interaction has been little explored in inhibitor design. This then positions the spiropyran amide carbonyl of **4.07** in close proximity to the active site serine, with the indole ring sitting on the outer edge of the S_1 binding pocket. The *N*-methyl group then projects into this pocket. The ethylene glycol linker on the benzopyran is positioned on the surface of the enzyme. The overall result is a somewhat unusual mode of binding to α-chymotrypsin, where the spiropyran provides a suitable scaffold for other key interactions to occur with the active site. It is noteworthy that our original design had the Phe mimetic of **4.07** interacting with the S_1 pocket rather than S_2' as is apparent from these studies. This difference is of little consequence to the current study, but it does present some intriguing future inhibitor design possibilities. It is also important to note that the ethylene glycol-based linker of **4.07** is positioned toward the enzyme surface of the protease and is thus suitably located for attachment to the MOF.

For comparison, the SP isomers of **4.08-4.11** were also docked into α-chymotrypsin, see supporting information for detail. All these structures bind to the active site of the enzyme with similar binding energies and docking energies compared to the SP isomer of **4.07**. Compounds **4.09** and **4.10** bind in essentially the same orientation as **4.07**, while **4.08** differs only in the orientation of the benzyl group (Supporting information, Figure S6-S8).

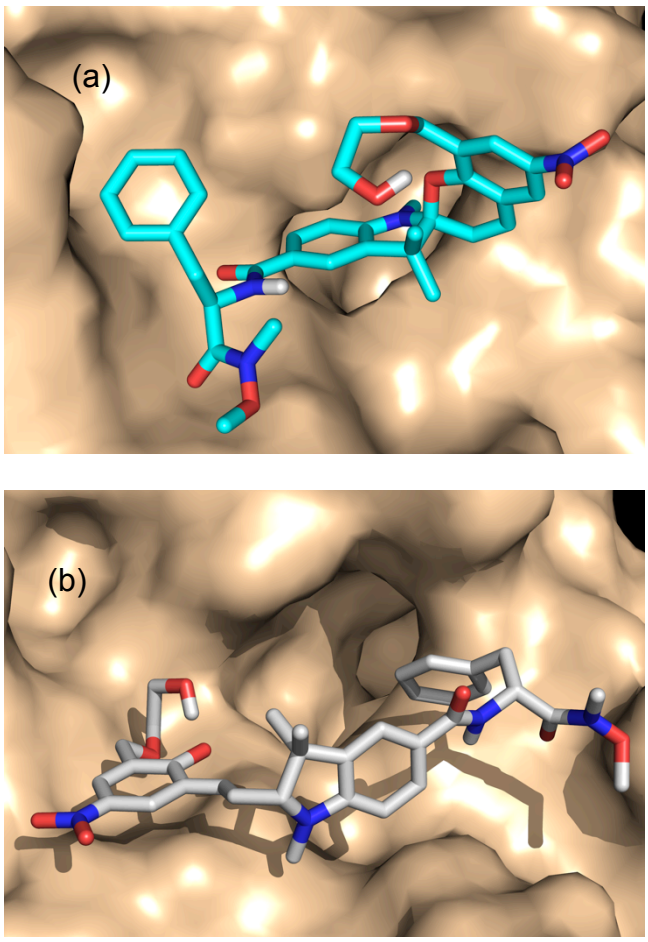

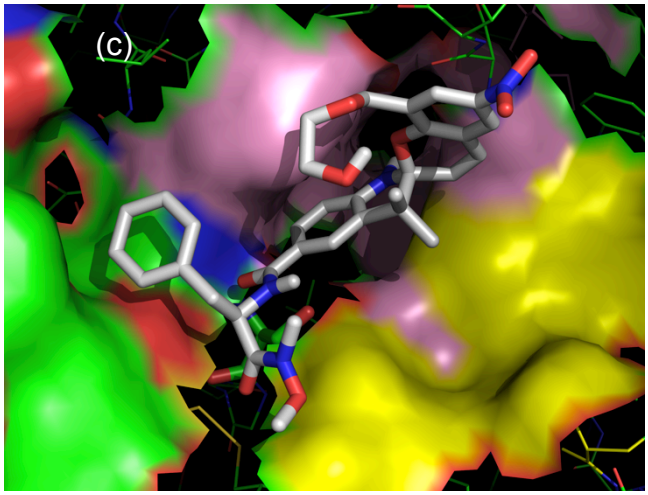

Figure 4.04 AutoDock4 results **4.07** in the active site of α-chymotrypsin (PDB code: 1GGD), (a) ring-closed SP **4.07**; (b) ring-opened MC **4.07**, and (c) key binding interactions of SP **4.07** with S2', S1, and S2 binding pockets highlighted in green, pink and yellow respectively.

4.3.5 Microstructured Optical Fibre-Based Experiments

Compound **4.07** was next attached to a silica-based suspended-core MOF (Supporting information, Figure S1) in order to probe its surface-based interactions with α-chymotrypsin as a step toward a functional sensor. All surface functionalization procedures were carried out under anhydrous conditions in a sealed metal chamber pressurized with N_2.[36] The fibre was first treated with pirahna solution (3:1 sulfuric acid : 30% H_2O_2 v/v) and the thus liberated free hydroxyl groups were reacted with 2.5% carboxyethylsilanetriol.[47] Steglich esterification[48] of the resulting carboxyl groups, with **4.07** in the presence of DIC, HOBt, and DMAP, to give the functionalized fibre (**Fibre-4.07**).

The ability of **4.07** to photoswitch when attached to the MOF was studied using the setup depicted in Figure 4.05. In particular, **Fibre-4.07** (SP isomer) was filled with Mili-Q water by capillary action and irradiated for 10 ms using a 532 nm laser and the resulting fluorescence was measured as shown in Figure 4.06.[36-37] The functionalized fibre was next irradiated with UV light (λ = 365 nm) for an extended period of 5 min in order to switch the surface attached SP-**4.07** to MC-**4.07** as per the solution experiments. Subsequent excitation of this isomer with 532 nm laser (as before) resulted in an enhanced (six-fold) average fluorescence relative to the SP isomer. This is consistent with the fluorescence characteristics of the MC isomer, where this isomer is known to have enhanced fluorescence due to π-conjugation as reported in literature.[28,43,49] (Figure 4.06, black, λ_{em} ~ 630 nm). Subsequent exposure of the **Fibre-4.07** to visible light for 5 min decreased the fluorescence intensity, as expected for a photostationary state enriched in SP isomer. Thus **4.07** is able to be reversibly photoswitched on fibre as per in solution. This is an important observation for sensor development.

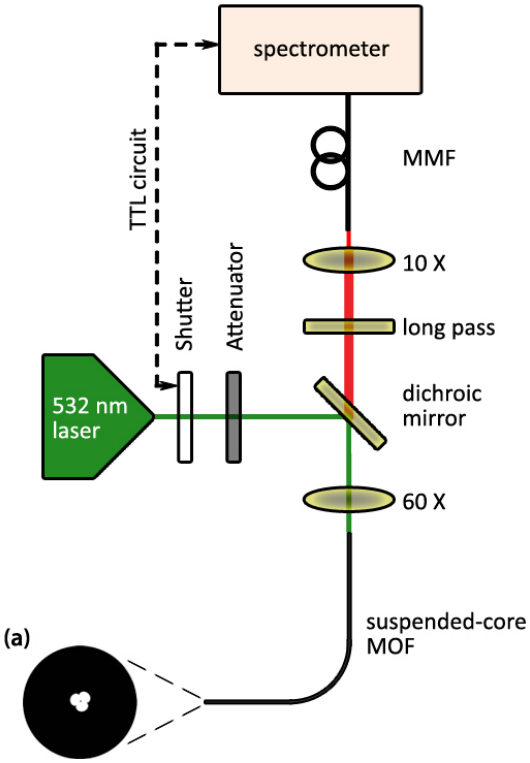

Figure 4.05 Optical set-up for measuring the fluorescence of a functionalized MOF. The area of illumination is shown by the dotted rectangle. (a) A cross section of the silica suspended-core fibre (see Figure S1 for SEM image).

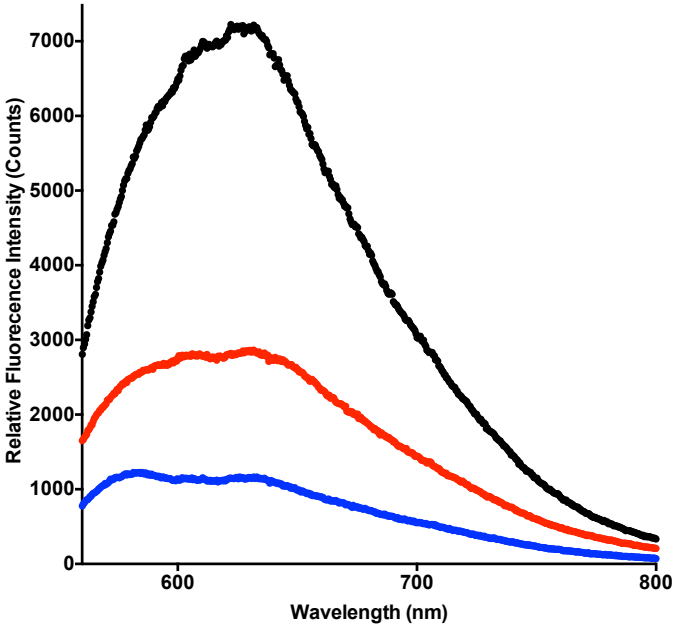

Figure 4.06 Fluorescence spectra of **Fibre-4.07** (SP) in water (blue), fibre-bound **4.07** in water irradiated with UV light (λ = 365 nm) (black) and **Fibre-4.07** subsequently irradiated with visible light (red). Fluorescence was induced by exposure of **Fibre-4.07** to 10 cycles of the 532 nm laser irradiation 10 ms per exposure. The spectra are averages of 10 fluorescence measurements of each sample.

Next, the fluorescence of **Fibre-4.07** (SP isomer) in the presence of α-chymotrypsin was measured to investigate enzyme binding. A new section of **Fibre-4.07** was filled with a solution of α-chymotrypsin in water (1 μM) over 5 min and the fluorescence was measured at 0, 10, 25, and 85 min by excitation with a 532 nm laser (10 x 10 ms pulses) in each case. After 10 min the fluorescence was observed to be 6-fold lower (c.f. Figure 4.07a, red and brown lines), which we suggest is the result of active site binding of the SP isomer of **4.07** that would quench the inhibitor's fluorescence. A similar decrease in fluorescence was observed in the solution-based experiments with compound **4.07** and α-chymotrypsin (see Figure S8 Supporting Information for detail). The fluorescence intensity increased gradually over the ensuring measurements (25, 85 min, see Figure 4.07a, blue and black curves respectively). This is consistent with slow but incomplete isomerism to the MC isomer in the dark,[50] with this isomer having an inherent enhanced fluorescence while also dissociating from the enzyme due to its weaker binding affinity as demonstrated in the solution-based experiments. In support, it is known that α-chymotrypsin has a greater affinity for non-polar inhibitors (e.g. the SP isomer) compared to polar inhibitors (e.g. MC isomer).[51]

Repeated photoswitching between the SP and MC isomer produced similar changes in fluorescence intensities (see Figure S9 Supporting Information for detail), which showed that MOF is a suitable platform for monitoring chymotrypsin activity reversibly. Finally, the experiment was repeated using water in place of α-chymotrypsin as a negative control. No significant change in fluorescence was apparent after 85 min (see Figure 4.08), which confirms that the earlier changes in fluorescence on fibre were due to the enzyme binding to **4.07**.

The binding of fibre-bound MC isomer with α-chymotrypsin was similarly investigated. The solution-filled section of the fibre was cleaved and discarded and the remaining section was infused with a fresh sample ofaα-chymotrypsin by capillary action over 5 min with concomitant UV (365 nm) irradiation in order to give a photostationary state enriched in the MC isomer. Fluorescence was measured at 0, 10, 25, and 85 min with laser irradiations (10 x 10 ms, 532 nm) as before, without any apparent significant change in fluorescence over the time course (see Figure 4.07b). This is consistent with the earlier solution-based observation that the MC isomer has significantly reduced activity and does not effectively bind to the protease. Small variations in fluorescence are likely a result of incomplete isomerization from the SP isomer to the MC isomer. This demonstrates that attaching **4.07** to fibre does not affect the relative binding affinities of the SP and MC isomers.

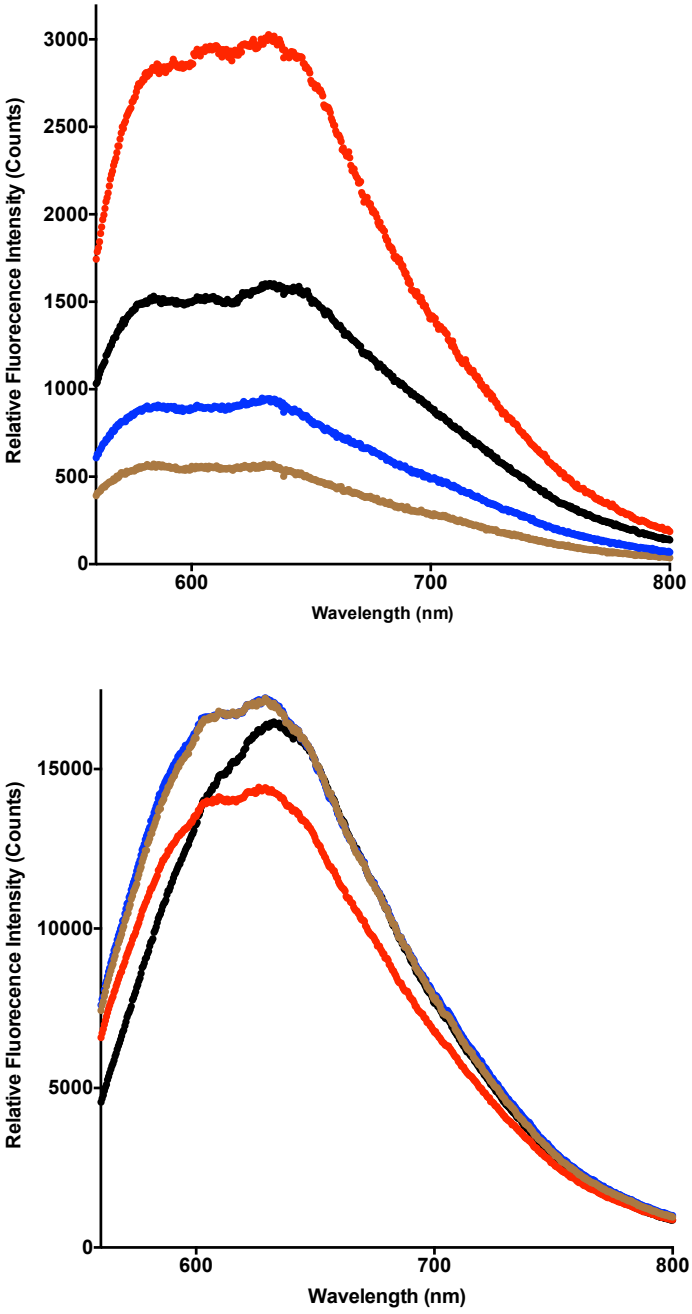

Figure 4.07 Fluorescent emissions of (a) SP of fibre-bound **4.07** with α-chymotrypsin left at room temperature for 0 min (red), 10 min (brown), 25 min (blue), and 85 min (black). The fibre-bound compound was excited by 10 pulses of 532 nm laser irradiation before each measurement; and (b) MC of fibre-bound **4.07** (isomerized under UV irradiation (λ = 365 nm)) with α-chymotrypsin left at room temperature for 0 min (red), 10 min (brown), 25 min (blue), and 85 min (black).

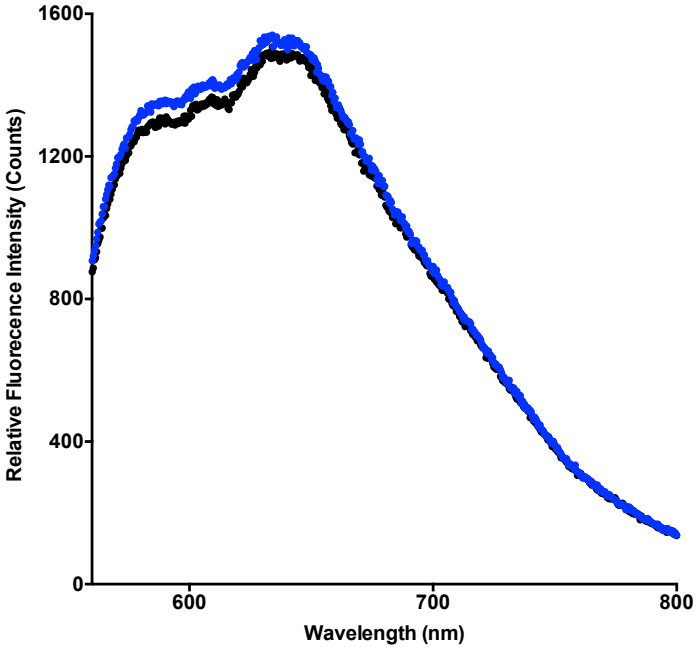

Figure 4.08 Fluorescence emissions of compound **4.07** incubated in Mili-Q water for 0 min (blue) and 85 min (black).

4.4 Conclusion

Here we report the development of the first examples of spiropyran-based protease inhibitors, which are able to undergo reversible photoisomerization between an active non-polar SP isomer and a significantly less active polar MC isomer upon UV/visible light irradiations. The inhibitors reported here were specifically designed to target α-chymotrypsin as a first step toward a more modular approach to a range of proteases.

The spiropyrans **4.01-4.11** were synthesized and assayed against α-chymotrypsin. The spiropyran cores alone (**4.01-4.03**) were active against α-chymotrypsin. The incorporation of phenylalanyl mimetic at the *C*-terminus (**4.04-4.10**) significantly improved the binding affinity. Compound **4.10** with an

additional *C*-terminal α-ketoester, was found to be the most active inhibitor in this series, with a K_i of 115 nM.

The Weinreb amide **4.07** was chosen as a stable analogue suitable for fibre functionalization while exhibiting reasonable activity against α-chymotrypsin (K_i = 86 μM). This compound was shown to bind as a competitive inhibitor by the Dixon plot and the *in silico* docking experiments. The UV irradiation of **4.07** in solution gave a photostationary state enriched in the MC isomer that was 6-fold less active against the enzyme than the SP isomer. This is consistent with the general observations that α-chymotrypsin has a greater affinity for non-polar inhibitors compared to polar inhibitors. A sample of **4.07** attached to a MOF (**Fibre-4.07**) could be reversibly photoisomerized to the MC isomer on fibre as per in solution.

Quenching of fluorescence (6-fold) was observed for the fibre-bound SP isomer of **4.07** after 10 min incubation with α-chymotrypsin, which is consistent with active-site binding. No significant change in fluorescence was apparent over 85 min incubation of the MC fibre-bound isomer with α-chymotrypsin. This is consistent with the earlier solution-based observation that the MC isomer has significantly reduced binding affinity compared to the SP isomer.

In this work we report a new class of spiropyran-based protease inhibitor, the inhibitory activity of which can be controlled by irradiation with light of a specific wavelength, both in solution and on attachment to a MOF. This

provides an important basis for probing and modulating enzyme activity in a confined and well-defined environment, and paves the way for potential real-time biosensing applications for *in vivo* disease diagnosis.

4.5 Experimental Section

4.5.1 General Information

Unless otherwise indicated, all starting materials, enzymes, chemicals and anhydrous solvents were purchased from Sigma Aldrich (NSW, Australia) and were used without further purification. UNIBOND C-18 reverse phase silica gel was purchased from Analtech Inc., USA. 3-(Chloromethyl)-2-hydroxy-5-nitrobenzaldehyde and compound **4.11** were prepared as previously described.[36] ^{1}H and ^{13}C NMR spectra were recorded on a Varian 500 MHz and a Varian Inova 600 MHz instruments in the indicated solvents. Chemical shifts are reported in ppm (δ). Signals are reported as s (singlet), br s (broad singlet), d (doublet), dd (doublet of doublets), t (triplet) or m (multiplet). High resolution mass spectra were collected using an LTQ Orbitrap XL ETD using flow injection, with a flow rate of 5 µL/min. Where indicated compounds were analyzed and purified by reverse phase HPLC, using an HP 1100 LC system equipped with a Phenomenex C-18 column (250 × 4.6 mm) for analytical traces and a Gilson GX-Prep HPLC system equipped with a Phenomenex C18 column (250 × 21.2 mm). H_2O/TFA (100/0.1 by v/v) and ACN/TFA (100/0.08 by v/v) solutions were used as aqueous and organic buffers. All graphs were generated using GraphPad Prism 6 software. A mercury lamp

(365 nm) and a halogen lamp (> 450 nm) were used as the UV and visible light sources in photoswitching experiments.

4.5.2 Chemical Syntheses

8-(2-(2-Ethoxyethoxy)ethoxy)-1',3',3'-trimethyl-6-nitrospiro[chromene-2,2'-indoline]-5'-carboxylic acid (4.01): To an ice-cooled solution of NaH (371 mg, 8.90 mmol) in anhydrous THF (15 ml) was added diethylene glycol monoethyl ether (747 mg, 5.57 mmol) dropwise under N_2. The mixture was stirred for 15 min with ice cooling and then a solution of 3-(chloromethyl)-2-hydroxy-5-nitrobenzaldehyde (1g, 4.64 mmol) in anhydrous THF (5 ml) was added dropwise. The mixture was allowed to warm to room temperature with stirring for 18 h under N_2. The mixture was cooled in ice before H_2O (160 ml) was added slowly to quench the reaction. The mixture was washed with CH_2Cl_2 (2 × 90 ml). The aqueous layer was acidified to pH 1 with 1 M aqueous HCl and extracted with ethyl acetate (3 × 90 ml). The organic phase was combined, dried over Na_2SO_4 and concentrated *in vacuo* to give **4.15** (1.12 g, 77%), which was used in the subsequent step without further purification. ^{1}H NMR (300 MHz, $CDCl_3$) δ 10.02 (s, 1H), 8.62 (s, 1H), 8.49 (s, 1H), 4.70 (s, 2H), 3.90-3.54 (m, 10H), 1.26-1.19 (t, *J* = 4.5 Hz, 3H); and MS: $[M]^+_{calcd}$ = 313.12, $[M]^+_{found}$ = 313.12.

To a solution of **4.15** (181 mg, 0.58 mmol) and **4.14** (125 mg, 0.58 mmol) in anhydrous ethanol (17 mM) was added Et_3N (59 mg, 0.58 mmol)). The mixture was refluxed for 3 h under N_2 and concentrated *in vacuo*. The crude

mixture was purified using C-18 reverse phase silica gel (35 % MeCN in H_2O) to give **1a** (80 mg, 27%)**.** ^{1}H NMR (600 MHz, CD_3OD) δ 8.14 (d, *J* = 2.6 Hz, 1H), 8.06 (d, *J* = 2.7 Hz, 1H), 7.91 (d, *J* = 8.2, 1H), 7.74 (s, 1H), 7.12 (d, *J* = 10.4 Hz, 1H), 6.63 (d, *J* = 8.2 Hz, 1H), 6.00 (d, *J* = 10.4 Hz, 1H), 4.37 – 4.25 (m, 2H), 3.59 – 3.38 (m, 10H), 2.79 (s, 3H), 1.32 (s, 3H), 1.20 (s, 3H), 1.14 (t, *J* = 7.0 Hz, 3H). ^{13}C NMR (151 MHz, CD_3OD) δ 156.2, 151.5, 140.8, 136.1, 131.0, 128.5, 128.4, 125.8, 124.3, 122.9, 121.6, 120.4, 118.6, 106.5, 105.9, 70.2, 70.0, 69.4, 66.2, 51.4, 39.0, 27.6, 24.8, 18.7, 14.0. HRMS (ESI) found $[M+H]^+$ 513.2230, $C_{27}H_{33}N_2O_8^+$ requires 513.2237.

8-(Azidomethyl)-1',3',3'-trimethyl-6-nitrospiro[chromene-2,2'-indoline]-5'-carboxylic acid (4.02): To a solution of sodium azide (166 mg, 2.60 mmol) in anhydrous DMSO (4.6 ml) was added 3-(chloromethyl)-2-hydroxy-5-nitrobenzaldehyde (500 mg, 2.30 mmol) in one portion. The mixture was stirred at room temperature under N_2 for 18 h. H_2O (5 ml) was added dropwise and the mixture was extracted with ethyl acetate (2 × 20 ml). The combined organic phase was washed with H_2O (20 ml), dried over Na_2SO_4 and concentrated *in vacuo* to yield **4.16** as a pale yellow solid (389 mg, 76%), which was subsequently used without further purification. ^{1}H NMR (500 MHz, $CDCl_3$) δ 12.01 (s, 1H), 10.02 (s, 1H), 8.55 (s, 1H), 8.48 (s, 1H), 5.30 (s, 1H), 4.56 (s, 2H), 1.55 (s, 1H); and MS: $[M]^+_{calcd}$ = 222.04, $[M]^+_{found}$ = 222.04.

To a solution of **4.16** (611 mg, 2.75 mmol) and **4.14** (593 mg, 2.75 mmol) in anhydrous ethanol (17 mM) was added Et_3N (278 mg, 2.75 mmol). The mixture was refluxed for 3 h under N_2 and then concentrated *in vacuo*. The

mixture was purified using C-18 reverse phase silica gel (25% MeCN in H_2O) to give **4.02** (150 mg, 13%). ^{1}H NMR (500 MHz, DMSO-d_6) δ 8.26 (s, 1H), 8.17 (s, 1H), 7.80 (d, *J* = 8.3 Hz, 1H), 7.68 (s, 1H), 7.28 (d, *J* = 10.5 Hz, 1H), 6.68 (d, *J* = 8.1 Hz, 1H), 6.06 (d, *J* = 10.5 Hz, 1H), 4.27 (d, *J* = 13.6 Hz, 1H), 4.23 (d, *J* = 13.6 Hz, 1H), 2.75 (s, 3H), 1.27 (s, 3H), 1.15 (s, 3H). ^{13}C NMR (151 MHz, DMSO-d_6) δ 167.7, 157.0, 151.0, 140.2, 135.8, 130.9, 128.5, 125.9, 123.1, 122.9, 121.1, 119.0, 106.7, 106.5, 51.6, 48.1, 28.5, 25.8, 19.6. HRMS (ESI) found $[M]^+$ 421.1381, $C_{21}H_{19}N_5O_5^+$ requires 421.1386.

8-((2-Hydroxyethoxy)methyl)-1',3',3'-trimethyl-6-nitrospiro[chromene-2,2'-indoline]-5'-carboxylic acid (4.03): To an ice-cooled solution of NaH (63 mg, 1.59 mmol) in anhydrous THF (2.8 ml) was added diethylene glycol monoethyl ether (99 mg, 1.59 mmol) dropwise at under N_2. The mixture was stirred for 15 min with ice cooling and then a solution of 3-(chloromethyl)-2-hydroxy-5-nitrobenzaldehyde (200 mg, 0.80 mmol) in anhydrous THF (0.7 ml) was added dropwise. The mixture was allowed to warmed to room temperature with stirring for 18 h under N_2. The mixture was cooled in ice before H_2O (35 ml/mmol aldehyde) was added slowly to quench the reaction. The mixture was washed with CH_2Cl_2 (2 × 20 ml). The aqueous layer was acidified to pH 1 with 1 M aqueous HCl and extracted with ethyl acetate (3 × 20 ml). The organic phase was combined, dried over Na_2SO_4 and concentrated *in vacuo* to give **4.17** (115 mg, 60%), which was used in the subsequent step without purification. ^{1}H NMR (500 MHz, $CDCl_3$) δ 11.92 (s, 1H), 10.01 (s, 1H), 8.57 (s, 2H), 8.50 (s, 1H), 4.85 (s, 2H), 2.25 – 2.11 (m, 2H), 1.58 (s, 1H), 1.25 (s, 1H); and MS: $[M]^+_{calcd}$ = 241.06, $[M]^+_{found}$ = 241.06.

To a solution of **4.17** (115 mg, 0.47 mmol) and **4.14** (101 mg, 0.47 mmol) in anhydrous ethanol (17 mM) was added Et_3N (47 mg, 0.47 mmol)). The mixture was refluxed for 3 h under N_2 and concentrated *in vacuo*. The crude mixture was purified using C-18 reverse phase silica gel (30% ACN in H_2O) to give **4.03** (93 mg, 45 %). ^{1}H NMR (500 MHz, CD_3OD) δ 8.19 (s, 1H), 8.07 (s, 1H), 7.92 (d, *J* = 8.2 Hz, 1H), 7.75 (s, 1H), 7.14 (d, *J* = 10.4 Hz, 1H), 6.64 (d, *J* = 8.2 Hz, 1H), 6.01 (d, *J* = 10.4 Hz, 1H), 4.57 (br s, 1H), 4.32 (s, 2H), 3.62 – 3.52 (m, 2H), 3.45 – 3.35 (m, 2H), 2.80 (s, 3H), 1.33 (s, 3H), 1.22 (s, 3H). ^{13}C NMR (151 MHz, CD_3OD) δ 157.7, 152.8, 142.5, 137.6, 132.4, 130.1, 127.5, 125.7, 124.4, 123.1, 122.1, 120.2, 108.1, 107.4, 73.7, 67.7, 62.4, 40.6, 29.2, 26.3, 20.3. HRMS (ESI) found $[M]^+$ 440.1581, $C_{23}H_{24}N_2O_7^+$ requires 440.1584.

General Procedure A for HATU-mediated Peptide Coupling

To a solution of carboxylic acid (1 equiv) in anhydrous DMF (40 mM) was sequentially added HATU (1 equiv) and the amine (1.2 equiv.). The mixture was stirred under N_2 for 15 min, cooled in an ice bath, and DIPEA (4 equiv) was added dropwise. The mixture was allowed to warm up to room temperature while stirring under N_2 for 18 h. 1 M aqueous HCl (10 ml/mmol of carboxylic acid) was added and the mixture was extracted with ethyl acetate (3 × 50 ml/mmol of carboxylic acid). The combined organic phase was washed with 1 M aqueous HCl (10 ml/mmol of carboxylic acid), saturated $NaHCO_3$ (10 ml/mmol of carboxylic acid) and brine (20 ml/mmol of carboxylic acid). The organic phase was dried over Na_2SO_4 and concentrated *in vacuo*.

The crude product was purified using C-18 reverse phase silica gel (30-50% MeCN in H_2O).

8-(2-(2-Ethoxyethoxy)ethoxy)-N-((R)-1-hydroxy-3-phenylpropan-2-yl)-1',3',3'-trimethyl-6-nitrospiro[chromene-2,2'-indoline]-5'-carboxamide (4.04): Compound **4.04** (96 mg, 62%) was prepared by coupling **4.01** with *L*-phenylalaninol **4.18** according to General Procedure A. ^{1}H NMR (600 MHz, CD_3OD) δ 8.19 (s, 1H), 8.08 (s, 1H), 7.79 – 7.61 (m, 1H), 7.51 (s, 1H), 7.33 – 7.21 (m, 2H), 7.19 – 7.15 (m, 1H), 7.13 (d, *J* = 10.4 Hz, 1H), 6.62 (d, *J* = 8.2 Hz, 1H), 6.00 (d, *J* = 10.4 Hz, 1H), 4.59 (br s, 1H), 4.41 – 4.23 (m, 3H), 3.75 – 3.59 (m, 2H), 3.55 – 3.37 (m, 10H), 3.13 – 2.95 (m, 1H), 2.95 – 2.83 (m, 1H), 2.78 (s, 3H), 2.65 (s, 2H), 1.37 (s, 3H), 1.22 (s, 3H), 1.14 (t, *J* = 7.0 Hz, 3H). ^{13}C NMR (151 MHz, CD_3OD) δ 168.8, 156.2, 150.6, 140.8, 138.7, 136.3, 128.9, 128.5, 128.0, 127.9, 125.9, 125.8, 125.5, 124.2, 121.6, 120.7, 120.5, 118.6, 106.5, 106.0, 70.1, 70.0, 69.4, 66.2, 63.0, 53.4, 51.5, 39.0, 36.6, 27.60, 24.70, 18.7, 14.0. HRMS (ESI) found $[M]^+$ 645.3055, $C_{36}H_{43}N_3O_8^+$ requires 645.3050.

8-(2-(2-Ethoxyethoxy)ethoxy)-N-((2R,3S)-1-carbomethoxy-1-hydroxy-3-phenylpropan-2-yl)-1',3',3'-trimethyl-6-nitrospiro[chromene-2,2'-indoline]-5'-carboxamide (4.05): Compound **4.05** (54 mg, 47%) was prepared by coupling of compound **4.01** with (2*R*,3*S*)-methyl 3-amino-2-hydroxy-4-phenylbutanoate **4.19**[38] according to General Procedure A. ^{1}H NMR (599 MHz, CD_3OD) δ 8.17 (s, 1H), 8.08 (s, 1H), 7.90 (s, 1H), 7.72 – 7.62 (m, 1H), 7.53 (s, 1H), 7.40 – 7.27 (m, 4H), 7.26 – 7.18 (m, 1H), 7.15 (d, *J* =

10.4 Hz, 1H), 6.65 (d, *J* = 8.2 Hz, 1H), 6.01 (d, *J* = 10.4 Hz, 1H), 4.71 (m, 1H), 4.58 (br s, 1H), 4.32 (s, 2H), 4.22 (s, 1H), 3.68 (s, 3H), 3.58 – 3.39 (m, 10H), 3.15 – 2.94 (m, 2H), 2.78 (s, 3H), 1.34 (s, 3H), 1.22 (s, 3H), 1.15 (t, *J* = 7.0 Hz, 3H). ^{13}C NMR (151 MHz, CD_3OD) δ 175.2, 170.2, 157.7, 152.3, 142.4, 139.7, 137.9, 130.6, 130.1, 129.7, 127.8, 127.4, 126.7, 125.8, 123.1, 122.3, 122.0, 120.2, 108.1, 107.6, 72.1, 71.7, 71.6, 71.0, 67.7, 55.6, 53.1, 52.8, 38.5, 29.2, 26.3, 20.2, 15.6. HRMS (ESI) found $[M]^+$ 703.3104, $C_{38}H_{45}N_3O_{10}^+$ requires 703.3105.

8-(Azidomethyl)-N-((R)-1-hydroxy-3-phenylpropan-2-yl)-1',3',3'-trimethyl-6-nitrospiro[chromene-2,2'-indoline]-5'-carboxamide (4.06): Compound **4.06** (120 mg, 87%) was prepared by coupling of compound **4.02** with *L*-phenylalaninol **4.18** according to General Procedure A. ^{1}H NMR (500 MHz, CD_3OD) δ 8.12 (s, 1H), 8.09 (s, 1H), 7.67 (d, *J* = 8.2 Hz, 1H), 7.56 (d, *J* = 6.0 Hz, 1H), 7.27 (m, 4H), 7.16 (m, 2H), 6.62 (d, *J* = 8.2 Hz, 1H), 6.02 (d, *J* = 10.4 Hz, 1H), 4.58 (s, 1H), 4.38 – 4.29 (m, 1H), 4.26 (d, *J* = 13.8 Hz, 1H), 4.18 (d, *J* = 13.8 Hz, 1H), 3.65 (d, *J* = 5.3 Hz, 2H), 3.10 – 2.85 (m, 2H), 2.81 (s, 3H), 1.34 (s, 3H), 1.21 (s, 3H). ^{13}C NMR (126 MHz, CD_3OD) δ 168.9, 156.8, 150.5, 140.7, 138.7, 136.01, 128.9, 128.4, 128.1, 127.9, 125.9, 125.6, 125.2, 123.0, 122.4, 120.7, 120.7, 119.2, 107.1, 106.0, 62.9, 53.4, 51.7, 36.6, 27.6, 24.9, 24.8, 18.7. HRMS (ESI) found $[M]^+$ 554.2278, $C_{30}H_{30}N_6O_5^+$ requires 554.2278.

8-((2-Hydroxyethoxy)methyl)-N-((R)-1-(methoxy(methyl)amino)-1-oxo-3-phenylpropan-2-yl)-1',3',3'-trimethyl-6-nitrospiro[chromene-2,2'-indoline]-5'-carboxamide (4.07): Compound **4.07** (74 mg, 57%) was

prepared by coupling of compound **4.03** with compound **4.21** according to General Procedure A. ^{1}H NMR (500 MHz, CD_3OD) δ 8.19 (s, 1H), 8.07 (s, 1H), 7.69 (d, *J* = 7.5 Hz, 1H), 7.58 (s, 1H), 7.29 (d, *J* = 3.4 Hz, 4H), 7.21 (br s, 1H), 7.13 (d, *J* = 10.4 Hz, 1H), 6.63 (d, *J* = 8.4 Hz, 1H), 6.00 (d, *J* = 10.5 Hz, 1H), 5.35 (br s, 1H), 4.30 (s, 1H), 3.80 (s, 3H), 3.56 (t, *J* = 4.6 Hz, 2H), 3.35 (d, *J* = 4.5 Hz, 2H), 3.20 (s, 3H), 3.18-3.02 (m, 2H), 2.78 (s, 3H), 1.34 (s, 3H), 1.21 (s, 3H). ^{13}C NMR (151 MHz, CD_3OD) δ 156.1, 150.9, 140.9, 136.3, 128.9, 128.6, 128.3, 128.0, 126.4, 125.8, 124.1, 121.5, 120.8, 120.4, 118.6, 106.5, 106.0, 72.1, 66.1, 60.8, 56.07, 51.5, 41.0, 29.4, 27.6, 23.0, 18.6, 16.0. HRMS (ESI) found $[M]^+$ 630.2694, $C_{34}H_{38}N_4O_8^+$ requires 630.2690.

General Procedure B for Dess-Martin Oxidation of Alcohol

To a solution of alcohol (1 equiv) in anhydrous CH_2Cl_2 (7 mM) under N_2 was added Dess-Martin periodinane (3 equiv) in one portion. The mixture was stirred at room temperature under N_2 for 1.5 h. The mixture was diluted with CH_2Cl_2 (100 ml/mmol of alcohol) and then $Na_2S_2O_3$ in saturated $NaHCO_3$ (10% w/v, 10 ml/mmol of alcohol) was added. The mixture was stirred for 15 min and the aqueous phase was separated and extracted with CH_2Cl_2 (50 ml/mmol of alcohol). The combined organic phase was dried over Na_2SO_4 and concentrated *in vacuo*. The crude product was purified using RP-HPLC.

8-((2-(2-Ethoxyethoxy)ethoxy)methyl)-1',3',3'-trimethyl-6-nitro-N-((R)-1-oxo-3-phenylpropan-2-yl)spiro[chromene-2,2'-indoline]-5'-carboxamide (4.08): Compound **4.04** was oxidized according to General Procedure B to

give compound **4.08** (3 mg, 8%). ^{1}H NMR (500 MHz, $CDCl_3$) δ 9.74 (s, 1H), 8.20 (s, 1H), 7.95 (d, *J* = 2.6 Hz, 1H), 7.54 (m, 2H), 7.40 – 7.18 (m, 5H), 6.96 (d, *J* = 10.4 Hz, 1H), 6.52 (d, *J* = 8.0 Hz, 1H), 5.84 (d, *J* = 10.2 Hz, 1H), 4.89 (s, 1H), 4.29 (s, 2H), 3.67 – 3.44 (m, 10H), 3.29 (m, 2H), 2.75 (s, 3H), 1.29 (s, 3H), 1.23 – 1.12 (m, 6H). ^{13}C NMR (151 MHz, CD_3OD) δ 168.9, 156.2, 150.6, 140.8, 139.2, 129.0, 128.9, 128.5, 128.1, 127.9, 127.3, 125.8, 125.8, 124.2, 121.6, 120.8, 118.6, 106.5, 105.9, 70.1, 70.0, 69.8, 66.1, 51.5, 39.0, 34.7, 34.6, 27.6, 24.7, 24.7, 18.7, 14.0. HRMS (ESI) found $[M]^+$ 643.2894, $C_{36}H_{41}N_3O_8^+$ requires 643.2898.

(3R)-Methyl 3-(8-((2-(2-ethoxyethoxy)ethoxy)methyl)-1',3',3'-trimethyl-6-nitrospiro[chromene-2,2'-indoline]-5'-ylcarboxamido)-2-oxo-4-phenylbutanoate (4.09): To a solution of **4.05** (33 mg, 0.047 mM) in anhydrous CH_2Cl_2 (2.4 ml) under N_2 was added Dess-Martin periodinane (20 mg, 0.047 mM) in one portion. The mixture was stirred at room temperature under N_2 for 3 h. The mixture was diluted with CH_2Cl_2 (4.7 ml) and $Na_2S_2O_3$ in saturated $NaHCO_3$ (10% w/v, 0.5 ml) was added. The mixture was stirred for 15 min and the aqueous phase was separated and extracted with CH_2Cl_2 (2.4 ml). The combined organic phase was dried over Na_2SO_4 and concentrated *in vacuo* to give the crude product as a dark red oil, which was purified by RP-HPLC to give **4.09** as a purple solid (2 mg, 6%). ^{1}H NMR (500 MHz, DMSO-d_6) δ 8.15 (s, 1H), 8.06 (s, 1H), 7.68 (d, *J* = 6.7 Hz, 1H), 7.56 (s, 1H), 7.28-7.20 (m, 5H), 7.12 (d, *J* = 10.4 Hz, 1H), 6.63 (d, *J* = 8.2 Hz, 1H), 5.99 (d, *J* = 10.3 Hz, 1H), 5.08 (s, 1H), 4.30 (s, 1H), 3.72 (s, 3H), 3.54-3.36 (m, 10H), 3.28-3.06 (m, 2H), 2.78 (s, 3H), 1.32 (s, 3H), 1.20 (s, 3H), 1.14 (t, *J* = 7.0 Hz,

3H). ^{13}C NMR (151 MHz, CD_3OD) δ 173.0, 168.8, 156.2, 149.4, 140.8, 138.5, 136.2, 129.0, 129.0, 128.5, 128.1, 127.8, 127.8, 126.4, 125.8, 125.8, 124.9, 124.2, 121.6, 120.7, 120.4, 118.6, 106.0, 105.9, 70.2, 70.1, 70.0, 70.0, 69.5, 66.2, 56.1, 51.5, 33.5, 27.6, 24.7, 18.6, 14.0. HRMS (ESI) found $[M]^+$ 701.2932, $C_{38}H_{43}N_3O_{10}^+$ requires 701.2948.

8-(Azidomethyl)-1',3',3'-trimethyl-6-nitro-N-((R)-1-oxo-3-phenylpropan-2-yl)spiro[chromene-2,2'-indoline]-5'-carboxamide (4.10): Compound **4.06** was oxidized according to General Procedure B to give **4.10** (7 mg, 10%). ^{1}H NMR (500 MHz, DMSO-d_6) δ 9.57 (s, 1H), 8.64 (d, *J* = 6.1 Hz, 1H), 8.25 (s, 1H), 8.16 (s, 1H), 7.70 (d, *J* = 8.2 Hz, 1H), 7.62 (s, 1H), 7.24 (m, 5H), 6.67 (d, *J* = 8.3 Hz, 1H), 6.04 (d, *J* = 10.4 Hz, 1H), 4.41 (m, 1H), 4.26 (d, *J* = 13.3 Hz, 1H), 4.18 (d, *J* = 13.3 Hz, 1H), 3.32-3.23 (m, 1H), 2.99 – 2.84 (m, 1H), 2.72 (s, 3H), 1.25 (s, 3H), 1.13 (s, 3H). ^{13}C NMR (151 MHz, CD_3OD) δ 169.1, 156.8, 150.5, 140.7, 138.7, 136.0, 1290.0, 128.4, 128.1, 127.9, 127.2, 125.8, 125.2, 123.0, 122.4, 120.7, 119.1, 107.1, 106.0, 97.8, 97.5, 55.8, 55.6, 51.7, 34.7, 27.6, 24.8, 18.7. HRMS (ESI) found $[M]^+$ 552.2138, $C_{30}H_{28}N_6O_5^+$ requires 552.2121.

3,3-Dimethyl-2-methyleneindoline-5-carboxylic acid (4.13): To a solution of 4-hydrazinobenzoic acid (2.00 g, 13.2 mmol) and 3-methyl-2-butanone (1.26 g, 14.4 mmol) in anhydrous ethanol was added 98% H_2SO_4 (0.4 ml) slowly. The reaction mixture was refluxed under N_2 for 18 h. The mixture was allowed to cool to room temperature and the resulting precipitate was removed by vacuum filtration. The filtrate was basified with saturated $NaHCO_3$

and washed with CH_2Cl_2 (2 × 15 ml). The pH of the aqueous phase was adjusted to 4 with 1 M aqueous HCl and extracted with CH_2Cl_2 (2 × 30 ml). The combined organic phase was dried over Na_2SO_4 and concentrated *in vacuo* to give **4.13** as a dark red solid (2.43 g, 91%). ^{1}H NMR (500 MHz, $CDCl_3$) δ 8.13 (d, *J* = 8.0 Hz, 1H), 8.04 (s, 1H), 7.63 (d, *J* = 8.5 Hz, 1H), 2.36 (s, 3H), 1.36 (s, 6H).

5-Carboxy-1,2,3,3-tetramethyl-3H-indolium iodide (4.14): To a solution of **4.13** (1.12 g, 5.5 mmol) in a mixture of anhydrous toluene and ACN (2 : 1, 30 ml) was added methyl iodide (782 mg, 5.5 mmol) dropwise. The mixture was refluxed for 18 h. After cooling to room temperature, the red precipitate was collected by vacuum filtration and washed with ethanol (5 ml) and hexane (30 ml) to yield **4.14** as a light grey solid (1.19 g, quant.). ^{1}H NMR (500MHz, DMSO-d_6) δ 8.36 (s, 1H), 8.17 (d, *J* = 8.0 Hz, 1H), 8.00 (d, *J* = 8.0 Hz, 1H), 3.97 (s, 3H), 2.79 (s, 3H), 1.55 (s, 6H).

(S)-2-Amino-N-methoxy-N-methyl-3-phenylpropanamide (4.21): To a solution of *N*-(*tert*-Butoxycarbonyl)-*L*-phenylalanine (500 mg, 1.88 mmol) in anhydrous CH_2Cl_2 (8 ml) was added BOP (833 mg, 1.88 mmol) and Et_3N (188 mg, 1.87 mmol). A solution of CH_3ONHCH_3.HCl (220 mg, 2.3 mmol) and Et_3N (155 mg, 1.5 mmol) in anhydrous CH_2Cl_2 (4.3 ml) was added to the mixture. The mixture was stirred under N_2 at room temperature for 21 h before quenched by 1 M aqueous HCl (20 ml). The mixture was diluted with DCM (50 ml) and the aqeous layer was separated and extracted with CH_2Cl_2 (2 × 50 ml). The combined organic phase was washed with 1M aqueous HCl (50 ml),

sat. $NaHCO_3$ (50 ml) and brine (50 ml), dried with Na_2SO_4 and concentrated *in vacuo* to give the crude product (630 mg), which was then dissolved in CH_2Cl_2 (24 ml). The solution was cooled on ice and then TFA (3 ml) was added. The mixture was stirred with ice cooling for 1 h. The volatiles were removed *in vacuo* to give the desired analog **4.21** as a white wax (188 mg, quant.) ^1H NMR (500MHz, $CDCl_3$) δ 7.35-7.11 (m, 5H), 5.15 (s, 1H), 4.95 (s, 1H), 3.65 (s, 3H), 3.16 (s, 3H), 3.10-2.81 (m, 2H).

4.5.3 Surface Attachment of 4.07 to a MOF (Fibre-4.07)

The MOFs used in this work were fabricated in-house. Details of the fibre and functionalization set-up have been reported previously.[36] The fibre was sealed into a metal chamber with a positive pressure of 50 psi applied to force solutions through the fibre. The inner surfaces of the fibre was washed with piranha solution (3:1 sulfuric acid : 30% H_2O_2 v/v, 1.5 ml) and carboxyethylsilanetriol in water (2.5% v/v, 9 ml) was forced through the fibre to functionalize the core surface via silanization.[47] A solution of **4.07** (0.5 mM), DIC (0.5 mM), HOBt (0.5 mM) and DMAP (0.3 mM) in ACN (10 ml) was then applied through the fibre overnight. The functionalized fibre (**Fibre-4.07**) was washed thoroughly with ACN (10 ml) and water (10 ml) for 6 h to remove unreacted **4.07** and other reagents.

4.5.4 Microstructured Optical Fibre (MOF) Experiments

All MOF experiments were conducted in the dark unless stated otherwise.

Fibre-4.07 was first coupled to an optical set-up as previously reported by Heng et al.[36] The fibre was filled with Mili-Q water for 5 min through capillary action. **Fibre-4.07** was excited by 10 pulses of laser irradiation (532 nm, 10 ms/pulse) and the resulting fluorescence emission after each pulse was measured by a spectrometer. **Fibre-4.07** was then irradiated with UV light (365 nm) generated from a mercury lamp for 5 min. **Fibre-4.07** was again subjected to 10 pulses of laser irradiation (532 nm, 10 ms/pulse) with the resulting fluorescence emissions measured similarly. **Fibre-4.07** was then irradiated with visible light generated from a halogen lamp (>450 nM) and was similarly subjected to laser irradiation with the fluorescence measured. The filled section of the fibre was cleaved and removed.

Fibre-4.07 (SP isomer) was then filled with a solution of α-chymotrypsin in Mili-Q water (1 μM) for 5 min and excited with 10 pulses of laser light (532 nm) as before for fluorescence measurements. **Fibre-4.07** (SP isomer) with α-chymotrypsin solution was left at room temperature for a total of 85 min with fluorescence measured at 10 min, 25 min and 85 min. 10 pulses of 532 nm laser light was used to induce fluorescence before each measurement. The solution-filled section of the fibre was cleaved and discarded and the remaining section of the fibre was filled with Mili-Q water over 5 min. **Fibre-4.07** was similarly excited with 10 laser pulses and the resulting fluorescence emission was measured. **Fibre-4.07** was left at room temperature for 85 min before the fluorescence was measured again. The solution-filled section of the fibre was again cleaved and the remaining section was filled with α-chymotrypsin in Mili-Q water (1 μM) for 5 min. **Fibre-4.07** was concomitantly

irradiated with UV light (365 nm) to allow isomerization to the corresponding MC isomer. **Fibre-4.07** (MC isomer) with α-chymotrypsin solution was left at room temperature for a total of 85 min with laser-induced fluorescence measured at 0 min, 10 min, 25 min and 85 min. The solution filled section of the fibre was cleaved and discarded.

4.6 Acknowledgements

We would like to thank Mr. Roman Kostecki, Dr. Herbert Foo, Mr. Daniel Stubing and Dr. Erik Schartner for their assistance with the fibre functionalization and all the fibre-based experiments. We also thank Mr. Jinxin Pei for his assistance for the *in silico* docking experiments and Dr. Ashok Pehere for assisting the synthesis of the weinreb amide.

4.7 Supporting Information

4.7.1 SEM Images of a Suspended-core Microstructured Optical Fibre

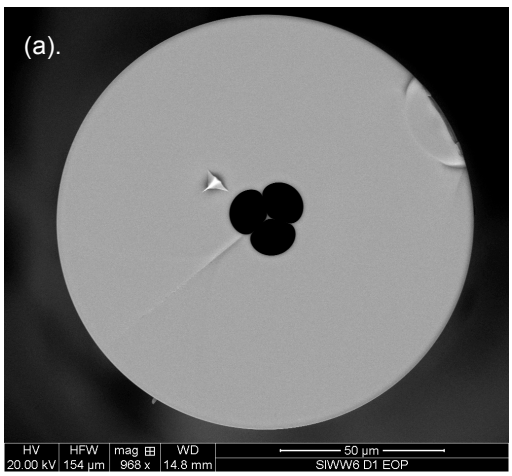

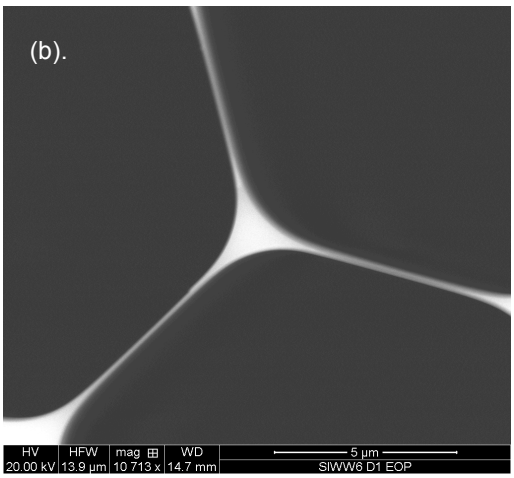

Figure S1. Scanning electron microscopic images of a suspended core microstructured optical fibre: (a) An image of the cross section of the MOF; (b) An expansion showing the core and sample chamber region of the MOF.

4.7.2 In vitro α-Chymotrypsin Assay

The assay was carried out with slight modification from literature.[25,52] The activity of α-chymotrypsin was assayed spectrophotometrically at 25 ºC using *Synergy H4 Hybrid Multi-Mode Microplate Reader* (Bio-Tek Instruments, Inc.). A solution of α-chymotrypsin (21.9 μg/mL) in 1 mM aqueous HCl was prepared fresh by a 1:40 dilution of a stock solution (874 μg/mL) in 1 mM aqueous HCl and kept on ice. A 1:100 dilution of the 21.9 μg/mL solution in ice-cold 1 mM aqueous HCl was prepared immediately before the start of each measurement. All compounds were analysed at 4-5 different inhibitor concentrations. The assay was conducted in black 96-well plates as below: To each well was added Ala-Ala-Phe-7-AMC (Sigma Aldrich, Castle Hill, NSW) substrate in DMSO (5 μL, final concentrations = 0.1-0.5 mM), α-chymotrypsin in 1 mM aqueous HCl (10 μL, final concentration = 4 nM), an inhibitor (0.01 nM-1 mM) in DMSO (10 μL) and N-[Tris(hydroxymethyl)methyl]-2-aminoethanesulfonic acid (TES) buffer (50 mM, pH 8.0, adjusted with NaOH) (175 μL). The excitation and emission wavelengths of the substrate were 380 nm and 460 nm respectively. Progress curves were monitored over 10 min for each concentration of every inhibitor. The K_i values of inhibitors were determined graphically according to Dixon[39]

using mean values of relative rates obtained from duplicate or triplicate measurements at two different concentrations.

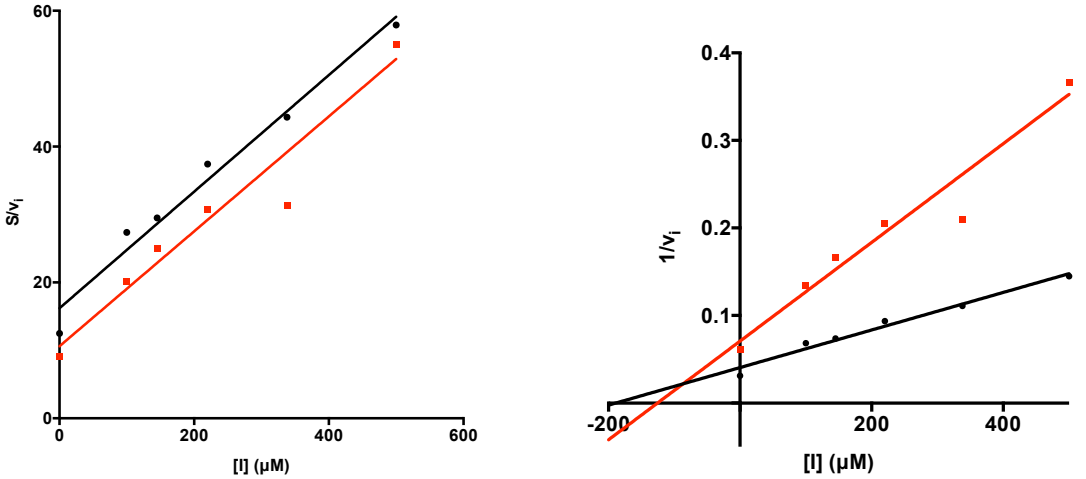

Figure S2. Left: Cornish-Bowden plot generated based on data of *in vitro* inhibition assay of **4.07** against α-chymotrypsin; right: Dixon plot generated based on data of *in vitro* inhibition assay of **4.07** against α-chymotrypsin. The red line in each plot represents the data set with substrate concentration of 150 μM (0.3 × K_m). The black line in each plot represents the data set with substrate concentration of 400 μM (0.8 × K_m).

4.7.3 In-Solution Photoisomerization of 4.07

A solution of **4.07** in MeOH (1 mM, 50 μL) was exposed to visible light (> 400 nm) for 15 min. UV/Vis absorption (λ = 300-700 nm) and fluorescence emission (λ_{ex} = 532 nm, λ_{em} = 300-700 nm) of this sample were measured using *Synergy H4 Hybrid Multi-Mode Microplate Reader*. The sample was irradiated with UV light at 365 nm for 15 min in the dark. UV-Vis absorption and fluorescence measurements were again measured. Compound **4.07** was

irradiated for 9 more cycles using both wavelengths with UV-Vis absorption and fluorescence measured after each cycle. The experiment was carried out in triplicate. The spectra and plots were generated with *GraphPad Prism 6*.

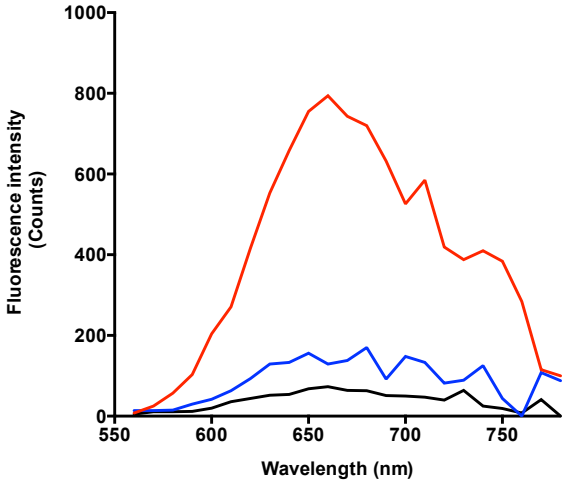

Figure S3. The fluorescence spectra (λ_{ex} = 532 nm) of **4.07** in MeOH under visible light (> 400 nm) (black), after irradiation with UV light (365 nm) for 15 min (red). Compound **4.07** was then isomerized by visible light irradiation again to produce spectrum in blue.

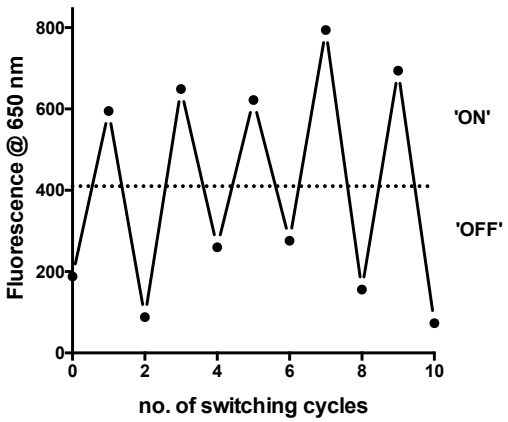

Figure S4. Fluorescence measurements (λ_{ex} = 532 nm, λ_{em} = 650 nm) of **4.07** after exposures to UV (365 nm) and visible light (> 400 nm) to induce

photoisomerization. Cycle 0 represents the state before **4.07** was irradiated with UV light. Cycles 1, 3, 5, 7 and 9 represent the state of **4.07** after irradiated with UV light for 15 min. Cycles 2, 4, 6, 8, and 10 represent the state of **4.07** after irradiated with visible light for 15 min.

4.7.4 In silico Docking Experiments

The coordinates of α-chymotrypsin (*Bos Taurus*) was obtained from Protein Data Bank (Entry: 1GGD). The molecular structures of the SP and MC isomers of **4.07** and the SP isomers of **4.08-4.10** were created with *GlycoBioChem PRODRG2 Server* (GlycoBioChem Ltd. University of Dundee, Scotland, UK) and subjected to energy minimization to optimize the conformations using *AutoDockTool* (The Scripps Research Institute, San Diego, CA, USA). The structures of **4.07-4.10** were separately docked into α-chymotrypsin using *AutoDock4*. A total of 25 docking runs and a maximum of 500,000 energy evaluations were performed on each structure using the Lamarckian Genetic Algorithm[46]. All the possible positions and orientations of ligands were attempted and representative conformations with the most favorable free energies were presented in Figures 4.05a-c and S5-S7. Various interactions involved in the protein/ligand complexes were analyzed also with *AutoDock4*. The inhibitor-enzyme complexes were visualized using *PyMol 1.3* (Schrödinger Inc., USA).

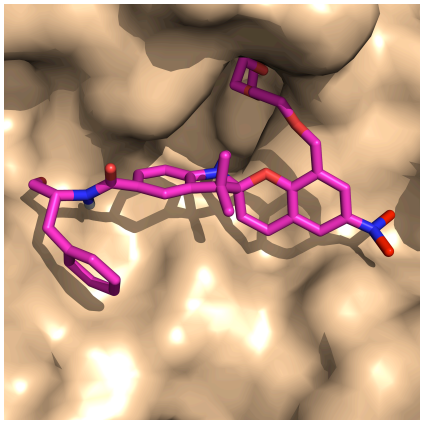

Figure S5. AutoDock4 results of docking of **4.08** in the active site of α-chymotrypsin (PDB entry: 1GGD).

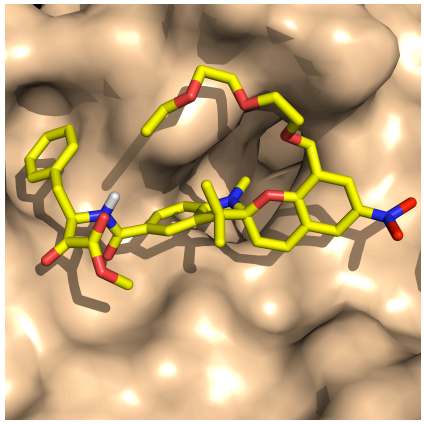

Figure S6. AutoDock4 results of docking of **4.09** in the active site of α-chymotrypsin (PDB entry: 1GGD).

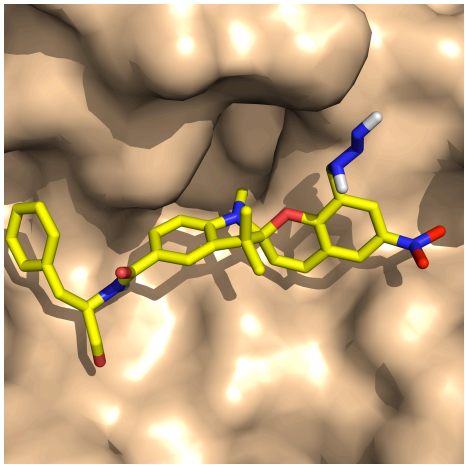

Figure S7. AutoDock4 results of docking of **4.10** in the active site of α-chymotrypsin (PDB entry: 1GGD).

4.7.5 Solution-based Binding of 4.07 with α-Chymotrypsin

A solution of compound **4.07** in DMSO (2 mM, 50 µL) was added to a solution of α-chymotrypsin in Mili-Q water (1 µM, 950 µL). This test sample together with a negative control containing the solution of α-chymotrypsin in water (1 µM, 950 µL), and a positive control containing the solution of compound **4.07** in DMSO (0.1 mM, 50 µL) were seperately incubated for 10 h at 25 ^{o}C under

ambient light (λ > 450 nm). After incubation, 200 μL of solution from each sample was transferred into a black 96-well plate for fluorescence measurements using *Synergy H4 Hybrid Multi-Mode Microplate Reader* (λ_{ex} = 532 nm). A solution containing both compound **4.07** (0.1 mM) and α-chymotrypsin (1 μM) in water (6% DMSO) without incubation (200 μL) was also added to the same plate for comparison. All samples were prepared in triplicate. The spectra produced were processed using *GraphPad Prism 6*.

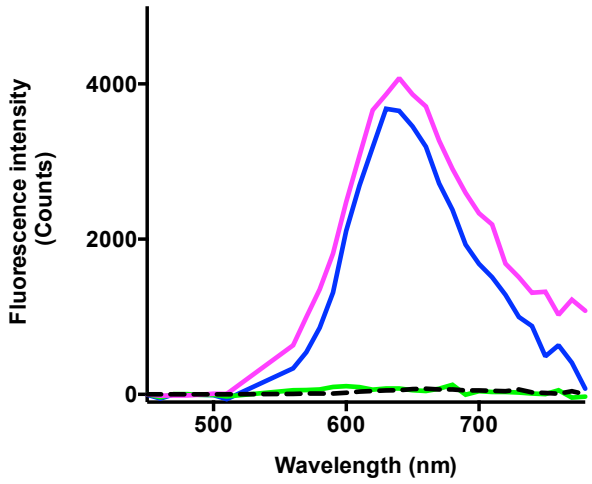

Figure S8. The fluorescence spectra (λ_{ex} = 532 nm) of i) α-chymotrypsin (1 μM) in water (black); ii) compound **4.07** (0.1 mM) in DMSO (blue); iii) compound **4.07** (0.1 mM) and α-chymotrypsin (1 μM) in water : DMSO (94:6) without incubation (magenta); and iv) compound **4.07** (0.1 mM) and α-chymotrypsin (1 μM) in water : DMSO (94:6) with 10-hour incubation at 25 ^{o}C (green).

4.8 References

(1) Bansal, A.; Zhang, Y. *Acc. Chem. Res.* **2014**, *47*, 3052.

(2) Szymanski, W.; Beierle, J. M.; Kistemaker, H. A. V.; Velema, W. A.; Feringa, B. L. *Chem. Rev.* **2013**, *113*, 6114.

(3) Chan, Y.-H.; Gallina, M. E.; Zhang, X.; Wu, I. C.; Jin, Y.; Sun, W.; Chiu, D. T. *Anal. Chem.* **2012**, *84*, 9431.

(4) Jung, H.-y.; You, S.; Lee, C.; You, S.; Kim, Y. *Chem. Commun.* **2013**, *49*, 7528.

(5) Willner, I.; Rubin, S.; Cohen, Y. *J. Am. Chem. Soc.* **1993**, *115*, 4937.

(6) Beharry, A. A.; Woolley, G. A. *Chem. Soc. Rev.* **2011**, *40*, 4422.

(7) Dohno, C.; Uno, S.-n.; Nakatani, K. *J. Am. Chem. Soc.* **2007**, *129*, 11898.

(8) Hamill, A. C.; Wang, S.-C.; Lee, C. T. *Biochemistry* **2005**, *44*, 15139.

(9) Wang, S.-C.; Lee, C. T. *The Journal of Physical Chemistry B* **2006**, *110*, 16117.

(10) Auernheimer, J. r.; Dahmen, C.; Hersel, U.; Bausch, A.; Kessler, H. *J. Am. Chem. Soc.* **2005**, *127*, 16107.

(11) Hohsaka, T.; Kawashima, K.; Sisido, M. *J. Am. Chem. Soc.* **1994**, *116*, 413.

(12) Banghart, M.; Borges, K.; Isacoff, E.; Trauner, D.; Kramer, R. H. *Nat Neurosci* **2004**, *7*, 1381.

(13) Pearson, D.; Downard, A. J.; Muscroft-Taylor, A.; Abell, A. D. *J. Am. Chem. Soc.* **2007**, *129*, 14862.

(14) Pearson, D.; Abell, A. D. *Organic & Biomolecular Chemistry* **2006**, *4*, 3618.

(15) Pearson, D.; Abell, A. D. *Chemistry – A European Journal* **2010**, *16*, 6983.

(16) Pearson, D.; Alexander N Fau - Abell, A. D.; Abell, A. D. *Chemistry – A European Journal* **2008**, *14*, 7358.

(17) Pearson, D. S., Alexander, N.A., Abell, A.D. *J. Pept. Sci.* **2006**, *12*, 167.

(18) Bieth, J.; Vratsanos, S. M.; Wassermann, N.; Erlanger, B. F. *Proceedings of the National Academy of Sciences* **1969**, *64*, 1103.

(19) Yoshino, J.; Kano, N.; Kawashima, T. *Dalton Transactions* **2013**, *42*, 15826.

(20) García-Amorós, J.; Velasco, D. *Beilstein Journal of Organic Chemistry* **2012**, *8*, 1003.

(21) Aizawa, M.; Namba, K.; Suzuki, S. *Arch. Biochem. Biophys.* **1977**, *182*, 305.

(22) Nakamoto, Y.; Karube, I.; Kobayashi, I.; Nishida, M.; Suzuki, S. *Arch. Biochem. Biophys.* **1979**, *193*, 117.

(23) Karube, I.; Suzuki, S. In *Enzyme Engineering*; Weetall, H., Royer, G., Eds.; Springer US: 1980, p 469.

(24) Madala, P.; Tyndall, J. D. A.; Nall, T.; Fairlie, D. P. *Chem. Rev. (Washington, DC, U. S.)* **2010**, ACS ASAP.

(25) Chua, K. C. H.; Pietsch, M.; Zhang, X.; Hautmann, S.; Chan, H. Y.; Bruning, J. B.; Gütschow, M.; Abell, A. D. *Angew. Chem. Int. Ed.* **2014**, *53*, 7828.

(26) Brieke, C.; Heckel, A. *Chemistry – A European Journal* **2013**, *19*, 15726.

(27) Levitus, M.; Glasser, G.; Neher, D.; Aramendía, P. F. *Chem. Phys. Lett.* **1997**, *277*, 118.

(28) Klajn, R. *Chem. Soc. Rev.* **2013**.

(29) Kohl-Landgraf, J.; Braun, M.; Özçoban, C.; Gonçalves, D. P. N.; Heckel, A.; Wachtveitl, J. *J. Am. Chem. Soc.* **2012**, *134*, 14070.

(30) Schechter, I.; Berger, A. *Biochem. Biophys. Res. Commun.* **1967**, *27*, 157.

(31) Appel, W. *Clin. Biochem. (Ottawa)* **1986**, *19*, 317.

(32) Angelastro, M. R.; Mehdi, S.; Burkhart, J. P.; Peet, N. P.; Bey, P. *J. Med. Chem.* **1990**, *33*, 11.

(33) Schellenberger, V.; Braune, K.; Hofmann, H. J.; Jakubke, H. D. *European journal of biochemistry / FEBS* **1991**, *199*, 623.

(34) Pearson, D.; Abell, A. D. *ARKIVOC (Gainesville, FL, U. S.)* **2008**, 85.

(35) Tulinsky, A.; Blevins, R. A. *J. Biol. Chem.* **1987**, *262*, 7737.

(36) Heng, S.; Nguyen, M.-C.; Kostecki, R.; Monro, T. M.; Abell, A. D. *RSC Advances* **2013**, *3*, 8308.

(37) Heng, S.; McDevitt, C. A.; Stubing, D. B.; Whittall, J. J.; Thompson, J. G.; Engler, T. K.; Abell, A. D.; Monro, T. M. *Biomacromolecules* **2013**, *14*, 3376.

(38) Peet, N. P.; Burkhart, J. P.; Angelastro, M. R.; Giroux, E. L.; Mehdi, S.; Bey, P.; Kolb, M.; Neises, B.; Schirlin, D. *J. Med. Chem.* **1990**, *33*, 394.

(39) Dixon, M. *Biochem. J* **1953**, *55*, 170.

(40) Tyndall, J. D. A.; Nall, T.; Fairlie, D. P. *Chem. Rev. (Washington, DC, U. S.)* **2005**, *105*, 973.

(41) Harvey, A. J.; Abell, A. D. *Tetrahedron* **2000**, *56*, 9763.

(42) Cornish-Bowden, A. *Biochem. J* **1974**, *137*, 143.

(43) Chen, J.; Zeng, F.; Wu, S. *ChemPhysChem* **2010**, *11*, 1036.

(44) Neidhart, D.; Wei, Y.; Cassidy, C.; Lin, J.; Cleland, W. W.; Frey, P. A. *Biochemistry* **2001**, *40*, 2439.

(45) Goodsell, D. S.; Morris, G. M.; Olson, A. J. *Journal of Molecular Recognition* **1996**, *9*, 1.

(46) Morris, G. M.; Huey, R.; Lindstrom, W.; Sanner, M. F.; Belew, R. K.; Goodsell, D. S.; Olson, A. J. *J. Comput. Chem.* **2009**, *30*, 2785.

(47) Debs, J. E.; Ebendorff-Heidepriem, H.; Quinton, J. S.; Monro, T. M. *Lightwave Technology, Journal of* **2009**, *27*, 576.

(48) Torrisi, V.; Amato, M. E.; Ballistreri, F. P.; Tomaselli, G.; Toscano, R. M.; Licciardello, A. *Surf. Interface Anal.* **2011**, *43*, 1095.

(49) Liao, B.; Long, P.; He, B.; Yi, S.; Ou, B.; Shen, S.; Chen, J. *Journal of Materials Chemistry C* **2013**, *1*, 3716.

(50) Shiraishi, Y.; Itoh, M.; Hirai, T. *PCCP* **2010**, *12*, 13737.

(51) Hedstrom, L. *Chem. Rev.* **2002**, *102*, 4501.

(52) Gendler, S. J.; Tökés, Z. A. *Biochimica et Biophysica Acta (BBA) - General Subjects* **1986**, *882*, 242.

Chapter 5

Experimental Procedures

5.1 General Procedures

5.1.1 NMR Spectroscopy

NMR spectra of all compounds in chapters 2-4 were obtained as described below: ^{1}H NMR and ^{13}C NMR spectra were obtained on a Varian 500 MHz and a Varian Inova 600 MHz instruments. Unless otherwise stated, all spectra were obtained at room temperature. Chemical shifts are reported in parts per million (ppm) on a δ scale (in which TMS is referenced to 0.00 ppm). Solvents used in NMR analysis (reference peak listed) are: $CDCl_3$ ($C\mathbf{H}Cl_3$ at δ_H 7.26 ppm, $\mathbf{C}DCl_3$ at δ_C 77.00 ppm); CD_3OD ($C\mathbf{H}D_2OD$ at δ_H 3.31 ppm, $\mathbf{C}D_3OD$ at δ_C 49.05 ppm); $(CD_3)_2SO$ ($(C\mathbf{H}D_2)_2SO$ at δ_H 2.50 ppm, $(\mathbf{C}D_3)_2SO$ at δ_C 39.70 ppm). Spin multiplicities are indicated by the following symbols: singlet (s), broad singlet (br s), doublet (d), doublet of doublet (dd), doublet of doublet of doublet (ddd), triplet (t), doublet of triplet (dt), quartet (q) and multiplet (m). All coupling constants (*J*) are reported in hertz (Hz).

5.1.2 Mass Spectrometry

High resolution mass spectra (HRMS) were collected using an LTQ Orbitrap XL ETD using flow injection, with a flow rate of 5 μL/min.

5.1.3 Infrared Spectroscopy

Infrared spectra were recorded on an ATI Mattson Genesis Series FTIR spectrophotometer as neat.

5.1.4 Chromatography

Thin-layer chromatography (TLC) was performed on Merck aluminium sheets with silica gel 60 F_{254}. Traces were visualised using short wave UV light or a suitable dip, including vanillin, ninhydrin and basic potassium permanganate.

Flash chromatography was performed using Scharlau silica gel 60, 230-400 mesh, under a positive pressure of nitrogen. The eluting solvents hexane, diethyl ether, ethyl acetate, dichloromethane and methanol were used as received. Petroleum ether and hexane were distilled to remove residual grease.

Reverse-phase flash chromatography was performed using Analtech or Sigma Aldrich C18 reverse-phase silica gel, 150 Å pore size, under a positive pressure of nitrogen. The eluting solvents Mili-Q water and HPLC-grade acetronitrile were used as received.

Reverse-phase high performance liquid chromatography (RP-HPLC) was performed using an HP 1100 LC system equipped with a Phenomenex C-18 column (250 × 4.6 mm) for analytical traces and a Gilson GX-Prep HPLC

system equipped with a Phenomenex C18 column (250 × 21.2 mm) for purification. H_2O/TFA (100/0.1 by v/v) and ACN/TFA (100/0.08 by v/v) solutions were used as aqueous and organic buffers.

5.1.5 Chemical Syntheses

All starting materials and reagents were obtained commercially and used without further purification unless stated otherwise. Dichloromethane was distilled over P_2O_5 and dried over 4 Å molecular sieves. Anhydrous *N,N*-dimethylformamide, methanol, ethanol and acetonitrile were purchased from Sigma-Aldrich (Castle Hill, NSW). Anhydrous tetrahydrofuran was obtained by fresh distillation from sodium/benzophenone under a nitrogen atmosphere. Oven-dried glassware was used in all reactions performed under an inert atmosphere (nitrogen or argon). Removal of volatiles *in vacuo* refers to the removal of solvents “under reduced pressure” by rotary evaporation (low vacuum pump) followed by application of high vacuum (oil pump) for a minimum of 60 min. All yields reported are isolated yields determined to be homogenous by NMR spectroscopy. All yields reported are isolated yields, judged to be homogeneous by TLC, analytical HPLC and NMR spectroscopy.

General procedure A: Dess-Martin oxidation

To a solution of the respective alcohol (1.0 equiv) in anhydrous DCM (250 ml/g of alcohol) was added Dess-Martin periodinane (3.0 equiv) under N_2 at room temperature. The mixture was stirred under N_2 at room temperature for

1.5 h. The reaction was quenched by slow addition of $Na_2S_2O_5$ (10 g/g of alcohol) in sat. $NaHCO_3$ (200 ml/g of $Na_2S_2O_5$). The aqueous phase was extracted with DCM (2 × 10 ml). The organic phase was combined and dried over $MgSO_4$. The solvent was removed *in vacuo* and the resultant crude product was purified with RP-HPLC to give the desired aldehyde.

General procedure B: Boc deprotection/methylation

To a solution of the respective N_α-Boc-protected carboxylic acid (1.0 equiv) in methanol (100 ml/g of acid) were added $SOCl_2$ (4.4 equiv) and anhydrous DMF (cat.) with cooling in an ice bath. The mixture was allowed to warm up to room temperature while stirring for 5 h. The solvent was removed *in vacuo* to give the desired product.

General procedure C: HATU peptide coupling

To a solution of the respective carboxylic acid (1.0 equiv) in anhydrous DMF (45 ml/g of acid) were added the corresponding amine (1.2 equiv), HATU (1.0 equiv) and HOBt (1.2 equiv). The mixture was stirred under N_2 for 15 min at room temperature before DIPEA (4.0 equiv) was added dropwise. The mixture was stirred under N_2 at room temperature for 21 h before acidified to pH 1 with 1 M HCl. The mixture was diluted with DCM (100 ml/g of acid). The organic phase was washed with 1 M HCl (80 ml/g of acid), sat. $NaHCO_3$ (2 × 150 ml/g of acid), H_2O (2 × 150 ml/g of acid) and brine (200 ml/g of acid) and dried over Na_2SO_4. The solvent was removed *in vacuo* and the resultant

crude product was purified with flash chromatography to give the desired coupling product.

General procedure D: NaOH Ester hydrolysis

To a solution of ester (1.0 equiv) 75.0 mg, 0.15 mmol) in THF/H_2O (1:1, 0.1 ml/mmol of ester) was added 2 M NaOH (8.0 equiv) in one portion. The mixture was stirred at room temperature for 18 h. THF was removed *in vacuo*. The solution was diluted with H_2O (4 ml/mmol of ester) and washed with Et_2O (4 ml/mmol of ester). The aqueous layer was neutralized to pH 7 by HCl (32%) and concentrated *in vacuo* to give the desired carboxylic acid.

General procedure E: TFA Boc deprotection

To an ice-cooled solution of Boc-protected amino acid (1.0 equiv) in DCM (50 ml/g of amino acid) was added TFA (50 ml/g of amino acid). The reaction was stirred for 30 min with ice cooling. The reaction was monitored by TLC. The volatile was removed *in vacuo* to give the desired free amine.

5.2 Synthesis for Chapter 2

(S)-N-((S)-4-Methyl-1-oxopentan-2-yl)-2,16-dioxo-3,20-diazabicyclo[15.2.1]icosa-1(19),17-diene-4-carboxamide ***2.12***[1]

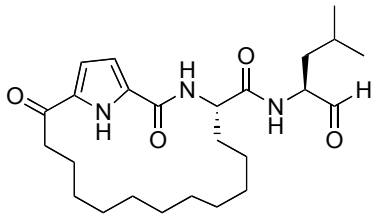

Compound **2.32** (190 mg, 0.42 mmol) was oxidised according to general procedure A to give compound **2.12** as a white solid (27 mg, 28%). ^{1}H NMR (300 MHz, $CDCl_3$) δ 10.33 (br s, 1H, pyrrole N**H**), 9.60 (s, 1H, C**H**O), 6.91 (s, 1H, pyrrole **H**), 6.81 (m, 1H, pyrrole **H**), 6.73 (s, 1H, N**H**), 6.59 (m, 1H, N**H**), 4.87 – 4.77 (m, 1H, NHC**H**CO), 4.62-4.53 (m, 1H, NHC**H**CHO), 2.90 (br s, 1H, COCH**H**$(CH_2)_{10}$), 2.67 (br s, 1H, COC**H**H$(CH_2)_{10}$), 2.21 – 2.09 (m, 1H, CO$(CH_2)_{10}$CH**H**), 1.80 – 1.64 (m, 4H, CHHC**H**$(CH_3)_2$ and $COCH_2C\mathbf{H}_2(CH_2)_8C\mathbf{H}H$), 1.53 – 1.43 (m, 2H, C**H**HCH$(CH_3)_2$), 1.43 – 1.35 (m, 1H, CO$(CH_2)_2$CH**H**), 0.97 (m, 6H, $CH_2CH(C\mathbf{H_3})_2$), 1.35 – 0.79 (m, 15H, CO$(CH_2)_2$C**H**H$(C\mathbf{H_2})_7$).

Macrocyclic aldehyde ***2.13***[1]

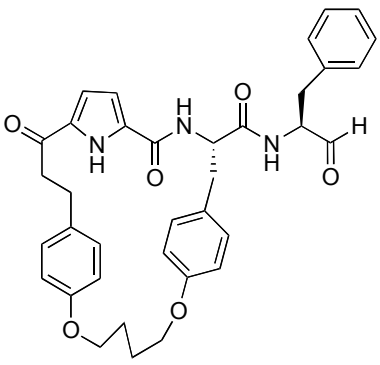

Compound **2.40** (69 mg, 0.11 mmol) was oxidised according to general procedure A to give compound **2.13** as a pale yellow oil (18.4 mg, 27%). ^{1}H NMR (300 MHz, $CDCl_3$) δ 9.89 (br s, 1H, pyrrole N**H**), 9.67 (s, 1H, C**H**O), 7.13 – 7.03 (m, 6H, Ar**H** and N**H**CHCHO), 6.98 (d, *J* = 8.5 Hz, 2H, OAr**H**), 6.90 (d, *J* = 8.5 Hz, 2H, OAr**H**), 6.75 (d, *J* = 8.5 Hz, 2H, OAr**H**), 6.62 (d, *J* = 8.5 Hz, 2H, OAr**H**), 6.14 – 6.12 (m, 1H, pyrrole **H**), 6.10-6.00 (m, 2H, pyrrole **H** and N**H**CHCO), 4.75 – 4.67 (m, 2H, C**H**CH_2Ar and NHC**H**CO), 4.00 – 3.76 (m, 4H, OC**H₂**$(CH_2)_2$C**H₂**O), 3.30 – 3.11 (m, 4H, CHCH**H**ArO, CHC**H₂**Ar and $ArCH_2CH$**H**), 3.02 – 2.86 (m, 3H, ArC**H₂**CH_2 and CHC**H**HArO), 2.70-2.68 (m, 1H, $ArCH_2C$**H**H), 1.92 (s, 4H, OCH_2C**H₂**C**H₂**CH_2O).

*^{13}C-labelled macrocyclic aldehyde **2.14***

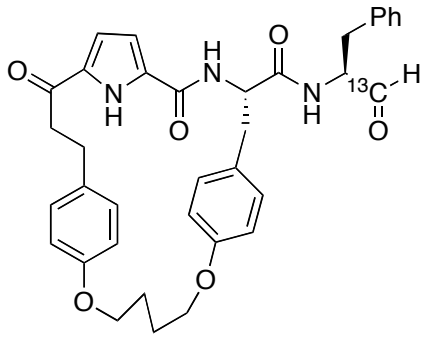

Compound **2.45** (38 mg, 0.06 mmol) was oxidized according to general procedure A to give compound **2.14** as a pale yellow oil (10 mg, 27%). ^{1}H NMR (300 MHz, $CDCl_3$) δ 9.90 (br s, 1H, pyrrole N**H**), 9.68 (d, *J* = 179.8 Hz, 1H, C**H**O), 7.20 – 7.07 (m, 6H, Ar**H** and N**H**CHCHO), 7.00 (d, *J* = 8.5 Hz, 2H, OAr**H**), 6.91 (d, *J* = 8.5 Hz, 2H, OAr**H**), 6.76 (d, *J* = 8.5 Hz, 2H, OAr**H**), 6.63 (d, *J* = 8.5 Hz, 2H, OAr**H**), 6.21 – 6.09 (m, 2H, pyrrole **H** and N**H**CHCO), 6.06-6.00 (m, 1H, pyrrole **H**), 4.81-4.69 (m, 2H, C**H**CH_2Ar and NHC**H**CO), 4.01 – 3.79 (m, 4H, OC**H₂**$(CH_2)_2$C**H₂**O), 3.30 – 3.09 (m, 4H, CHCH**H**ArO, CHC**H₂**Ar

and $ArCH_2CH\mathbf{H}$), 3.03 – 2.90 (m, 3H, $ArC\mathbf{H_2}CH_2$ and $CHC\mathbf{H}HArO$), 2.73-2.66 (m, 1H, $ArCH_2C\mathbf{H}H$), 1.94 (br s, 4H, $OCH_2C\mathbf{H_2}C\mathbf{H_2}CH_2O$).

Ethyl 1H-pyrrole-2-carboxylate ***2.16***[1]

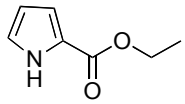

To a solution of sodium metal (1.5 g, 6.50 mmol) in anhydrous EtOH (20 ml) under N_2 was added a solution of **2.15** (9.0 g, 42.40 mmol) in anhydrous EtOH dropwise over 30 min. The mixture was stirred under N_2 for 30 min. The solvent was removed *in vacuo*. The resulting brown oil was resuspended in Et_2O (45 ml) and acidified to pH 0 with 3 M HCl (4.5 ml). The aqueous phase was extracted with Et_2O (45 ml). The combined organic phase was washed with sat. $NaHCO_3$ (45 ml) and dried over $MgSO_4$. The solvent was removed *in vacuo* and the resultant crude product was purified by flash chromatography in DCM to give compound **2.16** as a white solid (4.1 g, 67%). ^{1}H NMR (300 MHz, $CDCl_3$) δ 9.21 (br s, 1H, pyrrole N**H**), 6.97 – 6.90 (m, 2H, 2 × pyrrole **H**), 6.29 – 6.24 (m, 1H, pyrrole **H**), 4.32 (q, *J* = 7.1 Hz, 2H, $C\mathbf{H_2}CH_3$), 1.36 (t, *J* = 7.1 Hz, 3H, $CH_2C\mathbf{H_3}$).

3-(4-(Allyloxy)phenyl)propanoyl chloride ***2.18***[1]

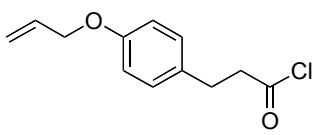

To an ice-cooled solution of **2.35** (1.6 g, 7.50 mmol) in anhydrous DCM (30 ml) was added $SOCl_2$ (5.4 g, 45.00 mmol) dropwise. The mixture was stirred for 10 min with ice cooling and then stirred at 40 ^{o}C for further 21 h. The

volatiles were removed *in vacuo* to give compound **2.18** as a yellow oil (1.6 mg, quant). ^{1}H NMR (300 MHz, $CDCl_3$) δ 7.10 (d, *J* = 8.6 Hz, 2H, OAr**H**), 6.86 (d, *J* = 8.6 Hz, 2H, OAr**H**), 6.12 – 5.97 (m, 1H, $OCH_2C\mathbf{H}CH_2$), 5.46 – 5.36 (m, 1H, $OCH_2CHCH\mathbf{H}$), 5.33 – 5.25 (m, 1H, $OCH_2CHC\mathbf{H}H$), 4.55 – 4.49 (m, 2H, $OC\mathbf{H_2}CHCH_2$), 3.17 (t, *J* = 7.4 Hz, 2H, $ArCH_2C\mathbf{H_2}$), 2.96 (t, *J* = 7.4 Hz, 2H, $ArC\mathbf{H_2}CH_2$).

*Methyl 5-undec-10-enoyl-1H-pyrrole-2-carboxylate **2.19***

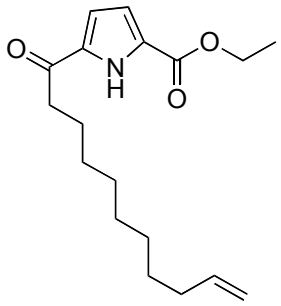

Method 1:[1] To a solution of **2.17** (4.1 g, 20.00 mmol) in nitromethane (27 ml) were added ethyl 1*H*-pyrrole-2-carboxylate **2.16** (1.4 g, 10.00 mmol) and $Yb(OTf)_3$ (620 mg, 1.00 mmol) and stirred for 21 h at room temperature. The mixture was diluted with DCM (250 ml) and washed with sat. $NaHCO_3$ (3 × 250 ml). The organic phase was dried over $MgSO_4$. The solvent was removed *in vacuo* to give a brown oil (5.5 g). The crude product was purified by flash chromatography (Et_2O:hexane 1:1) to give compound **2.19** as a yellow solid (443 mg, 16%).

Method 2: To a solution of **2.17** (4.1 g, 20.00 mmol) in nitromethane (27 ml) were added ethyl 1*H*-pyrrole-2-carboxylate **2.16** (1.4 g, 10.00 mmol) and $Yb(OTf)_3$ (620 mg, 1.00 mmol) and stirred for 48 h at room temperature. The mixture was diluted with DCM (250 ml) and washed with sat. $NaHCO_3$ (3 ×

250 ml). The organic phase was dried over $MgSO_4$. The solvent was removed *in vacuo* to give a brown oil (5.5 g). The crude product was purified by flash chromatography (Et_2O:hexane 1:1) to give compound **2.19** as a yellow solid (921 mg, 33%).

Method 3: To a solution of **2.17** (4.1 g, 20.00 mmol) in nitromethane (27 ml) were added ethyl 1*H*-pyrrole-2-carboxylate **2.16** (1.4 g, 10.00 mmol) and $Yb(OTf)_3$ (620 mg, 1.00 mmol) and stirred for 48 h at 45 ^oC. The mixture was diluted with DCM (250 ml) and washed with sat. $NaHCO_3$ (3 × 250 ml). The organic phase was dried over $MgSO_4$. The solvent was removed *in vacuo* to give a brown oil (5.5 g). The crude product was purified by flash chromatography (Et_2O:hexane 1:1) to give compound **2.19** as a yellow solid (1.81 g, 65%).

^1H NMR (300 MHz, $CDCl_3$) δ 9.78 (br s, 1H, pyrrole N**H**), 6.89 – 6.88 (m, 1H, pyrrole **H**), 6.85-6.83 (m, 1H, pyrrole **H**), 5.89 – 5.73 (m, 1H, $(CH_2)_8C\mathbf{H}CH_2$), 5.02 – 4.91 (m, 2H, $(CH_2)_8CHC\mathbf{H_2}$), 4.36 (q, *J* = 7.1 Hz, 2H, $OC\mathbf{H_2}CH_3$), 2.79 (t, *J* = 7.5 Hz, 2H, $COC\mathbf{H_2}$), 2.04 (q, *J* = 7.2 Hz, 2H, $(CH_2)_2(CH_2)_5C\mathbf{H_2}CHCH_2$), 1.75 – 1.58 (m, 2H, $CH_2C\mathbf{H_2}(CH_2)_6CHCH_2$), 1.42 – 1.24 (m, 13H, $(CH_2)_2(C\mathbf{H_2})_{\mathbf{5}}CH_2CHCH_2$ and $OCH_2C\mathbf{H_3}$).

Ethyl 5-(3-(4-(allyloxy)phenyl)propanoyl)-1H-pyrrole-2-carboxylate ***2.20***[1]

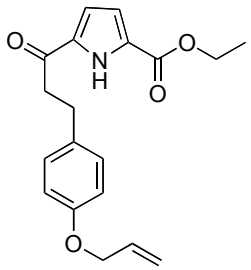

To a solution of **2.16** (2.3 g, 10.00 mmol) in nitromethane (27 ml) was added **2.17** (700 mg, 5.00 mmol) and $Yb(OTf)_3$ (310 mg, 0.50 mmol). The dark red mixture was stirred at 45 ^oC for 48 h. The reaction was quenched by addition of sat. $NaHCO_3$ (250 ml). The mixture was extracted with Et_2O (3 × 250 ml). The combined organic phase was washed with sat. $NaHCO_3$ (250 ml), H_2O (2 × 200 ml) and brine (250 ml) and dried over $MgSO_4$. The solvent was removed *in vacuo* and the resultant brown oil was purified by flash chromatography (Et_2O/hexane 2:3) to give compound **2.20** as a yellow solid (48 mg, 32%). ^1H NMR (300 MHz, $CDCl_3$) δ 9.81 (br s, 1H, pyrrole **H**), 7.13 (d, *J* = 8.6 Hz, 2H, OAr**H**), 6.89 – 6.79 (m, 4H, OAr**H** and pyrrole **H**), 6.12 – 5.98 (m, 1H, $OCH_2C\mathbf{H}CH_2$), 5.44 – 5.36 (m, 1H, $OCH_2CHCH\mathbf{H}$), 5.31 – 5.25 (m, 1H, $OCH_2CHC\mathbf{H}H$), 4.53 – 4.49 (m, 2H, $OC\mathbf{H_2}CHCH_2$), 4.36 (q, *J* = 7.1 Hz, 2H, $OC\mathbf{H_2}CH_3$), 3.13 – 3.06 (m, 2H, $ArCH_2C\mathbf{H_2}$), 3.02 – 2.97 (m, 2H, $ArC\mathbf{H_2}CH_2$), 1.37 (t, *J* = 7.1 Hz, 3H, $OCH_2C\mathbf{H_3}$).

(S)-Methyl 2-(5-undec-10-enoyl-1H-pyrrole-2-carboxamido)pent-4-enoate

2.21

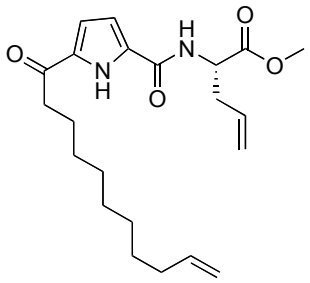

Method 1:[1] Compound **2.28** (290 mg, 1.04 mmol) was suspended in anhydrous DCM (13 ml) and compound **2.30** (216 mg, 1.31 mmol), EDCI (280 mg, 1.46 mmol) and HOBt (212 mg, 1.566 mmol) were added. The mixture was stirred under N_2 for 15 min. DIPEA (351 mg, 2.71 mmol) was added dropwise. The reaction mixture was stirred for 21 h under N_2. The mixture was diluted with DCM (50 ml) and acidified with 1 M HCl (20 ml). The aqueous phase was separated and extracted with DCM (2 × 50 ml). The combined organic phase was washed with 1 M HCl (50 ml), sat. $NaHCO_3$ (50 ml) and brine (50 ml) and dried over $MgSO_4$. The solvent was removed *in vacuo* to give a brown oil (564 mg), which was purified by flash chromatography (petroleum ether:EtOAc 3:1) to give compound **2.21** as a pale yellow oil (156 mg, 38%).

Method 2: Compound **2.28** (793 mg, 2.86 mmol) was coupled to compound **2.30** (546 mg, 3.29 mmol) according to general procedure C and the crude product was purified by flash chromatography (petroleum ether:EtOAc 3:1) to give compound **2.21** as a pale yellow oil (864 mg, 78%).

^{1}H NMR (300 MHz, $CDCl_3$) δ 9.99 (br s, 1H, pyrrole N**H**), 6.85 – 6.83 (m, 1H, pyrrole **H**), 6.62 – 6.65 (m, 1H, CON**H**CH), 6.61 (br s, 1H, pyrrole **H**), 5.65-5.76 (m, 1H, $CHCH_2C\mathbf{H}CH_2$), 5.77-5.84 (m, 1H, $(CH_2)_8C\mathbf{H}CH_2$), 5.16 (d, *J* = 13.3 Hz, 2H, $CHCH_2CHC\mathbf{H_2}$), 5.01 – 4.91 (m, 2H, $(CH_2)_8CHC\mathbf{H_2}$), 4.86 (q, *J* = 5.7 Hz, 1H, NHC**H**), 3.79 (s, 3H, $OC\mathbf{H_3}$), 2.77 (t, *J* = 7.5 Hz, 2H, $COC\mathbf{H_2}$), 2.72 – 2.54 (m, 2H, $NHCHC\mathbf{H_2}$), 2.03 (q, *J* = 6.8 Hz, 2H, $(CH_2)_2(CH_2)_5C\mathbf{H_2}CHCH_2$), 1.74 – 1.65 (m, 2H, $CH_2C\mathbf{H_2}(CH_2)_5CH_2CHCH_2$), 1.41 – 1.25 (m, 10H, $CH_2CH_2(C\mathbf{H_2})_5CH_2CHCH_2$).

(S)-Methyl 2-(5-(3-(4-(allyloxy)phenyl)propanoyl)-1H-pyrrole-2-carboxamido)-3-(4-(vinyloxy)phenyl)propanoate ***2.22***[1]

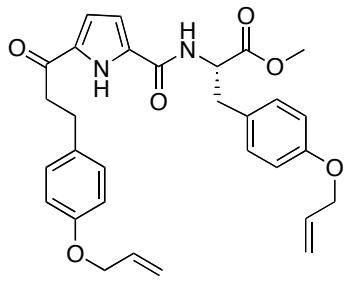

Compound **2.36** (272 mg, 0.90 mmol) was coupled to compound **2.38** (246 mg, 1.05 mmol) according to general procedure C and the crude product was purified by flash chromatography (petroleum ether:EtOAc 2:1) to give compound **2.22** as a pale yellow oil (500 mg, 78%). ^{1}H NMR (300 MHz, $CDCl_3$) δ 9.93 (br s, 1H, pyrrole N**H**), 7.13 (d, *J* = 8.6 Hz, 2H, OAr**H**), 7.00 (d, *J* = 8.6 Hz, 2H, OAr**H**), 6.85 (d, J = 8.6 Hz, 2H, OAr**H**), 6.82 (d, *J* = 8.6 Hz, 2H, OAr**H**), 6.80 – 6.77 (m, 1H, pyrrole **H**), 6.47 – 6.60 (m, 2H, pyrrole **H** and N**H**CH), 6.11 – 5.97 (m, 2H, 2 × $OCH_2C\mathbf{H}CH_2$), 5.44 – 5.35 (m, 2H, 2 × $OCH_2CHCH\mathbf{H}$), 5.31 – 5.24 (m, 2H, 2 × $OCH_2CHC\mathbf{H}H$), 5.00 (dt, *J* = 7.7, 5.5 Hz, 1H, NHC**H**),

4.53 – 4.47 (m, 4H, 2 × OC**H$_2$**CHCH$_2$), 3.76 (s, 3H, OC**H$_3$**), 3.16-3.13 (m, 2H, ArCH$_2$C**H$_2$**O), 3.11 – 3.04 (m, 2H, ArCH$_2$C**H$_2$**), 3.01 – 2.94 (m, 2H, ArC**H$_2$**CH).

*(S,Z)-methyl 2,16-dioxo-3,20-diazabicyclo[15.2.1]icosa-1(19),7,17-triene-4-carboxylate **2.23***

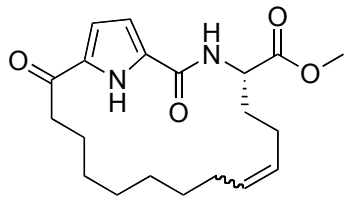

Method 1:[1] To a solution of **2.21** (100 mg, 0.25 mmol) in anhydrous DCM (250 ml) was added Grubb's 2nd generation catalyst (42 mg, 0.05 mmol) in one portion. The mixture was stirred for 18 h at 45 ^{o}C under N_2. The reaction was quenched by addition of activated charcoal and stirred at room temperature for 18 h. The solvent was removed *in vacuo* to give a brown oil (113 mg), which was purified by flash chromatography (petroleum ether:EtOAc 1:1) to give compound **2.23** as a yellow oil (26 mg, 28%).

Method 2: To a solution of **2.21** (100 mg, 0.25 mmol) in anhydrous DCM (250 ml) was added Grubb's 2nd generation catalyst (21 mg, 0.025 mmol). The mixture was heated to 45 ^{o}C and stirred for 1 h under a nitrogen atmosphere after the addition of the first portion. An additional portion of Grubb's 2nd generation catalyst (21 mg, 0.025 mmol) was added and the solution was stirred for 18 h at 45 ^{o}C. The reaction was quenched by addition of activated charcoal and stirred at room temperature for 18 h. The solvent was removed *in vacuo* to give a brown oil (122 mg), which was purified by flash

chromatography (petroleum ether:EtOAc 1:1) to give compound **2.23** as a yellow oil (45 mg, 50%).

Method 3: To a solution of **2.21** (500 mg, 1.25 mmol) in anhydrous DCM (500 ml) was added Grubb's 2nd generation catalyst (105 mg, 0.13 mmol). The mixture was heated to 45 ^{o}C and stirred for 1 h under a nitrogen atmosphere after the addition of the first portion. An additional portion of Grubb's 2nd generation catalyst (105 mg, 0.13 mmol) was added and the solution was stirred for 18 h at 45 ^{o}C. The reaction was quenched by addition of activated charcoal and stirred at room temperature for 18 h. The solvent was removed *in vacuo* to give a brown oil (782 mg), which was purified by flash chromatography (petroleum ether:EtOAc 1:1) to give compound **2.23** as a yellow oil (212 mg, 47%).

^{1}H NMR (300 MHz, $CDCl_3$) δ 9.99 (br s, 1H, pyrrole N**H**), 6.90 – 6.84 (m, 1H, pyrrole **H**), 6.63 – 6.59 (m, 1H, pyrrole **H**), 6.25 (d, *J* = 9.1 Hz, 1H, N**H**CHCO), 5.37 – 5.14 (m, 2H, NHCHCH_2C**H**C**H**), 4.89 (td, *J* = 9.1, 4.4 Hz, 1H, NHC**H**CO), 3.81 (s, 3H, OC**H_3**), 2.97 – 2.84 (m, 2H, COCH**H**$(CH_2)_7$ and NHCHCH**H**), 2.55 – 2.49 (m, 1H, COC**H**H$(CH_2)_7$), 2.24 – 2.14 (m, 1H, NHCHC**H**H), 1.90 – 1.87 (m, 2H, $COCH_2C$**H_2**$(CH_2)_6$), 1.82 – 1.73 (m, 2H $CO(CH_2)_7C$**H_2**), 1.41-1.23 (m, 3H, $CO(CH_2)_3$CH**H** and $CO(CH_2)_2$CH**H**C**H**H), 1.14 – 1.10 (m, 1H, $CO(CH_2)_2$C**H**H), 1.06 – 0.96 (m, 1H, $CO(CH_2)_5$CH**H**), 0.83-0.92 (m, 3H, $CO(CH_2)_4C$**H_2**C**H**H), 0.66 – 0.50 (m, 2H, $CO(CH_2)_6C$**H_2**).

*(S)-methyl 2,16-dioxo-3,20-diazabicyclo[15.2.1]icosa-1(19),17-diene-4-carboxylate **2.25***

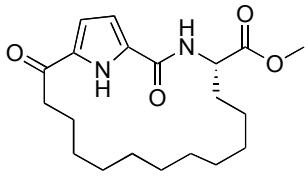

Method 1:[1] To a solution of compound **2.23** (49 mg, 0.14 mmol) in EtOAc (18 ml) was added Pd/C (5 mg, 10% w/w) was added to the solution and the mixture was stirred at room temperature under H_2 for 18 h. The mixture filtered through celite under vacuum and the solvent of the filtrate was removed *in vacuo* to give a yellow oil (56 mg). The crude product was purified by flash chromatography (petroleum ether:EtOAc 1:1) to give compound **2.25** as a pale yellow oil (12 mg, 24%).

Method 2: To a solution of compound **2.23** (150 mg, 0.43 mmol) in EtOAc (50 ml) was added Pd/C (75 mg, 50% w/w) was added to the solution and the mixture was stirred at room temperature under H_2 for 18 h. The mixture filtered through celite under vacuum and the solvent of the filtrate was removed *in vacuo* to give a yellow oil (161 mg). The crude product was purified by flash chromatography (petroleum ether:EtOAc 1:1) to give compound **2.25** as a pale yellow oil (100 mg, 66%).

Method 3: To a solution of compound **2.23** (265 mg, 0.74 mmol) in EtOAc (106 ml) was added Pd/C (88 mg, 33% w/w) was added to the solution and the mixture was stirred at room temperature under H_2 for 18 h. The mixture filtered through celite under vacuum and the solvent of the filtrate was

removed *in vacuo* to give a yellow oil (285 mg). The crude product was purified by flash chromatography (petroleum ether:EtOAc 1:1) to give compound **2.25** as a pale yellow oil (251 mg, 95%).

^{1}H NMR (300 MHz, $CDCl_3$) δ 10.30 (br s, 1H, pyrrole N**H**), 6.94 – 6.89 (m, 1H, pyrrole **H**), 6.73 (br s, 1H, pyrrole **H**), 6.17 (br s, 1H, N**H**CH), 4.93 (dt, *J* = 8.2, 4.0 Hz, 1H, NHC**H**), 3.79 (s, 3H, OC**H$_3$**), 2.90 (br s, 1H, COCH**H**), 2.62 (br s, 1H, COC**H**H), 2.27 – 2.13 (m, 1H, CO$(CH_2)_{10}$CH**H**), 1.89 – 1.65 (m, 3H, CO$(CH_2)_{10}$C**H**H and COCH_2C**H$_2$**), 1.38 – 1.14 (m, 12H, CO$(CH_2)_2$C**H$_2$**CH_2(C**H$_2$**)$_4$CH_2C**H$_2$**CH_2), 1.14 – 0.99 (m, 2H, CO$(CH_2)_3$C**H$_2$**), 0.94 – 0.79 (m, 2H, CO$(CH_2)_8$C**H$_2$**).

*Macrocyclic ester **2.26**[1]*

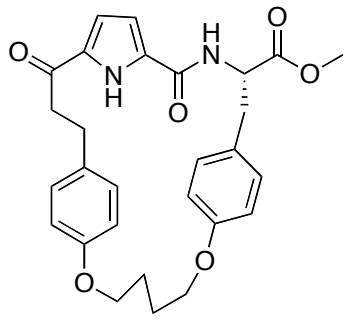

To a solution of **2.22** (260 mg, 0.53 mmol) in anhydrous DCM (100 ml) was added Grubb's 2nd generation catalyst (45 mg, 0.06 mmol). The mixture was heated to 45 ^{o}C and stirred for 1 h under a nitrogen atmosphere after the addition of the first portion. An additional portion of Grubb's 2nd generation catalyst (45 mg, 0.06 mmol) was added and the solution was stirred for 18 h at 45 ^{o}C. The reaction was quenched by addition of activated charcoal and stirred at room temperature for 18 h. The solvent was removed *in vacuo* and

the resultant crude product (295 mg) was dissolved in EtOAc (120 ml) under H_2. Pd/C (97 mg, 33% w/w) was added to the solution and the mixture was stirred at room temperature under H_2 for 3 h. The mixture was then filtered through celite and the solvent was removed *in vacuo.* The resultant crude product (293 mg) was purified by flash chromatography (petroleum ether:EtOAc 1:1) to give compound **2.28** as a clear oil (238 mg, 81%). ^{1}H NMR (300 MHz, $CDCl_3$) δ 9.73 (br s, 1H, pyrrole N**H**), 6.95 – 6.86 (m, 4H, OAr**H**), 6.72 (d, *J* = 8.3 Hz, 2H, OAr**H**), 6.64 (d, *J* = 8.3 Hz, 2H, OAr**H**), 6.18 (d, *J* = 7.6 Hz, 1H, N**H**CH), 6.14 – 6.07 (m, 2H, pyrrole **H**), 4.85 (q, *J* = 7.6 Hz, 1H, NHC**H**), 4.06 – 3.94 (m, 2H, C**H$_2$**OArCH$_2$CH), 3.88 (t, *J* = 5.8 Hz, 2H, (CH$_2$)$_2$ArOC**H$_2$**), 3.84 (s, 3H, OC**H$_3$**), 3.42 (dd, *J* = 14.0, 5.6 Hz, 1H, NHCHCH**H**), 3.17 – 3.04 (m, 1H, ArCH**H**CH$_2$), 3.03 – 2.91 (m, 3H, ArCH$_2$C**H$_2$** and NHCHC**H**H), 2.74 – 2.66 (m, 1H, ArC**H**HCH$_2$), 1.99 – 1.87 (m, 4H, OCH$_2$C**H$_2$**C**H$_2$**CH$_2$O).

5-Undec-10-enoyl-1H-pyrrole-2-carboxylic acid ***2.28***[1]

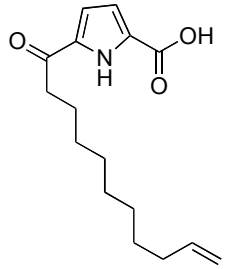

To a solution of **2.19** (1.14 g, 3.73 mmol) in THF/H_2O (1:1, 15 ml) was added KOH (1.68 g, 29.87 mmol) and stirred at 45 ^{o}C for 18 h. THF was removed *in vacuo* and the solution was diluted with water (100 ml). The solution was washed with Et_2O (50 ml). The aqueous phase was acidified with 3 M HCl to pH 1 and extracted with EtOAc (3 × 50 ml). The combined organic phase was

washed with water (50 ml) and dried over $MgSO_4$. The solvent was removed *in vacuo* to give compound **2.28** as a pale yellow solid (869 mg, 84%). ^{1}H NMR (300 MHz, $CDCl_3$) δ 10.46 (br s, 1H, pyrrole N**H**), 7.03 – 6.88 (m, 2H, pyrrole **H**), 5.89 – 5.72 (m, 1H, $(CH_2)_8CHCH_2$), 5.05 – 4.89 (m, 2H, $(CH_2)_8CHCH_2$), 2.83 (t, *J* = 7.5 Hz, 2H, $COCH_2$), 2.08 – 1.99 (m, 2H, $(CH_2)_2(CH_2)_5CH_2CHCH_2$), 1.78 – 1.69 (m, 2H, $CH_2CH_2(CH_2)_5CH_2CHCH_2$), 1.44 – 1.23 (m, 10H, $(CH_2)_2(CH_2)_5CH_2CHCH_2$).

(S)-1-Methoxy-1-oxopent-4-en-2-aminium chloride ***2.30***[1]

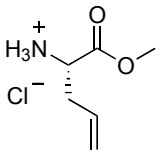

(*S*)-2-(*tert*-butoxycarbonylamino)-allylglycine **2.29** (500 mg, 4.34 mmol) was deprotected and methylated according to general procedure B to give compound **2.30** as a white solid (480 mg, quant). ^{1}H NMR (300 MHz, $CDCl_3$) δ 8.76 (br s, 3H, NH_3), 5.94 – 5.77 (m, 1H, CH_2CHCH_2), 5.33 (dd, *J* = 17.0, 10.1 Hz, 1H, $CHCH_2CHCHH$), 5.27 (dd, *J* = 17.0, 10.1 Hz, 1H, $CHCH_2CHCHH$), 4.25 (t, *J* = 5.9 Hz, 1H, $CHCH_2CHCH_2$), 3.81 (s, 3H, OCH_3), 2.85 (m, 2H, $CHCH_2CHCH_2$).

(S)-N-((S)-1-Hydroxy-4-methylpentan-2-yl)-2,16-dioxo-3,20-diazabicyclo[15.2.1]icosa-1(19),17-diene-4-carboxamide ***2.32***[1]

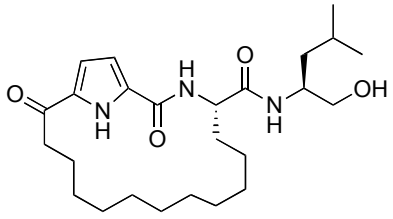

Compound **2.25** (250 mg, 0.69 mmol) was hydrolysed according to general procedure D to give compound **2.31** as a white solid (178 mg), which was coupled to *L*-leucinol according to general procedure C and the crude product was purified by flash chromatography (petroleum ether:EtOAc 1:4) to give compound **2.31** as a white solid (121 mg, 61%). ^{1}H NMR (300 MHz, $CDCl_3$) δ 12.18 (br s, 1H, pyrrole N**H**), 8.40 (d, *J* = 8.5 Hz, 1H, N**H**CHCO), 7.68 (d, *J* = 8.5 Hz, 1H, N**H**CHCH_2OH), 6.90 (s, 1H, pyrrole H), 6.81 (s, 1H, pyrrole H), 4.62 (t, *J* = 5.0 Hz, 1H, CH_2O**H**), 4.46 (t, *J* = 8.6 Hz, 1H, NHC**H**CO), 3.83 (br d, *J* = 4.4 Hz, 1H, NHC**H**CH_2OH), 3.28-3.35 (m, 1H, CH**H**OH), 3.20-3.25 (m, 1H, C**H**HOH), 2.88-2.95 (m, 1H, COCH**H**), 2.60-2.66 (m, 1H, COC**H**H), 1.75-1.80 (m, 1H, CO(CH_2)$_{10}$CH**H**), 1.64-1.67(m, 2H, COCH_2C**H**$_2$), 1.56-1.62 (m, 2H, CO(CH_2)$_{10}$C**H**H and CH_2C**H**(CH_3)$_2$), 0.83-1.36 (m, 18H, CO(CH_2)$_2$(C**H**$_2$)$_8$) and C**H**$_2$CH(CH_3)$_2$), 0.88 (d, *J* = 7.5 Hz, 3H, CH_2CH(C**H**$_3$)$_2$), 0.84 (d, *J* = 7.5 Hz, 3H, CH_2CH(C**H**$_3$)$_2$).

Methyl 3-(4-(allyloxy)phenyl)propanoate ***2.34***[1]

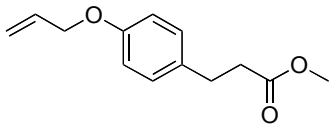

To a solution of methyl 3-(4-hydroxy-phenyl)propionate **2.33** (6.0 g, 33.60 mmol) in anhydrous DMF (50 ml) were sequentially added K_2CO_3 (9.0 g, 67.20 mmol), tetrabutylammonium iodide (1.2 g, 3.36 mmol) and allyl bromide (5.0 g, 42.00 mmol). The mixture was stirred at room temperature under N_2 for 18 h. The mixture was poured into ice water (400 ml) and extracted with EtOAc (4 × 100 ml). The organic phase was washed with 1 M HCl (150 ml), H_2O (2 × 150 ml) and brine (150 ml), and dried over Na_2SO_4. The solvent was

removed *in vacuo* to give compound **2.34** as a yellow oil (7.2 g, 97%). ^{1}H NMR (300 MHz, $CDCl_3$) δ 7.10 (d, J = 8.6 Hz, 2H, OAr**H**), 6.84 (d, J = 8.6 Hz, 2H, OAr**H**), 6.15 – 5.94 (m, 1H $OCH_2C\mathbf{H}CH_2$), 5.46 – 5.35 (m, 1H, $OCH_2CHCH\mathbf{H}$), 5.32 – 5.24 (m, 1H, $OCH_2CHC\mathbf{H}H$), 4.56 – 4.46 (m, 2H, $OC\mathbf{H_2}CHCH_2$), 3.66 (s, 3H, $OC\mathbf{H_3}$), 2.89 (t, J = 7.8 Hz, 2H, $ArCH_2C\mathbf{H_2}$), 2.60 (t, J = 7.8 Hz, 2H, $ArC\mathbf{H_2}CH_2$).

3-(4-(Allyloxy)phenyl)propanoic acid ***2.35***[1]

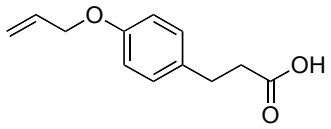

To a solution of **2.34** (7.2 g, 32.50 mmol) in THF/H_2O (170 ml, 50 ml) was added LiOH (3.9 g, 163.00 mmol) in one portion. The mixture was stirred at 35-40 ^{o}C for 3 h. The mixture was acidified to pH 0 with 1 M HCl. The mixture was extracted with EtOAc (3 × 300 ml). The organic phase was combined and washed with H_2O (2 × 300 ml). The aqueous phase was extracted with EtOAc (300 ml). The combined organic phase was dried over Na_2SO_4. The solvent was removed *in vacuo* to give compound **2.35** as a pale yellow solid (6.6 g, 99%). ^{1}H NMR (300 MHz, DMSO) δ 12.11 (br s, 1H, COO**H**), 7.12 (d, *J* = 8.7 Hz, 2H, OAr**H**), 6.84 (d, *J* = 8.7 Hz, 2H, OAr**H**), 6.12 – 5.92 (m, 1H, $OCH_2C\mathbf{H}CH_2$), 5.41 – 5.33 (m, 1H, $OCH_2CHCH\mathbf{H}$), 5.27 – 5.21 (m, 1H, $OCH_2CHC\mathbf{H}H$), 4.55 – 4.48 (m, 2H, $OC\mathbf{H_2}CHCH_2$), 2.74 (t, *J* = 7.6 Hz, 2H, $ArCH_2C\mathbf{H_2}$), 2.54 – 2.43 (m, 2H, $ArC\mathbf{H_2}CH_2$).

5-(3-(4-(Allyloxy)phenyl)propanoyl)-1H-pyrrole-2-carboxylic acid ***2.36***[1]

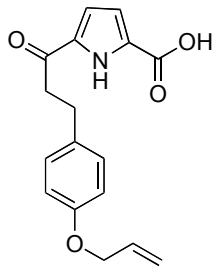

To a solution of **2.20** (740 mg, 2.26 mmol) in THF/H_2O (1:1, 14.8 ml) was added KOH (1010 mg, 18.10 mmol) in one portion and stirred at 40-50 ^oC for 18 h. The reaction mixture was cooled in an ice bath and partitioned between water (50 ml) and Et_2O (50 ml). The ice-cooled aqueous phase was acidified to pH 1 with HCl (32%). The precipitate was washed with ice-cold water and the volatiles were removed *in vacuo* overnight to give compound **2.36** as a pale yellow solid (578 mg, 85%). ^{1}H NMR (300 MHz, $CDCl_3$) δ 10.82 (br s, 1H, pyrrole N**H**), 7.14 (d, *J* = 8.5 Hz, 2H, OAr**H**), 7.02 – 6.98 (m, 1H, pyrrole **H**), 6.92 – 6.89 (m, 1H, pyrrole **H**), 6.85 (d, *J* = 8.5 Hz, 2H, OAr**H**), 6.13 – 5.97 (m, 1H, $OCH_2C\mathbf{H}CH_2$), 5.40 (d, *J* = 17.3, 1H, $OCH_2CHCH\mathbf{H}$), 5.28 (d, *J* = 10.5 Hz, 1H, $OCH_2CHC\mathbf{H}H$), 4.51 (d, *J* = 5.3 Hz, 2H, $OC\mathbf{H}_2CHCH_2$), 3.16 (t, *J* = 7.0 Hz, 2H, $ArCH_2C\mathbf{H_2}$), 3.01 (t, *J* = 7.0 Hz, 2H, $ArC\mathbf{H}_2CH_2$), COO**H** was not observed.

(S)-methyl 2-amino-3-(4-(vinyloxy)phenyl)propanoate ***2.38***[1]

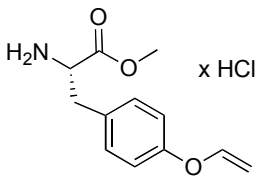

N_α-Boc-*L*-(allyl)tyrosine (1.0 g, 3.10 mmol) was reacted according to general procedure B to give compound **2.38** as a white solid (710 mg, quant). ^{1}H NMR (300 MHz, CD_3OD) δ 7.16 (d, *J* = 8.8 Hz, 2H, OAr**H**), 6.94 (d, *J* = 8.8 Hz, 2H,

OAr**H**), 6.12 – 5.98 (m, 1H, OC**H**CH_2), 5.43 – 5.35 (m, 1H, ArOCHCH**H**), 5.28 – 5.22 (m, 1H, ArOCHC**H**H), 4.55 (m, 2H, N**H_2**CH), 4.26 (dd, *J* = 7.4, 6.0 Hz, 1H, NH_2C**H**), 3.82 (s, 3H, OC**H_3**), 3.33 – 3.29 (m, 2H, CHC**H_2**Ar).

*Macrocyclic alcohol **2.40**[1]*

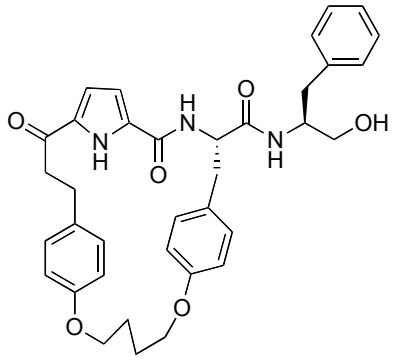

Compound **2.26** (238 mg, 0.49 mmol) was hydrolysed according to general procedure D to give compound **2.39** as a white powder (251 mg). Compound **2.39** (150 mg, 0.28 mmol) was subsequently coupled with *L*-phenylalaninol (63.6 mg, 0.42 mmol) according to general procedure C to give a yellow oil, which was purified by flash chromatography (petroleum ether:EtOAc 1:3) to give compound **2.40** as a white solid (82 mg, 48%). ^{1}H NMR (300 MHz, $CDCl_3$) δ 10.80 (br s, 1H, pyrrole N**H**), 7.82 (d, *J* = 8.4 Hz, 1H), 7.19 – 7.15 (m, 4H, Ar**H**), 7.14 – 7.10 (m, 1H, Ar**H**), 6.97 (d, *J* = 8.6 Hz, 2H, OAr**H**), 6.92 (d, *J* = 8.6 Hz, 2H, OAr**H**), 6.73 (d, *J* = 8.6 Hz, 2H, OAr**H**), 6.66 (d, *J* = 8.6 Hz, 2H, OAr**H**), 6.39 (d, *J* = 7.5 Hz, 1H, N**H**CHCO), 6.17 – 6.08 (m, 2H, 2 × pyrrole **H**), 5.14 (q, *J* = 6.9 Hz, 1H, C**H**CH_2ArO), 4.27 – 4.20 (m, 1H, C**H**CH_2Ar), 4.02 – 3.88 (m, 4H, OC**H_2**$(CH_2)_2$C**H_2**O), 3.85 – 3.73 (m, 3H, C**H_2**O**H**), 3.37 (dd, *J* = 14.1, 5.8 Hz, 1H, CHCH**H**ArO), 3.22 – 3.17 (m, 1H, ArCH_2CH**H**), 3.05 – 2.95 (m, 3H, ArC**H_2**CH_2 and CHC**H**HArO), 2.84 (d, *J* = 7.4 Hz, 2H, CHC**H_2**Ar), 2.75 – 2.68 (m, 1H, ArCH_2C**H**H), 2.00 – 1.87 (m, 4H, OCH_2C**H_2**C**H_2**CH_2O).

(S)-2-(tert-Butoxycarbonylamino)-L-phenylalaninol-1-^{13}C ***2.43***

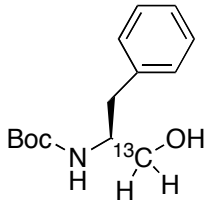

To a solution of *L*-phenylalanine-1-^{13}C (100 mg, 0.6 mmol) in THF/methanol (1:6, 50 ml) were added triethylamine (125 mg, 1.2 mmol) and Boc_2O (147 mg, 0.65 mmol). The mixture was stirred at room temperature for 18 h. The mixture was acidified to pH 0 with 1 M HCl (25 ml). The solvent was removed *in vacuo*. The pale yellow oil was partitioned between EtOAc (50 ml) and H_2O (50 ml). The aqueous phase was extracted with EtOAc (2 × 50 ml). The combined organic phase was washed with H_2O (50 ml) and brine (50 ml) and dried over Na_2SO_4. The solvent was removed *in vacuo* to give a clear oil (190 mg), which was dissolved in anhydrous THF (25 ml) and cooled in an ice bath. $LiAlH_4$ (90 mg, 2.5 mmol) was suspended in anhydrous THF (5 ml) and added dropwise to the reaction mixture under Ar. The mixture was allowed to warm up to room temperature and stirred under N_2 for 18 h. H_2O (2 ml) was added slowly to the ice-cooled reaction mixture. THF was removed *in vacuo*. The aqueous solution was acidified by 2 M HCl (20 ml) and extracted with EtOAc (4 × 20 ml). The combined organic phase was washed with brine (2 × 20 ml) and dried over $MgSO_4$. The solvent was removed *in vacuo* to give a clear oil (200 mg), which was purified by flash chromatography (petroleum ether:EtOAc 1:1) to give compound **2.43** as a white solid (166 mg, quant). ^{1}H NMR (300 MHz, $CDCl_3$) δ 7.39 – 7.09 (m, 5H, Ar**H**), 4.79 (br s, 1H, N**H**), 4.05 – 3.82 (m, 2H, CHC**H$_2$**Ar), 3.75 – 3.47 (m, 1H, CH_2O**H**), 2.94 (dd, *J* = 3.0 Hz, 9.0 Hz, 2H, C**H$_2$**OH), 1.42 (s, 9H, Boc (C**H$_3$**)$_3$CO).

*^{13}C-labelled macrocyclic alcohol **2.45***

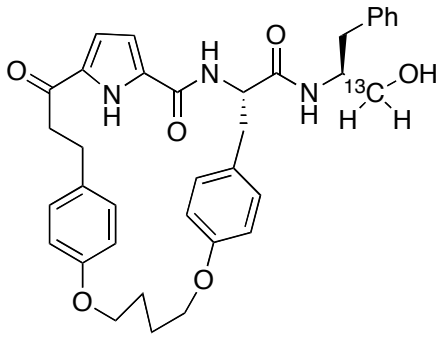

Compound **2.43** (48 mg, 0.19 mmol) was deprotected according to general procedure E to give compound **2.44** as a yellow oil (27.6 mg, 0.18 mmol), which was coupled to compound **2.39** (76 mg, 0.16 mmol) according to general procedure C to give a yellow oil (54 mg). The crude compound was purified by flash chromatography (petroleum ether:EtOAc 1:4) to give compound **2.45** as a white solid (38 mg, 39%). ^{1}H NMR (600 MHz, $CDCl_3$) δ 10.79 (br s, 1H, pyrrole N**H**), 7.72 (d, *J* = 8.3 Hz, 1H, N**H**CHCH$_2$OH), 7.33 – 7.23 (m, 5H, Ar**H**), 7.07 (d, *J* = 8.6 Hz, 2H, OAr**H**), 7.01 (d, *J* = 8.6 Hz, 2H, OAr**H**), 6.84 (d, *J* = 8.6 Hz, 2H, OAr**H**), 6.76 (d, *J* = 8.6 Hz, 2H, OAr**H**), 6.33 (d, *J* = 7.8 Hz, 1H, N**H**CHCO), 6.24 – 6.23 (m, 1H, pyrrole **H**), 6.16 – 6.14 (m, 1H, pyrrole **H**), 5.17 (q, *J* = 6.6 Hz, 1H, C**H**CH$_2$ArO), 4.39 – 4.30 (m, 1H, C**H**CH$_2$Ar), 4.12 – 3.97 (m, 4H, OC**H$_2$**(CH$_2$)$_2$C**H$_2$**O), 3.78-3.58 (m, 3H, C**H$_2$**O**H**), 3.47 (dd, *J* = 14.4, 5.4 Hz, 1H, CHCH**H**ArO), 3.32 – 3.23 (m, 1H, ArCH$_2$CH**H**), 3.16 – 3.03 (m, 3H, ArC**H$_2$**CH$_2$ and CHC**H**HArO), 3.00 – 2.88 (m, 2H, CHC**H$_2$**Ar), 2.85 – 2.77 (m, 1H, ArCH$_2$C**H**H), 2.00 – 1.92 (m, 4H, OCH$_2$C**H$_2$**C**H$_2$**CH$_2$O).

5.3 Synthesis for Chapter 3

*Boronic ester inhibitor **3.05***

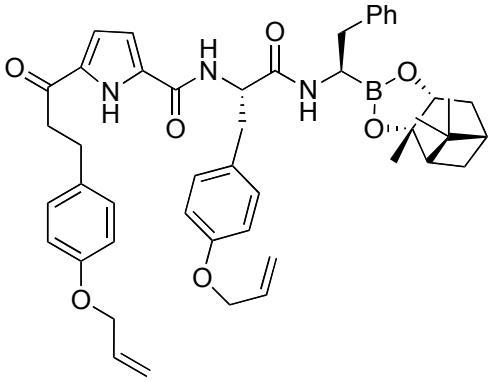

Carboxylic acid **3.09** (53 mg, 0.11 mmol) was coupled to compound **3.28** according to general procedure C and purified by RP-HPLC to give compound **3.05** as a clear oil (15 mg, 18%). ^{1}H NMR (599 MHz, $CDCl_3$) δ 9.91 (br s, 1H, pyrrole N**H**), 7.19 – 7.11 (m, 7H, Ar**H** and OAr**H**), 6.99 (d, *J* = 7.2 Hz, 2H, OAr**H**), 6.84 (d, *J* = 7.2 Hz, 2H, OAr**H**), 6.82 (d, *J* = 7.2 Hz, 2H, OAr**H**), 6.78 – 6.74 (m, 1H, pyrrole **H**), 6.65 (d, *J* = 8.4 Hz, 1H, N**H**CHCO), 6.48 – 6.45 (m, 1H, pyrrole **H**), 6.08 – 6.00 (m, 2H, 2 × $OCH_2C\mathbf{H}CH_2$), 5.96 (br s, 1H, N**H**CHB), 5.42 – 5.37 (m, 2H, 2 × $OCH_2CHCH\mathbf{H}$), 5.29 – 5.25 (m, 2H, 2 × $OCH_2CHC\mathbf{H}H$), 4.71 (q, *J* = 7.8 Hz, 1H, C**H**CH_2ArO), 4.51 – 4.48 (m, 3H, O**CH_2**$CHCH_2$ and C**H**CH_2Ar), 4.36 – 4.30 (m, 2H, O**CH_2**$CHCH_2$), 3.28 – 3.25 (m, 1H, pinanediol C**H**), 3.10 – 3.08 (m, 2H, C**H_2**Ar), 3.01 – 2.90 (m, 4H, O**CH_2CH_2**ArO), 2.70 – 2.65 (m, 2H, C**H_2**Ar), 2.38 – 2.32 (m, 1H, pinanediol CH**H**), 2.18 – 2.13 (m, 1H, pinanediol C**H**), 2.01 (t, *J* = 5.5 Hz, 1H, pinanediol C**H**), 1.92 – 1.85 (m, 2H, pinanediol C**H_2**), 1.38 (s, 3H, pinanediol C**H_3**), 1.28 (s, 3H, pinanediol C**H_3**), 1.15 (d, *J* = 10.8 Hz, 1H, pinanediol C**H**H), 0.95 (s, 3H, pinanediol C**H_3**). ^{13}C NMR (151 MHz, $CDCl_3$) δ190.2, 171.0, 159.2, 157.7,

157.0, 139.0, 133.4, 133.2, 133.1, 130.5, 129.7, 129.4, 129.2, 128.9, 128.4, 128.2, 126.4, 117.7, 115.6, 114.8, 110.3, 85.9, 77.9, 68.8, 54.0, 51.3, 40.9, 40.3, 39.5, 38.1, 37.8, 36.7, 35.5, 29.5, 28.5, 27.1, 26.3, 24.0. HRMS (ES) 784.4130 (MH^+); $C_{47}H_{54}BN_3O_7$ requires 784.4133.

*Boronic ester inhibitor **3.06***

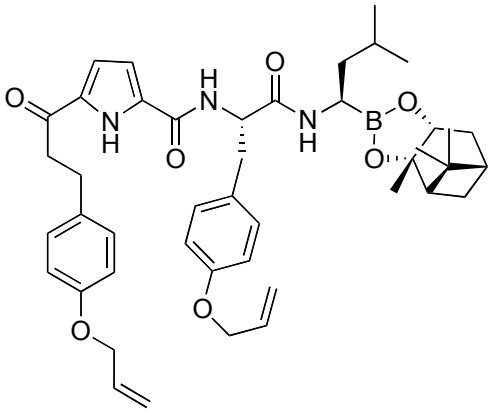

Carboxylic acid **3.09** (67 mg, 0.12 mmol) was coupled to compound **3.29** according to general procedure C and purified by RP-HPLC to give compound **3.06** as a clear oil (14 mg, 16%). ^{1}H NMR (500 MHz, $CDCl_3$) δ 10.36 (br s, 1H, pyrrole N**H**), 7.16 (d, *J* = 10.2 Hz, 2H, OAr**H**), 7.12 (d, *J* = 10.2 Hz, 2H, OAr**H**), 7.08 – 7.02 (m, 2H, OAr**H**), 6.84 (d, *J* = 10.2 Hz, 2H, OAr**H**), 6.83 – 6.78 (m, 2H, 2 × N**H**), 6.57 (br s, 1H, pyrrole **H**), 6.29 (br s, 1H, pyrrole **H**), 6.08 – 5.97 (m, 2H, 2 × $OCH_2C\mathbf{H}CH_2$), 5.42 – 5.34 (m, 2H, 2 × $OCH_2CHCH\mathbf{H}$), 5.29 – 5.24 (m, 2H, 2 × $OCH_2CHC\mathbf{H}H$), 4.89 – 4.84 (m, 1H, $C\mathbf{H}CH_2ArO$), 4.52 – 4.44 (m, 3H, $OC\mathbf{H_2}CHCH_2$ and NHC**H**B), 4.29 (d, *J* = 12.0 Hz, 2H, $OC\mathbf{H_2}CHCH_2$), 3.24 – 3.20 (m, 1H, pinanediol C**H**), 3.19 – 3.05 (m, 4H, $OC\mathbf{H_2}C\mathbf{H_2}Ar$), 3.00 – 2.90 (m, 3H, $C\mathbf{H_2}Ar$ and $C\mathbf{H}(CH_3)_2$), 2.36 – 2.30 (m, 1H, pinanediol CH**H**), 2.20 – 2.14 (m, 1H, pinanediol C**H**), 2.02 – 2.00 (m, 1H, pinanediol C**H**), 1.84 – 1.72 (m, 3H, $C\mathbf{H_2}CH(CH_3)_2$, pinaneldiol CH**H**), 1.38 (s, 3H, pinanediol $C\mathbf{H_3}$), 1.28 (s,

3H, pinanediol C**H**$_3$), 1.47 – 1.23 (m, 1H, pinanediol C**H**H), 1.21 – 1.18 (m, 1H, pinanediol C**H**H), 0.90 – 0.75 (m, 9H, pinanediol C**H**$_3$ and CH(C**H**$_3$)$_2$). ^{13}C NMR (126 MHz, $CDCl_3$) δ 190.3, 171.3, 159.6, 157.6, 157.0, 133.4, 133.2, 133.1, 130.5, 130.4, 129.2, 128.3, 117.6, 117.6, 115.8, 114.8, 110.6, 77.8, 68.8, 68.7, 53.9, 51.3, 40.3, 39.9, 39.5, 38.2, 37.8, 35.5, 29.6, 28.5, 27.1, 27.0, 26.3, 25.3, 24.0, 22.9, 21.9. HRMS (ES) 750.4203 (MH^+); $C_{44}H_{56}BN_3O_7$ requires 749.4211.

*Boronic ester inhibitor **3.07***

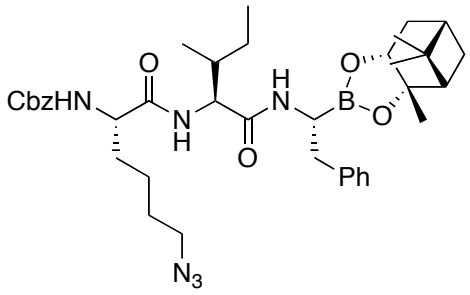

Compound **3.15** (65 mg, 0.16 mmol) was coupled to **3.28** (63 mg, 0.19 mmol) according to general procedure C to give the crude product as a yellow oil (90 mg). The crude product was purified by RP-HPLC to give compound **3.07** as a yellow oil (11 mg, 10%). ^{1}H NMR (300 MHz, $CDCl_3$) δ 7.38 – 7.27 (m, 7H, Cbz Ar**H** and Phe Ar**H**), 7.23 – 7.21 (m, 3H, Cbz Ar**H** and Phe Ar**H**), 6.50 (d, *J* = 7.0 Hz, 1H, N**H**), 6.44 (br s, 1H, N**H**), 5.21 (br s, 1H, N**H**), 5.05 (br s, 2H, Cbz C**H**$_2$), 4.33 – 4.27 (m, 2H, CbzNHC**H**CO and NHC**H**CH$_2$Ar), 4.11 – 4.04 (m, 1H, Ile **H**$_α$), 3.26 – 3.21 (m, 3H, C**H**$_2$N$_3$ and pinanediol C**H**) 2.98 (dd, *J* = 13.5, 5.5 Hz, 1H, CH**H**Ar), 2.78 (dd, *J* = 13.5, 10 Hz, 1H, C**H**HAr), 2.37 – 2.30 (m, 1H, pinanediol CH**H**), 2.17 – 2.10 (m, 1H, pinanediol C**H**), 2.00 (t, *J* = 5.5 Hz, 1H, pinanediol C**H**), 1.91 – 1.76 (m, 3H, Ile **H**$_β$ and C**H**$_2$CH$_2$CH$_2$CH$_2$N$_3$), 1.64 – 1.52 (m, 4H, pinanediol C**H**$_2$ and CH$_2$CH$_2$C**H**$_2$CH$_2$N$_3$), 1.45 – 1.33 (m, 4H,

$CH_2C\mathbf{H_2}CH_2CH_2N_3$ and $CH_3CHC\mathbf{H_2}CH_3$), 1.36 (s, 3H, pinanediol C$\mathbf{H_3}$), 1.27 (s, 3H, pinanediol C$\mathbf{H_3}$), 1.06 – 0.99 (m, 1H, pinanediol C**H**H), 0.87 – 0.83 (m, 9H, $C\mathbf{H_3}CHCH_2C\mathbf{H_3}$ and pinanediol C$\mathbf{H_3}$). ^{13}C NMR (126 MHz, $CDCl_3$) δ 171.3, 156.2, 139.5, 135.9, 129.0, 128.6, 128.3, 128.2, 126.4, 85.7, 67.3, 56.3, 55.0, 51.6, 51.0, 39.7, 38.1, 37.0, 35.8, 31.7, 28.6, 28.4, 27.1, 26.3, 24.6, 24.1, 22.6, 15.2, 11.3. HRMS (ES) 700.4108 (MH^+); $C_{38}H_{53}BN_6O_6$ requires 700.4120.

*Boronic ester inhibitor **3.08***

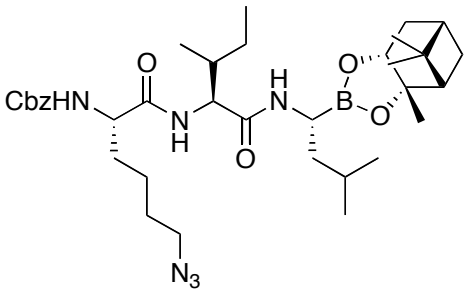

Compound **3.15** (50 mg, 0.12 mmol) was couple to **3.29** (36 mg, 0.12 mmol), according to general procedure C to give the crude product as a yellow oil (63 mg). The crude product was purified by RP-HPLC to give compound **3.08** as a yellow oil (12 mg, 15%). ^{1}H NMR (300 MHz, $CDCl_3$) δ 7.36 – 7.30 (m, 5H, Cbz Ar**H**), 6.69 – 6.64 (m, 1H, N**H**), 6.41 (br s, 1H, N**H**), 5.35 – 5.31 (m, 1H, N**H**), 5.10 (br s, 2H, Cbz C$\mathbf{H_2}$), 4.36 – 4.27 (m, 2H, CbzNHC**H**CO and NHC**H**CH_2Ar), 4.17 – 4.11 (m, 1H, Ile $\mathbf{H_\alpha}$), 3.27 – 3.20 (m, 3H, C$\mathbf{H_2}N_3$ and pinanediol C**H**), 2.39 – 2.30 (m, 1H, pinanediol CH**H**), 2.23 – 2.15 (m, 1H, pinanediol C**H**), 2.06 – 2.00 (m, 1H, pinanediol C**H**), 1.94 – 1.79 (m, 4H, Ile $\mathbf{H_\beta}$, Leu $\mathbf{H_\gamma}$ and $C\mathbf{H_2}CH_2CH_2CH_2N_3$), 1.69 – 1.54 (m, 4H, pinanediol C$\mathbf{H_2}$ and $CH_2CH_2C\mathbf{H_2}CH_2N_3$), 1.51 – 1.41 (m, 6H, $CH_2C\mathbf{H_2}CH_2CH_2N_3$, $C\mathbf{H_2}CH(CH_3)_2$ and $CH_3CHC\mathbf{H_2}CH_3$), 1.37 (s, 3H, pinanediol C$\mathbf{H_3}$), 1.29 (s, 3H, pinanediol C$\mathbf{H_3}$), 1.10 – 1.02 (m, 1H, pinanediol C**H**H), 0.96 – 0.83 (m, 15H, 2 × Leu C$\mathbf{H_3}$,

Ile 2 × C**H₃** and pinanediol C**H₃**). ^{13}C NMR (126 MHz, $CDCl_3$) δ 171.4, 156.2, 154.0, 136.0, 128.6, 128.3, 128.1, 67.3, 56.9, 55.1, 51.4, 51.0, 50.8, 39.9, 39.7, 39.6, 38.2, 37.0, 35.6, 32.0, 28.6, 28.4, 27.1, 26.3, 25.6, 25.5, 24.6, 24.0, 22.9, 22.6, 22.0, 15.3, 11.3. HRMS (ES) 665.4198 ($M\text{-}H^-$); $C_{35}H_{55}BN_6O_6$ requires 665.4205.

(*S*)-3-(4-(allyloxy)phenyl)-2-(5-(3-(4-(allyloxy)phenyl)propanoyl)-1*H*-pyrrole-2-carboxamido)propanoic acid **3.09**

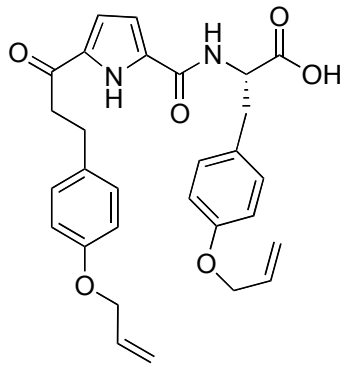

Compound **2.26** (271 mg, 0.54 mmol) was hydrolysed according to general procedure D to give the corresponding carboxylic acid **3.09** (286 mg, quant). ^{1}H NMR (500 MHz, $CDCl_3$) δ 7.12 (d, *J* = 4.2 Hz, 2H, OAr**H**), 7.09 (d, *J* = 4.2 Hz, 2H, OAr**H**), 7.00 (d, 1H, pyrrole **H**), 6.90 (d, *J* = 4.5 Hz, 1H, N**H**), 6.81 – 6.74 (m, 5H, 2 × OAr**H** and pyrrole **H**), 6.07 – 5.93 (m, 2H, 2 × $OCH_2C\mathbf{H}CH_2$), 5.39 – 5.28 (m, 2H, 2 × $OCH_2CHCH\mathbf{H}$), 5.22 – 5.15 (m, 2H, 2 × $OCH_2CHC\mathbf{H}H$), 4.70 (dd, *J* = 4.8, 8.1 Hz, 1H, C**H**CH_2ArO), 4.49 – 4.42 (m, 4H, 2 × O**CH_2**$CHCH_2$), 3.10 – 2.99 (m, 4H, O**CH_2CH_2**Ar), 2.95 – 2.85 (m, 2H, C**H_2**Ar)

(S)-6-Azido-2-(benzyloxycarbonylamino)hexanoic acid ***3.11***[2]

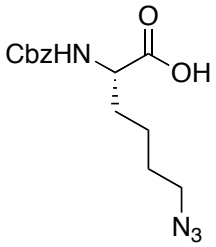

To a solution of (*S*)-6-amino-2-(benzyloxycarbonylamino)hexanoic acid (2.9 g, 10.27 mmol) in ACN (20 ml) and H_2O (10 ml) was added Et_3N (4.3 ml, 30.81 mmol) and $CuSO_4.5H_2O$ (26 mg, 0.10 mmol). The mixture was cooled in an ice bath while stirring for 30 min. A solution of triflic azide (2.7 g, 15.40 mmol) in ACN (40 ml) was added slowly to this ice-cooled mixture. The mixture was further stirred for 30 min with ice cooling and was allowed to warmed up to room temperature over 18 h. The volatiles were removed *in vacuo*. The mixture was diluted with H_2O (75 ml) and washed with EtOAc (3 × 75 ml). The aqueous phase was cooled in an ice bath and acidified to pH 1 with 2 M HCl. The acidified aqueous phase was then extracted with EtOAc (3 × 75 ml). The combined organic phase was washed with brine (100 ml) and dried over $MgSO_4$. The solvent was removed *in vacuo* and the resultant crude product (3.1 g) was purified by flash chromatography (DCM:MeOH 99:1) to give compound **3.11** as a white solid (907 mg, 29%). ^{1}H NMR (300 MHz, $CDCl_3$) δ 7.44 – 7.32 (m, 5H, Cbz Ar**H**), 5.28 (d, *J* = 8.2 Hz, 1H, N**H**), 5.11 (s, 2H, Cbz C$\mathbf{H_2}$), 4.42 (dd, *J* = 13.3, 7.9 Hz, 1H, $\mathbf{H_\alpha}$), 3.28 (t, *J* = 6.6 Hz, 2H, C$\mathbf{H_2}N_3$), 2.02 – 1.87 (m, 2H, C$\mathbf{H_2}CH_2CH_2CH_2N_3$), 1.68 – 1.38 (m, 4H, (C$\mathbf{H_2}$)$_2$CH_2N_3).

(2S,3R)-Methyl 2-((S)-6-azido-2-(benzyloxycarbonylamino)hexanamido)-3-methylpentanoate ***3.14***[2]

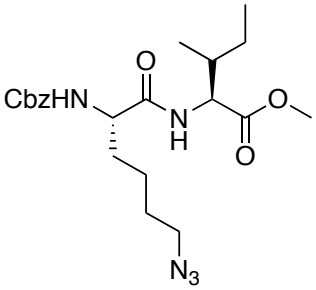

(2*S*,3*R*)-2-(*tert*-butoxycarbonylamino)-3-methylpentanoic acid (400 mg, 3.05 mmol) was deprotected and methylated according to general procedure B to give compound **3.13** as a clear oil (500 mg, quant) which was dissolved in anhydrous DCM (10 ml). EDCI (328 mg, 2.12 mmol), HOBt (329 mg, 2.44 mmol) and DIPEA (1.13 ml, 6.51 mmol) were added under N_2. The mixture was stirred for 18 h at room temperature under N_2 and quenched with 1 M HCl (10 ml). The mixture was diluted with DCM (50 ml) and the organic phase was separate and washed with 1 M HCl (20 ml), H_2O (2 × 20 ml) and brine (40 ml) and dried over $MgSO_4$. The solvent was removed *in vacuo* to give a clear oil (466 mg). The crude product was purified by flash chromatograhy (DCM:MeOH 99.5:0.5) to give compound **3.14** as a clear oil (460 mg, 36%). ^{1}H NMR (300 MHz, $CDCl_3$) δ 7.42 – 7.29 (m, 5H, Cbz Ar**H**), 6.47 (d, *J* = 8.4 Hz, 1H, N**H**), 5.36 (d, *J* = 7.3 Hz, 1H, N**H**), 5.12 (s, 2H, Cbz C$\mathbf{H_2}$), 4.57 (dd, *J* = 8.4, 4.8 Hz, 1H, $\mathbf{H_\alpha}$), 4.20 (q, *J* = 7.3 Hz, 1H, $\mathbf{H_\alpha}$), 3.74 (s, 3H, OC$\mathbf{H_3}$), 3.26 (t, *J* = 6.7 Hz, 2H, C$\mathbf{H_2}N_3$), 1.97 – 1.79 (m, 2H, C$\mathbf{H_2}CH_2CH_2CH_2N_3$), 1.74 – 1.54 (m, 3H, Ile $\mathbf{H_\beta}$ and $CH_2C\mathbf{H_2}CH_2CH_2N_3$), 1.51 – 1.32 (m, 3H $CH_2CH_2C\mathbf{H_2}CH_2N_3$ and $CH_3CHC\mathbf{H}HCH_3$), 1.22 – 1.06 (m, 1H, $CH_3CHCH\mathbf{H}CH_3$), 0.97 – 0.81 (m, 6H, 2 × Ile C$\mathbf{H_3}$).

(2S,3R)-2-((S)-6-Azido-2-(benzyloxycarbonylamino)hexanamido)-3-methylpentanoic acid ***3.15***[2]

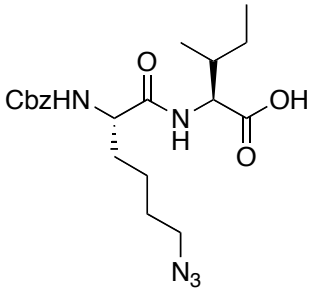

To an ice-cooled solution of **3.14** (437 mg, 1.01 mmol) in THF (9 ml) was added 1 M LiOH (120 mg, 5.05 mmol) slowly. The mixture was stirred for 16 h at room temperature and diluted with EtOAc (12 ml). The mixture was acidified with 2 M HCl to pH 7. The aqueous phase was separated and extracted with EtOAc (2 × 12 ml). The combined organic layer was washed wih brine (20 ml) and dried over $MgSO_4$. The solvent was removed *in vacuo* to give compound **3.15** as a pale yellow solid (395 mg, 93%). ^{1}H NMR (300 MHz, $CDCl_3$) δ 7.43 – 7.29 (m, 5H, Cbz Ar**H**), 6.66 (d, *J* = 8.5 Hz, 1H, N**H**), 5.50 (d, *J* = 8.3 Hz, 1H, N**H**), 5.12 (s, 2H, Cbz C$\mathbf{H_2}$), 4.58 (dd, *J* = 8.3, 4.7 Hz, 1H, $\mathbf{H_\alpha}$), 4.32 – 4.17 (m, 1H, $\mathbf{H_\alpha}$), 3.25 (t, *J* = 6.7 Hz, 2H, C$\mathbf{H_2}N_3$), 2.00 – 1.76 (m, 2H, C$\mathbf{H_2}CH_2CH_2CH_2N_3$), 1.74 – 1.52 (m, 3H, Ile $\mathbf{H_\beta}$ and $CH_2C\mathbf{H_2}CH_2CH_2N_3$), 1.52 – 1.34 (m, 3H, $CH_2CH_2C\mathbf{H_2}CH_2N_3$ and $CH_3CHC\mathbf{H}HCH_3$), 1.30 – 1.08 (m, 1H, $CH_3CHCH\mathbf{H}CH_3$), 0.92 (m, 6H, 2 × Ile C$\mathbf{H_3}$).

Isobutylboronic ester ***3.18***[3]

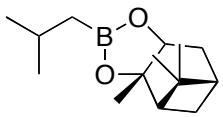

To a solution of isobutylboronic acid (100 mg, 0.86 mmol) in THF (1 ml) was added (+)-pinanediol (146 mg, 0.86 mmol). The mixture was stirred at room temperature for 21 h. The solvent was removed *in vacuo* and the resultant crude product (156 mg) was purified by flash chromatography (petroleum ether:EtOAc 50:1) to give compound **3.18** as a clear oil (97 mg, 45%). ^{1}H NMR (300 MHz, $CDCl_3$) δ 4.25 (dd, *J* = 8.7, 2.0 Hz, 1H, C**H**OB), 2.43 – 2.14 (m, 1H, pinanediol C**H**), 2.05 (t, *J* = 5.5 Hz, 1H, pinanediol C**H**), 1.97 – 1.78 (m, 1H, CH_3C**H**CH_3), 1.48 (td, *J* = 13.2, 6.6 Hz, 2H, C**H$_2$**B), 1.38 (d, *J* = 1.6 Hz, 3H, pinanediol C**H$_3$**), 1.30 – 1.27 (m, 4H, 2 × pinanediol C**H$_2$**), 0.90 – 0.81 (m, 2 × pinanediol C**H$_3$** and C**H$_3$**CHC**H$_3$**CH_2B, 12H).

(Dichloromethyl)lithium ***3.19***

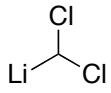

Method 1:[4] A solution of n-butyllithium (1.1 g, 1.92 mmol) in anhydrous THF (7.4 ml) was cooled in MeOH/$N_{2(l)}$ bath and anhydrous DCM (140 µl, 2.12 mmol) was added under Ar. The mixture was stirred with cooling in MeOH/$N_{2(l)}$ bath for 40 min. The mixture was used in the subsequent step without isolation and purification.

Method 2:[5] A solution of LDA (1.6 ml, 3.21 mmol) in anhydrous THF (7.4 ml) was cooled in acetone/$CO_{2(s)}$ bath and anhydrous DCM (0.5 ml, 4.70 mmol)

was added dropwise under Ar. The mixture was stirred with cooling in acetone/$CO_{2(s)}$ bath for 30 min. The mixture was used in the subsequent step without isolation and purification.

*Monochloroisobutylboronic ester **3.20**[4]*

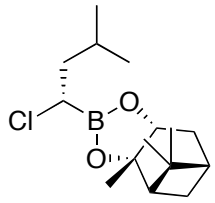

A solution of **3.18** (632 mg, 2.68 mmol) in anhydrous THF (8 ml) was cooled in acetone/$CO_{2(s)}$ bath and a solution of **3.19** (3.21 mmol) in anhydrous THF (7.4 ml) was added dropwise. The mixture was stirred with cooling in acetone/$CO_{2(s)}$ bath under N_2 for 15 min before well-dried $ZnCl_2$ powder (585 mg, 4.29 mmol) was added. The mixture was stirred with cooling in acetone/$CO_{2(s)}$ bath under N_2 for 3 h and was gradually warmed to room temperature. NH_4Cl (10%, 10 ml) was added. The mixture was extracted with petroleum ether (3 × 20 ml). The combined organic phase was dried over Na_2SO_4. The solvent was removed *in vacuo* to give compound **3.20** as a pale yellow oil (612 mg, 76%). ^{1}H NMR (300 MHz, $CDCl_3$) δ 4.38 – 4.34 (m, 1H, ClC**H**B), 3.54 (m, 1H, pinanediol C**H**), 2.43 – 2.17 (m, 2H, pinanediol C**H**H), 2.09 (t, *J* = 5.4 Hz, 1H, pinanediol C**H**), 1.99 – 1.73 (m, 3H, CH_3C**H**CH_3 and pinanediol CH**H**), 1.69 – 1.60 (m, 1H, pinanediol C**H**H), 1.42 (s, 3H, pinanediol C**H$_3$**), 1.30 (s, 3H, pinanediol C**H$_3$**), 1.19 (d, *J* = 11.0 Hz, 1H, pinanediol CH**H**), 0.92 (q, *J* = 6.5 Hz, 6H, C**H$_3$**CHC**H$_3$**), 0.85 (s, 3H, pinanediol C**H$_3$**).

Dimethyl dichloromethylboronate ***3.22***[4]

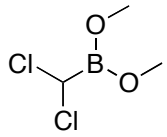

A solution of n-butyllithium (384 mg, 6.00 mmol) in anhydrous THF (12 ml) was cooled in $MeOH/N_{2(l)}$ bath and anhydrous DCM (0.43 ml, 6.60 mmol) was added under Ar. The mixture was stirred with cooling in $MeOH/N_{2(l)}$ bath for 40 min. Trimethylborate (686 mg, 6.60 mmol) was added in one portion and the mixture was further stirred with cooling in $MeOH/N_{2(l)}$ bath for 40 min. The reaction was quenched with 5 M HCl (1.2 ml). The mixture was warmed to room temperature. The aqueous phase was extracted with Et_2O (2 × 5 ml). The combined organic phase was dried over Na_2SO_4. The solvent was removed *in vacuo* to give compound **3.22** as a pale yellow oil which upon standing, turned to a pale yellow solid (582 mg, quant). The product was used in the subsequent step without isolation.

(+)-Pinanediol dichloromethaneboronate ***3.23***[4]

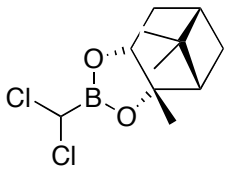

To a solution of **3.22** (290 mg, 1.85 mmol) in Et_2O (0.5 ml) was added (+)-pinanediol (142 mg, 1.00 mmol). The mixture was stirred at room temperature for 18 h. The solvent was removed *in vacuo* to give a clear oil (243 mg), which was purified by flash chromatography (petroleum ether:EtOAc 200:1) to give compound **3.23** as a clear oil (204 mg, 87%). ^1H NMR (300 MHz, $CDCl_3$) δ 5.40 (s, 1H, $Cl_2C\mathbf{H}B$), 4.47 (d, *J* = 8.7 Hz, 1H, C**H**OB), 2.46 – 2.22 (m, 2H,

pinanediol C**H** and C**H**H), 2.13 (t, *J* = 5.4 Hz, 1H, pinanediol C**H**), 2.00 – 1.90 (m, 2H, pinanediol C$\mathbf{H_2}$), 1.46 (s, 3H, pinanediol C$\mathbf{H_3}$), 1.31 (s, 3H, pinanediol C$\mathbf{H_3}$), 1.21 (d, *J* = 11.3 Hz, 1H, pinanediol CH**H**), 0.85 (s, 3H, pinanediol C$\mathbf{H_3}$).

(+)-Pinanediol 1-chloro-2-phenyl-1-boronate ***3.24***[4]

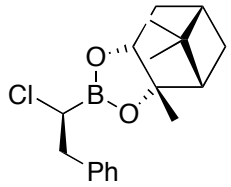

A solution of **3.23** (1 g, 3.80 mmol) in Et_2O (15 ml) was cooled in acetone/$CO_{2(s)}$ bath under N_2 and benzylmagnesium bromide (743 mg, 3.80 mmol) and well-dried $ZnCl_2$ powder (373 mg, 2.74 mmol) were added. The mixture was stirred under N_2 for 18 h while gradually warming up to room temperature. The solid residue formed was removed under vacuum and the filtrate was washed with NH_4Cl (10%, 2 × 50 ml) and dried over Na_2SO_4. The solvent was removed *in vacuo* to give a clear oil (987 mg), which was purified by flash chromatography (petroleum ether:EtOAc 200:1) to give compound **3.24** as a clear oil (819 mg, 68%). ^{1}H NMR (300 MHz, $CDCl_3$) δ 7.40 – 7.21 (m, 5H, Ar**H**), 4.38 – 4.31 (m, 1H, ClC**H**B), 3.71 – 3.60 (m, 1H, C**H**OB), 3.26 – 3.04 (m, 2H, C$\mathbf{H_2}$Ar), 2.40 – 2.27 (m, 1H, pinanediol C**H**H), 2.23 – 2.12 (m, 1H, pinanediol C**H**), 2.06 (t, *J* = 5.5 Hz, 1H, pinanediol C**H**), 1.94 – 1.81 (m, 2H, pinanediol C$\mathbf{H_2}$), 1.35 (s, 3H, pinanediol C$\mathbf{H_3}$), 1.28 (s, 3H, pinanediol C$\mathbf{H_3}$), 1.07 (d, *J* = 11.0 Hz, 1H, pinanediol CH**H**), 0.83 (s, 3H, pinanediol C$\mathbf{H_3}$).

(+)-Pinanediol 1-chloro-3-methylbutane-1-boronate ***3.25***[4]

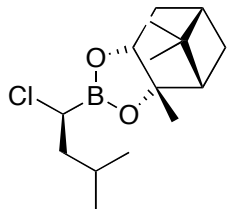

A solution of **3.23** (1.0 g, 3.80 mmol) in Et_2O (15 ml) was cooled in acetone/$CO_{2(s)}$ bath under N_2 and isobutylmagnesium bromide (613 mg, 3.80 mmol) and well-dried $ZnCl_2$ powder (373 mg, 2.74 mmol) were added. The mixture was stirred under N_2 for 18 h while gradually warming up to room temperature. The solid residue formed was removed under vacuum and the filtrate was washed with NH_4Cl (10%, 2 × 50 ml) and dried over Na_2SO_4. The solvent was removed *in vacuo* to give a clear oil (770 mg), which was purified by flash chromatography (petroleum ether:EtOAc 200:1) to give compound **3.25** as a clear oil (540 mg, 50%). ^{1}H NMR (300 MHz, $CDCl_3$) δ 4.41 – 4.31 (m, 1H, ClC**H**B), 3.59 – 3.49 (m, 1H, C**H**OB), 2.44 – 2.19 (m, 2H, pinanediol C**H**H and C**H**), 2.10 (t, *J* = 5.4 Hz, 1H, pinanediol C**H**), 1.97 – 1.83 (m, 3H, pinanediol C**H$_2$** and CH_2C**H**$(CH_3)_2$), 1.83 – 1.74 (m, 1H, C**H**HCH$(CH_3)_2$), 1.68 – 1.59 (m, 1H, CH**H**CH$(CH_3)_2$), 1.42 (s, 3H, pinanediol C**H$_3$**), 1.30 (s, 3H, pinanediol C**H$_3$**), 1.19 (d, *J* = 11.0 Hz, 1H, pinanediol CH**H**), 0.93 (q, *J* = 6.7 Hz, 6H, $CH_2CH(CH_3)_2$), 0.85 (s, 3H, pinanediol C**H$_3$**).

(+)-Pinanediol 1-chloro-2-phenyl-1-boronate hydrochloride ***3.28***[4]

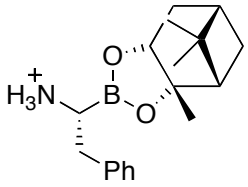

Method 1: A solution of **3.24** (132 mg, 0.42 mmol) in anhydrous THF (1.4 ml) was cooled in acetone/$CO_{2(s)}$ bath under Ar and 1 M LiHMDS in THF (451 µl, 0.45 mmol) was added dropwise. The mixture was stirred under N_2 for 18 h while gradually warming to room temperature. The solvent was removed *in vacuo* and the resulting solid was resuspended in anhydrous petroleum ether (0.5 ml). The insoluble residues were removed under vacuum. The filtrate was cooled in acetone/$CO_{2(s)}$ bath and 2 M HCl in anhydrous Et_2O (630 µl, 1.26 mmol) was added dropwise. The mixture was stirred for 12 h while gradually warming up to roomed temperature. The precipitate formed were collected by filtration, washed with ice-cold petroleum ether (10 ml) and dried to give compound **3.28** as a white solid (25 mg, 20%).

Method 2: A solution of **3.24** (1400 mg, 4.40 mmol) in anhydrous THF (12 ml) was cooled in acetone/$CO_{2(s)}$ bath and freshly prepared LiHMDS (800 mg, 4.78 mmol) in THF (4.8 ml) was added dropwise under N_2. The mixture was stirred under N_2 for 18 h while gradually warming to room temperature. The solvent was removed *in vacuo* and the resulting solid was resuspended in anhydrous petroleum ether (5 ml). The insoluble residues were removed under vacuum. The filtrate was cooled in acetone/$CO_{2(s)}$ bath and 2 M HCl in anhydrous Et_2O (6.6 ml, 13.20 mmol) was added dropwise. The mixture was stirred for 12 h while gradually warming up to room temperature. The

precipitate formed were collected by filtration, washed with ice-cold petroleum ether (50 ml) and dried to give compound **3.28** as a white solid (460 mg, 35%).

Method 3: A solution of HMDS (35 mg, 0.22 mmol) in anhydrous THF (120 µl) was cooled in MeOH/$N_{2(l)}$ bath under Ar and n-BuLi (14 mg, 0.22 mmol) was added dropwise. The mixture was stirred under Ar for 1 h with cooling in MeOH/$N_{2(l)}$ bath. The resulting solution was added to a solution of **3.24** (65 mg, 0.20 mmol) in anhydrous THF (0.55 ml). The mixture was stirred under Ar for 18 h while gradually warming up to room temperature. The solvent was removed *in vacuo* and the resulting solid was resuspended in anhydrous petroleum ether (0.2 ml). The insoluble residues were removed under vacuum. The filtrate was cooled in acetone/$CO_{2(s)}$ bath and 2 M HCl in anhydrous Et_2O (300 µl, 0.60 mmol) was added dropwise. The mixture was stirred for 12 h while gradually warming up to roomed temperature. The precipitate formed were collected by filtration, washed with ice-cold petroleum ether (2 ml) and dried to give compound **3.28** as a white solid (49 mg, 79%).

^{1}H NMR (300 MHz, DMSO) δ 7.95 (br s, 3H, N**H$_3$**), 7.38 – 7.21 (m, 5H, Ar**H**), 4.38 (d, *J* = 8.8 Hz, 1H, **H$_\alpha$**), 3.16-3.02 (m, 2H, C**H$_2$**Ar), 2.98 – 2.84 (m, 1H, C**H**OB), 2.34 – 2.22 (m, 1H, pinanediol C**H**H), 2.13-2.03 (m, 1H, pinanediol C**H**), 1.93 (t, *J* = 5.4 Hz, 1H, pinanediol C**H**), 1.74-1.65 (m, 2H, pinanediol C**H$_2$**), 1.31 (s, 3H, pinanediol C**H$_3$**), 1.23 (s, 3H, pinanediol C**H$_3$**), 0.95 (d, *J* = 10.9 Hz, 1H, pinanediol CH**H**), 0.80 (s, 3H, pinanediol C**H$_3$**).

(+)-Pinanediol 1-amino-3-methylbutane-1-boronate hydrochloride ***3.29***[4]

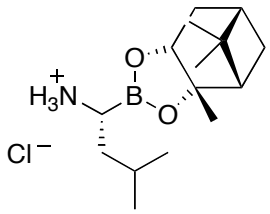

A solution of HMDS (155 mg, 0.96 mmol) in anhydrous THF (0.5 ml) was cooled in MeOH/$N_{2(l)}$ bath under Ar and n-BuLi (61 mg, 0.96 mmol) was added dropwise. The mixture was stirred under Ar for 1 h with cooling in MeOH/$N_{2(l)}$ bath. The resulting solution was added to a solution of **3.25** (285 mg, 0.96 mmol) in anhydrous THF (3.5 ml). The mixture was stirred under Ar for 18 h while gradually warming up to room temperature. The solvent was removed *in vacuo* and the resulting solid was resuspended in anhydrous petroleum ether (10 ml). The insoluble residues were removed under vacuum. The filtrate was cooled in acetone/$CO_{2(s)}$ bath and 2 M HCl in anhydrous Et_2O (1450 µl, 2.89 mmol) was added dropwise. The mixture was stirred for 12 h while gradually warming up to roomed temperature. The precipitate formed were collected by filtration, washed with ice-cold petroleum ether (10 ml) and dried to give compound **3.29** as a white solid (163 mg, 60%). ^{1}H NMR (300 MHz, DMSO) δ 7.79 (br s, 3H, N**H**$_3$), 4.49 – 4.42 (m, 1H, **H**$_\alpha$), 2.83 – 2.74 (m, 1H, C**H**OB), 2.39 – 2.29 (m, 1H, pinanediol C**H**H), 2.25 – 2.16 (m, 1H, pinanediol C**H**), 2.01 (t, *J* = 5.5 Hz, 1H, pinanediol C**H**), 1.92 – 1.85 (m, 1H, CH_3C**H**CH_3), 1.82 – 1.62 (m, 2H, pinanediol C**H**$_2$), 1.55 – 1.41 (m, 2H, C**H**$_2$CH(CH_3)$_2$), 1.37 (s, 3H, pinanediol C**H**$_3$), 1.26 (s, 3H, pinanediol C**H**$_3$), 1.15 – 1.07 (m, 1H, pinanediol CH**H**), 0.91-0.85 (m, 6H, C**H**$_3$CHC**H**$_3$), 0.83 (s, 3H, pinanediol C**H**$_3$).

5.4 X-Ray Crystallography

X-ray crystallography was performed by Dr. John Bruning (School of Biological Sciences, the University of Adelaide) using the Braggs X-ray facility.

TLCK-treated α-chymotrypsin purchased from Worthington Biochemical and compound **2.13** were dissolved in 0.1 M HEPES buffer (pH 7) and crystallized by sitting-drop vapour diffusion method. The crystals formed were harvested and mounted onto a Rigaku 007 X-ray goniometer (rotating copper anode, I = 1.54 Å). The crystal was cryo-protected using an Oxford cryostream. The diffraction was detected using a R-axis IV^{++} detector. The data was processed using iMasflm. Molecular replacement was conducted using Phaser. Cell refinement was undertaken with Pheonix. Values in parentheses correspond to the last shell. Data validation and Ramachandran values were calculated using Molprobity. The following parameters were used:

Wavelength (Å)	1.54
Resolution range (Å)	35 – 2.2
Space Group	$P2_1$
Unique Reflections	43565 (4172)
Multiplicity	4.5 (3.9)
Completeness (%)	98.5 (93.8)
Mean I/ sigma (I)	6.1 (2.9)
Wilson B-factor	21.1

R-merge	8.6 (29.3)
R-pim	4.9 (17.8)
R-factor	20.6 (25.3)
R-free	26.8 (36.3)
Protein Subunits in ASU	4
Total Number of Atoms	7479
Macromolecule Atoms	6794
Ligands Atoms	180
Water Atoms	505
Protein Residues	928
RMS bonds (Å)	0.012
RMS angles (^{o})	1.38
Ramachandran favoured (%)	96.1
Average B-factor Total	10.0
Macromolecule B-factor	9.9
Solvent B-factor	11.5

5.5 *In vitro* Assay with Purified Rabbit 20S Proteasome[2]

The activity of the 20S proteasome was assayed spectrophotometrically at 37 ^{o}C with a Synergy H4 Hybrid Multi-Mode Microplate Reader. The 20S proteasome and fluorogenic substrates were purchased from Boston Biochem and Sapphire Bioscience respectively. The substrates Suc-Leu-Leu-Val-Tyr-AMC (Suc-LLVY-AMC), Boc-Leu-Arg-Arg-AMC (Boc-LLR-AMC), and Ac-Nle-

Pro-Nle-Asp-AMC (Ac-nLPnLD-AMC) were used to determine chymotrypsin-like (CT-L), trypsin-like (T-L) and caspase-like (C-L) activities of the 20S proteasome, respectively. A solution of the proteasome (40 ng/μL) in buffer (20 mM Tris, pH 7.8) was prepared immediately before the assay. The three substrates were separately dissolved in the same buffer to achieve the concentration of 62.5 μM. The inhibitor solutions (250 pM – 250 μM) were prepared in DMSO. The assay was performed in black 96-well plates in the presence of 2% v/v DMSO. To each well was added 9 μL of the proteasome solution (40 ng/μL) and 1 μL of the inhibitor solution (250 pM – 250 μM). The mixture was incubated at room temperature for 15 min. Fluoregenic substrate (40 μL, 62.5 μM) was added to each well and the plate was incubated for 2 h at 37 ^{o}C. The fluorescence produced by the hydrolysed AMC was detected by a Synergy H4 Hybrid Multi-Mode Microplate Reader (λ_{ex} = 380 nm and λ_{em} = 460 nm). Uninhibited enzyme activity was determined by adding DMSO instead of inhibitor solution. Non-enzymatic hydrolysis of the substrates was analyzed by adding buffer instead of enzyme solution, and found to be negligible. The rate of enzyme-catalyzed hydrolysis of substrate in the absence of inhibitor was determined in each experiment and was set to 100%. The data was processed using Microsoft Excel for Mac 2011 and plotted using GraphPad Prism 6. A minimum of three biological replicates was performed for each data point.

5.6 *In vitro* Assay with the Proteasome in Whole Cell Extracts[6]

In vitro assays with cytosolic proteasome were conducted by Ms. Alaknanda Alaknanda in the Cancer Therapeutic Group, Hanson Institute, Adelaide.

Cell-free extracts were prepared as previously described.[6] The cellular extract (2 µg) was pre-incubated for 90 min at 37 ^{o}C with a titration (0-5 µM) of the indicated proteasome inhibitors. To the mixture, 40 µl of fluorogenic peptide substrates Suc-LLVY-AMC (CT-L activity, 100 µM), Boc-LSTR-AMC (T-L, 600 µM) and Ac-nLPnLD-AMC (C-L activity, 100 µM) in buffer (20 mM Tris-HCl, pH 7.5) were added. Fluorescence emitted by proteasomal cleavage of the substrates (λ_{ex} = 380 nm, λ_{em} = 460 nm) was monitored every 30 min using a Fluostar Optima Flurometer to quantify the hydrolysed AMC. The data was analysed and plotted using GraphPad Prism 6.

5.7 Cell Cytotoxicity Assays[2]

Cell cytotoxicity assays were conducted by Ms. Alaknanda Alaknanda in the Cancer Therapeutic Group, Hanson Institute, Adelaide.

Cell viability assays were performed as previously described.[2] Briefly, cells were seeded in 96-well plates at a density of 3 × 10^4 cells per well in the presence and the absence of the indicated inhibitors. Cells were harvested 48 h post-treatment, centrifuged at 1,300 *g*, washed in phosphate-buffered saline, and stained with 7-amino-actinomycin-D solution (2 µg/mL) (Invitrogen,

Carlsbad, CA) for 10 min at room temperature. Cell viability was determined using FACS Calibur flow cytometer (Becton Dickinson Immunocytometry Systems) and analyzed using FLOWJO (Tree Star, Inc.) and GraphPad Prism 6 (GraphPad Software Inc.).

5.8 ^{13}C NMR Experiments of Labelled Inhibitor 2.14 and α-chymotrypsin

Solution A was prepared by suspending compound **2.14** (2.6 mM) in 20% DMSO-d_6 in D_2O (1.05 ml) and filtering to remove the insoluble residues. Solution B was prepared by dissolving α-chymotrypsin (2.6 mM) in 20% DMSO-d_6 in D_2O (1.05 mL). Solution C was prepared by dissolving compound **2.13** (2.6 mM) in 20% DMSO-d_6 in D_2O (1.05 mL). Solution D was prepared by combining solutions A (350 µL) and B (350 µL). Solution E was prepared by combining solutions C (350 µL) and B (350 µL) All solutions were placed in separate glass NMR tubes and incubated at room temperature for 1 h with occasional inversions. ^{1}H NMR and ^{13}C NMR were collected for each solution using a Varian Inova 600 MHz instrument. The NMR spectra were processed by VnmrJ 3.2A.

5.9 Determining the Concentration of a saturated solution of 2.14 in DMSO/H_2O by RP-HPLC

Solutions of **2.14** in DMSO (100 µL, concentration = 0.2, 0.3, 0.4, 1, 1.5 and 2 mM) were prepared and 20 µL of each solution was analysed by RP-HPLC using an HP 1100 LC system equipped with a Phenomenex C-18 column

(250 × 4.6 mm). A UV spectrum (λ = 280 nm) of each sample was obtained. The absolute integral of the major peak at 18.1 min was calculated for each sample, with results listed in Table 2.04, Chapter 2. The integrals were plotted against the calculated amount of **2.14** injected to construct a standard curve, as shown in Figure 2.14, Chapter 2. Next, an excess amount of **2.14** was suspended in 7.5% DMSO in H_2O with stirring at room temperature for 1 h. The sample was centrifuged and filtered to give a homogeneous solution and 20 μL of this solution was similarly analysed by RP-HPLC to give a UV spectrum. The absolute intergral of the peak at 18.1 min (**2.14**) was compared with the standard curve to identify a concentration of 0.69 mM.

5.10 *In vitro* α-Chymotrypsin Assay

The activity of α-chymotrypsin was assayed spectrophotometrically at 25 ºC using Synergy H4 Hybrid Multi-Mode Microplate Reader. A solution of α-chymotrypsin (21.9 μg/mL) in 1 mM aqueous HCl was prepared freshly by a 1:40 dilution of a stock solution (874 μg/mL) in 1 mM aqueous HCl and kept on ice. A 1:100 dilution of the 21.9 μg/mL solution in ice-cold 1 mM aqueous HCl was prepared immediately before the start of each measurement. The assay was conducted in black 96-well plates as below: To each well was added AAF-AMC (Sigma Aldrich, Castle Hill, NSW) substrate in DMSO (5 μL, final concentrations = 0.5 mM), α-chymotrypsin in 1 mM aqueous HCl (10 μL, final concentration = 4 nM), DMSO (0, 15 or 35 μL) and Mili-Q water (185, 160, or 150 μL). The total volume in each well was 200 μL. The excitation and

emission wavelengths are 380 nm and 460 nm respectively. Progress curves were monitored over 10 min. The assay was conducted in triplicate.

5.11 NMR Spectra of Compounds 3.05, 3.06 and 3.08

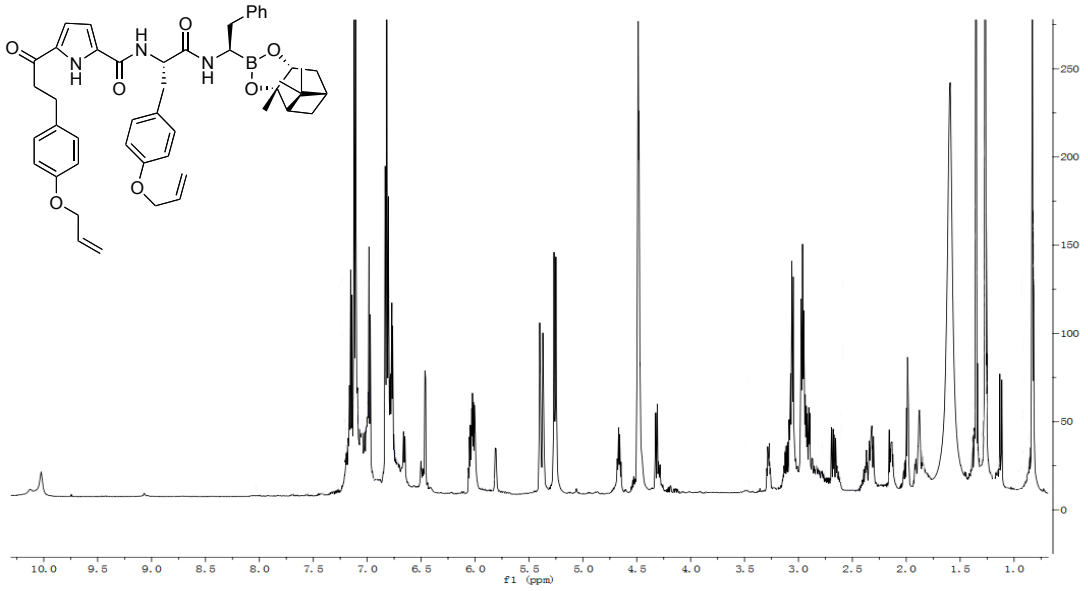

Figure 5.01 ^{1}H NMR spectrum of compound **3.05**.

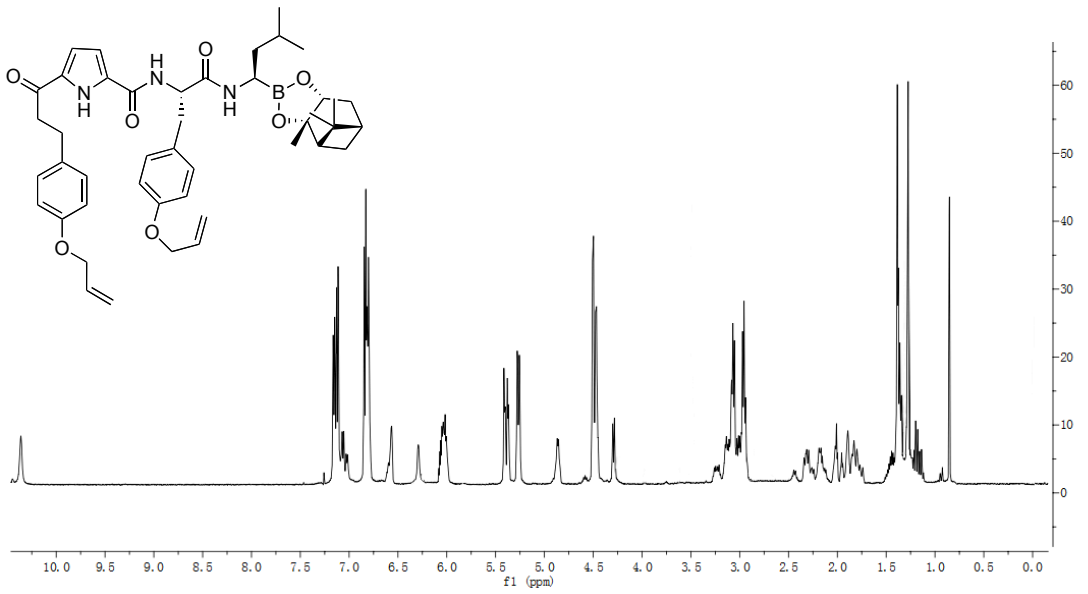

Figure 5.02 ^{1}H NMR spectrum of compound **3.06**.

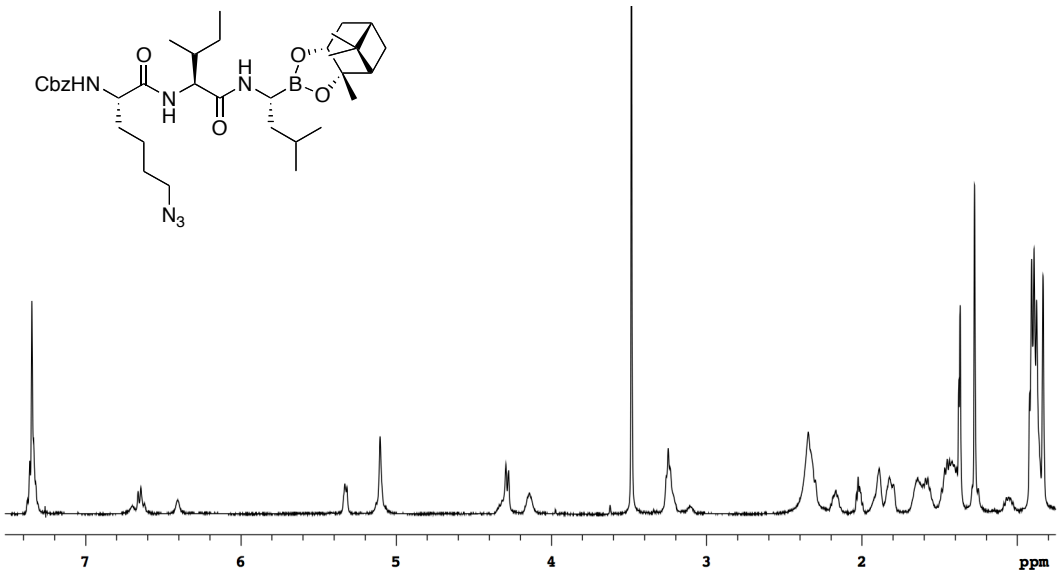

Figure 5.03 ^{1}H NMR spectrum of compound **3.08**.

5.12 References

(1) Chua, K. C. H.; Pietsch, M.; Zhang, X.; Hautmann, S.; Chan, H. Y.; Bruning, J. B.; Gütschow, M.; Abell, A. D. *Angew. Chem. Int. Ed.* **2014**, *53*, 7828.

(2) Neilsen, P. M.; Pehere, A. D.; Pishas, K. I.; Callen, D. F.; Abell, A. D. *ACS Chemical Biology* **2012**, *8*, 353.

(3) Matteson, D. S.; Sadhu, K. M.; Lienhard, G. E. *J. Am. Chem. Soc.* **1981**, *103*, 5241.

(4) Zhu, Y.; Zhao, X.; Zhu, X.; Wu, G.; Li, Y.; Ma, Y.; Yuan, Y.; Yang, J.; Hu, Y.; Ai, L.; Gao, Q. *J. Med. Chem.* **2009**, *52*, 4192.

(5) Matteson, D. S.; Sadhu, K. M. *J. Am. Chem. Soc.* **1983**, *105*, 2077.

(6) Kisselev, A. F.; Goldberg, A. L. In *Methods Enzymol.*; Raymond, J. D., Ed.; Academic Press: 2005; Vol. Volume 398, p 364.